

Thesis for the degree

Doctor of Philosophy

**Few Body Interactions
Near Central Massive Objects**

Hagai Binyamin Perets

Adviser: Prof. Tal Alexander

May 2009

Submitted to the scientific council of the

Weizmann Institute of Science, Rehovot, Israel

*The cobble stones of black and white,
The flowers of amazing red,
The smell of every springing hour,
And shining memories of May -*

*All for you, to keep to take,
To think about your way.
To feel, to taste,
To see the light
Of everlasting life and might.*

Few body interactions near central massive objects

ABSTRACT

The configuration of a central massive object interacting gravitationally with much lighter objects around it (so called near Keplerian system) appears on many astrophysical scales. At the largest scales massive black holes (MBHs; thought to exist in most if not all galactic nuclei,) and the stellar systems around them, exemplify such systems. Close interactions of stars with MBHs lead in many cases to catastrophic outcomes; a star or a binary star could be disrupted following a close encounter with the MBH; a compact object, such as a stellar black hole, neutron stars or a white dwarf may in-spiral to the MBH, through gravitational wave (GW) emission. In this Thesis the dynamics of stars and their close interactions near MBHs are studied. We explore several directions including the effects of massive perturbers such as giant molecular clouds on the dynamics of stars near MBHs; the close interaction of stars and binary stars with MBHs and their rates; and the origin and dynamical evolution of hypervelocity stars ejected by MBHs. We show that massive perturbers can accelerate relaxation processes in Galactic nuclei by orders of magnitude. Scattering of stars by such perturbers can explain the origin of the young stars observed very close to the MBH in the Galactic center, as well as the origin of hypervelocity stars observed in the Galactic halo. Massive perturbers could also have a major role in the coalescence of binary MBHs and induce their merger in short times, leading to their in-spiral through GW emission, likely to be observable with future space programs. We also obtained strong constraints on the origin of hypervelocity stars, and found a novel method to use them as probes of the Galactic potential at large scales.

אינטראקציות רב-גופיות ליד עצמים מסיביים

מערכות רב גופיות המורכבות מעצם מסיבי בנוסף למספר גופים קלים הנעים סביבו קיימות בטבע כמערכות בסדרי גודל שונים. בין הגדולות שבהן נמצאות מערכות כוכבים סביב חורים שחורים מסיביים (חש"מים); גופים אלו נמצאים ככל הנראה במרכזן של רוב ואולי אפילו כל הגלקסיות). אינטראקציות קרובות בין חש"מים אלו לבין כוכבים עשויות להוביל להריסת הכוכבים, ועצמים קומפקטיים כגון חורים שחורים כוכביים, כוכבי ניטרונים או ננסים לבנים עשויים ליפול אל חש"מים תוך כדי פליטת גלי כבידה. בתזה זו אנו עוסקים בנושאים אלו - תנועתם של כוכבים והאינטראקציות הבין-גופיות שלהם קרוב לחש"מים. מספר כיווני מחקר שונים מופיעים בתזה, וביניהם ההשפעה של עצמים מסיביים כגון עננים בין כוכביים על מערכות כוכבים ליד חש"מים; אינטראקציות קרובות של כוכבים וכוכבים כפולים עם חש"מים וקצביהן; וכן מקורם ותנועתם של כוכבים על-מהירים המועפים על ידי חש"מים. אנו מראים כי עננים בין כוכביים יכולים להאיץ תהליכי רלקסציה במרכזי גלקסיות, וכי תהליכים אלו מגבירים באופן משמעותי את קצב האינטראקציות הקרובות של כוכבים עם חש"מים. אנו מראים כי בכך הם עשויים להסביר הן את מקורם של הכוכבים הצעירים הנצפים ליד החש"מ במרכז הגלקסיה שלנו (שנתפסו על ידי החש"מ כתוצאה מהריסתם הגיאומטרית של כוכבים כפולים), הן את מקורם של כוכבים על-מהירים שנצפו בגלקסיה שלנו, והן את האופן בו שני חש"מים מתנגשים ומתחברים (תוך כדי פליטת גלי כבידה) לאחר התנגשות הגלקסיות בהן התקיימו. בנוסף אנו מציעים שיטה להשתמש בתצפיות של כוכבים על-מהירים לשם מדידת הפוטנציאל הכבידתי של הגלקסיה במרחקים גדולים (ובכך גם למדוד את החומר האפל הקיים בגלקסיה).

Acknowledgments

My PhD studies have been a great experience for me; the people I met and corresponded with, the excitement and fun in learning and thinking on new ideas and revealing the beauty of the world through scientific exploration, all contributed to this wonderful scientific adventure. I owe this great experience to many people to whom I would like to thank.

I would like to thank my adviser, Tal Alexander, who had to suffer my unfocused and eclectic methods of work, my sometimes strange ideas and my constant push towards directions not at all related to my studies, and to roads not usually taken. I am forever in debt for his open mindedness in letting me freely explore all these directions and at the same time always pointing me back to the rigorous science on which scientific work is based upon. More importantly, I would like to thank Tal for his kindness, patience and support, even at difficult times.

Beside my adviser, I have been fortunate to have good friends who made this journey much easier. Clovis Hopman have had a major contribution in guiding me into the world of massive black holes and stellar dynamics. Our many walks and talks in Weizmann, Leiden and other places have always been islands of pleasant tranquility and fun for me. To Smadar Naoz I owe a handful of gratitude for being a close friend throughout my academic studies. Always encouraging and supportive, she has made both our collaboration and my general studies much more enjoyable. Beside spending time on delightful discussions on both science and life in general, I would like to thank Yoav Lahini for introducing me to the world of quantum optics, which I never thought would be one of my fields of study. Avishay Gal-Yam opened more than one door for me, both to the science of supernovae and to the ways in which collaborative science could be done at its best. Moreover, since our acquaintance I was always sure to find in him a trustful listener and good council both in scientific issues and in more general questions and problems I encountered.

I would also like to express special gratitude to Avi Loeb and David Merritt for their invaluable help and council in both scientific and academic issues, and for many enlightening discussions.

Throughout my studies I have had many collaborators. Beside those mentioned above I would like to especially thank some of my closer collaborators from whom I have learned much. These include my MSc adviser, Ofer Biham with whom I have had a fruitful collaboration, since my MSc studies and to this day; Ariel Amir and Gabor Kupa with whom I both shared a room and many discussions, and I have also been fortunate to directly work with, and finally also to Dan Fabrycky, from whom I learned

a lot even though our work was done only through email correspondence.

The great environment in the Weizmann Institute and specifically in the Benozio center for astrophysics contributed much to my studies. My knowledge of physics, astrophysics and scientific presentations and analysis have gained much from my discussions and meetings with the astrophysics group faculty including Eli Waxman, Moti Milgrom and Volodia Usov (and Tal and Avishay mentioned earlier). I owe as much to my current and past colleagues in the physics and astrophysics group, including Amir Sagiv, Uri Keshet, Clovis Hopman, Rani Budnik, Boaz Katz, Gabor Kuti, Itay Rabinak, Ehud Eilon, Doron Kushnir, Michal Bregman, Muhammed Akashi, Assaf Sternberg, Michael Kiewe, Yair Arcavi, Roni Ilan, Ariel Amir and Yoav Lahini and the members of the “Physics Pirate Seminar”.

Finally, I would have never completed my PhD studies without the love and support of my family; Ruti, my wife, and my two children, Galia and Yuval who have always given me the right perspective of the most important things in life.

Hagai Perets
May 2009

Preface

The configuration of a central massive object interacting gravitationally with much lighter objects around it (so called near Keplerian system) appears on many astrophysical scales; from planets and asteroids around the sun in our own solar system; through binary and triple stars orbiting each other; and up to stars in the center of our Galaxy (or in other galaxies) orbiting a massive black hole. The technological improvements in the last decade have enabled the unprecedented detailed observations of such astrophysical systems. For example, it is now possible to resolve and follow the trajectories of single stars in the center of our Galaxy; hundreds of extrasolar planets have been discovered and their orbital characteristics measured; and in the solar system, binary asteroids have been observed as well as a wealth of single and binary minor planets found to orbit the sun beyond the orbit of Neptune. The observational study of the dynamics of such newly discovered types of gravitational systems presents many theoretical questions and challenges to our understanding of their formation and evolution. These questions are the main focus of my PhD studies.

During my PhD I have studied several different subjects, most of which are related to the dynamics of stars near massive black holes (MBHs) and some to the dynamics of triple systems such as triple stars and binary minor planets orbiting the sun. In this thesis I present my work on stellar dynamics near MBHs in Galactic nuclei. The appendix includes additional studies done during my PhD, in other fields of astrophysics and quantum physics, which are not directly related to the main theme of this thesis.

The submitted and published papers presented below are preceded by an introductory section and concluded by a discussion and summary section. The introduction presents the basic concepts and processes that are relevant for understanding the main concepts presented in this thesis. These include a description of various few-body interactions of single and binary stars with a MBH, and the interactions of stars and massive objects near MBHs. The latter interactions are presented in the context of relaxation processes, which govern the dynamics of stars near MBHs, and lead to scattering of stars into them. These parts greatly benefitted from the excellent reviews[1, 2] by my adviser, Tal Alexander, and the PhD thesis of my colleague and collaborator Clovis Hopman[59]. In addition, the introduction briefly reviews the stellar population near the MBH in our Galactic center and the population of hypervelocity stars, which are likely ejected from this region. As discussed below, the origin and evolution of these stellar populations are closely related to, and may result from, few body interactions near the massive black hole in the Galactic center.

Contents

1	Introduction	14
1.1	Close interactions with massive black holes	15
1.1.1	Tidal disruption by a massive black hole	15
1.1.2	Binary disruption by a massive black hole	16
1.1.3	Ejection by a binary MBH	17
1.1.4	Gravitational wave inspirals	17
1.1.4.1	Extreme mass ratio inspirals	17
1.1.4.2	High mass ratio inspirals	18
1.2	Loss-cone theory	18
1.3	Relaxation processes in galactic nuclei	21
1.3.1	Two body relaxation	22
1.3.2	Massive perturbers	23
1.3.2.1	Massive perturbers and the loss-cone	23
1.3.3	Resonant relaxation	24
1.4	The young stars in the Galactic center	27
1.5	Hypervelocity stars	28
2	Massive perturber-driven interactions between stars and a massive black hole	31
3	Massive perturbers and the efficient coalescence of binary massive black holes	45
4	Dynamical and evolutionary constraints on the nature and origin of hypervelocity stars	60
5	Runaway and hypervelocity stars in the Galactic halo: Binary rejuvenation and triple disruption	68
6	The Galactic potential and the asymmetric distribution of hypervelocity stars	80
7	Dynamical evolution of the young stars in the Galactic center: N-body simulations of the S-stars	87

<i>CONTENTS</i>	13
8 Conclusions	94
I Appendix	98
9 Molecular hydrogen formation on amorphous silicates under interstellar conditions	99
10 Realization of quantum walks with negligible decoherence in waveguide lattices	104
11 On the triple origin of blue stragglers	109
12 Kozai cycles, tidal friction and the dynamical evolution of binary minor planets	119
13 A new type of stellar explosions	125
14 Glossary, quantities and useful relations	154
14.1 GLOSSARY	154
14.2 SOME ASTROPHYSICAL QUANTITIES AND USEFUL RELATIONS	156
15 Bibliography	158
16 List of publications	164

Chapter 1

Introduction

Observations of individual stars in our own Galactic center, show their orbit to be consistent with a Keplerian orbit around a point mass of $M_{BH} = (3.6 \pm 0.3) \times 10^6 M_\odot$ [109, 1, 29]. The analysis of such orbits give a direct evidence for the existence of a supermassive ultra-compact object, and serves as evidence that our Galaxy harbors a massive black hole (MBH) in its center. The evidence for the existence of a MBH in our own Galaxy, and additional mounting evidence for the existence of extra-galactic MBHs (although less direct), both in the local Universe and at high redshifts (where MBHs are the engines of quasars; [122]), have made the MBH hypothesis to be generally accepted by most astronomers [e.g. 77] and today MBHs are thought to exist in most galactic nuclei. Indirect measurements of MBHs masses in other galactic nuclei show them to have a wide range of masses in the range $10^6 M_\odot \lesssim M_{BH} \lesssim 10^9 M_\odot$ [65, 76, 39, 30].

Far from the MBH, its mass M_\bullet can be neglected and the potential is dominated by the stars. If the stars far away from the MBH can be characterized by a velocity dispersion σ , the MBH will become the dominant component of the potential within the radius of influence,

$$r_h = \frac{GM_\bullet}{\sigma^2}. \quad (1.1)$$

If the velocity dispersion near r_h is comparable with the velocity dispersion at the effective radius, r_h and σ are related by the so-called empirical $M_\bullet - \sigma$ relation [31, 38, 117]

$$M_\bullet = 1.3(\pm 0.36) \times 10^8 M_\odot \left(\frac{\sigma}{200 \text{ km s}^{-1}} \right)^{4.72(\pm 0.36)}, \quad (1.2)$$

in which case the radius of influence is uniquely determined by the mass of the MBH. Such relation points to the fact that the evolution of MBHs in galactic nuclei is closely related to the evolution of larger scale structure of galaxies. The study of the dynamics near MBHs is therefore not only important to the understanding of galactic nuclei, but may also have significant implications for the evolution of galaxies as a whole.

Typically MBHs are thought to exist in dense stellar clusters. The high densities, especially in the closest environment of the MBHs, inside the radius of influence, make close interactions between stars and the MBHs inevitable. The observable outcomes of such strong encounters can be used as signatures for the existence of MBHs. Moreover, they can teach us about the dynamics and conditions in the close environment of MBHs in galactic nuclei, and even serve to probe the fundamental physics of general relativity (GR) and gravitational waves (GWs) physics. The interaction between a star or a stellar binary and a MBH are usually well approximated as a two-body problem, in which other effects (such as tidal effects or GW emission) can be treated as perturbations. It is the two-body approach that allows, for example, the precise determinations of the mass of the Galactic MBH. The outcome of a close interaction between the MBH and a star is in many cases catastrophic, leading to the disruption of the star or the binary. The rate of such interactions is therefore determined by the continuous rate at which stars are scattered onto the MBH, replacing those previously disrupted by it. The orbital parameters of stars and the structure of stellar systems near MBHs change through relaxation processes. Some of these could be very rapid processes working on short dynamical timescales, introduced through a prompt major change in the system such as violent relaxation following galactic mergers. Other processes work continuously but over longer times. This thesis is focused on the few body interactions of stars in the environment of MBHs, the relaxation processes governing these interactions, their outcomes, and their observational and theoretical implications.

In the following we describe various close interactions of stars with MBHs, we then briefly explain the “loss cone” theory which describes the way in which relaxation processes are responsible for such interactions and determine their rates. These are followed by a discussion of various relaxation processes which can play a role in the dynamics of galactic nuclei and determine the long term evolution of stars, and their relation to the loss cone theory. Finally we give brief overview of our Galactic center stellar environment and of hypervelocity stars observed in our galaxy, of which much of this work is related to.

1.1 Close interactions with massive black holes

1.1.1 Tidal disruption by a massive black hole

In most theoretical analyses of large stellar systems, stars are treated as point masses. Since most stars reside in stellar systems where the rate of physical collisions between stars is negligibly small, such point mass treatment assumptions are quite valid. However, in dense stellar systems, and specifically in galactic nuclei, very close encounters between stars or close encounters with an MBH, may become important, in which case the finite size of stars must be taken into account.

When a star is scattered very close to an MBH, the differential effect of the force exerted on one side of the star, and the force exerted on its far side, i.e. the tidal force, can be quite large. When the tidal force becomes strong enough to overcome the gravitational well which holds the star together, the star is disrupted. Such catastrophic

outcome typically occurs when the star passes closer than its tidal radius, defined by

$$r_t \sim \left(\frac{M_\bullet}{M_\star} \right)^{1/3} R_\star, \quad (1.3)$$

where M_\star and R_\star are the mass and radius of the star, respectively.

For low mass MBHs ($< \text{few} \times 10^7 M_\odot$) the tidal radius of stars is much larger than their physical radius, and stars are disrupted upon close encounters with the MBH. However, for higher mass MBHs, the Schwarzschild radius $r_\bullet = 2GM_\bullet/c^2$, can be larger than the tidal radius of the stars. In such cases, stars could be swallowed whole by the MBH without a tidal disruption outcome. Therefore only low mass MBHs may contribute to tidal disruption events. Tidal disruption events may result in highly luminous events observable to large distances. The rates of such tidal disruption events are theoretically estimated to be of $\sim 10^{-4}$ events per year [119], for galaxies harboring low mass MBHs. Observationally, several luminous bursts in galactic nuclei have been suggested as candidates for tidal disruption events in the literature [46, 47], although a conclusive evidence for the tidal disruption origin of these events have not yet been reported.

1.1.2 Binary disruption by a massive black hole

A close pass of a binary star near a massive black hole results in an exchange interaction, in which one star is ejected at high velocity, while its companion is captured by the MBH and is left bound to it. Such interaction occurs because of the tidal forces exerted by the MBH on the binary components. Typically, a binary (with mass, M_b , and semi-major axis, a_b), is disrupted when it crosses the tidal radius of the binary given by

$$r_t = \left(\frac{M_\bullet}{M_b} \right)^{1/3} a_b, \quad (1.4)$$

note that here the binary mass, M_b , and the semi-major axis of the binary, a_b , replace the mass and radius of a single star in Eq. 1.3 given above.

The capture probability and the semi-major axis distribution of captured stars were estimated by simulations, showing that most binaries approaching the MBH within the tidal radius $r_t(a)$ (Eq. 1.3) are disrupted [56, 57, 17]. The harmonic mean semi-major axis for 3-body exchanges with equal mass binaries was found to be [56]

$$\langle a_1 \rangle \simeq 0.56 \left(\frac{M_\bullet}{M_{\text{bin}}} \right)^{2/3} a \simeq 0.56 \left(\frac{M_\bullet}{M_{\text{bin}}} \right)^{1/3} r_t, \quad (1.5)$$

where a is the semi-major axis of the infalling binary and a_1 that of the captured star (the MBH-star “binary”). Most values of a_1 fall within a factor 2 of the mean. This relation maps the semi-major axis distribution of the infalling binaries to that of the captured stars: the harder the binaries, the more tightly bound the captured stars. The periastron of the captured star is at r_t , and therefore its eccentricity is very high [56, 82],

$$e = 1 - r_t/a_1 \simeq 1 - 1.8(M_{\text{bin}}/M_\bullet)^{1/3} \gtrsim 0.97 \quad (1.6)$$

for values typical of CO binaries and the MBH in the GC ($M_{\text{bin}} = 1 - 10 M_{\odot}$; $M_{\bullet} = 3.6 \times 10^6 M_{\odot}$). The velocity at infinity of the ejected star (neglecting the Galactic potential) is

$$v_{\text{BH}}^2 = \sqrt{2} \left(\frac{GM_{\text{bin}}}{a} \right) \left(\frac{M_{\bullet}}{M_{\text{bin}}} \right)^{1/3} \propto M_{\text{bin}}^{2/3} / a$$

(an equal mass binary with periapse at r_t is assumed; Hills 55), i.e. the harder the binary, the higher is v_{BH} .

Various phenomena associated with such exchange interactions were suggested and explored. Studies by Hills [55], and Yu & Tremaine [123], explored the ejection of hypervelocity stars from the GC following tidal disruption by the MBH. This mechanism was also suggested [51, 123, 96] in respect to the origin of the young massive stars observed near the Galactic MBH (the ‘S-stars’; [29, 49]; see also section 1.4).

Other less massive binaries and/or compact object (COs; or compact remnants; CR), such as white dwarfs (WDs), neutron stars (NSs) or stellar black holes (SBHs) binaries could also be disrupted by the MBH [64, 82] and be captured close to it, but these are more difficult to directly observe. Captured compact objects in the GC and in other galactic nuclei could potentially be observed by the planned LISA mission through the GW emission of such objects that inspiral into the MBH [82] or flyby near it.

1.1.3 Ejection by a binary MBH

Binary MBHs (BMBHs) form in the aftermath of galactic mergers, when the two MBHs sink by dynamical friction to the center of the merged galaxy. Once the binary hardens, the orbital decay continues by 3-body interactions with stars that are deflected to the center and extract energy from the binary, until the orbit becomes tight enough for efficient GW emission, which rapidly leads to coalescence of the BMBH. Stars scattered close the BMBH orbit, i.e. within its semi-major axis, a_{BMBH} closely interact with the BMBH, and are ejected by it with high velocities. Such ejected stars are typically lost from the system (although some fraction of them could infall again on to the BMBH [83]), and stars are needed to replenish those lost stars in order to further dissipate the orbital energy of the BMBH and lead to its coalescence. Simulations show that when the replenishment of stars occurs only through two-body stellar relaxation alone, the interaction rate is too slow for the BMBH to coalesce within a Hubble time (e.g. Berczik et al. 14; see review [80]), and the inspiral of BMBH is stalled when the BMBH semi-major axis is typically at the order of a pc. This “last parsec stalling problem” appears to contradict the circumstantial evidence that most galactic nuclei contain only a single MBH [15, 80], and suggests that additional relaxation processes such as studied in this thesis have a role in the evolution of BMBHs.

1.1.4 Gravitational wave inspirals

1.1.4.1 Extreme mass ratio inspirals

For a compact remnant (CR) orbiting a MBH of a few million M_{\odot} , typically $r_{\bullet} \gg r_t$ and tidal effects are entirely negligible everywhere. This implies that such a CR can come

close to the Schwarzschild radius without being tidally disrupted. However, if the CR orbit is close enough to the central black hole (e.g. it was scattered into highly eccentric orbit, with very small pericenter distance to the MBH), the gravitational radiation reaction is efficient before the star is re-scattered by the surrounding star cluster. Then, the orbit is gradually circularized over several consecutive orbits and the star is captured by the central black hole and finally swallowed by it. Although the initial orbit is typically very eccentric ($e \gg 0$) at the beginning of the formation of this system, the eccentricity is reduced to a moderate value before the final inspiral to the MBH by dissipation of its orbital energy through GWs emission. Such GWs sources are amongst the most exciting and plausible targets of the *Laser Interferometer Space Antenna (LISA)*, and sources with orbital periods of $1 \text{ s} < P < 10^4 \text{ s}$ at distances of $\sim 1 \text{ Gpc}$ are expected to be detected by *LISA*. Because of the large difference between the mass of the MBH and the CR, such sources are known as “extreme mass ratio inspirals” (EMRIs).

The energy lost to GWs emission can be calculated for a given CR orbit around the MBH. For a star with eccentricity e and peri-apse r_p , the energy $\Delta \mathcal{E}_{\text{GW}}$ emitted by GWs per orbit is given by [101, 110]

$$\Delta \mathcal{E}_{\text{GW}} = \frac{8\pi}{5\sqrt{2}} f(e) \frac{M_\star c^2}{M_\bullet} \left(\frac{r_p}{r_\bullet} \right)^{-7/2}; \quad f(e) = \frac{1 + \frac{73}{24}e^2 + \frac{37}{96}e^4}{(1+e)^{7/2}}. \quad (1.7)$$

The CR can only survive such a close passage if its angular momentum is larger than the angular momentum of the last stable orbit, which for an orbit of energy $\ll c^2$ is

$$J_{\text{LSO}} = \frac{4GM_\bullet}{c}, \quad (1.8)$$

and orbits with $J < J_{\text{LSO}}$ are therefore lost from the system.

1.1.4.2 High mass ratio inspirals

As mentioned earlier (section 1.1.3), following galactic mergers, the MBHs in each of the galactic cores inspiral to the newly formed galactic core of the merged galaxy. If efficient mechanism brings the two MBHs come close enough (see Eq. 1.7), GWs emission becomes important and dominate the orbital evolution of the newly formed BMBH, leading eventually to its final inspiral and merger. Such high mass ratio inspirals are also thought to be important GWs sources for the *LISA* mission, and are expected to give crucial information about inspiral processes and MBHs mergers in galactic nuclei.

1.2 Loss-cone theory

In both prompt disruption processes (such as tidal disruption) and GW inspiral processes occurring near a MBH there exists a minimal angular momentum, so that stars with J smaller than this minimum are tidally disrupted or swallowed by the MBH. This minimum is known as the angular momentum of the *loss-cone*,

$$J_{lc} = \max \left[J_{\text{LSO}}, \sqrt{2GM_\bullet r_t} \right], \quad (1.9)$$

where it is assumed that $1 - e \ll 1$. The distribution function of stars near a MBH in the presence of a loss-cone, and the rate at which stars are scattered into the loss-cone and accreted by the MBH has been studied extensively [e.g. 34, 71, 10, 25, 75, 114, 119]. Here we give a short summary of the main results.

The two-body relaxation time T_r (see section 1.3.1) is both the time-scale for changes in orbital energy, and the time-scale for a change in angular momentum by an amount of the circular angular momentum J_c . Since two-body relaxation is a random walk process, this implies that for times $\delta t < T_r$, the angular momentum changes by an amount $\delta J = \sqrt{\delta t / T_r} J_c$, and in particular, the change in angular momentum per orbital period, P , is

$$\Delta J_p = \sqrt{P / T_r} J_c. \quad (1.10)$$

Similarly, the time-scale for a change in angular momentum of order unity is given by

$$T_{Jr} = \left(\frac{J}{J_c} \right)^2 T_r. \quad (1.11)$$

Therefore, usually

$$\frac{J}{J_c} \ll \frac{E}{E_c},$$

and scattering in angular momentum is the dominant process in replenishing the loss cone.

For processes where the star is promptly destroyed by the MBH, two different energy regimes are considered in loss-cone theory [71]. Close to the MBH, the orbital period is short, and the change in angular momentum per orbit is smaller than the size of the loss-cone ($\Delta J_p \ll J_{lc}$). Since star travels all through J -space in a relaxation time, the rate at which stars of given orbital energy enter the loss-cone is estimated as

$$\Gamma_{\text{empty}}(\mathcal{E}) \sim \frac{N(\mathcal{E}) \ln(J_c / J_{lc})}{T_r(\mathcal{E})}, \quad (1.12)$$

where $N(\mathcal{E})d\mathcal{E}$ is the number of stars per with energies in the range $(\mathcal{E}, \mathcal{E} + d\mathcal{E})$; where the logarithmic term $\ln(J_c / J_{lc})$ appears due to the mild deviation of the distribution of stars around the MBH from a strictly isotropic distribution ([71]; the boundary conditions at the loss cone requires the DF to fall to zero, but only logarithmically in J). This regime is known as the “empty loss-cone” regime, because the area in angular momentum space with $J < J_{lc}$ is not populated by stars.

The opposite situation arises far away from the MBH, where $\Delta J_p \gg J_{lc}$. In that case the stars jump in and out the loss-cone on their way to the MBH, so that the loss-cone is full; this implies that at every orbital period a fraction $(J_{lc} / J_c)^2$ of the stars reach the MBH, so that the rate per energy is

$$\Gamma_{\text{full}} \sim \frac{N(\mathcal{E}) [J_{lc} / J_c(\mathcal{E})]^2}{P(\mathcal{E})}. \quad (1.13)$$

Within the radius of influence of the MBH, and assuming a Bahcall & Wolf cusp (see Eq. 1.16), $\Gamma(\mathcal{E})$ grows with decreasing energy in the empty loss-cone regime, and decreases with energy in the full loss-cone regime. The event rate is therefore dominated by stars near the critical energy where $\Delta J_p \sim J_{lc}$.

The total rate of close interaction events, Γ_{lc} , is set by the replenishment rate of stars into the loss-cone. Close to the MBH, where the relative size of the loss-cone in phase-space is large, relaxation is too slow to replenish the lost stars, and the loss-cone is on average empty. Farther out, where the loss-cone is small, relaxation can replenish the lost stars, the loss-cone is full, and the local replenishment rate is maximal. Nevertheless, the contribution to the total replenishment rate from the full loss-cone regions of phase-space, where the timescales are longer and the stellar densities lower, remains small compared to that from the empty loss-cone regions [71].

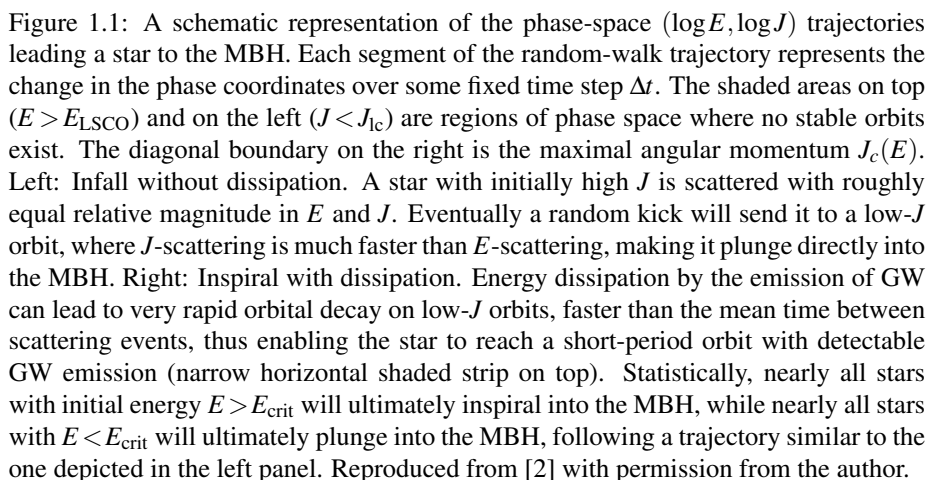
The observational and theoretical interest in such close interactions motivated numerous investigations of alternative efficient loss-cone replenishment mechanism, such as 2-body relaxation in non-spherically symmetric potentials [75, 15], chaotic orbits in triaxial potentials [87, 81, 44, 58], relaxation by massive perturbers [124, 96], resonant relaxation [106, 105, 61, 68], or perturbations by a massive accretion disk or a secondary IMBH [102, 70]. Some of the work in this thesis is related to such relaxation processes which go beyond the two-body stellar relaxation process, including massive perturbers induced relaxation and resonant relaxation, we briefly overview these processes in section 1.3.

Close interactions with a MBH (see section 1.1) fall in two dynamical categories [3]: infall processes, such as tidal disruption, where the star is destroyed promptly on its first close encounter with the MBH, and inspiral processes, such as GW EMRI events, where multiple consecutive close encounters are required for the orbit to gradually decay. The infall takes about an orbital period, the time to fall from the point of deflection to the center, whereas the inspiral process takes much longer, depending on the energy extraction efficiency of the dissipational mechanism involved (e.g. GW emission). In most cases the dissipated energy is a steeply decreasing function of the periape (e.g. Eq. 1.7) and so the inspiral time scales with the number of periape passages, and hence with the initial orbital period.

An infall or inspiral event can occur only if the star, once deflected into the loss-cone, avoids being re-scattered out of it (and in the case of inspiral, also avoids being scattered directly into the MBH). Because inspiral processes are slow, stars can avoid re-scattering, complete the inspiral and decay to an interesting, very short period orbit with high emitted dissipative power, only if they are deflected into the loss cone from an initially short period orbit, with $E > E_{\text{crit}}$. Figure 1.1 shows a schematic description of the phase-space evolution of infalling and inspiraling stars, and the emergence of a critical energy scale. For inspiral by GW emission into a $M_{\bullet} \sim O(10^6 M_{\odot})$ MBH, E_{crit} corresponds to an initial distance scale of $r_{\text{crit}} \sim 0.01$ pc (the *ansatz* $r \leftrightarrow E = GM_{\bullet}/2a$, is assumed here, where a is the Keplerian semi-major axis). The EMRI event rate is then approximately [60]

$$\Gamma_{\text{lc}} \sim N_{\text{GW}}(< r_{\text{crit}})/T_R(r_{\text{crit}}) \propto N_{\text{GW}}(< r_{\text{crit}})N_{\star}(< r_{\text{crit}})/\tau_{\text{dyn}}(r_{\text{crit}}), \quad (1.14)$$

where $N_{\text{GW}}(< r)$ is the number of potential GW sources (compact remnants) within distance r of the MBH. A critical energy can be similarly defined for infall processes. Because infall is much faster than inspiral, E_{crit} is much lower (r_{crit} much larger). For example, the critical radius for tidal disruption in the GC is $r_{\text{crit}} \sim \text{few pc}$ [71, 114, 75]. Most of the stars that infall or inspiral originate near r_{crit} .



1.3 Relaxation processes in galactic nuclei

Dynamical relaxation by star-star interactions is inherent to the discreteness of stellar systems. In the absence of additional mechanisms to randomize stars in phase-space, standard 2-body stellar relaxation assures a minimal degree of randomization, albeit one that could sometimes be too slow to be of practical interest. In the following we will shortly review various relaxation processes near MBHs, including both the 2-body relaxation and other relaxation processes which go beyond the standard stellar relaxation, and operate on much shorter timescales, or else operate in a qualitatively different way: massive perturbers, resonant relaxation and binary heating.

1.3.1 Two body relaxation

The stellar densities in galactic nuclei are typically high. Two-body gravitational encounter are therefore important in these systems. The typical timescale for an order unity change in the kinetic energy of stars, due to two-body gravitational encounters between stars in such systems is the two-body relaxation time. One can estimate the two body relaxation time of a system following a simple derivation [24, 16].

Let a stellar system consist of N stars of average mass m per star, and let R be the size of the system. The number density of stars is $n \sim N/R^3$. The two-body relaxation time in the system can be estimated in the following manner. The change in the velocity v of a star in a single encounter is

$$(\delta v_{\perp})_1 \sim \frac{Gm}{b^2} \frac{2b}{v} \sim \frac{2Gm}{bv},$$

where b is the impact parameter in the encounter, and G is the gravitational constant. In multiple encounters this adds randomly, so $(\delta v_{\perp})^2$ grows with time. The rate of increase of the mean square is then

$$\begin{aligned} \frac{d}{dt}(\delta \bar{v}_{\perp})^2 &\sim \int_{b_{min}}^{b_{max}} (\delta v_{\perp})_1^2 n v 2\pi b db \\ &\sim \frac{8\pi G^2 m^2 n}{v} \int_{b_{min}}^{b_{max}} \frac{db}{b} \\ &\sim \frac{8\pi G^2 m^2 n}{v} \ln \left(\frac{b_{max}}{b_{min}} \right). \end{aligned}$$

The relaxation time is then

$$T_r = \frac{v^2}{\frac{d}{dt}(\delta \bar{v}_{\perp})^2} \sim \frac{v^3}{8\pi G^2 m^2 n \ln \Lambda}, \quad (1.15)$$

where $\Lambda = b_{max}/b_{min}$ is called the Coulomb logarithm, in analogy to the Coulomb logarithm used in plasma physics. Typically the velocity v used in such formulation is replaced by the characteristic velocity dispersion of the system, σ . For example, in the Galactic center, it is estimated that $t_r \approx \text{few Gyr}$ [5, 1, 62].

The fact that the relaxation time is shorter than the Hubble time, implies that the system may relax to a quasi steady state configuration. A detailed analysis for a system composed of single mass stars near a MBH was first performed by Bahcall & Wolf [9], who derived the Fokker-Planck equations for a stellar system dominated by the potential of a MBH. Formally, a Maxwellian velocity distribution solves these equations, but this ignores the fact that a MBH acts as a mass sink: stars coming too close to the MBH are tidally disrupted or swallowed directly, so that the distribution function vanishes at some high energy. Bahcall & Wolf found another solution which does obey the boundary conditions to the Fokker-Planck equations, and this solution implies that the spatial distribution of stars near a MBH is a power law,

$$n_*(r) \propto r^{-\alpha}; \quad \alpha = 7/4. \quad (1.16)$$

In a subsequent paper, Bahcall & Wolf [10] extended their results to a multi-mass population, in which each species is distributed according to different (approximate) power laws. The most massive stars have the steepest power laws, which is a result of mass-segregation (see also 62; 35). The existence of a Bahcall & Wolf cusp near MBHs has now been confirmed numerically by many different theoretical models, including Monte Carlo models [36], Fokker-Planck models [25, 85] and N -body simulations [13, 103]. Note, however, that the BW solution is obtained when massive objects (e.g. stellar black holes) dominate the population, otherwise even stronger segregation occurs [4].

1.3.2 Massive perturbers

1.3.2.1 Massive perturbers and the loss-cone

As shown above, the relaxation time (Eq. 1.15) is proportional to $(M_*^2 n_*)^{-1}$. Typically two-body relaxation takes into account only mutual scattering by gravitational encounters between stars. However, when the system also contains a few very massive objects such as giant molecular clouds (GMCs), stellar clusters, or intermediate mass MBHs (IMBHs; if such exist), these massive perturbers (MPs) of mass $M_p \gg M_*$ and space density $n_p = N_p/V \ll n_*$ will scatter stars at a rate of $\Gamma_p \sim n_p (M_* + M_p)^2 / v^3 \sim n_p M_p^2 / v^3$. Therefore, MPs could well dominate the relaxation even if they are very rare, as long as

$$\mu_2 \equiv M_p^2 N_p / M_*^2 N_* > 1. \quad (1.17)$$

Efficient relaxation by MPs was first suggested by Spitzer & Schwarzschild [112, 113] to explain stellar velocities in the Galactic disk. Its relevance for replenishing the loss-cone was subsequently investigated in the context of Solar system dynamics for the scattering of Oort cloud comets to the Sun [54, 11], and more recently as a mechanism for establishing the M_\bullet/σ correlation by fast accretion of stars and dark matter [124]. In this thesis the focus is on the consequences of MPs for the replenishment of the loss-cone, and the implications for stellar populations in the Galaxy (chapter 2), the coalescence of binary MBHs (chapter 3) and for the cosmic rates of GW inspirals (chapters 2 and 3).

Loss-cone replenishment by MPs can be described by the standard loss-cone formalism (e.g. [121]) with only few modifications [96]. The large size of the MPs is taken into account by decreasing the Coulomb logarithm accordingly; the orbital averaging of phase-space diffusion due to scattering by stars is done incoherently (sum of squares), while for rare MPs, where there may be on average less than one scattering events per orbital period, the averaging is done coherently (square of sums).

The relative contributions of relaxation by stars and relaxation by MPs to the total loss-cone replenishment rate depend on the size of r_{crit} relative to the spatial distribution of the MPs (r_{crit} increases with the loss-cone size, and in the case of inspiral also with the efficiency of the dissipative process). MPs are extended objects, which cannot survive in the strong tidal field of the MBH (IMBHs could be the one exception).

Generally, MPs in galactic centers could also be affected by an intense central radiation field, whether the AGN's or the stars', or by outflows associated with accretion on a MBH. These processes introduce an inner cutoff r_{MP} to the MP distribution. A plausible estimate is $r_{\text{MP}} \gtrsim \ell(r_h)$. This is the case in the GC, where the clumpy circumnuclear gas ring lies outside the central 1.5 pc, on a scale comparable to r_h . The event rates of processes such as tidal disruption of single stars ($r_{\text{crit}} \sim r_h$) or GW EMRI ($r_{\text{crit}} \ll r_h$), where stellar relaxation by itself efficiently fills the loss-cone at $r_{\text{crit}} < r < r_{\text{MP}}$, will not be much enhanced by additional relaxation due to MPs (the stellar distribution function (DF) cannot be more random than isotropic). In contrast, the event rates of processes whose loss-cone is large, and which would have remained empty beyond r_{MP} in the absence of MPs, can be increased by orders of magnitude by the presence of MPs. Most of the enhancement is due to MPs near r_{MP} [96].

Here we consider two processes with large loss-cones, where MPs play an important role: the tidal disruption of stellar binaries leading to the capture of one star around the MBH and the ejection of the other as a HVS (see section 1.1.2), and the orbital decay of a binary MBH of total mass by interactions with stars (see section 1.1.3). Detailed discussion of these processes and their outcomes is given in chapters 2-7.

1.3.3 Resonant relaxation

The effect of 2-body relaxation on a test star is incoherent: the star experiences randomly oriented, uncorrelated perturbations from the ambient stars, and as a result its orbit deviates in a random-walk fashion from its original phase-space coordinates (in a stationary spherical smoothed potential where E and J would have been conserved in the continuum limit, $\Delta E \propto \sqrt{t}$ and $\Delta J \propto \sqrt{t}$ (Eqs. 1.15 and 1.11) due to 2-body interactions (see section 1.3.1). Resonant relaxation (RR) [106, 105] is a form of accelerated relaxation of the orbital angular momentum, which occurs when approximate symmetries in the potential restrict the orbital evolution of the perturbing stars. This happens in the almost Keplerian potential near a MBH, where the orbits are approximately fixed ellipses (the potential of the enclosed stellar mass far from the MBH, or General Relativistic (GR) precession near the MBH, eventually leads to deviations from pure elliptical orbits), or in a non-Keplerian, but nearly spherically symmetric potential around a MBH, where the orbits approximately conserve their angular momentum and move on rosette-like planar orbits (the fluctuations in the potential due to stellar motions eventually lead to deviations from strictly planar orbits). As long as the symmetry is approximately conserved, on times shorter than the coherence timescale t_ω , the orbit of a test star with semi-major axis a experiences correlated (coherent) perturbations, which can be described as a constant residual torque exerted by the superposed potentials of the $N_*(< a)$ randomly oriented elliptical “mass wires” (in a Keplerian potential) or “mass annuli” (in a non-Keplerian spherical potential) that represent the orbitally-averaged mass distribution of individual perturbing stars. The magnitude of the residual torque is then $J \sim N_*^{1/2}(< a)GM_*/a$ and the change in the angular momentum of the test star increases linearly with time, $\Delta J \sim Jt$ (for $t < t_w$). The orbital energy, on the other hand, remains unchanged, since the potential is constant.

RR in a Keplerian potential is called *scalar* RR since it changes both the magnitude

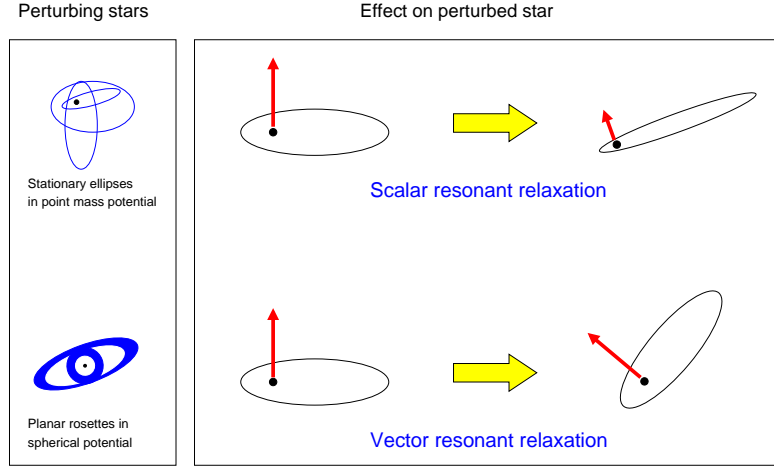


Figure 1.2: A sketch comparing the symmetries leading to scalar and vector RR. Top: The torques by fixed elliptical “mass wires” in a Keplerian potential lead to rapid changes in both the direction and magnitude of the orbital angular momentum of a test star. Bottom: The torques by fixed “mass annuli” in a non-Keplerian spherical potential lead to rapid changes in the direction, but not in the magnitude of the orbital angular momentum of a test star. Figure reproduced from [2] with permission from the author.

and direction of \mathbf{J} . Scalar RR can therefore change a circular orbit into an almost radial, MBH-approaching one. In contrast, RR in a non-Keplerian spherical potential is called *vector* RR since, for reasons of symmetry, it changes only the direction of \mathbf{J} , but not its magnitude (Fig. 1.2). Vector RR can randomize the orbital orientations, but does not play a role in supplying stars to the loss-cone.

On timescales longer than the coherence time, the orbital orientations of the perturbing stars drift, and coherence is lost. the maximal change in angular momentum during the linear coherence time, $\Delta J_\omega \sim \dot{J} t_\omega$ then becomes the “mean free path” for a random walk in J -space, whose time-step is t_ω . On timescales longer than the coherence time, the angular momentum changes incoherently $\propto \sqrt{t}$, but much faster than it would have in the absence of RR. The energy is unaffected by RR and always evolves incoherently $\propto \sqrt{t}$ on the long non-resonant relaxation timescale (e.g., see Fig. 1 in chapter 7). The RR timescale T_{RR} is defined, like the incoherent 2-body relaxation timescale, as the time to change J by order J_c (Eqs. 1.15 and 1.11), $T_{RR} \sim (J_c / \Delta J_\omega)^2 t_\omega$, which can be expressed as [61]

$$T_{RR} = A_{RR}^\omega \frac{N_*(< a)}{\mu^2(< a)} \frac{P^2(a)}{t_\omega} \simeq \frac{A_{RR}^\omega}{N_*(< a)} \left(\frac{M_\bullet}{M_*} \right)^2 \frac{P^2(a)}{t_\omega}, \quad (1.18)$$

where μ is the relative enclosed enclosed stellar mass, $\mu = N_* M_* / (M_\bullet + N_* M_*)$, P is the radial orbital period, and the last approximate equality holds in the Keplerian regime. Here and below, the constants A_{RR}^ω are numerical factors of order unity that

depend on the specifics of the coherence-limiting process, on the orbital characteristics of the test star, and probably also on the parameters of the stellar distribution. These constants are not well-determined at this time.

The coherence time depends on the symmetry assumed and on the process that breaks it. For a non-relativistic near-Keplerian potential, the limiting process is precession due to the potential of the distributed stellar mass¹,

$$t_\omega = t_M \sim \frac{M_\bullet}{N_\star(<a)M_\star} P(a). \quad (1.19)$$

Remarkably, the resulting RR timescale does not depend on N_\star . Close to the MBH is much shorter than the non-coherent 2-body relaxation timescale (here denoted for emphasis as T_{NR}),

$$T_{RR}^M = A_{RR}^M \frac{M_\bullet}{M_\star} P(a) \sim \frac{N_\star(<a)M_\star}{M_\bullet} T_{NR}. \quad (1.20)$$

Yet closer to the MBH, it is GR precession that limits the coherence,

$$t_\omega = t_{GR} = \frac{8}{3} \left(\frac{J}{J_{\text{LSO}}} \right)^2 P(a), \quad (1.21)$$

where $J_{\text{LSO}} = 4GM_\bullet/c$ is the last stable orbit for $\varepsilon \ll c^2$. The GR precession is prograde, while that due to the distributed mass is retrograde, and so they may partially cancel each other. Their combined effect on the scalar RR timescale is

$$T_{RR}^s \simeq \frac{A_{RR}^s}{N_\star(<a)} \left(\frac{M_\bullet}{M_\star} \right)^2 P^2(a) \left| \frac{1}{t_M} - \frac{1}{t_{GR}} \right|. \quad (1.22)$$

Since t_M increases with r , while t_{GR} decreases with r , scalar RR is fastest at some finite distance from the MBH, which typically coincides with $\sim r_{\text{crit}}/2$ for LISA EMRI targets.

Precession does not affect vector RR. The coherence in a non-Keplerian spherical potential is limited by the change in the total gravitational potential $\phi = \phi_\bullet + \phi_\star$ caused by the fluctuations in the stellar potential, ϕ_\star , due to the realignment of the stars as they rotate by π on their orbits,

$$t_\omega = t_\phi = \frac{\phi}{\dot{\phi}_\star} \sim \frac{N_\star^{1/2}(<a)}{2\mu} P(a) \simeq \frac{M_\bullet}{2N_\star^{1/2}(<a)M_\star} P(a), \quad (1.23)$$

where the last approximate equality holds in the Keplerian regime. The vector RR timescale is obtained by substituting t_ϕ in Eq. (1.18),

$$T_{RR}^v = 2A_{RR}^v \frac{N_\star^{1/2}(<a)}{\mu(<a)} P(a) \simeq 2A_{RR}^v \left(\frac{M_\bullet}{M_\star} \right) \frac{P(a)}{N_\star^{1/2}(<a)}, \quad (1.24)$$

where vector RR is much faster than scalar RR.

¹The enclosed stellar mass $N_\star M_\star$ changes the Keplerian period $P \propto M_\bullet^{-1/2}$ by $\Delta P/P = N_\star M_\star / 2M_\bullet = \Delta\phi/2\pi$. Identifying de-coherence with a phase drift $\Delta\phi = \pi$ then implies $t_M \sim (\pi/\Delta\phi)P$.

1.4 The young stars in the Galactic center

One of the most surprising observations in recent years was the discovery of a young stellar population very close to the MBH in the central pc of the GC [48, 29]. Star formation so close to the MBH is thought to be inhibited by the tidal forces from the MBH, which would disrupt any star forming molecular cloud progenitor. Many alternative formation scenarios have been suggested in the literature to explain these stars [1]. Since much of this thesis is related to the stellar population in the GC, its origin and evolution, I present a short overview of the stellar populations in the GC, and specifically the young stellar population.

The properties of the stellar population in the central pc of the Galaxy are observed to change with decreasing distance from the MBH, once at ~ 0.4 pc and then again at ~ 0.04 pc. Both the stellar spatial distribution and the stellar population outside ~ 0.4 pc are a continuation of the large scale $n_\star \propto r^{-2}$ mixed distribution of old and young stars in the inner 100 pc [43]. The old population is dynamically relaxed and follows the Galactic rotation pattern [79, 52, 42].

Inside ~ 0.4 pc the stellar spatial distribution flattens to $n_\star \propto r^{-1.4}$ [43]. On approximately the same length-scale (whether or not this is a coincidence is unclear), there appears a dominant population of massive young stars [33, 6, 66, 48, 89, 29, 12, 74]. This population consists of dynamically unrelaxed blue supergiants with distinctive helium emission lines in their infrared spectra [115, 42, 41]. The lack of hydrogen lines and evidence of outflow in the spectral line shapes (“P Cygni profiles”) identify them as WR stars or Luminous Blue Variables [86]. WRs are stars with masses of order $\text{few} \times 10 M_\odot$ and lifespans of $\text{few} \times 10^6$ yr undergoing rapid mass loss by a stellar wind, which removes the hydrogen-rich envelope and uncovers the helium-rich core. LBVs are WR progenitors that are still in the process of losing their envelopes. There are tentative detections of X-ray emission from the shocked winds of a couple of these stars [8].

The emission line stars co-rotate tangentially in an opposite direction to the Galactic rotation, in one or possibly two partially overlapping disk-like structures [69, 43, 90, 116, 12, 74, ; the existence of a second disk is still debated]. The two disks are strongly inclined relative to each other. In projection on the plane of the sky, the inner disk appears to rotate clock-wise, and the outer disk counter-clockwise. The inner extent of the disk population is ~ 0.04 pc.

Inside ~ 0.04 pc the population changes again. There are no bright giants, red or blue, and only faint blue stars are observed there. This population is known as the “S-stars” or “S-cluster”, after their identifying labels. Deep near-IR photometric [66, 43] and spectroscopic [40, 27, 32, 45, 48] observations of that region were all consistent with the identification of these stars as massive MS stars. It is now spectroscopically confirmed [48, 29, 78] that the S-stars are B0–B9 MS stars (corresponding to masses in the range $\sim 3 M_\odot - \sim 15 M_\odot$). The rotational velocities (stellar spin) are similar to those of Solar neighborhood stars of the same spectral type. Thus, there is no indication of anything unusual about the S-stars, apart for their location very near the MBH. Astrometric observations [108, 29, 49, 50] indicate that, unlike the emission line stars farther out, the S-stars orbits appear random (isotropic) and uncorrelated with the orientation of either disk. There are some marginal statistical indications of a bias toward radial

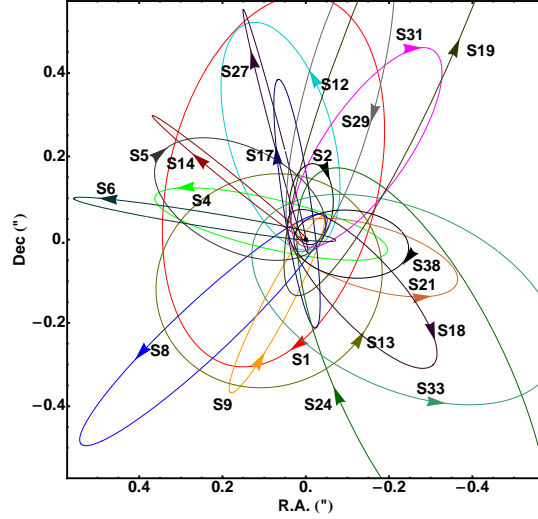


Figure 1.3: a Orbits of S-stars in the Galactic center, as measured by Gillessen et al. [50].

orbits, i.e. bias towards higher eccentricities than expected for a thermal distribution of eccentricities ([12, 50]; see Figure 1.3). As we show in chapters 7, the origin and dynamical evolution of these stars is closely related to the few body interactions between the stars and with the MBH (chapters 2, 7).

The brightest star in the S-cluster, S2/S0-2 ($K = 13.9$ mag), is a transitional O8–B0 star with a mass of $\sim 15 M_{\odot}$ [78], effective temperature of $\sim 30,000$ K, intrinsic bolometric luminosity of $L \sim 10^3 L_{\odot}$ and a main sequence lifespan of $\sim 10^7$ yr. All the other stars in the cluster are less massive, longer-lived, cooler and fainter. A B9 MS star has a mass of $\sim 3 M_{\odot}$, a radius of $\sim 2.1 R_{\odot}$ and a main sequence lifespan of $\sim 4 \times 10^8$ yr. A typical star would correspond to a B2 main sequence star, with a mass of $\sim 10 M_{\odot}$, a radius of $\sim 4.5 R_{\odot}$ and main sequence lifespan of $\sim 2 \times 10^7$ yr ([26, 107]). It is not clear what is the relation, if any, between the population of the He stars on the 0.04–0.4 pc scale and the S-cluster stars inside 0.04 pc (see discussion in chapter 7).

1.5 Hypervelocity stars

Hypervelocity stars (HVSs) are stars with extremely high peculiar velocities relative to the velocity distribution of their parent population. In recent years several HVSs have been observed in the Galactic halo, some of them unbound to the Galaxy (with velocities beyond the escape velocity; [23]). From these a Galactic population of 96 ± 10 such HVSs was inferred [23], up to the 100 kpc distance limit of the survey. Many similar bound HVSs (with velocities lower than the escape velocity) have been observed. Most of the observed HVSs are B-type stars ([20, 19, 21, 22, 23, 28]; future observations of HVSs of other stellar types are discussed in [64, 18, 63]). Given the color selection

of the targeted survey for these stars [19], such stars could be either main sequence (MS; or blue straggler) B stars or hot blue horizontal branch (BHB) stars. Currently only three of the stars in the survey have unambiguous spectral identification and were found to be MS stars [37, 73, 104]. HVSs might also be detected in the future in M31 [111].

Extreme velocities as found for these stars suggest a dynamical origin from an interaction with the massive black hole (MBH) in the GC. Several scenarios have been suggested for ejection of HVSs; a disruption of a stellar binary by the MBH in the GC [55, 123, 96], an interaction of a single star with an intermediate mass black hole (IMBH) which inspirals to the GC [53, 123, 67], or interaction with stellar black holes (SBHs) in the GC [123, 84, 88]. The later two scenarios scatter HVSs mostly from regions very close to the MBH (< 0.01 pc) where as the binary disruption scenario mostly eject HVSs that evolved in binaries much further from the MBH ($\gtrsim 2$ pc). The IMBH inspiral scenario is a discrete event, which does not occur continuously (although a sequence of several IMBH inspirals may eject HVSs semi-continuously; [72]) where the binary disruption or SBHs kicks are continuous processes leading to a constant rate of HVSs ejection.

Chapters 4-6 discuss in length and explore various issues concerning the origin and characteristics of HVSs, and their observational constraints, as well as suggest a novel use of HVSs as probes of the Galactic dark mass component and the Galactic potential.

Brief description of work presented in this thesis

In this Thesis the dynamics of stars near massive black holes and their outcomes are studied in detail, and the results are applied to a number of astrophysical applications. The Thesis is based on several published papers, and contains the following work, described here briefly. The full papers appear in chapters 2-9 of this thesis.

In *Massive Massive perturber-driven interactions between stars and a massive black hole* we explored the role of MPs in deflecting stars and binaries to almost radial (“loss-cone”) orbits, where they pass near the central MBH, interact with it at periape, and are ultimately destroyed. We compiled the MP mass function from published observations, and showed that MPs in the nucleus of the Galaxy (mainly giant molecular clouds), shorten the relaxation timescale by 10^{2-7} relative to 2-body relaxation by stars alone in these regions. We showed that this increases by 10^{1-3} the rate of *large*-periape interactions with the MBH, where loss-cone refilling by stellar 2-body relaxation is inefficient. We extended the Fokker-Planck loss-cone formalism to approximately account for relaxation by rare encounters with MPs. We showed that binary stars–MBH exchanges driven by MPs can explain the origin of the young main sequence B stars that are observed very near the Galactic MBH, and increase by orders of magnitude the ejection rate of hyper-velocity stars.

In *Massive perturbers and the efficient coalescence of binary massive black holes* we showed that dynamical relaxation in the aftermath of a galactic merger, and the ensuing formation of a binary massive black hole (BMBH), are dominated by MPs. MPs accelerate relaxation by orders of magnitude relative to 2-body stellar relaxation alone, and efficiently scatter stars into the binary MBH’s orbit. The 3-body star–binary

MBH interactions shrink the binary MBH to the point where energy loss from the emission of GWs leads to rapid coalescence, much shorter than a Hubble time and the estimated inspiral times found in previous theoretical estimates, which did not take these MPs into account.

In *Dynamical and evolutionary constraints on the nature and origin of hypervelocity stars* we use observations of the Galactic center stellar population and dynamical and evolutionary arguments to constrain the nature and origin of HVSs. We show that the IMBH inspiral scenario requires too many main sequence B stars to exist close to the MBH at the time of inspiral. Scattering by SBHs also require too many B stars to be observed in the GC, but it may contribute a small fraction of the currently observed HVSs. The binary disruption scenario is still consistent with current observations. In addition we show that due to the conditions close to the MBH most binary star systems are not expected to survive for long in this region. Consequently, unique stellar populations that require long evolution in binaries are not expected to be ejected as HVSs in the BHs scattering mechanisms.

In *Runaway and hypervelocity stars in the Galactic halo: Binary rejuvenation and triple disruption* we study the possibilities of ejecting binary runaway and hypervelocity stars and show that such binaries could have been ejected in triple disruptions and other dynamical interactions with stars or with MBHs. We show that currently observed “too young” stars in the halo could have been ejected from the Galactic disk or the Galactic center and be observable in their current position if they were ejected as binaries, and were then rejuvenated through merger of or mass accretion between the binary components. In addition, we suggest that triple disruptions by the MBH in the Galactic center could also capture binaries in close orbits near the MBH, some of which may later evolve to become more massive rejuvenated stars.

In *The Galactic potential and the asymmetric distribution of hypervelocity stars* we proposed a novel method to probe and constrain the Galactic potential, using the asymmetric radial velocity distribution of hypervelocity stars, to identify the stellar type of the stars in the HVSs survey and to estimate the number of HVSs in the Galaxy.

In *Dynamical evolution of the young stars in the Galactic center: N-body simulations of the S-stars* we use *N*-body simulations to study the evolution of the orbital eccentricities of the S-stars and constrain their origin. We chose initial conditions motivated by two competing models for their origin: formation in a disk followed by inward migration; and exchange interactions involving a binary star. We find that the latter model could produce the currently observed orbital properties of the S-stars, where as the disk migration scenario produces orbits which are much less eccentric than observed, and is therefore unlikely to produce the S-stars.

Chapter 2

Massive perturber-driven interactions between stars and a massive black hole

Perets, Hopman, & Alexander

The Astrophysical Journal, Volume 656, Issue 2, pp. 709-720 (2007)

MASSIVE PERTURBER–DRIVEN INTERACTIONS BETWEEN STARS AND A MASSIVE BLACK HOLE

HAGAI B. PERETS,¹ CLOVIS HOPMAN,¹ AND TAL ALEXANDER²

Faculty of Physics, Weizmann Institute of Science, Rehovot, Israel; hagai.perets@weizmann.ac.il,
 clovis.hopman@weizmann.ac.il, tal.alexander@weizmann.ac.il

Received 2006 June 19; accepted 2006 October 13

ABSTRACT

We study the role of massive perturbers (MPs) in deflecting stars and binaries to almost radial (“loss cone”) orbits, where they pass near the central massive black hole (MBH), interact with it at periaapse, and are ultimately destroyed. MPs dominate dynamical relaxation when the ratio of the second moments of the MP and star mass distributions, $\mu_2 \equiv N_p \langle M_p^2 \rangle / N_* \langle M_*^2 \rangle$, satisfies $\mu_2 \gg 1$. We compile the MP mass function from published observations and show that MPs in the nucleus of the Galaxy (mainly giant molecular clouds), and plausibly in late-type galaxies generally, have $10^2 \lesssim \mu_2 \lesssim 10^8$. MPs thus shorten the relaxation timescale by 10^1 – 10^7 relative to two-body relaxation by stars alone. We show that this increases by 10^1 – 10^3 the rate of *large*-periaapse interactions with the MBH, where loss cone refilling by stellar two-body relaxation is inefficient. We extend the Fokker-Planck loss cone formalism to approximately account for relaxation by rare encounters with MPs. We show that binary star–MBH exchanges driven by MPs can explain the origin of the young main-sequence B stars that are observed very near the Galactic MBH and can increase by orders of magnitude the ejection rate of hypervelocity stars. In contrast, the rate of *small*-periaapse interactions of single stars with the MBH, such as tidal disruption, is only increased by a factor of a few. We suggest that MP-driven relaxation plays an important role in the three-body exchange capture of stars on very tight orbits around the MBH. These captured stars may later be disrupted by the MBH via tidal orbital decay or direct scattering into the loss cone; captured compact objects may inspiral into the MBH by the emission of gravitational waves from zero-eccentricity orbits.

Subject headings: black hole physics — galaxies: nuclei — ISM: clouds —
 open clusters and associations: general — stars: kinematics

Online material: color figures

1. INTRODUCTION

There is compelling evidence that massive black holes (MBHs) lie in the centers of all galaxies (Ferrarese & Merritt 2000; Gebhardt et al. 2003; Shields et al. 2003), including the center of our Galaxy (Eisenhauer et al. 2005; Ghez et al. 2005). The MBH affects the dynamics and evolution of the galaxy’s center as a whole (e.g., Bahcall & Wolf 1976), and it also strongly affects individual stars or binaries that approach it. Such close encounters, which may be extremely energetic or involve non-gravitational interactions or post-Newtonian effects, have been the focus of many studies (see review by Alexander 2005). These processes include the destruction of stars by the MBH, either by falling whole through the event horizon, or by being first tidally disrupted and then accreted (e.g., Rees 1988); tidal scattering of stars on the MBH (Alexander & Livio 2001); the capture and gradual inspiral of stars into the MBH, accompanied by the emission of gravitational waves or by tidal heating (e.g., Alexander & Hopman 2003; Alexander & Morris 2003); or dynamical exchange interactions in which incoming stars or binaries energetically eject a star tightly bound to the MBH and are captured in its place very near the MBH (e.g., Alexander & Livio 2004; Gould & Quillen 2003).

The interest in such processes is driven by their possible implications for the growth of MBHs, for the orbital decay of a MBH binary, for the detection of MBHs, for gravitational wave (GW) astronomy, as well as by observations of unusual stellar phenomena in our Galaxy; for example, the puzzling young pop-

ulation of B stars very near the Galactic MBH (Eisenhauer et al. 2005), or the hypervelocity B stars at the edge of the Galaxy (Brown et al. 2005; Fuentes et al. 2006; Brown et al. 2006a), possibly ejected by three-body interactions of a binaries with the MBH (Hills 1991).

Here we focus on close encounters with the MBH whose ultimate outcome (“event”) is the elimination of the incoming object from the system, whether on the short infall (dynamical) time, if the event is prompt (e.g., tidal disruption or three-body exchange between a binary and the MBH), or on the longer inspiral time, if the event progresses via orbital decay (e.g., GW emission or tidal capture and heating). Such processes are effective only when the incoming object follows an almost zero angular momentum (“loss cone”) orbit with periaapse closer to the MBH than some small distance q . To reach the MBH, or to decay to a short-period orbit, both the infall and inspiral times must be much shorter than the system’s relaxation time t_r (Alexander & Hopman 2003). The fraction of stars initially on loss cone orbits is very small, and they are rapidly eliminated. Subsequently, the close encounter event rate is set by the dynamical processes that refill the loss cone.

The loss cone formalism used for estimating the event rate (Frank & Rees 1976; Lightman & Shapiro 1977; Cohn & Kulsrud 1978) usually assumes that the system is isolated and that the refilling process is two-body relaxation. This typically leads to a low event rate, set by the long two-body relaxation time.

Two-body relaxation, which is inherent to stellar systems, ensures a minimal loss cone refilling rate. Other more efficient but less general refilling mechanisms were also studied with the aim of explaining various open questions (e.g., the stalling problem of MBH binary coalescence: Berczik et al. 2005; Merritt & Wang

¹ Also at Leiden University, Leiden Observatory, Leiden, Netherlands.

² William Z. and Eda Bess Novick Career Development Chair.

2005; Berczik et al. 2006; or MBH feeding: Zhao et al. 2002; Miralda-Escudé & Kollmeier 2005) or in the hope that they may lead to significantly higher event rates for close encounter processes. These mechanisms include chaotic orbits in triaxial potentials (Norman & Silk 1983; Gerhard & Binney 1985; Merritt & Poon 2004; Holley-Bockelmann & Sigurdsson 2006) (the presence of a MBH may, however, destroy the triaxiality near the center; Merritt & Quinlan 1998; Holley-Bockelmann et al. 2002; Sellwood 2002); increased fraction of low angular momentum orbits in nonspherical potentials (Magorrian & Tremaine 1999; Berczik et al. 2006); accelerated resonant relaxation of angular momentum near the MBH where the orbits are Keplerian (Rauch & Tremaine 1996; Rauch & Ingalls 1998; Hopman & Alexander 2006a; Levin 2007); and perturbations by a massive accretion disk or an intermediate-mass black hole (IMBH) companion (Polnarev & Rees 1994; Zhao et al. 2002; Levin et al. 2005). Most of these mechanisms require special circumstances to work (e.g., specific asymmetries in the potential) or are short-lived (e.g., the IMBH will eventually coalesce with the MBH).

Here we explore another possibility that is more likely to apply generally: accelerated relaxation and enhanced rates of close encounters driven by massive perturbers (MPs). Efficient relaxation by MPs was first suggested by Spitzer & Schwarzschild (1951, 1953) to explain stellar velocities in the Galactic disk. MPs remain an important component in modern models of galactic disk heating (see, e.g., Villumsen 1983, 1985; Lacey 1984; Jenkins & Binney 1990; Hänninen & Flynn 2002 and references therein). A similar mechanism was suggested to explain the spatial diffusion of stars in the inner Galactic bulge (Kim & Morris 2001). In addition to dynamical heating, efficient relaxation by MPs was suggested as a mechanism for loss cone replenishment and relaxation, both in the context of scattering of Oort cloud comets to the Sun (Hills 1981; Bailey 1983) and the scattering of stars to a MBH in a galactic nucleus (Zhao et al. 2002). Zhao et al. (2002) suggested MPs as a mechanism for establishing the M_\bullet - σ relation (Ferrarese & Merritt 2000; Gebhardt et al. 2000) by fast accretion of stars and dark matter. They also noted the possibility of increased tidal disruption flares and accelerated MBH binary coalescence due to MPs. In this study we investigate in detail the dynamical implications of loss cone refilling by MPs. We evaluate its effects on the different modes of close interactions with the MBH, in particular three-body exchanges, which were not considered by Zhao et al. (2002), and apply our results to the Galactic center (GC), where observations indicate that dynamical relaxation is very likely dominated by MPs.

This paper is organized as follows. In § 2 we present the main concepts and procedures of our calculations. The observational data and theoretical predictions about MPs in the inner ~ 100 pc of the GC are reviewed in § 3. In § 4 we explore the implications of relaxation by MPs for various types of interactions with the MBH. We summarize our results in § 5.

2. LOSS CONE REFILLING

In addition to stars, galaxies contain persistent dense structures³ such as molecular clouds, open clusters, and globular clusters with masses up to 10^4 – $10^7 M_\odot$. Such structures can perturb stellar orbits around the MBH much faster than two-body stellar relaxation (hereafter “stellar relaxation”), provided that they are numerous enough. This condition can be quantified by considering a test star randomly scattered by perturbers with masses in the interval $(M_p, M_p + dM_p)$ and number density $(dN_p/dM_p)dM_p$,

approaching it with relative velocity v on orbits with impact parameters in the interval $(b, b + db)$. The minimal impact parameter still consistent with a small-angle deflection is $b_{\min} = 2GM_p/v^2$ (the capture radius), where v is on the order of the local velocity dispersion σ . Defining $B \equiv b/b_{\min} \geq 1$, the encounter rate is then

$$\begin{aligned} \frac{d^2\Gamma}{dM_p db} dM_p db &\sim \frac{dN_p}{dM_p} dM_p v b_{\min}^2 2\pi B dB \\ &= \frac{G^2}{v^3} \frac{dN_p}{dM_p} M_p^2 dM_p 2\pi B dB. \end{aligned} \quad (1)$$

The total rate is obtained by integrating over all MP masses and over all impact parameters between b_{\min} and b_{\max} . Here we are interested in perturbations in the specific angular momentum J of a star relative to the central MBH, and so $b_{\max} \sim r$, the radial distance of the star from the center. MPs with substantially larger impact parameters are much less efficient because their effect on the MBH-star pair is tidal rather than direct.

The relaxation rate due to all MPs at all impact parameters is then

$$\begin{aligned} t_r^{-1} &= \int_{b_{\min}}^{b_{\max}} db \int dM_p \frac{d^2\Gamma}{dM_p db} \left(\frac{\delta v}{v}\right)^2 \\ &\sim \log \Lambda \frac{G^2}{v^3} \int dM_p \frac{dN_p}{dM_p} M_p^2, \end{aligned} \quad (2)$$

where $(\delta v/v)^2 \propto 1/B$ is the weighted deflection and $\log \Lambda = \log(b_{\max}/b_{\min})$ is the Coulomb logarithm (here the dependence of $\log \Lambda$ and v on M_p is assumed to be negligible). For stars, typically $\log \Lambda \gtrsim 10$; the omission of large-angle scattering by encounters with $b < b_{\min}$ is thus justified because it introduces only a relatively small logarithmic correction. This formulation of the relaxation time is equivalent to its conventional definition (Spitzer 1987) as the time for a change of order unity in v^2 by diffusion in phase space due to scattering, $t_r \sim v^2/D(v^2)$, where $D(v^2)$ is the diffusion coefficient.

If the stars and MPs have distinct mass scales with typical number densities N_\star and N_p and rms masses $\langle M_\star^2 \rangle^{1/2}$ and $\langle M_p^2 \rangle^{1/2}$ [where $\langle M^2 \rangle \equiv \int M^2 (dN/dM) dM/N$], then MPs dominate if the ratio of the second moments of the MP and star mass distributions, $\mu_2 \equiv N_p \langle M_p^2 \rangle / N_\star \langle M_\star^2 \rangle$, satisfies $\mu_2 \gg 1$ (note that for a continuous mass spectrum, this condition is equivalent to $-d \log N/d \log M < 2$).

As discussed in detail in § 3, the central ~ 100 pc of the Galactic center contain 10^8 – $10^9 M_\odot$ in stars and about 10^6 – $10^8 M_\odot$ in MPs such as giant molecular clouds or open clusters of masses 10^3 – $10^8 M_\odot$ (Oka et al. 2001; Figer et al. 2002, 2004; Vollmer et al. 2003; Güsten & Philipp 2004; Borissova et al. 2005). An order-of-magnitude estimate indicates that MPs in the GC can reduce the relaxation time by several orders of magnitude:

$$\begin{aligned} \frac{t_{r,\star}}{t_{r,\text{MP}}} &= \mu_2 \sim \frac{(N_p M_p) M_p}{(N_\star M_\star) M_\star} \\ &= 10^4 \left(\frac{N_\star M_\star / N_p M_p}{10} \right)^{-1} \frac{M_p / M_\star}{10^5}. \end{aligned} \quad (3)$$

Note that μ_2 does not include possible modifications in the value of $\log \Lambda$ for MPs due to their much larger size, which may decrease this ratio by $O(10)$. This estimate is borne out by more detailed calculations (Fig. 1 and Tables 1 and 2), using the formal definition $t_r = v^2/D(v_\parallel^2)$ with $M_\star \rho_\star \rightarrow \int (dN_p/dM_p) M_p^2 dM_p$

³ Structures that persist at least as long as the local galactic dynamical time and are substantially denser than the ambient stellar mass distribution.

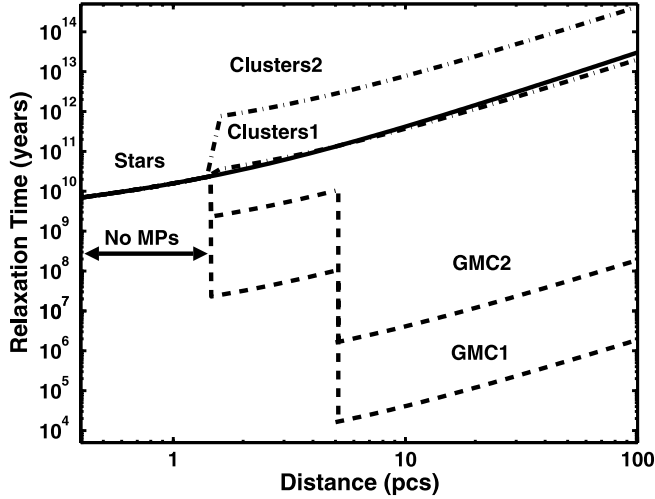


FIG. 1.—Relaxation time as a function of distance from the MBH, for stars (solid line) and for each of the four MP models separately, as listed in Table 2: clusters (dash-dotted lines) and GMCs (dashed lines). The discontinuities are artifacts of the assumed sharp spatial cutoffs on the MP distributions. Two-body stellar processes dominate close to the MBH, where no MPs are observed to exist. However, at larger distances massive clumps (at $1.5 \text{ pc} < r < 5 \text{ pc}$) and GMCs (at $5 \text{ pc} < r < 100 \text{ pc}$) are much more important. [See the electronic edition of the *Journal* for a color version of this figure.]

(e.g., Binney & Tremaine 1987, their eqs. [8-69]–[8-70]). A similar result is indicated by simulations of spatial diffusion of stars in the central 100 pc (Kim & Morris 2001).

2.1. Noncoherent Loss Cone Refilling

The Fokker-Planck approach to the loss cone problem (e.g., Cohn & Kulsrud 1978) assumes that the effects of multiple small perturbations on the orbit of a test star dominate over the rarer strong close encounters ($b_{\text{max}}/b_{\text{min}} \gg 1$) and that the cumulative effect can be described as diffusion in phase space. The change in the angular momentum of the test star then grows non-coherently, $\Delta J \propto \sqrt{t}$. The change over one orbital period P is $J_D = J_c(E)(P/t_r)^{1/2}$, where $J_c = [2(\psi - E)]^{1/2}r$ is the maximal (circular) angular momentum for a stellar orbit of specific relative energy $E = -v^2/2 + \psi(r)$ and $\psi \equiv -\phi$ is the negative of the gravitational potential, so that $E > 0$ for bound orbits. The magnitude of J_D relative to the J magnitude of the loss cone,

$$J_{lc} \simeq \sqrt{2GM_\bullet q}, \quad (4)$$

where q is the periaapse distance to the MBH, determines the mode of loss cone refilling. The relative volume of phase space occupied by the loss cone, $J_{lc}^2/J_c^2(E)$, increases with E (decreases with r), while P decreases. Near the MBH (high E), $J_D \ll J_{lc}$, stars diffuse slowly into the loss cone and are promptly destroyed over an orbital

period, leaving the loss cone always nearly empty. In this empty loss cone regime, the loss cone is relatively large, but the refilling rate is set by the long relaxation timescale (e.g., Lightman & Shapiro 1977):

$$\left(\frac{d\Gamma}{dE}\right)_{\text{empty}} \simeq \frac{N_\star(E)}{\log(J_c/J_{lc})t_r} = \frac{J_D^2(E)}{J_c^2(E)} \frac{1}{\log[J_c(E)/J_{lc}]} \frac{N_\star(E)}{P(E)}, \quad (5)$$

where $N_\star(E)$ is the stellar number density per energy interval.

Far from the MBH (low E), $J_D \gg J_{lc}$, stars diffuse into the loss cone many times over one orbit, and the loss cone is always nearly full. In this full loss cone regime, the refilling rate is set by the short orbital time, but the loss cone is relatively small:

$$\left(\frac{d\Gamma}{dE}\right)_{\text{full}} \simeq \frac{J_{lc}^2}{J_c^2(E)} \frac{N_\star(E)}{P(E)}. \quad (6)$$

Note that here and elsewhere we make the simplifying approximation that the period is a function of energy only, which is true only for motion in a Keplerian potential.

The total contribution to loss cone refilling is dominated by stars with energies near the critical energy E_c (equivalently, the critical typical radius r_c), separating the two regimes (Lightman & Shapiro 1977; see § 4). Within r_c ($E > E_c$), an object, once deflected into the loss cone, can avoid being scattered out of it before reaching the MBH.⁴ The empty and full loss cone regimes of infall processes can be interpolated to give a general approximate expression for the differential event rate for these noncoherent encounters (e.g., Young 1977):

$$\frac{d\Gamma}{dE} \simeq \frac{j^2(E)}{J_c^2(E)} \frac{N_\star(E)}{P(E)}, \quad (7)$$

$$j^2(E) \equiv \min\left\{\frac{J_D^2(E)}{\log[J_c(E)/J_{lc}]}, J_{lc}^2\right\}, \quad (8)$$

where j is the loss cone–limited angular momentum change per orbit, which expresses the fact that the loss cone can at most be completely filled during one orbit.

⁴ In the case of inspiral, E_c is determined by the condition $J_D = J_{lc}$ over the inspiral time (Hopman & Alexander 2005), rather than the much shorter orbital period, which results in a much smaller r_c than for direct infall. Inspiring stars with $E > E_c$ can avoid being scattered directly into the MBH before completing the orbital decay. There is no contribution to inspiral events from regions outside r_c ($E < E_c$), since the probability of an object to remain on its low- J trajectory over the many orbital periods required to complete the inspiral, is vanishingly small.

TABLE 1
NUMBER OF OBSERVED MASSIVE PERTURBERS IN THE GALACTIC CENTER

MP Type	r^a (pc)	N_p	M_p (M_\odot)	$\langle M_p^2 \rangle^{1/2}$ (M_\odot)	R_p (pc)	References
Observed GMCs	<100	~ 100	10^4 – 10^8	3×10^6 – 3×10^7	5	1, 2
Observed clusters	<100	~ 10	10^2 – 10^5	4.8×10^3 – 2.4×10^4	1	3, 4, 5, 6, 7
Observed clumps	1.5–3	~ 25	10^2 – 10^5	3.7×10^3 – 4.1×10^4	0.25	8, 9

^a Projected distance range enclosing observed MPs.

REFERENCES.—(1) Oka et al. 2001; (2) Güsten & Philipp 2004; (3) Figer et al. 1999; (4) Figer et al. 2002; (5) Figer 2004; (6) Maillard et al. 2004; (7) Borissova et al. 2005; (8) Genzel et al. 1985; (9) Christopher et al. 2005.

TABLE 2
MASSIVE PERTURBER MODELS

Model	r^a (pc)	N_p^b	M_p (M_\odot)	β	(μ_M, σ_M)	R_p (pc)	$\mu_2^{\text{obs}c}$
GMC1	5–100	100	$10^5\text{--}5 \times 10^7$	1.2	...	5	2×10^8
	1.5–5	30	$3 \times 10^3\text{--}10^5$	[1.1] ^d	(10.04, 0.65)	...	5500
GMC2	5–100	100	$10^4\text{--}5 \times 10^6$	1.2	...	5	2×10^6
	1.5–5	30	$7 \times 10^2\text{--}10^4$	1.7	44
Clusters1	1.5–100	10	$5 \times 10^2\text{--}7 \times 10^4$	1.3	...	1	27
Clusters2	1.5–100	10	$3 \times 10^2\text{--}10^4$	[1.9] ^d	(8.16, 1.1)	1	1
Stars	5–100	2×10^8	1	~ 0	1
	1.5–5	8×10^6	1	~ 0	1

^a Distance range enclosing observed MPs.

^b We assume that $N_p(r) \propto r^{-2}$ in the given range.

^c The quantity $\mu_2^{\text{obs}} = \sum_i M_{p,i}^2 / N_* M_*^2$, where $M_{p,i}$ is the observed MP's mass.

^d Best power-law fit, not used for modeling.

2.2. Coherent Loss Cone Refilling

The loss cone formalism can be generalized to deal with MPs in an approximate manner with only a few modifications. The capture radius for MPs may be smaller than their size. Since the MP mass profile is centrally concentrated, we adopt the modified definition

$$b_{\min} = \max(0.1R_p, 2GM_p/v^2), \quad (9)$$

where $v^2 = GM(<r)/r$. This results in $\log \Lambda \sim 6$ for MPs, less than the typical value for relaxation by stars. Nevertheless, the error introduced by neglecting encounters with $b < b_{\min}$ is still not very large because penetrating encounters are much less efficient. However, the assumption of multiple noncoherent encounters with MPs over one orbital period of the test star is not necessarily justified because of their small number density.

To address this, we modify the treatment of the empty loss cone regime (the contribution to the event rate from regions where the loss cone is already filled by stellar relaxation cannot be increased by MPs; see § 4). We define rare encounters as those with impact parameters $b \leq b_1$, where b_1 is defined by

$$P \int_{b_{\min}}^{b_1} db (d\Gamma/db) = 1. \quad (10)$$

The differential rate is estimated simply by $d\Gamma/db = N_p v 2\pi b$. When $P \int_{b_1}^{b_{\max}} db (d\Gamma/db) > 1$, with $b_{\max} = r$, all encounters with $b > b_1$ are defined as frequent encounters that occur more than once per orbit and add noncoherently.⁵ Note that even when $P \int_{b_1}^{b_{\max}} db (d\Gamma/db) > 1$ for all MPs, perturbations by rare, very massive MPs may still occur less than once per orbit. Our treatment is approximate. A complete statistical treatment of this situation lies beyond the scope of this study.

When the typical number of encounters per orbit is less than 1, the fractional contributions from different individual encounters, δJ , should be averaged coherently ($\Delta J \propto t$), subject to the limit that each encounter can at most fill the loss cone. The loss cone–limited change in angular momentum per orbit due to rare encounters is therefore

$$j_R^2(E) = \left[P \int_{b_{\min}}^{b_1} db \frac{d\Gamma}{db} \min(\delta J, J_{lc}) \right]^2. \quad (11)$$

⁵ In the marginal cases of $P \int_{b_{\min}}^{b_{\max}} db (d\Gamma/db) < 1$ or $P \int_{b_1}^{b_{\max}} db (d\Gamma/db) < 1$, all encounters are considered rare.

In contrast, frequent uncorrelated collisions add up noncoherently ($\Delta J \propto \sqrt{t}$), and it is only their final value that is limited by the loss cone (individual steps δJ may exceed J_{lc} , but they can then be partially canceled by opposite steps during the same orbit). The loss cone–limited change in angular momentum per orbit due to frequent encounters is therefore

$$j_F^2(E) = \min \left[\frac{1}{\log(J_c/J_{lc})} P \int_{b_1}^{b_{\max}} db \frac{d\Gamma}{db} \delta J^2, J_{lc}^2 \right]. \quad (12)$$

The total loss cone–limited angular momentum change per orbit is then approximated by

$$j^2 = \min(j_R^2 + j_F^2, J_{lc}^2), \quad (13)$$

and the differential event rate is calculated by equation (7).

The contribution of rare encounters is evaluated in the impulse approximation by setting $\delta J \sim GM_p r / bv$ in equation (11). We find that the contribution by GC MPs (§ 3) is generally small. Frequent encounters are the regime usually assumed in the Fokker-Planck treatment of the loss cone problem (e.g., Lightman & Shapiro 1977). To evaluate the contribution of frequent encounters, we do not calculate δJ directly, but instead calculate the subexpression $I = P \int_{b_1}^{b_{\max}} db (d\Gamma/db) \delta J^2$ in equation (12) in terms of the b -averaged diffusion coefficient $D(v_t^2)$, after averaging over the orbit between the periape r_p and apoaape r_a and averaging over the perturber mass function (this is essentially equivalent to the definition of J_D in terms of t_r ; § 2.1),

$$I = \int dM_p \left[2 \int_{r_p}^{r_a} \frac{r^2 D(\Delta v_t^2)}{v_r} dr \right] \\ \simeq \int dM_p \left[2 \int_0^{2r} \frac{r^2 D(\Delta v_\perp^2)}{v} dr \right]. \quad (14)$$

The assumptions involved in the last approximate term (Magorrian & Tremaine 1999) are that the star is on a nearly radial orbit ($v_r \rightarrow v$, $r_p \rightarrow 0$, $r_a \rightarrow 2r$) and that $D(v_t^2)$ (the diffusion coefficient of the transverse velocity relative to the MBH) can be approximated by $D(\Delta v_\perp^2)$ (the diffusion coefficient of the transverse velocity relative to the stellar velocity \mathbf{v}), given explicitly by (Binney & Tremaine 1987, their eq. [8-68])

$$D(\Delta v_\perp^2) = \frac{8\pi G^2 (dN_p/dM_p) M_p^2 \ln \Lambda}{v} K \left(\frac{v}{\sqrt{2}\sigma} \right), \quad (15)$$

where $K(x) \equiv \text{erf}(x)(1 - 1/2x^2) + \exp(-x^2)/\sqrt{\pi}x$ and where a spatially homogeneous distribution of MPs with a Maxwellian velocity distribution of rms one-dimensional velocity σ was assumed.

To summarize, the event rates are calculated as follows. For each perturber model (Table 2), we integrate over the stellar distribution [$N_* = 1.2 \times 10^6 (r/0.4 \text{ pc})^{-2}$, for $r > 0.4 \text{ pc}$ and $M_* = 1 M_\odot$] in terms of r , using N_* to derive the appropriate density of perturbed objects (single stars, § 4.1; binaries, § 4.2). At each r , we calculate b_{\min} (eq. [9]), b_1 (eq. [10]), j_R (eq. [11]), and j_F (eq. [12]). The integral I (eq. [14]) is evaluated by taking $v^2 \rightarrow GM(<r)/r$ and correcting approximately for the difference relative to the exact calculation. We use j (eq. [13]) to calculate the differential event rate $d\Gamma/dr$ (eq. [7]), with the *Ansatz* that $E \rightarrow GM(<r)/2a$, where $a \equiv (4/5)r$ is an effective semi-major axis, which is motivated by the fact that for a Keplerian isothermal eccentricity distribution, $\langle r \rangle = a(1 + \langle e^2 \rangle/2) = (5/4)a$. The total event rate is calculated by carrying the integration over r in the region where MPs exist, between r_{MP} and r_{out} (§ 3).

3. MASSIVE PERTURBERS IN THE GALACTIC CENTER

MPs can dominate relaxation only when they are massive enough to compensate for their small space densities. Here we consider only MPs with masses $M_p \geq 10^2 M_\odot$. Such MPs could be molecular clouds of different masses, in particular giant molecular clouds (GMCs), open or globular stellar clusters, and perhaps also IMBHs. As discussed below, observations of the Galaxy reveal enough MPs to dominate relaxation in the central 100 pc. We adopt here a conservative approach and include in our modeling only those MPs that are directly observed in the Galaxy, namely, GMCs and young clusters. We briefly discuss theoretical predictions for two other classes of MPs, dynamically evolved “submerged” clusters and IMBHs, that could well be common in galactic centers and contribute to efficient relaxation.

The dynamically dominant MPs are GMCs. Emission-line surveys of the central $\sim 100 \text{ pc}$ reveal ~ 100 GMCs with estimated masses in the range $10^4 - 5 \times 10^7 M_\odot$ and sizes of $R_p \sim$ a few pc (Miyazaki & Tsuboi 2000; Oka et al. 2001; Güsten & Philipp 2004). We selected for analysis individual, reliably identified GMCs in the central 0.7° of the Galaxy ($\sim 100 \text{ pc}$ of the GC) from the sample observed by Oka et al. (2001). Figure 2 shows the empirical GMC mass function using the Oka et al. (2001) virial mass estimates as an upper mass limit and adopting a lower limit 10 times smaller, following Miyazaki & Tsuboi (2000), who found that LTE mass estimates are typically an order of magnitude lower than the virial ones. Note that the more recent GMC CO(1–0) molecular line observations by Oka et al. (2001), which we use here, indicate a more massive and flatter mass function than that derived for their earlier CS(1–0) molecular line observations (Miyazaki & Tsuboi 2000). This is probably due to the higher sensitivity of the CO(1–0) line to lower density molecular gas (M. Tsuboi 2006, private communication).

Inside the inner 5 pc of the GC (a volume smaller or comparable to that of a GMC or a stellar cluster), the most massive local structures are the molecular gas clumps observed in the circumnuclear gaseous disk and its associated spiral-like structures (Genzel et al. 1985; Christopher et al. 2005). Their sizes are $\sim 0.25 \text{ pc}$ and their masses are estimated to be in the range $10^3 - 10^5 M_\odot$, where the lower estimates are based on the assumption of optically thin HCN(1–0) line emission and the upper estimates are based on the optically thick assumption, which also coincides with the virial estimates.

It is possible to obtain a model-independent estimate of the effect of the *observed* MPs on the relaxation time by directly

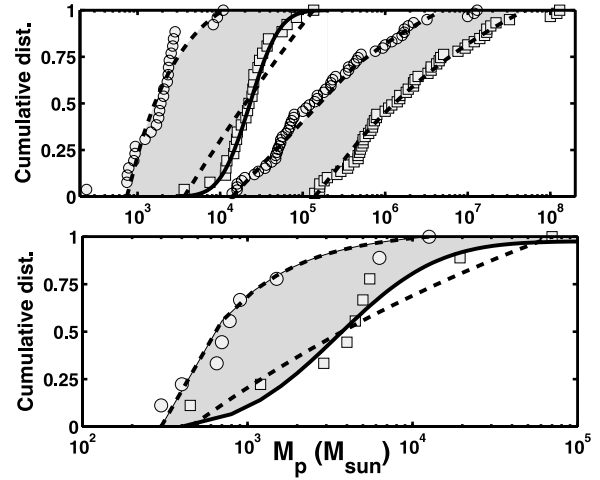


FIG. 2.—Cumulative mass functions of observed MPs in the GC (symbols) with best-fit power-law distributions (dashed lines), $dN/dM \propto M^{-\beta}$, or lognormal distributions (solid lines), $dN/dM \propto \text{LN}(\mu_M, \sigma_M)$ (see text). *Top*: Lower (circles) and upper (squares) estimates for the masses of observed molecular clumps (Christopher et al. 2005; left) and GMCs (Oka et al. 2001; right) in the GC. The best-fit power-law indices for the GMCs are $\beta_{\text{up}} = \beta_{\text{low}} = 1.2$, and for the clumps, $\beta_{\text{up}} = 1.1$ and $\beta_{\text{low}} = 1.7$. The upper estimates of the clump masses are better fitted by a LN distribution with $\mu_M = 8.2$ and $\sigma_M = 0.65$. *Bottom*: Same as above, but for GC clusters (Figer et al. 1999; Figer 2004; Borissova et al. 2005), with $\beta_{\text{up}} = 1.3$ and $\beta_{\text{low}} = 1.9$, and $\mu_M = 10$ and $\sigma_M = 1.1$ for the upper mass estimate.

calculating the quantity $\mu_2^{\text{obs}} = \sum_i M_{p,i}^2 / N_* M_*^2$, which is listed in Table 2. The observed GMC masses show that $\mu_2^{\text{obs}} \sim 2 \times 10^6 - 10^8$ on the 100 pc scale, and $\mu_2^{\text{obs}} \sim 6 \times 10^1 - 10^3$ on the 5 pc scale. This clearly indicates that MPs dominate the relaxation on all relevant length scales where MPs exist. For the purpose of our numeric calculations below, it is convenient to describe the differential mass function analytically.

Here we model the data as either a power-law ($dN_p/dM_p \propto M_p^{-\beta}$) or a lognormal (LN) distribution ($dN_p/dM_p \propto \exp[-(\log M_p - \mu_M)/2\sigma_M^2]/(2\pi)^{1/2} M_p \sigma_M$, where μ_M and σ_M are the mean and standard deviation of $\log M_p$), whichever fits the data better. Figure 2 shows that the power-law distribution is a good fit for the mass function of the GMCs (Miyazaki & Tsuboi 2000) and for the lower estimate of the gas clumps. For the upper estimate of the molecular gas clumps, the mass function is better fitted by a LN distribution. It should be emphasized that our results and conclusions are determined primarily by the large values of μ_2 , not by the detailed form of the mass function. We repeated our calculations with several alternative distributions and found qualitatively similar results. The assumed high-mass cutoff of the mass function is important, as it determines the magnitude of μ_2 . Figure 2 shows that our models do not extrapolate beyond the maximum observed MP masses (and even fall below them for GMCs). Our analytical models thus provide a faithful and robust representation of the MP mass function.

We obtained best-fit power-law indices β and best-fit LN moments μ_M and σ_M for the lower and upper mass estimates and then chose the mass function model that best described the data. The cumulative mass functions and best fits are shown in Figure 2 and are listed in Table 1. Both the GMCs’ upper mass estimate ($1.4 \times 10^5 M_\odot \leq M_p \leq 5 \times 10^7 M_\odot$) and the lower mass estimates ($1.4 \times 10^4 M_\odot \leq M_p \leq 5 \times 10^6 M_\odot$) are well fitted by a power-law distribution with $\beta = 1.2$ (models GMC1 and GMC2 in Table 2). The clumps’ lower mass estimates ($2.4 \times 10^2 M_\odot \leq M_p \leq 1.1 \times 10^4 M_\odot$) are best fitted by a power-law distribution with $\beta \simeq 1.1$. The clumps’ upper mass estimates

$(3.6 \times 10^3 M_\odot \leq M_p \leq 1.35 \times 10^5 M_\odot)$ are best fitted by a LN distribution with $\mu_M = 8.16$ and $\sigma_M = 0.65$ (the power-law fit is for $\beta \simeq 1.7$; see models GMC1 and GMC2 in Table 1). The space density of such clumps falls rapidly inside the inner ~ 1.5 pc.

Stellar clusters are another class of MPs, which are of minor dynamical significance in this context. About 10 young stellar clusters with masses in the range 10^2 – $10^5 M_\odot$ and sizes of order $R_p \sim 1$ pc were observed (Figer et al. 1999, 2002; Maillard et al. 2004; Figer et al. 2004; Borissova et al. 2005). Again, we fit the lower mass estimates (3×10^2 – $1.3 \times 10^4 M_\odot$) with a power-law distribution with $\beta \simeq 1.3$ and the upper mass estimates (4.5×10^2 – $7 \times 10^4 M_\odot$) with a LN distribution with $\mu_M = 10$ and $\sigma_M = 1.1$ (the power-law fit is for $\beta \simeq 1.9$). The cumulative mass functions and best fits are shown in Figure 2 and are listed in Table 1.

It is interesting to note in passing that all MPs have very similar mass functions, but the clusters have a lower mass range, as might be expected if these GMCs are the progenitors of young GC clusters. This is similar to the relation observed between galactic disk clusters and GMCs (Lada & Lada 2003).

On the basis of the current observations of the nine confirmed clusters in the GC, we find that they are dynamically insignificant compared to the GMCs. Nevertheless, their contribution to the relaxation is comparable to that of the stars when the upper mass estimate is assumed (Fig. 1 and Table 2). Clusters could play a larger role in relaxation if there are many more yet undiscovered ones in the GC. On the basis of dynamical simulations, Portegies Zwart et al. (2006) suggest that there may be $O(100)$ evolved young clusters in the region that are undetected against the field stars because of their low surface density. However, Figer et al. (2002) argue that these massive clusters, if they exist, should have been observed. Two young GC cluster candidates were recently discovered by Borissova et al. (2006), one of which may be more massive than $10^4 M_\odot$. It is thus possible that the GC harbors some additional undetected massive clusters, although probably not as many as suggested by Portegies Zwart et al. (2006). Such young clusters may produce IMBHs by runaway stellar collisions (e.g., Portegies Zwart et al. 2004; Gürkan et al. 2004), which would then sink to the center by dynamical friction, dragging with them the cluster core. Portegies Zwart et al. (2006) estimate that many IMBHs may have migrated to the central 10 pc of the GC in this way; however, there is as yet no conclusive observational evidence supporting this idea.

The MBH's dynamical influence extends up to a radius r_h containing $O(M_\bullet)$ mass in stars, which in the GC falls in the range 2–4 pc, depending on the operative definition of r_h and the uncertainties in the value of M_\bullet and of the density of the surrounding stellar cluster (see Alexander 2005, § 3.1.2). Thus, most Galactic MPs, and in particular the very massive ones, lie outside r_h . Table 1 summarizes the estimated properties of the observed MPs.

The observed MP species vary in their spatial distributions and mass functions, which are not smooth or regular, and their distribution constantly changes as their orbits decay by dynamical friction and new MPs are formed and destroyed. It is thus likely that the presently observed MPs are but one realization of a much smoother and regular (well mixed) underlying distribution. Consequently, we construct several simplified MP models for our numeric calculations (Table 2) that are based on the observed properties of the MPs (§ 4) and our best fits for their mass functions. The simplifications involve the following assumptions. (1) A smooth, spherically symmetric MP number density distribution, $N_p(r) \propto r^{-2}$, between the cutoffs $r_{\text{MP}} < r < r_{\text{out}}$ (r_{out} does not play an important role, see below), with a random velocity field. (2) A single or broken power-law MP mass function, or a LN mass function. (3) A single-mass stellar population of $1 M_\odot$

stars with a number density distribution $N_*(r) \propto r^{-2}$ outside the inner 1.5 pc (i.e., a constant MP-to-star ratio). (4) Mutually exclusive perturber types (i.e., a single type of perturber is assumed to dominate relaxation, as indicated by the detailed calculations presented in Fig. 1).

The five perturber models are detailed in Table 2: Stars, Clusters1, Clusters2, GMC1, and GMC2, which represent, respectively, the case of relaxation by stars only, by heavy or light stellar clusters, and by heavy GMCs or light GMCs. Table 2 also lists μ_2^{obs} , the observed ratio of the second moment of the various MPs to that of the stars.

4. MASSIVE PERTURBER-DRIVEN INTERACTIONS WITH A MBH

The maximal differential loss cone refilling rate, which is also the close encounter event rate, $d\Gamma/dE$, is reached when relaxation is efficient enough to completely refill the loss cone during one orbit (eq. [7]). Further decrease in the relaxation time does not affect the event rate at that energy. MPs can therefore increase the differential event rate over that predicted by stellar relaxation only at high enough energies, $E > E_c$ (equivalently, at small enough typical radii, $r < r_c$), where slow stellar relaxation fails to refill the empty loss cone. The extent of the empty loss cone region increases with the maximal periaapse q , which in turn depends on the close encounter process of interest. For example, the tidal disruption of an object of mass M and size R occurs when $q < r_t$, the tidal disruption radius:

$$r_t \simeq R(M_\bullet/M)^{1/3}. \quad (16)$$

This approximate disruption criterion applies both for single stars ($M = M_*$, $R = R_*$) and for binaries, where M is the combined mass of the binary components and R is the binary's semimajor axis, a . Stellar radii are usually much smaller than typical binary separations, but stellar masses are only ~ 2 times smaller than binary masses. Binaries are therefore disrupted on larger scales than single stars. In the GC this translates to an empty (stellar relaxation) loss cone region extending out to $r_c^s \sim 3$ pc for single stars and out to $r_c^b > 100$ pc for binaries. In the GC, $r_{\text{MP}} \lesssim r_c^s \ll r_c^b$, and so MPs are expected to increase the binary disruption rate by orders of magnitude, but increase the single-star disruption rate only by a small factor. This is depicted qualitatively in Figure 3, which shows the local rates ($d\Gamma/d \log r$) for disruption of single stars and binaries due to stellar relaxation or relaxation by a simplified one-component MP model.

Figure 3 also shows that the MP-induced disruption rate is dominated by binaries originating near the *inner* cutoff, r_{MP} [in the following discussion the initial orbital energy of the disrupted objects is expressed by the corresponding radius of a circular orbit, $r \sim GM(<r)/2E$]. This is qualitatively different from the usual case of stellar tidal disruption induced by stellar relaxation, which mainly occurs inside r_c^s and is dominated by stars originating near the *outer* limit, which is $\min(r_c^s, r_h)$; usually $r_c^s \sim r_h$ (Lightman & Shapiro 1977). The difference can be understood by considering the r dependence of $d\Gamma/d \log r$. Neglecting logarithmic terms, the empty and full local loss cone rates are, respectively (eqs. [5] and [6]),

$$\frac{d\Gamma_e}{d \log r} \sim \frac{N_*(<r)}{t_r(r)}, \quad (17)$$

$$\frac{d\Gamma_f}{d \log r} \sim \frac{M_\bullet}{M_\bullet + M_*(<r)} \frac{q}{r} \frac{N_*(<r)}{P(r)}, \quad (18)$$

where $N_*(<r)$ is the number of stars enclosed within r .

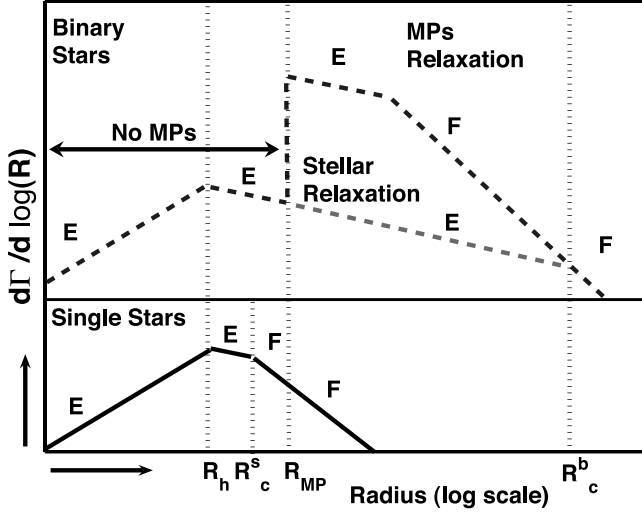


FIG. 3.—Schematic representation of the local contribution to the tidal disruption rate for a single-component MP model (e.g., GMC2 without the central clumps, so that $r_{\text{MP}} = 5$ pc). *Top*: Disruption rate of binaries (a constant binary fraction is assumed here for simplicity) due to stellar relaxation (lower dashed line) and MPs (upper dashed line). *Bottom*: Disruption rate of single stars for both perturber models. Empty and full loss cone regimes are denoted by “E” and “F,” respectively. The initial orbital energy of the disrupted objects is expressed by the corresponding radius of a circular orbit, r . For $r < r_h$, stellar density and velocity distributions of $N_*(r) \propto r^{-3/2}$ and $\sigma(r) \propto r^{-1/2}$ are assumed; for $r > r_h$, $N_*(r) \propto r^{-2}$ and $\sigma(r) = \text{constant}$. The transition from the empty to full loss cone regime (for stellar relaxation) occurs at the critical radius $r_c^s < r_{\text{MP}}$ for single stars and at $r_c^b \gg r_{\text{MP}}$ for binaries. [See the electronic edition of the *Journal* for a color version of this figure.]

Inside r_h , the potential is dominated by the MBH [$M_*(< r)/M_\bullet \ll 1$], $N_* \propto r^{-\alpha_1}$, with $\alpha_1 < 2$ for most dynamical scenarios (e.g., Bahcall & Wolf 1977; Young 1980), and the velocity dispersion is Keplerian, $\sigma \propto r^{-1/2}$. The orbital period scales as $P \propto r^{3/2}$, and $t_r \sim (M_\bullet/M_*)^2 P / [(\log N_*) N_*]$. The local disruption rates are then $d\Gamma_e/d \log r|_{r < r_h} \propto r^{9/2-2\alpha_1}$ and $d\Gamma_f/d \log r|_{r < r_h} \propto r^{1/2-\alpha_1}$. For plausible values of $1/2 < \alpha_1 < 9/4$, Γ_e increases with r , whereas Γ_f decreases with r , so the rate is dominated by stars near r_c (Lightman & Shapiro 1977). Outside r_h , the stellar distribution is usually assumed to be nearly isothermal, $N_* \propto r^{-\alpha_2}$ with $\alpha_2 \sim 2$ and a velocity dispersion $\sigma \sim \text{constant}$, and the potential is dominated by the stars [$M_\bullet \ll M_*(< r) \propto r^{3-\alpha_2}$]. The orbital period scales as $P \propto r^{\alpha_2/2}$, and $t_r \sim N_* P / \log N_*$. The local disruption rates are then $d\Gamma_e/d \log r|_{r > r_h} \propto r^{-\alpha_2/2} \sim r^{-1}$ and $d\Gamma_f/d \log r|_{r > r_h} \propto r^{-1-\alpha_2/2} \sim r^{-2}$. For $\alpha_2 \sim 2$, both rates increase toward small radii. Since for most Galactic MP types $r_{\text{MP}} > r_h$, the disruption rate is dominated by stars near r_{MP} . For example, when the loss cone is empty, $\sim 50\%$ of the total rate is due to MPs at $r < 2r_{\text{MP}}$; when the loss cone is full, $\sim 75\%$ of the total rate is due to MPs at $r < 2r_{\text{MP}}$.

4.1. Interactions with Single Stars

GMCs, gas clumps, and clusters in the GC are abundant only beyond the central $r_{\text{MP}} \sim 1.5$ pc, whereas the empty loss cone regime for tidal disruption of single stars extends only out to $r_c^s \sim 3$ pc. For inspiral processes such as GW emission, r_c is ~ 100 times smaller still (Hopman & Alexander 2005, 2006b). The effect of such MPs on close encounter events involving single stars is thus suppressed (weaker tidal effects by MPs at $r > r_c^s$ are not considered here). This is contrary to the suggestion of Zhao et al. (2002), who assumed that the effect of MPs fully extends to the empty loss cone regime. We find that the enhancement of MPs over stellar relaxation to the single-star disruption rate is small,

less than a factor of 3, and is due to stars scattered by gas clumps in the small empty loss cone region between $r_{\text{MP}} \sim 1.5$ pc and $r_c^s \sim 3$ pc. A possible exception to this conclusion is the hypothesized population of IMBHs (Portegies Zwart et al. 2006), not modeled here, whose distribution could extend to the inner 1 pc (e.g., the IMBH candidate in IRS 13; Maillard et al. 2004; but see Schödel et al. 2005; Paumard et al. 2006).

4.2. Interactions with Stellar Binaries

The empty loss cone region for binary-MBH interactions extends out to >100 pc because of their large tidal radius. On these large scales MPs are abundant enough to dominate the relaxation processes. Here we focus on three-body exchange interactions (Hills 1991, 1992; Yu & Tremaine 2003), which lead to the disruption of the binary, the energetic ejection of one star, and the capture of the other star on a close orbit around the MBH.

Various phenomena associated with such exchange interactions were suggested and explored. Hills (1988), and later Yu & Tremaine (2003), Gualandris et al. (2005), Ginsburg & Loeb (2006), and Bromley et al. (2006), studied hypervelocity stars ejected from the GC following tidal disruption by the MBH. Gould & Quillen (2003) suggested this mechanism to explain the origin of the young stars near the Galactic MBH. Miller et al. (2005) proposed that compact objects captured following a binary disruption event will eventually be sources of GWs from zero-eccentricity orbits, in contrast to high-eccentricity sources typical of single-star inspiral (Hopman & Alexander 2005).

The event rates estimated by these authors vary substantially. Hills (1988) assumed a full loss cone and a fraction $f_{\text{bin}} = 0.02$ of the stars in binaries with small enough semimajor axes to produce a high-velocity star ($a < 0.1$ AU) and derived a three-body exchange rate of $\sim 10^{-3} (f_{\text{bin}}/0.02) \text{ yr}^{-1}$. Yu & Tremaine (2003) took into account the empty loss cone regime and argued for a higher fraction of relevant binaries ($f_{\text{bin}} = 0.04$ for binaries with $a < 0.3$ AU that can survive 0.8 pc from the MBH), thereby obtaining a rate of $\sim 2.5 \times 10^{-6} (f_{\text{bin}}/0.04) \text{ yr}^{-1}$, 3 orders of magnitude smaller than that estimated by Hills. These calculations assumed the same binary separation for all binaries and a constant binary fraction at all distances from the MBH (two possibilities were considered, $a = 0.3$ AU and $a = 0.03$ AU).

The binary fraction and typical binary semimajor axis depend on the binary mass and on the rate at which binaries evaporate by encounters with other stars. This depends in turn on the stellar densities and velocities and therefore on the distance from the MBH. Here we take these factors into account and estimate in detail the three-body exchange rate for MP-driven relaxation. The rate is proportional to the binary fraction in the population, which is the product of the poorly known binary initial mass function (IMF) in the GC and the survival probability against binary evaporation.

We assume for simplicity equal-mass binaries, $M_{\text{bin}} = 2M_*$, since the observations indicate that moderate mass ratios dominate the binary population (Duquennoy & Mayor 1991; Kobulnicky et al. 2006). The evaporation timescale at a distance r from the center for a binary of semimajor axis a composed of two equal-mass stars of mass M_* and lifetime t_* is (e.g., Binney & Tremaine 1987)

$$t_{\text{evap}}(M_*, a, r) = \frac{M_{\text{bin}}}{\langle M_* \rangle} \frac{\sigma(r)}{16\sqrt{\pi}\rho(r)Ga \ln \Lambda_{\text{bin}}}. \quad (19)$$

The Coulomb factor for binary evaporation, $\Lambda_{\text{bin}} = a\sigma^2/4G\langle M_* \rangle$, expresses the fact that the binary is only affected by close perturbations at distances smaller than $\sim a/2$. The MPs considered

TABLE 3
TOTAL BINARY DISRUPTION RATE AND NUMBER OF CAPTURED YOUNG STARS

MODEL	DISRUPTION RATE (yr ⁻¹)		YOUNG STARS ^a		YOUNG HVSS ^b
	$r < 0.04$ pc	$r < 0.4$ pc	$r < 0.04$ pc	$0.04 \text{ pc} < r < 0.4 \text{ pc}$	
GMC1	1.1×10^{-4}	3.2×10^{-4}	39.4	5.2	342
GMC2	2.8×10^{-5}	1.8×10^{-4}	6	1.4	49
Clusters1	6.4×10^{-7}	9.7×10^{-7}	0.19	0.004	1.9
Clusters2	2.6×10^{-8}	4×10^{-8}	0.01	10^{-4}	0.1
Stars	3.4×10^{-7}	5.3×10^{-7}	0.15	0.003	1.3
Observed	?	?	10–35 ^c	?	43 ± 31^d

^a Main-sequence B stars with a life span of $t < 5 \times 10^7$ yr.

^b Main-sequence B stars with a life span of $t < 4 \times 10^8$ yr. Note that only 20% of these ejected stars could be observed in regions covered by current surveys (i.e., between 20 and 120 pc from the GC; Brown et al. 2006a).

^c There are ~ 10 stars with derived values of $a \lesssim 0.04$ pc, with a total of $\gtrsim 30$ stars observed in the area.

^d Estimated from the observed 5 hypervelocity stars.

here are extended objects (Table 2) and therefore do not affect the binary evaporation timescale (IMBH MPs could be a possible exception). Although binary evaporation is a stochastic process and the actual time to evaporation differs from binary to binary, we expect a small scatter in the evaporation rate, $\Delta t_{\text{evap}}^{-1}/t_{\text{evap}}^{-1} \ll 1$, because evaporation is a gradual process caused by numerous weak encounters. Evaporation is thus better approximated as a fixed limit on the binary lifetime rather than as a Poisson process (where $\Delta t_{\text{evap}}^{-1}/t_{\text{evap}}^{-1} = 1$). The maximal binary lifetime is then $\tau = \min[t_H, t_*(M_*, t_{\text{evap}}(M_*, a, r))]$, where t_H is the Hubble time, taken here to be the age of the Galaxy. It is well established that the central 100–200 pc of the GC have undergone continuous star formation over the lifetime of the Galaxy (Serabyn & Morris 1996; Figer et al. 2004). Assuming a constant star formation rate over time t_H , the differential binary distribution at time t is $dN_{\text{bin}}/da|_t = f_{\text{bin}} df/da|_0 \Gamma_* \min(t, \tau)$, where $df/da|_0$ is the normalized initial semimajor axis distribution, which can be observed in binaries in low-density environments where $t_{\text{evap}} \rightarrow \infty$, and Γ_* is the single-star formation rate, which is normalized to the observed present-day stellar density by setting $t = t_H$ and taking $t_{\text{evap}} \rightarrow \infty$ for single stars, so that $\Gamma_* = N_*/\min(t_H, t_*)$. The present-day binary semimajor axis distribution is therefore

$$\left. \frac{dN_{\text{bin}}}{da} \right|_{t_H} = f_{\text{bin}}(M_*) \left. \frac{df}{da} \right|_0 N_*(r) \min \left\{ 1, \frac{t_{\text{evap}}(M_*, a, r)}{\min[t_H, t_*(M_*)]} \right\}. \quad (20)$$

The capture probability and the semimajor axis distribution of captured stars were estimated by simulations (Hills 1991, 1992; Yu & Tremaine 2003). Numeric experiments indicate that between 0.5 and 1.0 of the binaries that approach the MBH within the tidal radius $r_t(a)$ (eq. [16]) are disrupted. Here we adopt a disruption efficiency of 0.75. The harmonic mean semimajor axis for three-body exchanges with equal-mass binaries was found to be (Hills 1991)

$$\langle a_1 \rangle \simeq 0.56 \left(\frac{M_*}{M_{\text{bin}}} \right)^{2/3} a \simeq 0.56 \left(\frac{M_*}{M_{\text{bin}}} \right)^{1/3} r_t, \quad (21)$$

where a is the semimajor axis of the infalling binary and a_1 is that of the captured star (the MBH-star “binary”). Most values of a_1 fall within a factor of 2 of the mean. This relation maps the semimajor axis distribution of the infalling binaries to that of the captured stars: the harder the binaries, the more tightly bound the captured stars. The velocity at infinity of the ejected star (neglecting the Galactic potential) is $v_\infty^2 = 2^{1/2} (GM_{\text{bin}}/a)(M_*/M_{\text{bin}})^{1/3} \propto$

$M_{\text{bin}}^{2/3}/a$ (an equal-mass binary with periastron at r_t is assumed; Hills 1988). The harder the binary, the higher the value of v_∞ . The periastron of the captured star is at r_t , and therefore its eccentricity is very high (Hills 1991, 1992; Miller et al. 2005): $e = 1 - r_t/a_1 \simeq 1 - 1.8(M_{\text{bin}}/M_*)^{1/3} \gtrsim 0.98$ for values typical of the GC.

We now consider separately the implications of three-body exchange interactions of the MBH with old ($t_* \gtrsim t_H$) binaries and massive young ($t_* < 5 \times 10^7$ yr) binaries.

4.2.1. Low-Mass Binaries

The properties of binaries in the inner GC are at present poorly determined. The period distribution of solar neighborhood binaries can be approximated by a lognormal distribution with a median period of 180 yr ($a \sim 40$ AU; Duquennoy & Mayor 1991). The total binary fraction of these binaries is estimated at $f_{\text{bin}} \sim 0.3$ (Lada 2006). Adopting these values for the GC, the total binary disruption rate by the MBH can then be calculated, as described in § 2, by integrating dN_{bin}/da (eq. [20]) over the binary a -distribution and over the power-law stellar density distribution of the GC up to 100 pc (Genzel et al. 2003). Table 3 lists the capture rates for the different perturber models, assuming a typical old equal-mass binary of $M_{\text{bin}} = 2 M_\odot$.

The old, low-mass binary disruption rate that we derive for stellar relaxation alone is $\sim 5 \times 10^{-7} \text{ yr}^{-1}$, which is ~ 5 times lower than, but still in broad agreement with, the result of Yu & Tremaine (2003). Their rate is somewhat higher because they assumed a constant binary fraction and a constant semimajor axis for all binaries, even close to the MBH, where these assumptions no longer hold.

MPs increase the binary disruption and high-velocity star ejection rates by factors of $\sim 10^1$ – 10^3 and effectively accelerate stellar migration to the center. This can modify the stellar distribution close to the MBH by introducing a “source term” to the stellar current into the MBH. Low-mass stars are at present too faint to be directly observed in the GC. However, such a source term may have observable consequences, since it can increase the event rate of single-star processes such as tidal disruption, tidal heating, and GW emission from compact objects, in particular from compact objects on zero-eccentricity orbits (Miller et al. 2005; in contrast, GW from inspiraling single stars occurs on high-eccentricity orbits; Hopman & Alexander 2005). We calculated numerical solutions of the Fokker-Planck equation for the stellar distribution around the MBH with a captured-star source term. These preliminary investigations (H. B. Perets et al. 2007, in preparation) confirm that the total accumulated mass of captured stars does not exceed the dynamical constraints on the

extended mass around the MBH (Mouawad et al. 2005), because two-body relaxation and likely also resonant relaxation (Rauch & Tremaine 1996; Hopman & Alexander 2006a) scatter enough of them into the MBH or to wider orbits.

4.2.2. Young Massive Binaries

MPs may be implicated in the puzzling presence of a cluster of main-sequence B stars ($4 M_{\odot} \lesssim M_{\star} \lesssim 15 M_{\odot}$) in the inner $\sim 1''$ (~ 0.04 pc) of the GC. This so-called S cluster is spatially, kinematically, and spectroscopically distinct from the young, more massive stars observed farther out, on the ~ 0.05 – 0.5 pc scale, which are thought to have formed from the gravitational fragmentation of one or two gas disks (Levin & Beloborodov 2003; Genzel et al. 2003; Milosavljević & Loeb 2004; Paumard et al. 2006). There is, however, still no satisfactory explanation for the existence of the seemingly normal young massive main-sequence stars of the S cluster, so close to a MBH (see review of proposed models by Alexander 2005; also a recent model by Levin 2007).

Here we revisit an idea proposed by Gould & Quillen (2003), which is that the S stars were captured near the MBH by three-body exchange interactions with infalling massive binaries. Originally, this exchange scenario lacked a plausible source for the massive binaries. Gould & Quillen speculated that they originated in an unusually dense and massive young cluster on an almost radial infall trajectory, but they concluded that such a finely tuned scenario seems unlikely. Furthermore, a massive cluster is expected to leave a tidally stripped tail of massive stars beyond the central 0.5 pc (Kim et al. 2004; Gürkan & Rasio 2005), which are not observed (Paumard et al. 2006). Alternatively, it must contain an unusually massive central IMBH to hold it together against the tidal field of the GC (Hansen & Milosavljević 2003). However, such a massive IMBH is well beyond what is predicted by simulations of IMBH formation by runaway collisions (Gürkan et al. 2004; Gürkan & Rasio 2005) or anticipated by extrapolating the M - σ relation (Ferrarese & Merritt 2000; Gebhardt et al. 2000) to clusters.

MP-driven three-body exchanges circumvent the problems of the cluster infall scenario by directly bringing massive *field* binaries to r_i , without requiring massive clusters of unusual, perhaps even impossible properties. The ongoing star formation in the central ~ 100 pc implies the presence of a large reservoir of massive stars there, which are indeed observed in the central few tens of pc both in dense clusters and in the field (Figer et al. 1999; Figer 2003; Muno et al. 2006). It is plausible that a high fraction of them are in binaries. It is assumed here that the field binaries are dynamically relaxed, which is reasonable in view of the fact that MP relaxation times are shorter or comparable to their typical stellar lifetimes over most of the range of GMC-dominated MP models.

We model the binary population of the GC in the S star mass range, $4 M_{\odot} \lesssim M_{\star} \lesssim 15 M_{\odot}$, by assuming equal-mass binaries that follow the single-star mass function with an initial binary fraction of $f_{\text{bin}} \sim 0.75$, as observed elsewhere in the Galaxy (Lada 2006; Kobulnicky et al. 2006). Because the stellar evolutionary life span of such stars is relatively short, massive binaries are essentially unaffected by dynamical evaporation. We assume star formation at a constant rate for 10 Gyr with a Miller-Scalo IMF (Miller & Scalo 1979) and use a stellar population synthesis code (Sternberg et al. 2003) with the Geneva stellar evolution tracks (Schaller et al. 1992) to estimate that the present-day number fraction of stars in the S star mass range is 3.5×10^{-4} (and less than 0.01 of that for $M_{\star} > 15 M_{\odot}$ stars). Note that if star formation in the GC is biased toward massive stars (Figer 2003; Stolte et al. 2005), this estimate should be revised upward. We adopt the observed solar neighborhood distribution of the semimajor

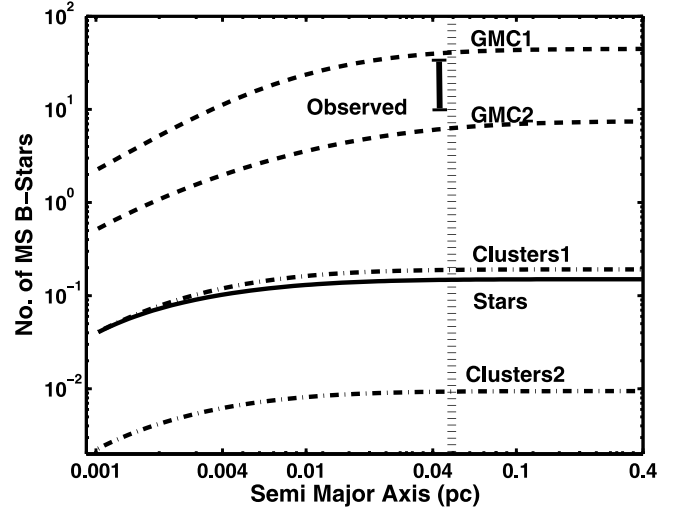


FIG. 4.—Cumulative number of young B stars in the GC (see also Table 3) as predicted by the MP models and by stellar two-body relaxation (listed in Table 2). The vertical bar represents the total number of observed young stars inside 0.04 pc (Eisenhauer et al. 2005; S. Gillessen 2006, private communication). The hatched vertical line marks the approximate maximal distance within which captured B stars are expected to exist. [See the electronic edition of the *Journal* for a color version of this figure.]

axis of massive binaries, which is lognormal with $\langle \log a \rangle = -0.7 \pm 0.6$ AU (i.e., 63% of the binaries with $a = 0.2^{+0.60}_{-0.15}$ AU; 91% with $a = 0.2^{+2.96}_{-0.19}$ AU; Garmany et al. 1980; Kobulnicky et al. 2006). Massive binaries are thus typically harder than low-mass binaries and will be tidally disrupted (eq. [16]) closer to the MBH and leave a more tightly bound captured star.

We represent the massive binaries by binaries composed of equal-mass stars in the midrange of the S star masses, with $M_{\text{bin}} = 15 M_{\odot}$ and $t_{\star}(7.5 M_{\odot}) \simeq 5 \times 10^7$ yr, and integrate over the stellar distribution and the binary a -distribution as before, to obtain the rate of binary disruptions, Γ , the mean number of captured massive stars in a steady state, $N_{\star} = \Gamma t_{\star}$, and their semimajor axis distribution (eq. [21]). Table 3 compares the number of captured young stars in a steady state for the different MP models, both on the $r < 0.04$ pc scale (the S cluster) and on the 0.04 pc $< r < 0.4$ pc scale (the stellar rings), with current observations (Eisenhauer et al. 2005; Paumard et al. 2006).

The S stars are found in the central < 0.04 pc (Ghez et al. 2005; Eisenhauer et al. 2005). If they were captured by binary disruptions, they must have originated from massive binaries with $a \lesssim 3.5$ AU. This is consistent with the semimajor axis distribution of massive binaries. The number of captured massive stars falls rapidly beyond 0.04 pc (Table 3) because wide massive binaries are rare. This capture model thus provides a natural explanation for the central concentration of the S cluster (Fig. 4). The absence of more massive stars in the S cluster ($M_{\star} > 15 M_{\odot}$; spectral type O V) is a statistical reflection of their much smaller fraction in the binary population. Figure 4 and Table 3 compare the cumulative semimajor axis distribution of captured B stars, as predicted by the different MP models, with the total number of young stars observed in the inner 0.04 pc (~ 35 stars; Eisenhauer et al. 2005; Ghez et al. 2005; Paumard et al. 2006). Of these, only ~ 10 have full orbital solutions (in particular, solutions for a and e) at present. For the others, we assume the *Ansatz* that a is similar to the observed projected position. The numbers predicted by the GMC-dominated MP models are consistent with the observations, unlike the stellar relaxation model, which falls short by 2 orders of magnitude.

The binary capture model predicts that captured stars have very high initial eccentricities. Most of the solved S star orbits do have $e > 0.9$, but a couple have $e \sim 0.3\text{--}0.4$ (Eisenhauer et al. 2005). Normal, noncoherent stellar relaxation is slow, even after taking into account the decrease in t_r toward the center due to mass segregation (Hopman & Alexander 2006b). It is unlikely that it could have decreased the eccentricity of these stars over their relatively short lifetimes. However, the much faster process of resonant relaxation (Rauch & Tremaine 1996) may be efficient enough to randomize the eccentricity of a fraction of the stars, and it could thus possibly explain the much larger observed spread in eccentricities (Hopman & Alexander 2006a). Additional orbital solutions and a better estimate of the efficiency of resonant relaxation in the GC are required for more detailed comparisons between observations and the MP model predictions.

4.2.3. Hypervelocity Stars

Each captured star is associated with an ejected companion, which in some cases is launched with a very high velocity. The one-to-one correspondence between the number of captured S stars and the number of early-type hypervelocity stars (HVSs) is thus a generic prediction of binary capture models. The MP capture scenario specifically implies the continuous and isotropic ejection of both young and old HVSs from the GC. Recent observations of HVSs (Brown et al. 2005; Hirsch et al. 2005; Edelmann et al. 2005; Brown et al. 2006a, 2006b) are consistent with a GC origin and favor a steady state temporal distribution and an isotropic spatial distribution over a burstlike nonspherical distribution that is expected for HVSs triggered by the infall of a cluster (Levin 2006; Haardt et al. 2006; Baumgardt et al. 2006).

Two of the recently observed HVSs ($v \sim 560\text{--}710 \text{ km s}^{-1}$; Brown et al. 2005, 2006a; Fuentes et al. 2006; Edelmann et al. 2005; Brown et al. 2006b) were spectrally identified as late B V young massive stars [masses of $3\text{--}5 M_\odot$, main-sequence life spans of $(1\text{--}4) \times 10^8 \text{ yr}$, and a number fraction of $\sim 10^{-3}$ in the population], implying a total population of 43 ± 31 such HVSs in the Galaxy (Brown et al. 2006a). We model the parent binaries of these HVSs by equal-mass binaries of $M_{\text{bin}} = 8 M_\odot$ and $t_*(4M_\odot) = 2 \times 10^8 \text{ yr}$. The ejection velocity was found in numerical simulations (Hills 1988; Bromley et al. 2006) to scale as

$$v_\infty = 1776 \text{ km s}^{-1} \left(\frac{a}{0.1 \text{ AU}} \right)^{-1/2} \left(\frac{M_{\text{bin}}}{2 M_\odot} \right) \left(\frac{M_\bullet}{3.7 \times 10^6 M_\odot} \right)^{1/6}. \quad (22)$$

To reproduce the high HVS velocities, we consider binaries with $a < 1 \text{ AU}$, which are tidally disrupted at $r_t < 3.7 \times 10^{-4} \text{ pc}$ and eject a HVS with $v_\infty \gtrsim 900 \text{ km s}^{-1}$, the escape velocity from the bulge (Haardt et al. 2006). Taking only the GMCs into account, we predict that tens to hundreds of such HVSs exist in the Galaxy, in agreement with the deduced HVS populations, whereas stellar relaxation predicts only 1.3 such stars (see Table 3).

We note that Brown et al. (2006a) used the 10^{-5} yr^{-1} total rate of hypervelocity star ejection calculated by Yu & Tremaine (2003); including binaries of all stellar types, assuming stellar relaxation only, and normalized to a fiducial 10% binary fraction) to estimate the number of late B V HVSs in a Salpeter IMF at $10\text{--}25 M_\odot$. This theoretical prediction seems to be in rough agreement with the observations (and contradicts our much lower estimate of 1.3 HVSs). However, the rates of Yu & Tremaine are inapplicable here and lead to a significant overestimate of the number of HVSs because their binary population model is not appropriate for massive binaries in the GC. On the one hand, the young binary

population does not extend all the way to the center, as assumed by Yu & Tremaine for the general binary population (following Paumard et al. [2006], who do not find any B V stars between 0.5 and 1 pc of the GC, we truncate the massive binary population inside 1.5 pc). The massive binary population in the GC is a few times 10 smaller than that implied by a simple scaling of the Yu & Tremaine general binary population. On the other hand, the binary fraction of young massive binaries is 70%, rather than 10% (§ 4.2.2). We conclude that the agreement found by Brown et al. is accidental and that binary disruption by stellar relaxation is insufficient to explain the number of observed HVSs, whereas MP-induced relaxation can reproduce the observations.

5. SUMMARY

Relaxation by MPs dominates relaxation by two-body stellar interactions when the ratio between the second moments of their respective mass functions satisfies $\mu_2 = N_p \langle M_p^2 \rangle / N_\star \langle M_\star^2 \rangle \gg 1$. We show that Galactic MPs (mostly GMCs and smaller molecular gas clumps that exist outside the inner few pc) dominate and accelerate relaxation in the inner $\sim 100 \text{ pc}$ of the GC. This is plausibly the case in the centers of late-type galaxies in general. There is also evidence for molecular gas in the centers of early-type galaxies (e.g., Rupen 1997; Knapp 1999), which suggests that MPs may dominate relaxation there as well and lead to the relaxation of the central regions of galactic bulges in general.

Relaxation determines the rate at which stars and binaries are deflected to nearly radial (loss cone) orbits that bring them closer to the MBH than some critical periastron q , where they undergo a strong destructive interaction with it. The size of q depends on the nature of the interaction of interest (e.g., tidal disruption, three-body exchange). It is much larger for binaries than for single stars due to the binary's larger effective size.

We extend loss cone theory to approximately treat rare encounters with MPs and apply it to explore the implications of MPs on the rates of different types of close encounters. The rate reaches its maximum when loss cone orbits are replenished by scattering within an orbital time (the full loss cone regime). This is more easily achieved when the phase-space volume of the loss cone is small; that is, when q is small. MPs thus affect only those processes with large q whose loss cones are too large to be efficiently replenished by stellar encounters (the empty loss cone regime).

We show that MPs will not contribute much to the disruption of single stars in the GC, whose loss cone is efficiently replenished by stars outside the central $\sim 2 \text{ pc}$ (MPs may accelerate the consumption of stars by more massive MBHs, where q is significantly larger, or the capture of stars in accretion disks). However, MPs will enhance by factors of $10\text{--}1000$ the tidal disruption rate of infalling binaries, which result in the capture of one of the stars on a tight orbit around the MBH and the ejection at high velocity of the other star (Hills 1991, 1992; Yu & Tremaine 2003). The enhancement of the event rates is dominated by the innermost MPs, and so the uncertainty in determining the MP distribution on the smallest scales dominates the uncertainties in the total event rate. Detailed observations of MPs in the inner GC allow us to robustly predict their effects in the Galaxy. We show that MP-induced disruptions of relatively rare massive binaries can naturally explain the puzzling presence of apparently normal main-sequence B stars in the central 0.04 pc of the GC (Eisenhauer et al. 2005) and at the same time can account for the observed HVSs that are well on their way out of the Galaxy (Brown et al. 2005; Edelmann et al. 2005; Hirsch et al. 2005; Brown et al. 2006a, 2006b; Bromley et al. 2006). Tidal disruptions of the many more faint low-mass binaries can efficiently supply single stars on very eccentric tight

orbits near the MBH. Such an increase in the number of stars in tight orbit near the MBH may increase the rates of single-star processes such as tidal disruption and heating or GW emission from tightly bound compact objects (Miller et al. 2005).

Finally, MP-induced interactions also have cosmological implications for the coalescence of binary MBHs following galactic mergers (Zhao et al. 2002). We suggest that MPs can accelerate the dynamical decay of binary MBHs by efficiently supplying stars for the slingshot mechanism and thereby help solve the “last parsec” stalling problem. MP-driven loss cone refilling will operate even in the case of a spherical potential, where other

suggested mechanisms are inefficient, thus allowing MBHs to coalesce on the dynamical timescale of the galactic merger. A detailed treatment of this idea will be presented elsewhere (H. B. Perets & T. Alexander 2007, in preparation).

We are grateful to M. Tsuboi for help in interpreting the giant molecular cloud data. T. A. is supported by ISF grant 928/06, Minerva grant 8563, and a New Faculty grant by Sir H. Djangoly, CBE, of London, UK. C. H. was supported by a Veni scholarship from the Netherlands Organization for Scientific Research (NWO).

REFERENCES

- Alexander, T. 2005, *Phys. Rep.*, 419, 65
 Alexander, T., & Hopman, C. 2003, *ApJ*, 590, L29
 Alexander, T., & Livio, M. 2001, *ApJ*, 560, L143
 ———. 2004, *ApJ*, 606, L21
 Alexander, T., & Morris, M. 2003, *ApJ*, 590, L25
 Bahcall, J. N., & Wolf, R. A. 1976, *ApJ*, 209, 214
 ———. 1977, *ApJ*, 216, 883
 Bailey, M. E. 1983, *MNRAS*, 204, 603
 Baumgardt, H., Gualandris, A., & Portegies Zwart, S. 2006, *MNRAS*, 372, 174
 Berczik, P., Merritt, D., & Spurzem, R. 2005, *ApJ*, 633, 680
 Berczik, P., Merritt, D., Spurzem, R., & Bischof, H.-P. 2006, *ApJ*, 642, L21
 Binney, J., & Tremaine, S. 1987, *Galactic Dynamics* (Princeton: Princeton Univ. Press)
 Borissova, J., Ivanov, V. D., Minniti, D., & Geisler, D. 2006, *A&A*, 455, 923
 Borissova, J., Ivanov, V. D., Minniti, D., Geisler, D., & Stephens, A. W. 2005, *A&A*, 435, 95
 Bromley, B. C., Kenyon, S. J., Geller, M. J., Barcikowski, E., Brown, W. R., & Kurtz, M. J. 2006, *ApJ*, 653, 1194
 Brown, W. R., Geller, M. J., Kenyon, S. J., & Kurtz, M. J. 2005, *ApJ*, 622, L33
 ———. 2006a, *ApJ*, 640, L35
 ———. 2006b, *ApJ*, 647, 303
 Christopher, M. H., Scoville, N. Z., Stolovy, S. R., & Yun, M. S. 2005, *ApJ*, 622, 346
 Cohn, H., & Kulsrud, R. M. 1978, *ApJ*, 226, 1087
 Duquennoy, A., & Mayor, M. 1991, *A&A*, 248, 485
 Edelman, H., Napiwotzki, R., Heber, U., Christlieb, N., & Reimers, D. 2005, *ApJ*, 634, L181
 Eisenhauer, F., et al. 2005, *ApJ*, 628, 246
 Ferrarese, L., & Merritt, D. 2000, *ApJ*, 539, L9
 Figer, D. F. 2003, *Astron. Nachr. Suppl.*, 324, 255
 ———. 2004, in *ASP Conf. Ser. 322, The Formation and Evolution of Massive Young Star Clusters*, ed. H. J. G. L. M. Lamers et al. (San Francisco: ASP), 49
 Figer, D. F., Kim, S. S., Morris, M., Serabyn, E., Rich, R. M., & McLean, I. S. 1999, *ApJ*, 525, 750
 Figer, D. F., Rich, R. M., Kim, S. S., Morris, M., & Serabyn, E. 2004, *ApJ*, 601, 319
 Figer, D. F., et al. 2002, *ApJ*, 581, 258
 Frank, J., & Rees, M. J. 1976, *MNRAS*, 176, 633
 Fuentes, C. I., Stanek, K. Z., Gaudi, B. S., McLeod, B. A., Bogdanov, S., Hartman, J. D., Hickox, R. C., & Holman, M. J. 2006, *ApJ*, 636, L37
 Garmany, C. D., Conti, P. S., & Massey, P. 1980, *ApJ*, 242, 1063
 Gebhardt, K., et al. 2000, *ApJ*, 539, L13
 ———. 2003, *ApJ*, 583, 92
 Genzel, R., Crawford, M. K., Townes, C. H., & Watson, D. M. 1985, *ApJ*, 297, 766
 Gerhard, R., et al. 2003, *ApJ*, 594, 812
 Gerhard, O. E., & Binney, J. 1985, *MNRAS*, 216, 467
 Ghez, A. M., Salim, S., Hornstein, S. D., Tanner, A., Lu, J. R., Morris, M., Becklin, E. E., & Duchêne, G. 2005, *ApJ*, 620, 744
 Ginsburg, I., & Loeb, A. 2006, *MNRAS*, 368, 221
 Gould, A., & Quillen, A. C. 2003, *ApJ*, 592, 935
 Gualandris, A., Portegies Zwart, S., & Sipior, M. S. 2005, *MNRAS*, 363, 223
 Gürkan, M. A., Freitag, M., & Rasio, F. A. 2004, *ApJ*, 604, 632
 Gürkan, M. A., & Rasio, F. A. 2005, *ApJ*, 628, 236
 Güsten, R., & Philipp, S. D. 2004, in *The Dense Interstellar Medium in Galaxies*, ed. S. Pfalzner et al. (Heidelberg: Springer), 253
 Haardt, F., Sesana, A., & Madau, P. 2006, *Mem. Soc. Astron. Italiana*, 77, 653
 Häneninen, J., & Flynn, C. 2002, *MNRAS*, 337, 731
 Hansen, B. M. S., & Milosavljević, M. 2003, *ApJ*, 593, L77
 Hills, J. G. 1981, *AJ*, 86, 1730
 ———. 1988, *Nature*, 331, 687
 ———. 1991, *AJ*, 102, 704
 ———. 1992, *AJ*, 103, 1955
 Hirsch, H. A., Heber, U., O’Toole, S. J., & Bresolin, F. 2005, *A&A*, 444, L61
 Holley-Bockelmann, K., Mihos, J. C., Sigurdsson, S., Hernquist, L., & Norman, C. 2002, *ApJ*, 567, 817
 Holley-Bockelmann, K., & Sigurdsson, S. 2006, *MNRAS*, submitted (astro-ph/0601520)
 Hopman, C., & Alexander, T. 2005, *ApJ*, 629, 362
 ———. 2006a, *ApJ*, 645, 1152
 ———. 2006b, *ApJ*, 645, L133
 Jenkins, A., & Binney, J. 1990, *MNRAS*, 245, 305
 Kim, S. S., Figer, D. F., & Morris, M. 2004, *ApJ*, 607, L123
 Kim, S. S., & Morris, M. 2001, *ApJ*, 554, 1059
 Knapp, G. R. 1999, in *ASP Conf. Ser. 163, Star Formation in Early-Type Galaxies*, ed. J. Cepa & P. Carral (San Francisco: ASP), 119
 Kobulnicky, H. A., Fryer, C. L., & Kiminki, D. C. 2006, *ApJ*, submitted (astro-ph/0605069)
 Lacey, C. G. 1984, *MNRAS*, 208, 687
 Lada, C. J. 2006, *ApJ*, 640, L63
 Lada, C. J., & Lada, E. A. 2003, *ARA&A*, 41, 57
 Levin, Y. 2006, *ApJ*, 653, 1203
 ———. 2007, *MNRAS*, 374, 515
 Levin, Y., & Beloborodov, A. M. 2003, *ApJ*, 590, L33
 Levin, Y., Wu, A., & Thommes, E. 2005, *ApJ*, 635, 341
 Lightman, A. P., & Shapiro, S. L. 1977, *ApJ*, 211, 244
 Magorrian, J., & Tremaine, S. 1999, *MNRAS*, 309, 447
 Maillard, J. P., Paumard, T., Stolovy, S. R., & Rigaut, F. 2004, *A&A*, 423, 155
 Merritt, D., & Poon, M. Y. 2004, *ApJ*, 606, 788
 Merritt, D., & Quinlan, G. D. 1998, *ApJ*, 498, 625
 Merritt, D., & Wang, J. 2005, *ApJ*, 621, L101
 Miller, G. E., & Scalo, J. M. 1979, *ApJS*, 41, 513
 Miller, M. C., Freitag, M., Hamilton, D. P., & Lauburg, V. M. 2005, *ApJ*, 631, L117
 Milosavljević, M., & Loeb, A. 2004, *ApJ*, 604, L45
 Miralda-Escudé, J., & Kollmeier, J. A. 2005, *ApJ*, 619, 30
 Miyazaki, A., & Tsuboi, M. 2000, *ApJ*, 536, 357
 Mouawad, N., Eckart, A., Pfalzner, S., Schödel, R., Moutakka, J., & Spurzem, R. 2005, *Astron. Nachr.*, 326, 83
 Muno, M. P., Bower, G. C., Burgasser, A. J., Baganoff, F. K., Morris, M. R., & Brandt, W. N. 2006, *ApJ*, 638, 183
 Norman, C., & Silk, J. 1983, *ApJ*, 266, 502
 Oka, T., Hasegawa, T., Sato, F., Tsuboi, M., Miyazaki, A., & Sugimoto, M. 2001, *ApJ*, 562, 348
 Paumard, T., et al. 2006, *ApJ*, 643, 1011
 Polnarev, A. G., & Rees, M. J. 1994, *A&A*, 283, 301
 Portegies Zwart, S. F., Baumgardt, H., Hut, P., Makino, J., & McMillan, S. L. W. 2004, *Nature*, 428, 724
 Portegies Zwart, S. F., Baumgardt, H., McMillan, S. L. W., Makino, J., Hut, P., & Ebisuzaki, T. 2006, *ApJ*, 641, 319
 Rauch, K. P., & Ingalls, B. 1998, *MNRAS*, 299, 1231
 Rauch, K. P., & Tremaine, S. 1996, *NewA*, 1, 149
 Rees, M. J. 1988, *Nature*, 333, 523
 Rupen, M. P. 1997, in *ASP Conf. Ser. 116, The Nature of Elliptical Galaxies*, ed. M. Arnaboldi et al. (San Francisco: ASP), 322
 Schaller, G., Schaerer, D., Meynet, G., & Maeder, A. 1992, *A&AS*, 96, 269
 Schödel, R., Eckart, A., Iserlohe, C., Genzel, R., & Ott, T. 2005, *ApJ*, 625, L111
 Sellwood, J. A. 2002, in *The Shapes of Galaxies and Their Dark Halos*, ed. P. Natarajan (Singapore: World Scientific), 123
 Serabyn, E., & Morris, M. 1996, *Nature*, 382, 602
 Shields, G. A., Gebhardt, K., Salviander, S., Wills, B. J., Xie, B., Brotherton, M. S., Yuan, J., & Dietrich, M. 2003, *ApJ*, 583, 124
 Spitzer, L. 1987, *Dynamical Evolution of Globular Clusters* (Princeton: Princeton Univ. Press)
 Spitzer, L., Jr., & Schwarzschild, M. 1951, *ApJ*, 114, 385
 ———. 1953, *ApJ*, 118, 106

- Sternberg, A., Hoffmann, T. L., & Pauldrach, A. W. A. 2003, *ApJ*, 599, 1333
Stolte, A., Brandner, W., Grebel, E. K., Lenz, R., & Lagrange, A.-M. 2005, *ApJ*, 628, L113
Villumsen, J. V. 1983, *ApJ*, 274, 632
———. 1985, *ApJ*, 290, 75
Vollmer, B., Zylka, R., & Duschl, W. J. 2003, *A&A*, 407, 515
Young, P. 1980, *ApJ*, 242, 1232
Young, P. J. 1977, *ApJ*, 215, 36
Yu, Q., & Tremaine, S. 2003, *ApJ*, 599, 1129
Zhao, H., Haehnelt, M. G., & Rees, M. J. 2002, *NewA*, 7, 385

ERRATUM: “MASSIVE PERTURBER–DRIVEN INTERACTIONS BETWEEN STARS
AND A MASSIVE BLACK HOLE” (ApJ, 656, 709 [2007])

HAGAI B. PERETS, CLOVIS HOPMAN, AND TAL ALEXANDER
Faculty of Physics, Weizmann Institute of Science, POB 26, Rehovot 76100, Israel

There is an error in the plotted cumulative mass function of the giant molecular clouds in Figure 2 (top panel, two rightmost curves). Due to a misinterpretation of the mass estimates in Table 1 of T. Oka et al. (ApJ, 562, 348 [2001]), Figure 2 includes 12 (out of 60) data points that are multiple entries for the same clouds, expressing alternative mass estimation assumptions (we thank R. O’Leary for pointing this out and T. Oka for clarifying the issue). The corrected observed ratio of second moments of the mass function μ_2 in Table 2 should be modified downward to 10^8 for model GMC1 and to 10^6 for model GMC2. However, the analytic power-law fit for the mass function that was actually used in the numerical calculations was very conservative to begin with, and still conservatively underestimates μ_2 by a factor of 2. Therefore, the results presented in the paper remain unchanged.

Chapter 3

Massive perturbers and the efficient coalescence of binary massive black holes

Perets & Alexander

The Astrophysical Journal, Volume 677, Issue 1, pp. 146-159 (2008)

MASSIVE PERTURBERS AND THE EFFICIENT MERGER OF BINARY MASSIVE BLACK HOLES

HAGAI B. PERETS AND TAL ALEXANDER¹

Faculty of Physics, Weizmann Institute of Science, P.O. Box 26, Rehovot 76100, Israel;
 hagai.perets@weizmann.ac.il, tal.alexander@weizmann.ac.il

Received 2007 May 15; accepted 2007 December 3

ABSTRACT

We show that dynamical relaxation in the aftermath of a galactic merger and the ensuing formation and decay of a binary massive black hole (MBH) are dominated by massive perturbers (MPs) such as giant molecular clouds or clusters. MPs accelerate relaxation by orders of magnitude compared to two-body stellar relaxation alone, and efficiently scatter stars into the binary MBH’s orbit. The three-body star-binary MBH interactions shrink the binary MBH to the point where energy losses from the emission of gravitational waves (GWs) lead to rapid coalescence. We model this process based on observed and simulated MP distributions and take into account the decreased efficiency of the star-binary MBH interaction due to acceleration in the galactic potential. We show that mergers of gas-rich galactic nuclei lead to binary MBH coalescence well within the Hubble time. Moreover, lower mass binary MBHs ($<10^8 M_\odot$) require only a few percent of the typical gas mass in a postmerger nucleus to coalesce in a Hubble time. The fate of a binary MBH in a gas-poor galactic merger is less certain, although massive stellar structures (e.g., clusters, stellar rings) could likewise lead to efficient coalescence. These coalescence events are observable by their strong GW emission. MPs thus increase the cosmic rate of such GW events, lead to a higher mass deficit in the merged galactic core, and suppress the formation of triple-MBH systems and the resulting ejection of MBHs into intergalactic space.

Subject headings: black hole physics — galaxies: clusters: general — galaxies: nuclei — stars: kinematics

Online material: color figures

1. INTRODUCTION

There is compelling evidence that massive black holes (MBHs) exist in the centers of most galaxies (Ferrarese & Merritt 2000; Gebhardt et al. 2003; Shields et al. 2003). It is believed that galaxies grow by successive mergers, during which the two MBHs sink to the center of the newly formed galaxy by dynamical friction and form a “hard” binary MBH (BMBH) (Begelman et al. 1980) with a semimajor axis of

$$a_h = \left[Q / (1 + Q)^2 \right] r_h(M_{12}) / 4, \quad (1)$$

where $M_{12} = M_1 + M_2$ is the mass of the binary, $Q \equiv M_2/M_1 \leq 1$ is the mass ratio, and $r_h(M_{12})$ is the radius of dynamical influence of the BMBH,² where typically $a_h \sim 1\text{--}10$ pc. After the BMBH hardens, it continues to shrink by losing energy and angular momentum to stars, which are ejected from the system (the “slingshot effect”; Saslaw et al. 1974), or to gas, with which it interacts dynamically. Once the separation further decreases by 2–3 orders of magnitude, the BMBH rapidly decays by the emission of gravitational waves (GWs) until the two MBHs coalesce.

In mergers induced by interactions with stars, the merger time-scale depends on the rate at which new stars are supplied to BMBH-crossing orbits (“loss cone” trajectories). Simulations show that this supply rate is typically not high enough; the BMBH stalls before reaching a separation small enough for efficient decay by GW emission, and fails to coalesce in a Hubble time, t_H (e.g., Berczik et al. 2005; see review by Merritt & Milosavljević 2005).

This result appears to contradict the circumstantial evidence that most galactic nuclei contain only a single MBH (Berczik et al. 2006; Merritt & Milosavljević 2005), and furthermore, it implies few such very strong GW sources, which future GW detectors, such as the *Laser Interferometric Space Antenna (LISA)*, hope to detect.

Several mechanisms have been suggested as means of accelerating BMBH coalescence (see Merritt et al. 2007 for a recent overview and discussion), either involving interactions with stars (“dry mergers”) or with gas (“wet mergers”). These include re-ejection of stars that had a previous interaction with the BMBH but were not ejected from the galactic core (Milosavljević & Merritt 2003; Berczik et al. 2005), BMBHs embedded in dense gas (e.g., Ivanov et al. 1999; Escala et al. 2005; Dotti et al. 2007), interactions of the BMBH with a third MBH (Makino & Ebisuzaki 1994; Blaes et al. 2002; Iwasawa et al. 2006), and accelerated BMBH coalescence due to accelerated loss cone replenishment in nonaxisymmetric potential (Yu 2002; Berczik et al. 2006) or in a steep cusp (Zier 2006, 2007). It is still unclear whether these mechanisms are efficient enough, or whether they occur commonly enough to solve the stalling problem. Efficient direct interaction with gas requires the BMBH to be embedded in a very dense massive central gas concentration. However, it is unknown whether such amounts of gas exist there. For example, the central ~ 2 pc of the Galactic center (GC) are gas-depleted (Christopher et al. 2005), and other galaxies also show central gas cavities in their nuclei (Sakamoto et al. 1999). The gas may also be dispersed by the accreting BMBH before the merger is completed (Merritt & Milosavljević 2005), and may not be efficient for minor mergers (Escala et al. 2005, but see Dotti et al. 2007). It is likewise unknown whether the nonaxisymmetric potential assumed by the dry-merger scenario of Berczik et al. (2006) is generally present in the postmerger galaxy on the relevant scales. Even if that is the case, actual demonstration of rapid BMBH

¹ The William Z. and Eda Bess Novick career development chair.

² Defined here as the radius that encloses a stellar mass of $2M_{12}$ (Merritt & Szell 2006). The threshold semimajor axis for a hard BMBH is sometimes defined in terms of σ^2 , the typical velocity dispersion in the center; $a_h = GM_1M_2\mu/4\sigma^2$, where $\mu = M_1M_2/M_{12}$ is the reduced mass. However, this is ill defined, since σ^2 usually varies with distance from the BMBH.

TABLE 1
OBSERVED AND SIMULATED PROPERTIES OF MASSIVE PERTURBERS

MP Type	M_p (M_\odot)	Mass Profile	$\langle M_p^{2/3} \rangle$ (M_\odot)	R_p (pc)	References
GMCs in the GC	10^4 – 10^8	Power law ($\beta = 1.2$)	4×10^5	5	Oka et al. (2001); Güsten & Philipp (2004); Perets et al. (2007)
Young clusters in the GC	10^3 – 10^5	Power law ($\beta = 1.2$)	3×10^4	1	Figer et al. (1999, 2002); Maillard et al. (2004); Borissova et al. (2005); Perets et al. (2007)
Globular clusters in the Galaxy.....	$10^{2.5}$ – $10^{6.5}$	Log normal	1.9×10^5	5	Mandushev et al. (1991)
Young clusters in galaxies.....	$10^{4.5}$ – $10^{6.5}$	Power law ($\beta = 2$)	4.3×10^5	3	Zhang & Fall (1999); Kravtsov & Gnedin (2005); Larsen (2006)

coalescence still awaits future N -body simulations with realistically high N (Berczik et al. 2006).

Here we explore another possibility likely to apply in most mergers: BMBH coalescence driven by massive perturbers (MPs), such as giant molecular clouds (GMCs) or stellar clusters, in the postmerger galaxy. MPs accelerate relaxation and scatter stars into the BMBH orbit at high rates. Efficient relaxation by MPs was first suggested by Spitzer & Schwarzschild (1951, 1953) to explain stellar velocities in the galactic disk. MPs remain an important component in modern models of galactic disk heating (see e.g., Villumsen 1983, 1985; Lacey 1984; Jenkins & Binney 1990; Hänninen & Flynn 2002, and references therein). A similar mechanism was proposed to explain the spatial diffusion of stars in the inner Galactic bulge (Kim & Morris 2001). In addition to dynamical heating, efficient relaxation by MPs was suggested as a mechanism for loss cone replenishment and relaxation, both in the context of the scattering of Oort cloud comets to the Sun (Hills 1981; Bailey 1983) and the scattering of stars to a MBH in a galactic nucleus (Zhao et al. 2002). Zhao et al. (2002) also noted the possibility of increased tidal disruption flares and accelerated MBH binary coalescence due to MPs. Recently, Perets et al. (2007, hereafter Paper I) studied in detail MP-driven interactions of single and binary stars with a single MBH.

In this study we apply the methods developed in Paper I to investigate MP-driven interactions of stars with a BMBH and the consequences for BMBH coalescence. We explore different MP populations and merger scenarios based on the available observations and simulations, and estimate the BMBH coalescence rate. We also discuss additional implications: the mass deficit in the galactic cores and the suppression of triple-MBH formation in galactic mergers.

This paper is organized as follows. We begin with a general overview of our calculations and the new results (§ 2). In § 3, we briefly summarize the physics of MP-driven loss cone replenishment, which are derived in detail in Paper I. The observations and theoretical predictions of MPs in the inner hundreds of pc of galactic nuclei are reviewed in § 4 and used to construct the MP models used in our calculations in § 5. In § 6, we briefly review

the dynamics of BMBH mergers; a detailed technical discussion is presented in Appendices A and B. We then present our procedure for modeling the dynamical evolution of the BMBH coalescence under various assumptions in § 6 and analyze the results of our calculations in § 7. We explore their implications in § 8 and discuss and summarize our results in § 9.

2. OVERVIEW OF THE CALCULATIONS AND NEW RESULTS

This paper presents a first detailed study of the impact of MPs on BMBH mergers. In this section, we give an overview of the methods, calculations, and modeling that we use to study the dynamics of BMBH mergers by MP-induced slingshot events, and to estimate the merger timescale and the associated mass ejection from the nucleus. These are described in detail in §§ 3–6 and in the appendices. We then briefly list the new results derived here and their implications. These are described and discussed in detail in §§ 7 and 8.

MPs shorten the BMBH merger timescale by accelerating the supply rate of stars to the loss cone (see § 3). The application of loss cone theory to the BMBH merger problem requires a model of the MP properties: their mass, size, number, and spatial distributions. We review the available observations and numerical simulations of MPs in merging galaxies of different morphological types (§ 4, Tables 1 and 2). We then construct a few generic models for various types of merger scenarios, with and without MPs, based on these data and on theoretical results (§ 5, Table 3).

To evolve the BMBH in time in the context of a given merger scenario (defined by a BMBH mass ratio and a MP model; see § 6), we execute the following steps. (1) We establish the BMBH's initial semimajor axis at the stalling point, where two-body stellar relaxation can no longer efficiently resupply the loss cone. The stalling radius is estimated semianalytically by the formulas derived in Appendix A, which are based on the N -body simulations of Merritt (2006). (2) At each time step, we calculate the rate at which stars are scattered into the loss cone by MPs from all radii, taking into account the BMBH's instantaneous separation (Paper I; § 3). (3) We calculate the hardness of the encounter (the ratio between

TABLE 2
MASS FRACTION OF OBSERVED AND PREDICTED MASSIVE PERTURBERS IN GALACTIC NUCLEI

Galaxy	MP Type	$M_p^{\text{tot}}/M_{\text{dyn}}$	References
Milky Way	GMCs	$\text{few} \times 0.1$	Oka et al. (2001); Güsten & Philipp (2004)
	Clusters	10^{-4}	Figer et al. (1999, 2002); Maillard et al. (2004); Borissova et al. (2005)
Spirals.....	GMCs	0.1–0.3	Koda et al. (2005); Güsten & Philipp (2004); Sakamoto et al. (1999); Young & Scoville (1991)
Elliptical mergers (Sim.).....	Clusters	0.2^a	Li et al. (2004); Prieto & Gnedin (2006)
Ellipticals (Obs.).....	GMCs	10^{-3} – 10^{-2}	Rupen (1997); Knapp (1999)
ULIRGs.....	GMCs	0.3–0.6	Sanders & Mirabel (1996)
Merger (Obs.).....	GMCs	0.3–0.6	Evans et al. (2002); Sakamoto et al. (2006); Cullen et al. (2007)
Merger (Sim.).....	GMCs	0.3–0.6	Barnes & Hernquist (1992)

^a Assumed, based on simulations. See text.

TABLE 3
MASSIVE PERTURBER MODELS IN GALACTIC MERGERS

Merger Model	Q	r/r_h^a	$M_p^{\text{tot}}/M_{\text{dyn}}^{\text{tot}}$	M_p (M_\odot)	β^b	R_p (pc)	μ_2^c
Major.....	1	2–30	1/2	$5 \times 10^4 - 1 \times 10^7$	1.2	5	3×10^7
Minor.....	0.05	2–30	1/3	$5 \times 10^4 - 1 \times 10^7$	1.2	5	5×10^6
Elliptical.....	1	2–30	1/5	$1 \times 10^5 - 1 \times 10^7$	2	3	5×10^5
Stars.....	...	1–30	1	1	...	0	1

^a Spatial extent of the MP distribution, assuming $N_p(r) \propto r^{-2}$.

^b Assuming $dN_p/dM_p \propto M_p^{-\beta}$.

^c $\mu_2 \equiv N_p \langle M_p^2 \rangle / N_* \langle M_*^2 \rangle$, where $\langle M^2 \rangle = \int M^2 (dN/dM) dM / N$.

the encounter velocity and the BMBH orbital velocity) due to the acceleration of the infalling star in the galactic potential, as derived in Appendix B2. This effect, which has been neglected in previous studies, significantly decreases the energy extraction efficiency of the encounter. (4) We estimate the average amount of BMBH orbital energy extracted by the interaction with the stars scattered into the loss cone. This is based on numerical experiments of isolated three-body encounters (Quinlan 1996, hereafter Q96), which are adapted in Appendix B1 to take into account the changing hardness of the encounter in the course of the BMBH evolution. (5) We include the energy extraction by GW emission, which increasingly dominates the last stages of the merger. (6) We update the BMBH semimajor axis according to the extracted energy by both the slingshot effect and GW emission. (7) We end the dynamical calculation when the emitted GW power exceeds that extracted by dynamical interactions, and the BMBH enters the final rapid GW-induced decay phase leading to coalescence.

Our new results and their implications are as follows. (1) The inferred properties and numbers of MPs in postmerger galactic nuclei are high enough to effectively reduce the relaxation times there by orders of magnitude. Consequently, BMBH decay due to MP-induced dynamical interactions with stars is efficient enough in most mergers to lead to coalescence within a Hubble time (typically within $10^8 - 10^9$ yr), thereby solving the “last parsec” problem. The rates of GW emission from BMBH coalescence should thus trace the galactic merger rates. (2) Since the MP-induced dynamical phase of BMBH mergers is rapid, we predict that most BMBHs will be observed either electromagnetically at separations larger than the hardening radius (>1 pc) or by GW emission at much smaller separations (typically $\ll 1$ pc) during the GW-dominated decay phase. (3) In most cases the BMBH coalescence takes less than the typical time between major galactic mergers. Therefore, the formation of triple MBHs through multiple galactic mergers is unlikely, and ejection of MBHs from unstable triples should be rare. (4) The ejection of stars by the slingshot effect removes mass from the galactic core (“mass deficit”). The more the BMBH can decay, the larger the total ejected mass. The spatial scale of the deficit reflects the origin of the scattered stars. We point out that the magnitude and spatial extent of the deficit can be used to discriminate between merger mechanisms. Specifically, the MP-induced BMBH merger mechanism predicts a larger mass deficit over a larger spatial extent than that due to stalled mergers by stellar relaxation alone.

3. LOSS CONE REFILLING BY MASSIVE PERTURBERS

In Paper I, we presented a detailed quantitative analysis of the MP-induced resupply of stars to nearly radial, “loss cone” orbits, which bring them within some threshold distance q from the central mass (MBH or BMBH), where they undergo a strong inter-

action with it (“event”) and are thereby removed (scattered or destroyed). We showed that the resupply rate by MPs is orders of magnitude faster than that by stellar two-body relaxation alone. This translates to an accelerated rate of close interactions with the central object. Here we present a brief qualitative summary of the results of Paper I and their implications.

A star with orbital energy in the range $(E, E + dE)$ on a nearly radial loss cone orbit with angular momentum $J < J_{\text{lc}}$ will reach the MBH and be removed in about a single dynamical (or orbital) time $P(E)$. When the resupply rate of such stars is slower than the rate at which they are removed ($\sim 1/P$), the phase-space region $(dE, J < J_{\text{lc}})$ is nearly empty of stars. Conversely, when the resupply rate is higher than $1/P$, that phase-space region is nearly full, and its phase-space distribution is nearly isotropic. At that point the rate at which stars with energy E interact with the central mass reaches its maximal value; further scattering cannot increase the rate. When the resupply of stars is driven by stellar two-body relaxation, tightly bound regions of phase space (high E , small typical r) are empty, since the angular size of the loss cone is large, the period is short, and removal is fast. Conversely, loosely bound regions (low E , large typical r) are full. Most of the contribution to the total resupply rate comes from stars with energies near the transition between the empty and full loss cone regimes, where $P \sim t_r$, the relaxation time (Frank & Rees 1976; Lightman & Shapiro 1977). This simple picture changes when MPs dominate relaxation, because their distribution does not necessarily follow that of the stars, and their properties (mass, size) may change with distance from the center.

MPs of mass M_p and space density n_p dominate dynamical relaxation over scattering by stars of mass M_* and space density n_* when the ratio of the second moments of the mass distributions satisfies $\mu_2 \equiv n_p M_p^2 / n_* M_*^2 \gtrsim t_r^* / t_r^{\text{MP}} \gg 1$. The quantity μ_2 thus expresses the MP enhancement factor of the relaxation time-scale up to the ratio of the Coulomb logarithms for star-star and star-MP scatterings, which takes into account the extended size of the MPs. This can be shown by considering first close encounters at the “capture radius” $r_c \sim GM_p/v^2$, where v is the typical relative velocity. The “ $nv\Sigma$ ” rate of such encounters with a test star is then $t_r^{-1} \sim nvr_c^2 \propto n_p M_p^2/v^3$. Integration over all encounter distances further decreases the relaxation time by a Coulomb logarithm factor that depends on the size of the system and, if $R_p > r_c$, also on R_p , the size of the MP.³ The impact of fast, MP-induced relaxation on the rate at which stars enter the loss cone can be incorporated into standard loss cone theory (e.g., Lightman & Shapiro 1977; Young 1977) by replacing the relaxation time due to scattering by stars with that due to MPs, with

³ For example, on a scale of $r \sim 50$ pc, where the velocity dispersion is $\sigma \sim \mathcal{O}(100 \text{ km s}^{-1})$ and for MPs of typical size $R_p \sim 5$ pc, $\Lambda_* \sim r\sigma^2/GM_*$, $\Lambda_{\text{MP}} \sim r/R_p$, and $\log \Lambda_*/\log \Lambda_{\text{MP}} \sim 8$.

the only modification being the separate treatment of rare scattering events.

The effect of MPs on the BMBH loss cone depends on the typical distance from the center and on the BMBH's stage of dynamical evolution. Far from the BMBH, MPs fill the loss cone and drive the resupply rate to its maximal value, while closer to the BMBH, even MPs cannot fill the loss cone, although they still increase the supply rate by a large factor of $\sim \mu_2$. Closer still, the tidal field of the BMBH gradually limits the size and mass of the MPs to the point at which stellar relaxation re-emerges as the dominant relaxation mechanism (see Fig. 3 in Paper I). The demarcation between the full and empty loss cone regions changes with time as the BMBH decays, the size of the loss cone decreases, and the empty loss cone region contracts. Irrespective of these details, the overall effect of MPs is to dramatically increase the loss cone resupply rate over what would be expected from slow stellar two-body relaxation alone.

We calculate the loss cone resupply rate with some simplifying approximations. We assume a spherically symmetric distribution, the *Ansatz* $E \leftrightarrow GM(<r)/2r$, and the Keplerian expression for the orbital period $P(E)$. We also make the conservative assumption that one class of massive perturbers dominates relaxation, and neglect the contributions from other mass components (e.g., stars). The full expressions for the supply rates of stars deflected from a typical radius r in the empty loss and full loss cone regimes (§ 2 in Paper I) can be respectively approximated by

$$\begin{aligned} \frac{d\Gamma_e}{d \log r} &\sim \frac{N_*(<r)}{\log(r/q)t_r}, \\ \frac{d\Gamma_f}{d \log r} &\sim \frac{q}{r} \frac{N_*(<r)}{P(r)}, \end{aligned} \quad (2)$$

where $N_*(<r)$ is the number of stars enclosed within r , and where the dependence on the MP's properties enters through the relaxation time, $t_r = t_r^{\text{MP}} \propto \mu_2 t_r^*$. The total loss cone refilling rate is then given by integrating over the contributions from all radii, taking into account the fact that the refilling rate does not exceed the full loss cone rate,

$$\Gamma(q) = \int \frac{d\Gamma(q)}{dr} dr = \int \min \left[\frac{d\Gamma_e(q)}{dr}, \frac{d\Gamma_f(q)}{dr} \right] dr. \quad (3)$$

In the context of BMBH decay, the rate (eq. [3]) implicitly depends on time through the evolution of $q = a(t)$, and the rate, in turn, affects the evolution of a through the BMBH evolution equation (eq. [7], below). The BMBH is evolved in time by iterative numerical integration of the coupled rate and evolution equations.

The effects of MPs are significant in situations where perturbations by stars alone are not efficient enough to refill the loss cone on the orbital timescale. MPs are most effective for large- q processes, such as close interactions between binaries and a single MBH (where q is the tidal disruption radius of the binary), or interactions of single stars with a BMBH (where q is the BMBH's semimajor axis). This is because the larger q is, the lower is the empty loss cone refilling rate relative to that needed to completely fill the loss cone [i.e., $\Gamma_e/\Gamma_f \propto (r/q)/\log(r/q)$ is a decreasing function of q for $r/q \gg 1$; see eq. (2)].

4. MASSIVE PERTURBERS IN GALACTIC NUCLEI

The space density of MPs is much smaller than that of stars, so to dominate relaxation ($\mu_2 \gg 1$) they must be significantly more massive. Here we consider only MPs with masses $M_p \geq 10^4 M_\odot$,

such as stellar clusters and GMC gas clumps. Intermediate-mass black holes (IMBHs) could be very effective MPs, but these are not considered here, since it is still unclear whether they actually exist. A summary of the observed properties of MPs and those derived from simulations is presented in Tables 1 and 2.

The lifespan of a single MP is affected by many factors, such as collisions with other MPs or the central galactic tidal field, which can disrupt them if they approach the center on an eccentric orbit or sink there by dynamical friction. GMCs can also be dispersed by strong radiation from stars and by supernovae. Thus, individual MPs are not expected to survive much longer than a few local dynamical times, a time substantially shorter than the galactic merger timescale (roughly the galactic dynamical time), which in turn may be much shorter than the time required for a BMBH merger. However, MPs do not have to exist individually much longer than a local dynamical time to have a strong effect on relaxation. It is sufficient that the overall MP population maintain a steady state by the continuous formation or supply of new MPs to replace those destroyed. There is both observational and theoretical support for the long-term persistence of large populations of MPs in galactic nuclei.

Observation of the GC indicates the steady state existence of a large population of short-lived MPs over a Hubble time. As reviewed in detail in Paper I, observations of dense gas in the central ~ 100 pc of the GC reveal $N_p \sim 100$ GMCs with a typical mass of $\langle M_p \rangle \sim 10^5 M_\odot$ (Table 1) (Oka et al. 2001). GMCs and young stellar clusters are stages in the path of star formation, and so the star formation rate can be used to estimate the MP mass supply rate. Figer et al. (2004) show that the star formation history in the central projected 30 pc of the GC is well described by continuous star formation over 10 Gyr at a rate of $0.02 M_\odot \text{ yr}^{-1}$. Extrapolated out to 100 pc in the $n_* \sim r^{-2}$ stellar distribution of the inner bulge, this corresponds to $dM_*/dt \sim 0.05 M_\odot \text{ yr}^{-1}$. Since the mean star formation efficiency (fraction of mass turned into stars) is on average very low, $f_* \sim \text{few} \times 0.01$ (Myers et al. 1986), the star formation rate translates to an MP mass supply rate of $dM/dt \sim (dM_*/dt)/f_* \sim \mathcal{O}(1 M_\odot \text{ yr}^{-1})$, and an MP formation or supply rate of

$$\Gamma_p \sim \frac{dM/dt}{\langle M_p \rangle} \sim 5 \times 10^{-5} \text{ yr}^{-1} \left(\frac{f_*}{0.01} \right)^{-1} \left(\frac{\langle M_p \rangle}{10^5 M_\odot} \right)^{-1}. \quad (4)$$

The mean lifetime of such GMCs is then

$$t_p \sim \frac{N_p}{\Gamma_p} \sim 2 \times 10^6 \text{ yr} \left(\frac{f_*}{100} \right) \left(\frac{\langle M_p \rangle}{10^5 M_\odot} \right) \left(\frac{N_p}{100} \right), \quad (5)$$

which is comparable to the dynamical timescale at ~ 100 pc. We therefore conclude that the observed MPs in the GC, together with the inferred star formation rate and history, are fully consistent with such a steady state MP population persisting over a Hubble time.

Simulations of gas in galactic nuclei also show highly inhomogeneous quasi-steady state conditions, with a very broad mass spectrum extending over ~ 7 orders of magnitude (Wada 2001; Wada & Norman 2001). The nuclear MP population in the Galaxy is probably representative of that in the nuclei of other spiral galaxies, where similar amounts of dense gas are observed (Koda et al. 2005; Sakamoto et al. 1999; Young & Scoville 1991). Furthermore, estimates of the gas supply timescales for starbursts in other galaxies also suggest continuous gas supply over 10^8 – 10^9 yr (Leitherer 2001).

The MP contents in the nuclei of postmerger galaxies are expected to be still larger than in the Galaxy, which does not appear to have undergone a recent major merger. This is indeed observed in ULIRGS (Sanders & Mirabel 1996), in merging galaxies (Evans et al. 2002; Sakamoto et al. 2006; Cullen et al. 2007), and also in simulations (Barnes & Hernquist 1992).

We now turn to a detailed discussion of the observed and inferred properties of MPs in galactic nuclei of different types. These form the basis of the MP models used in our numerical analysis of BMBH mergers.

4.1. Massive Perturbers in Spiral Galaxies

The ~ 100 GMCs observed in the GC, with masses in the range $10^4 - 10^7 M_\odot$, contain a few $\times 0.01$ of the total dynamical mass on the few $\times 100$ pc scale and a few $\times 0.1$ in the central ~ 100 pc (see Paper I for an extended discussion of the properties of MPs in our GC). In contrast, the central ~ 2 pc of the GC contain negligible amounts of gas. Single molecular clouds cannot be resolved in the nuclei of other spiral galaxies, but the total fraction of gas and its distribution are usually quite similar to those observed in the GC (e.g., Sakamoto et al. 1999; Sawada et al. 2004; see review by Henkel et al. 1991). CO observations show that the gas contains very dense large clumps that account for up to $\lesssim 50\%$ of the total gas contents in these regions (Downes et al. 1993; Downes & Solomon 1998).

In addition to GMCs, many globular clusters (Friel 1995; Ashman & Zepf 1998) and open clusters may, in the course of their evolution, spiral into the galactic nucleus, or form inside it (e.g., Gnedin et al. 1999). For example, the Galaxy contains hundreds of $\sim 10^3 M_\odot$ open clusters and a few $\times 10^5 M_\odot$ globular clusters (Meylan & Mayor 1991; Friel 1995). Many more are observed in other galaxies (Ashman & Zepf 1998). If some of these clusters contain IMBHs, they will contribute to the MP population even after the disruption of the host cluster (Ebisuzaki et al. 2001; Miller & Hamilton 2002), and will sink all the way to the center.

4.2. Massive Perturbers in Elliptical Galaxies

The gas fraction in elliptical galaxies is typically 10–100 times smaller than in spiral galaxies (Rupen 1997; Knapp 1999). However, in some elliptical galaxies, it is comparable to or even larger than that in spirals. Such gas-rich ellipticals are thought to have been formed recently in a merger of two late-type galaxies (e.g., Wiklind et al. 1997). In particular, ultraluminous infrared galaxies (ULIRGs; see review by Sanders & Mirabel 1996) have extreme amounts of gas, 10–100 times more than in the Galaxy, and can have as much gas mass as stellar mass, or even more. Elliptical galaxies may well be evolved merger products, where most of the dense gas in the core has formed stars (e.g., Bender & Saglia 1999). In that case, it is plausible that the main type of MPs would be the stellar clusters that were born from the GMCs, rather than the GMCs themselves. Observations of stellar rings and disks in the cores of elliptical galaxies indeed suggest that present-day stellar structures reflect earlier gaseous structures (Downes & Solomon 1998). This is also consistent with the fact that ellipticals have larger numbers of globular clusters than spirals, and that mergers are associated with the formation of massive clusters (Ashman & Zepf 1998; Zhang & Fall 1999; Kravtsov & Gnedin 2005; Larsen 2006).

4.3. Formation of Massive Perturbers in Galactic Mergers

Simulations of mergers of gas-rich spirals indicate that $\gtrsim 50\%$ of the total gas mass in both galaxies is driven into the central few $\times 100$ pc of the newly formed galaxy (Barnes & Hernquist 1991, 1996), where it probably forms massive clumps. In merg-

ers of two gas-poor ellipticals, stellar clusters may play a similar role. Many of the newly formed stellar clusters will probably survive in the merged nucleus (Portegies Zwart et al. 2002). In addition, many old globular clusters will fall directly into the nucleus in the course of the merger (Gnedin & Prieto 2006) or sink in by dynamical friction (Capuzzo-Dolcetta 1993). While most will probably be disrupted (O. Gnedin 2006, private communication), a significant fraction could survive (e.g., simulations by Miocchi et al. 2006). This central accumulation of young and old stellar clusters could significantly shorten the relaxation time. Further simulations are needed to address these questions quantitatively.

5. MODELING MASSIVE PERTURBER-DRIVEN BMBH COALESCENCE

Based on the observations and simulations described above, we formulate three representative merger scenarios that include MPs, and compare them to a merger scenario in which only stellar two-body relaxation plays a role. The model parameters are listed in Table 3.

The major merger scenario consists of a $Q = 1$ merger of two gas-rich galaxies. It is assumed that the merger triggers a large gas inflow to the center, increasing the amount of gas there to $\sim 1/2$ of the total dynamical mass (~ 5 times more than presently in the center of the Milky Way; the mass of the cold gas in postmerger galaxies can be even higher, but we take into account only the densest regions that correspond to the more massive MPs). It is further assumed that the MPs are similar to massive GMCs in our GC, that they have a power-law mass function, $dN_p/dM_p \propto M_p^{-\beta}$ with $\beta = 1.2$ (see MP model GMC1 in Paper I for details), and that their spatial distribution is isotropic.⁴

The minor merger scenario consists of a $Q = 0.05$ merger between a large, massive gas-rich galaxy and a much smaller galaxy, which only slightly perturbs the large galaxy and triggers only a moderate gas inflow into the center. It is assumed that the nuclear gas mass is $\sim 1/3$ of the total dynamical mass (~ 1.5 times more than presently in the center of the Milky Way). The MP properties are the same as in the major merger scenario.

In the elliptical merger scenario we attempt to model a $Q = 1$ merger of two equal-mass, gas-poor elliptical galaxies. We assume that the MPs are mostly stellar systems such as clusters or spiral structures. Lacking secure observations, we model the MPs after results from simulations (Li et al. 2004; Prieto & Gnedin 2006). These simulations show that both the total cluster birthrate and the massive cluster birthrate peak at the center of the galaxy (Li et al. 2004). We assume that the MP mass fraction is 0.2 of the total dynamical mass and that the cluster mass function is a power law with $\beta = 2$ for $10^5 M_\odot \leq M_p \leq 10^7 M_\odot$, following the results of Prieto & Gnedin (2006). Finally, we consider, for comparison, a model that assumes that relaxation in the postmerger galaxy is due to stellar two-body interactions only.

In our calculations we assume that the stellar distribution over the entire relevant distance range can be approximated by a singular isothermal stellar distribution,

$$\rho(r) = \frac{\sigma_\infty^2}{2\pi Gr^2}, \quad (6)$$

where the velocity dispersion σ_∞ , and hence the normalization, is determined by the empirical M_\bullet/σ relation (e.g., Wang &

⁴ While the geometry of the central molecular zone of the Galaxy is flattened, its height of a few $\times 10$ pc implies that it is nearly isotropic on the scale of interest of ~ 100 pc.

Merritt 2004). The MP distribution is assumed to follow the stars down to a minimal radius r_{MP} , where the MPs are destroyed either by the central tidal field, the radiation of the accreting BMBH, or the outflows associated with the accretion or star formation triggered by the merger. The exact value of r_{MP} is uncertain, since the processes involved in the destruction of the MPs are complex, and the inner cusp may be flattened due to previous mergers (Milosavljević et al. 2002). Here it is assumed that $r_{\text{MP}} = 2r_h$.⁵ In the GC, $r_{\text{MP}} \sim 4-8$ pc. At $r > r_{\text{MP}}$, our assumed minimal GMC mass of $5 \times 10^4 M_\odot$ is consistent with observations (Backer & Sramek 1999; Oka et al. 2001). This minimal radius is probably a conservative estimate, since transient dense clumps and dense cluster cores can survive even at smaller distances, as seen in observations in our GC (Christopher et al. 2005), and as found in simulations (Wada & Norman 2001; Portegies Zwart et al. 2003).

6. BMBH MERGER DYNAMICS

A BMBH merger progresses through three stages (see Merritt 2006). (1) First, there is a gradual decay by dynamical friction to the point where the separation between the two MBHs is $r_{12} \sim r_h(M_1)$. (2) Rapid decay then brings about the formation of a bound Keplerian pair [when $r_{12} < r_h(M_1)$], initially by dynamical friction on M_2 and later by the slingshot effect. This is followed by a slowdown of the decay when $a \sim a_h$ and stalling, unless the loss cone is replenished by a process more efficient than diffusion due to two-body relaxation. (3) Ultimately, the BMBH orbital decay rate is dominated by GW emission, leading to final coalescence. The operational definition of the stalling separation a_s at time t_s is the point at which the decay rate sharply decreases. Typically $a_s \sim \mathcal{O}(a_h)$ (see Appendix A).

The slingshot effect occurs when q , the periaapse distance of the star from the BMBH center of mass, is on the order of the BMBH semimajor axis a . Such stars are ejected and lost from the system, either directly or after several repeated interactions with the BMBH, and on average extract energy $\Delta E(q)$ from the BMBH. The evolution of the BMBH energy, or equivalently, the decrease in a , is given by

$$\frac{d}{dt} \left(\frac{GM_1 M_2}{2a} \right) = \int_0^\infty \frac{d\Gamma}{dq} \Delta E(q) dq \equiv \Gamma(a) \langle \Delta E \rangle(a), \quad (7)$$

where $\Gamma(a)$ is the supply rate of stars that approach the BMBH on orbits with $q < a$, and $\langle \Delta E \rangle \propto a^{-1}$ is the appropriately weighted mean extracted energy (Milosavljević & Merritt 2003; Merritt & Milosavljević 2005; see detailed discussion in Appendix B1). It then follows from equation (2) that the dynamical decay rate in the two regimes scales as $\dot{a}_{\text{dyn}} \propto -a/\log(r/a)$ or $\propto -a^2$, respectively, so that in both cases the dynamical hardening rate decreases as a decreases. Note that in the hard BMBH limit ($a \rightarrow 0$), when the loss cone is small and therefore full, $d(1/a)/dt \sim \text{const}$ (Q96).

When the BMBH separation becomes small enough, the orbital decay rate due to GW emission, \dot{a}_{GW} , becomes higher than the dynamical decay rate. We conservatively assume circular BMBHs (eccentric BMBHs coalesce faster in the GW-emission-dominated phase). The decay rate on a circular orbit due to the emission of GW is (Peters 1964)

$$\dot{a}_{\text{GW}} = -\frac{64}{5} \frac{G^3 \mu M_{12}^2}{c^5 a^3}, \quad (8)$$

⁵ Note that the M_\bullet/σ and M_\bullet/M_b relations (M_b is the mass of the bulge, with typical length scale r_b) then imply that $r_{\text{MP}} \propto r_b$.

which increases as a decreases. The time to decay to $a = 0$ from an initial semimajor axis a is

$$t_{\text{GW}} = \frac{5}{256} \frac{c^5}{G^3} \frac{a^4}{\mu M_{12}^2}. \quad (9)$$

Since \dot{a}_{dyn} decreases with a , while \dot{a}_{GW} increases, there exists a transition BMBH separation, a_{GW} , such that $\dot{a}_{\text{dyn}}(a_{\text{GW}}) = \dot{a}_{\text{GW}}(a_{\text{GW}})$. Once the BMBH shrinks to a_{GW} , the coalescence is inevitable as long as $t_{\text{GW}}(a_{\text{GW}}) < t_h$ and as long as the BMBH remains unperturbed. The total time from the hardening semimajor axis a_h to the coalescence is then

$$t_c = t_{\text{dyn}}(a_h \rightarrow a_{\text{GW}}) + t_{\text{GW}}(a_{\text{GW}} \rightarrow 0). \quad (10)$$

The dynamical decay timescale $t_{\text{dyn}}(a_h \rightarrow a_{\text{GW}})$ is on the order of the time it takes the BMBH to intercept and interact with stars whose total mass equals its own, $t_{\text{dyn}} \sim M_{12}/[M_\bullet \Gamma(a_{\text{GW}})]$, where Γ is evaluated at a_{GW} , where the rate is slowest.⁶ This estimate neglects the possibility that a fraction of the stars are not ejected from the loss cone, but return to interact again with the BMBH. This can further accelerate the decay, but is not enough in itself to prevent stalling (Milosavljević & Merritt 2003).

In order to calculate the MP-induced coalescence time, it is necessary to compute both the rate at which stars are scattered by MPs into the BMBH and the energy they extract from the BMBH. Based on results from three-body scattering experiments (Hills 1983; Q96; Sesana et al. 2006, 2007), we assume that a star whose periaapse distance q from the BMBH's center of mass is smaller than the BMBH separation a interacts strongly with the MBH and is then ejected from the system. We omit the possibility of re-ejection, and we neglect soft scattering events ($q > a$) since these are inefficient in extracting energy from the BMBH (see Sesana et al. 2006 and Appendix B1). We thus obtain a conservative upper limit on the coalescence time.

Beginning with a hard BMBH of separation $a(t=0) = a_s$ (Appendix A), we define the time-dependent loss cone periaapse as $q = a(t)$ and calculate the loss cone rate $\Gamma(q)$ using the methods described in Paper I and summarized here in § 2. We follow the evolution of the BMBH separation by numerically integrating the evolution equation with time steps small enough such that $da \ll a$ (see Milosavljević & Merritt 2003 and Sesana et al. 2006, 2007 for a similar approach) until the orbital decay is dominated by GW emission (eq. [10]), which is effectively the coalescence time t_c . In simplified notation, the evolution equation (eq. [B15]) is

$$\frac{d \log a}{dt} = -2 \frac{M_\bullet}{M_{12}} \int \bar{C}(a, r) \frac{d\Gamma(a)}{dr} dr, \quad (11)$$

where $d\Gamma/dr$ is the differential loss cone replenishment rate, and \bar{C} is the mean value of the dimensionless energy, $C \equiv M_{12} \Delta E / 2M_\bullet E_{12}$, exchanged between the scattered star and the BMBH (see detailed derivation and numeric estimation in Appendix B1; $C = 1$ corresponds to the case where the specific energy carried

⁶ Every star that passes near the binary MBH extracts from it binding energy on the order of $M_\bullet \varepsilon_{12}$, where $\varepsilon_{12} = G\mu/2a$ is the specific energy of the BMBH, so that $dE = -GM_1 M_2 / 2a^2 da = (M_\bullet G\mu/2a) \Gamma(a) dt$. Integrating between $a_h \gg a_{\text{GW}}$, with $\Gamma(a) \sim |(a/r) N_\star(<r)/P(r)|_{r_{\text{MP}}}$ (when the loss cone is filled by MPs that orbit as close as r_{MP} from the MBH) yields $t_{\text{dyn}} \simeq M_{12}/M_\bullet \Gamma(a_{\text{GW}})$.

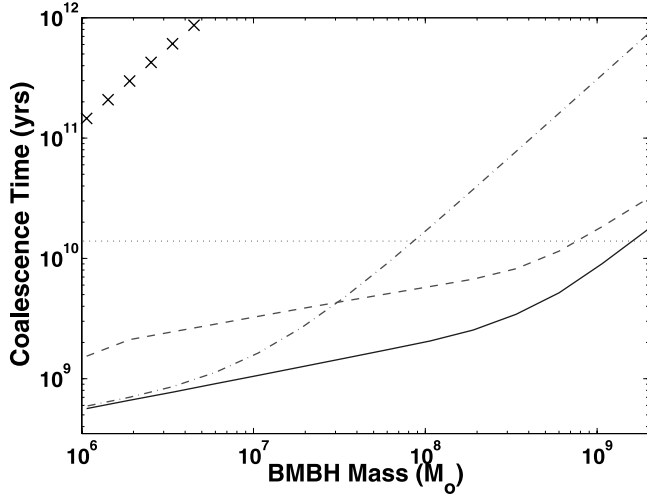


FIG. 1.—Dynamical decay times, t_{dyn} , of BMBHs from a_h to a_{GW} as a function of the BMBH mass (the time to final GW-induced decay, t_{GW} , from a_{GW} to $a = 0$ is negligible compared to the initial dynamical decay phase). Different merger scenarios are shown (Table 3): major mergers (solid line), minor mergers (dashed line), and elliptical mergers (dash-dotted line). Without MPs (crosses, for $Q = 1$), the decay times are longer than the age of the universe (horizontal line) for all BMBH mass in this range. [See the electronic edition of the Journal for a color version of this figure.]

by the star equals twice that of the BMBH). The quantity $\bar{C}(a, r)$ depends on the hardness parameter of the encounter $\zeta \equiv \sigma(r)/V_{12}(a)$, defined as the ratio between the typical initial velocity of the scattered star far from the BMBH, $\sigma(r)$, and the orbital velocity of the BMBH, $V_{12} = (GM_{12}/a)^{1/2}$. An additional r -dependence is introduced by the acceleration of the star toward the BMBH by galactic potential, which increases the relative velocity between the BMBH and the star at the point of encounter beyond what it would have been if the star fell toward an isolated BMBH (see Appendix B2), and decreases the efficiency of the slingshot effect (Fig. 3). This non-negligible effect, taken into account here, was neglected in previous estimations of the BMBH coalescence times (Sesana et al. 2006; Q96).

7. RESULTS

Figure 1 shows the total decay time of BMBHs in the mass range $M_{12} = 10^6 - 10^9 M_\odot$ for different merger scenarios. Stellar two-body relaxation cannot replenish the loss cone fast enough. In the absence of MPs, the merger proceeds in the empty loss cone regime, where the timescale is set by the slow relaxation time (eq. [2]), leading to merger times orders of magnitude longer than t_H . In contrast, when the MP number density is high enough, or when the loss cone is small enough (lower BMBH mass), the loss cone is full, the merger time is the shortest possible, and is determined by the size of the loss cone and by the dynamical time (eq. [2]). These conditions hold for gas-rich mergers across almost the entire mass range ($M_{12} \lesssim \text{few} \times 10^8 M_\odot$), and are also true for lower mass BMBHs in mergers of elliptical galaxies ($M_{12} \lesssim \text{few} \times 10^6 M_\odot$). For higher BMBH masses, there are not enough MPs to refill the loss cone. However, the merger still evolves a factor of $\sim \mu_2$ faster than it would with stellar relaxation alone (Table 3), until the BMBH separation decreases, the loss cone is filled, and the scattering rate reaches its maximal value. This fast MP-driven evolution continues until the BMBH shrinks to the point at which stellar relaxation alone can fill the loss cone. Since the BMBH spends most of its time in those late stages, the overall decrease in the total dynamical merger time,

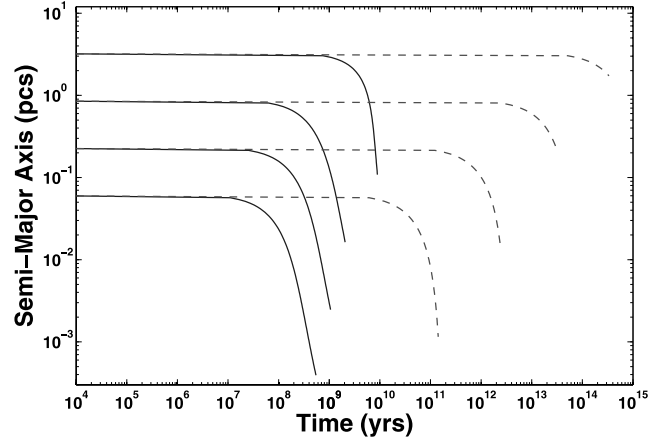


FIG. 2.—Evolution of the BMBH separation from a_s to a_{GW} in a major merger due to three-body scatterings of stars. The evolution in the major merger scenario with MP-induced relaxation (solid lines) is compared to that with stellar relaxation (dashed lines) for BMBH masses of 10^6 , 10^7 , 10^8 , and $10^9 M_\odot$ (from bottom up). [See the electronic edition of the Journal for a color version of this figure.]

t_{dyn} , is intermediate between the maximal possible value of $\sim \mu_2^{-1}$ and that due to stars alone (eq. [3]), $1 \ll t_{\text{dyn}}^{\text{MP}}/t_{\text{dyn}}^* \ll \mu_2^{-1}$.

The results indicate that MPs drive rapid coalescence of BMBHs in less than t_H in most minor and major mergers. Moreover, for most BMBHs, coalescence occurs in less than 1 Gyr, which is comparable to the dynamical timescale of the galactic merger itself (Barnes & Hernquist 1992). Our results indicate that massive BMBHs ($M_{12} \gtrsim 10^8 M_\odot$) in gas-poor ellipticals may take $\gg t_H$ to coalesce. However, these estimates omit processes that could shorten the coalescence time by an additional factor of a few, such as re-ejection of loss cone stars (Milosavljević & Merritt 2003; Berczik et al. 2005). We find that MP-induced loss cone refilling is effective in driving BMBHs of $M_{12} \sim 10^7 M_\odot$ ($10^8 M_\odot$, $10^9 M_\odot$) to coalescence in a Hubble time, if 0.005 (0.05, 0.5) of the total mass density in the galactic nucleus is in clumped gas components with a mass function such as that observed in the GC (Fig. 1). The cores of low-mass ellipticals with $M_{12} < 10^8 M_\odot$ quite possibly contain some clumped gas (up to 0.02 of the MPs assumed in our major merger model; see Table 2). Such clumps are sufficient for inducing rapid coalescence even in such systems, even if relaxation by stellar clusters or other coherent stellar structures is too slow.

Figure 2 shows the evolution of the BMBH separation for $M_{12} = 10^6$, 10^7 , 10^8 , and $10^9 M_\odot$ in major mergers ($Q = 1$), with and without MPs. The BMBH separation is evolved up to the point where the decay is dominated by GWs, and coalescence follows soon after (the transition criterion $\dot{a}_{\text{dyn}} = \dot{a}_{\text{GW}}$ and eq. [8] imply that the evolution curves steepen sharply beyond the transition point). The evolution of BMBHs with MP relaxation exhibits a short initial stalled phase, where the initially large loss cone is empty even in the presence of MPs, followed by a phase of rapid decay. It should be noted that the decay phase does not display the $a \propto t^{-1}$ evolution of a hard BMBH, expected when $\bar{C} \simeq \text{const}$. The acceleration of the infalling stars in the Galactic potential softens the encounter with the BMBH and substantially reduces the energy extraction efficiency. Figure 3 shows that this efficiency strongly depends on both the distance from which stars are deflected to the BMBH and the BMBH separation. It should be emphasized that acceleration by the galactic potential cannot not be neglected, since it substantially reduces the efficiency of any BMBH slingshot mechanism, in particular those for which the

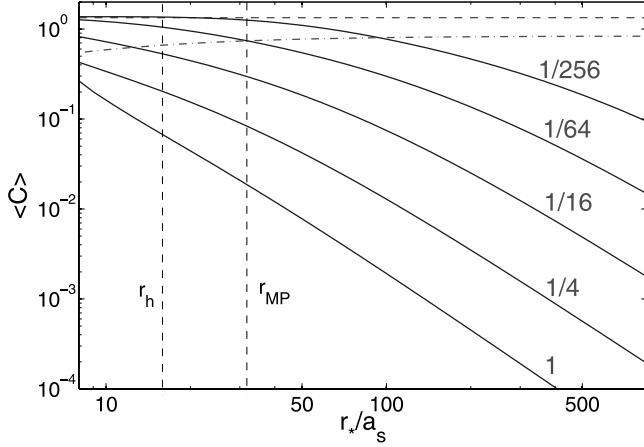


FIG. 3.—Dependence of the mean dimensionless extracted energy, $\bar{C}_{\text{eff}} = \bar{C}(Q, \zeta_{\text{eff}})$ (eq. [B14]) for $Q = 1$, on the point of origin of the deflected star, r_*/a_s , for different stages of the BMBH evolution, a/a_s (indicated by the numbers adjacent to the lines), taking into account the acceleration in the Galactic potential. The dashed horizontal line at the top is the asymptotic value of \bar{C}_{eff} in the hard limit ($a/a_s \rightarrow 0$). The dash-dotted line is the value of \bar{C} for the case $a/a_s = 1$, when the Galactic potential is neglected. The vertical lines indicate the BMBH's radius of dynamical influence, r_h , and the inner cutoff of the MP distribution, r_{MP} . Most of the stars are deflected toward the BMBH from $r_* \gtrsim r_{\text{MP}}$. [See the electronic edition of the Journal for a color version of this figure.]

potential gradient is steep (e.g., Zier, 2006, 2007) or those for which stars are deflected toward the MBH from very large distances (e.g., Berczik et al., 2006).

8. IMPLICATIONS OF MP-INDUCED BMBH COALESCENCE

8.1. Observations of BMBHs

BMBHs can be observed as resolved objects in the initial dynamical friction stage, when $a > a_h$, and possibly also in the second dynamical decay stage when $a_{\text{GW}} < a < a_h$ (in particular massive BMBHs, whose a_h is large; see eq. [1]). They may be detected indirectly (see review by Komossa 2006) or by GW emission in the last GW-driven decay stage, when $a \lesssim a_{\text{GW}}$. Efficient MP-driven BMBH mergers progress rapidly through the second dynamical decay stage. Thus, a prediction of the MP merger scenario is that observed BMBHs should fall into a bimodal distribution: those with $a > a_h$ and those with $a \lesssim a_{\text{GW}}$, where $a_{\text{GW}} \ll a_h$. In contrast, dynamical scenarios that lead to stalling, such as relaxation by stars alone, imply that BMBHs with $a \lesssim a_h$ should be common.

The few direct and indirect observations of BMBHs available today are consistent with the predictions of the MP scenario. There are two known resolved double active galactic MBHs, NGC 6240 with $a = 1.4$ kpc (Komossa et al. 2003), and 0402+379 with $a = 7$ pc (Rodríguez et al. 2006), just outside its hardening separation $a_h \sim 3.5$ pc for $M_{12} \sim 1.5 \times 10^8 M_\odot$. X-ray-shaped radio galaxies, double-double radio galaxies, with pairs of coaligned symmetric double-lobed radio structures, and AGNs, with semi-periodic light curves or double-peaked emission lines, were suggested as signatures of close ($a \ll 1$ pc) or recently merged BMBHs (Komossa 2006).

The detection of the GW signal from coalescing BMBHs would constitute direct evidence of such events. Our calculations show that for most galaxy mergers, the BMBH would coalesce within t_H , and so the BMBH coalescence rate should follow the galaxy merger rate. In that case, the cosmic rate of these GW events could be as high as 10^2 yr^{-1} (Haehnelt 1994; Sesana et al. 2004; Enoki et al. 2004).

8.2. Triple MBHs and MBH Ejection

The galaxy merger rate in dense clusters may be high enough ($> 10^{-9} \text{ yr}^{-1}$; Mamon 2006) for a second merger to occur before the first BMBH coalesces. This would result in the formation of an unstable triple-MBH system, which will eject one of the MBHs at high velocity (Saslaw et al. 1974). This scenario was suggested as a possible solution for the stalling problem, as the third component may drive the BMBH to high eccentricities and to much more rapid coalescence (Blaes et al. 2002; Iwasawa et al. 2006; Hoffman & Loeb 2007).

Because MPs accelerate BMBH coalescence in most mergers, our results indicate that triple-MBH systems and high-velocity MBHs ejected by the slingshot mechanism should be rare⁷ (Fig. 1). Because of the rapid BMBH decay, in those cases where a triple MBH is formed, it is expected that it will be hierarchical. This would typically lead to fast coalescence of the inner BMBH (Makino & Ebisuzaki 1994; Iwasawa et al. 2006), followed by the MP-driven decay and coalescence of the newly formed central MBH with the outer MBH.

8.3. Mass Deficits

The large number of stars ejected from the system during the BMBH coalescence could change the stellar distribution of the BMBH environment. It has been suggested that the mass deficit observed in some bright elliptical galaxies is the result of such events (Milosavljević et al. 2002; Ravindranath et al. 2002; Graham 2004; Ferrarese et al. 2006). The total mass of ejected stars in the dynamical decay phase depends only on the initial and final BMBH separations,

$$M_{\text{ej}}(t) \equiv M_* \int_0^t dt' \int dE \mathcal{F}(E, t') \sim \mathcal{J} M_{12} \ln \frac{a(0)}{a(t)}, \quad (12)$$

where \mathcal{F} is the flux of stars supplied to the loss cone, and \mathcal{J} is a numerical factor approximately equal to $1/2\bar{C}$ (Q96; Milosavljević & Merritt 2003; Sesana et al. 2007).

Previous studies of the mass deficit (Milosavljević et al. 2002; Merritt 2006) took into account only the stars evacuated from the core before the BMBH stalled at $a \sim a_h$ because of inefficient stellar relaxation. We note that there are between 2 and 7 further e -foldings between a_h and a_{GW} (Fig. 2). As a result, when the BMBH merger is driven all the way to a_{GW} , the mass deficit will grow substantially (this was recently also noted by Merritt et al. 2007). When the merger is driven by MPs, the mass deficit will be on the $\sim (1-2)r_{\text{MP}}$ scale, where most of the scattered stars originate. We calculated the total mass of stars that originated from such distances and that were ejected from the core during coalescence. We found that these amount to approximately 30%–40% of the total stellar mass in these regions.

We note that generally, the magnitude and spatial scale of the mass deficit could, in principle, discriminate between different proposed solutions for the stalling problem. In mergers driven by nonaxisymmetric potentials, most stars originate from large radii (Berczik et al. 2006), where the enclosed number of stars is very large. The fractional, spatially averaged mass deficit will therefore be very small and harder to detect. In contrast, scenarios that assume very steep cusps (Zier 2006, 2007) lead to substantial central mass depletion. Even in gas-induced mergers (Escala et al. 2005; Dotti et al. 2007), in which stars play a minor role, there

⁷ Recent observations of an apparently hostless quasar (Magain et al. 2005) were interpreted as an ejected MBH (Haehnelt et al. 2006; Hoffman & Loeb 2006, 2007), but see Merritt et al. (2006) for an opposing view.

may be an indirect mass deficit effect caused by the inhibition of star formation due to heating of the gas by the inspiraling BMBH.

9. DISCUSSION AND SUMMARY

We have shown that it is very likely that MPs play a dominant role in the aftermath of galactic mergers. They shorten the relaxation timescale in the galactic nuclei by orders of magnitudes compared to two-body stellar relaxation alone, and drive the newly formed BMBH to rapid coalescence by the slingshot effect. The MP mechanism requires only the existence of sufficiently large inhomogeneities in the galactic mass distribution. Since these occur naturally over a wide range of conditions, the MP mechanism is robust and probably accelerates most BMBH mergers. The one possible exception may be mergers of two gas-poor elliptical galaxies, where GMCs are less common. However, simulations indicate that stellar clusters can play the role of MPs and drive an efficient merger even in most of these cases.

We conclude that most BMBHs are expected to coalesce within t_H , even in cases where previous theoretical modeling, which did not consider accelerated relaxation by MPs, predicts that the merging BMBH will stall. This conclusion is based on conservative assumptions. We considered only circular BMBHs, whereas eccentric BMBHs coalesce even faster in the GW-emission-dominated phase, and we neglected the possible concurrent effects of any of the other orbital decay mechanisms proposed in the literature. It thus appears likely the BMBH coalescence is in fact achieved on timescales $\ll t_H$, which implies that BMBH coalescence GW events occur at the cosmic rate of galactic mergers. Specifi-

cally, we predict that low-mass BMBHs, which are prospective *LISA* targets, should coalesce within a merger dynamical time, $10^8 - 10^9$ yr.

Efficient MP-driven BMBH coalescence has additional implications, which we have discussed briefly here. Fast BMBH mergers decrease the probability of nuclei containing triple MBHs, and hence of ejected MBHs, since in most cases, the BMBH coalescence time is shorter than the mean time between galactic collisions. During the final stage of the merger, when the BMBH separation shrinks from the hardening radius to the final GW radius, a large number of stars will be ejected from the nuclei. We find that this additional ejection stage could appreciably increase the mass deficit of the newly formed nucleus beyond what is predicted when taking into account only the earlier stages of the merger (Merritt 2006).

In summary, we have shown that the plausible existence of MPs in galactic nuclei shortens the relaxation time by orders of magnitude. In particular, MPs accelerate the dynamical decay of BMBHs by efficiently supplying stars for the slingshot mechanism. This prevents stalling (the “last parsec problem”) and allows the final coalescence of the BMBH by GW emission within a Hubble time.

T. A. is supported by ISF grant 928/06, Minerva grant 8563 and a New Faculty grant by Sir H. Djangoly, CBE, of London, UK. H. P. would like to thank the Israeli Commercial and Industrial Club for their support through the Ilan Ramon scholarship.

APPENDIX A

THE STALLING RADIUS

This appendix presents a simple analytic approximation for the stalling separation, a_s , as a function of the premerger galactic density profile and the BMBH mass ratio Q , which is based on the N -body simulations of Merritt (2006). Typically, $a_s \sim a_h$ (eq. [1]) up to a factor of a few. Assumption of the *Ansatz* $a_s \rightarrow a_h$ in the evaluation of the BMBH coalescence time can lead to inaccuracies of up to a factor of a few, in particular for $Q \rightarrow 1$.

Merritt (2006) modeled typical galactic cores in large N -body simulations of BMBH coalescence by Dehnen configurations (Dehnen 1993),

$$\rho = \frac{M}{[4\pi/(3-\gamma)]d^3} \frac{1}{(r/d)^\gamma(1+r/d)^{4-\gamma}}, \quad (\text{A1})$$

where M is the total stellar mass, d is a scale length, and $-\gamma$ is the logarithmic slope at $r \ll d$. A central MBH of mass $M_1/M = 0.01$ was added to the initial density distribution. We assume here that the results derived for this particular class of models also apply, at least approximately, to other initial density distributions and MBH-to-stellar cluster mass ratios.

Merritt (2006) finds that the stalling radius can be described to a good approximation, independently of γ , by

$$a_s = 0.2Q/(1+Q)^2 r'_h(M_{12}) = 0.8[r'_h(M_{12})/r_h(M_{12})]a_h, \quad (\text{A2})$$

where $r'_h(M_{12})$ is the radius of influence of the BMBH at the stalling time t_s after the scouring effect of the binary formation, which is estimated as follows. The ejected mass at t_s can be approximated analytically:

$$\frac{\Delta M}{M_{12}} \simeq 0.7Q^{0.2}. \quad (\text{A3})$$

The postmerger radius of influence r'_h can typically be estimated to better than 3% (Fig. 4) by assuming that the post density profile resembles the original profile, except for the removal of ΔM from the center further out, so that

$$M(<r'_h) = 2M'_{12} \equiv 2M_{12} + \Delta M = M_1(1+Q)(2+0.7Q^{0.2}). \quad (\text{A4})$$

The enclosed stellar mass in the initial Dehnen distribution is $M(<r) = M[r/(r+d)]^{3-\gamma}$, and so

$$r'_h(M_{12})/r_h(M_{12}) = \left[(2M_{12}/M)^{1/(\gamma-3)} - 1 \right] / \left[(2M'_{12}/M)^{1/(\gamma-3)} - 1 \right]. \quad (\text{A5})$$

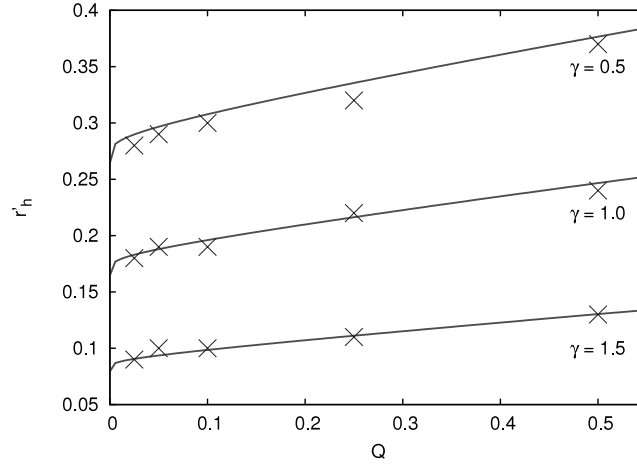


FIG. 4.—Influence radius in the postmerger galaxy at the stalling time, r_h' , as function of Q , for initial Dehnen density profiles with $\gamma = 0.5, 1.0$, and 1.5 (top to bottom), as derived by Merritt (2006) in N -body simulations (crosses), and by the approximate analytical expression, eq. (A5) (solid lines). [See the electronic edition of the Journal for a color version of this figure.]

The correction is thus a function of the inner cusp slope only. The stalling separation (eq. [A2]) is a rising function of Q . For $Q \rightarrow 0$, $a_s \rightarrow 0.8a_h$ irrespective of M_{12}/M or γ . For $Q \rightarrow 1$, $M_{12}/M = 0.01$, and $\gamma = 2$, $a_s \rightarrow 2.2a_h$.

APPENDIX B

BMBH ENERGY EXTRACTION BY INTERACTIONS WITH STARS

This appendix details how the mean BMBH energy that is extracted by an encounter with a star from the galactic core is estimated using results of isolated three-body scattering experiments, which are available in the literature.

B1. ADAPTATION OF RESULTS FROM SCATTERING EXPERIMENTS

The rate at which the BMBH changes its binding energy $E_{12} = GM_1M_2/2a$ due to the interaction of stars is

$$\frac{dE_{12}}{dt} = \int_0^\infty \langle \Delta E(b; Q, \xi) \rangle 2\pi b \frac{d\Gamma}{db} db, \quad (\text{B1})$$

where b is the impact parameter, $\xi = v/V_{12}$ is the hardness parameter (v is the velocity of the incoming star at infinity relative to the BMBH center of mass, ignoring the potential of the galaxy), and $V_{12} = (GM_{12}/a)^{1/2}$ is the BMBH's circular velocity in the reduced-mass system. The quantity $\langle \Delta E(b; Q, \xi) \rangle$ is the mean energy extracted by the star from the BMBH orbit averaged over the BMBH orbital parameters, and $2\pi b(d\Gamma/db)db$ is the rate at which stars are deflected into orbits with impact parameters in the range $(b, b + db)$. In a Keplerian system, the impact parameter $b \equiv xb_0$, with $b_0^2 = 2GM_{12}a/v^2 = 2a^2/\xi^2$ (Q96), is related to the periaapse distance $r_p \equiv ya$ by $b^2 = r_p^2(1 + 2GM_{12}/r_p v^2)$, which can be written as

$$x^2 = \xi^2 y^2 / 2 + y; \quad y = \left(\sqrt{1 + 2\xi^2 x^2} - 1 \right) / \xi^2. \quad (\text{B2})$$

The extracted energy $\langle \Delta E \rangle$ is a function of r_p , the mass ratio Q , and the hardness parameter ξ . It was derived numerically by Monte Carlo simulations of three-body scattering (Hills 1983; Q96; Sesana et al. 2006), which show that it is large and fairly constant for $r_p/a \lesssim 0.5-2$ and then falls rapidly to zero for $r_p/a \gtrsim 0.5-2$ (see also Zier 2007 for an extended discussion of the r_p -dependence of the extracted energy). Unfortunately, the behavior of $\langle \Delta E(b; Q, \xi) \rangle$ as a function of its parameters has only been partially documented. Hills (1983) studied the dependence on b and Q only in the $\xi \rightarrow 0$ limit, for specific values of the BMBH orbital eccentricities. Sesana et al. (2006) show plots only for $\xi \rightarrow 0$, while Q96 explored the full range of values for ξ and Q and averaged over the eccentricity, but integrated over the b -dependence. For that reason, it is not possible to use these results to evaluate equation (B1) explicitly, and it is necessary to resort to an approximate formulation. Following the trends seen in the $\xi \rightarrow 0$ simulation results, we adopt here a step function approximation, which is based on the assumption that the $\langle \Delta E \rangle$ is roughly constant between $b = 0$ and an effective maximal impact parameter b_1 ; we therefore write

$$\frac{dE_{12}}{dt} \sim \Delta \bar{E}_1 \Gamma(b_1), \quad (\text{B3})$$

where the b -averaged extracted energy is defined as

$$\Delta \bar{E}_1 \equiv \overline{\langle \Delta E(Q, \xi) \rangle} = \int_0^{b_1} 2\pi b \langle \Delta E(b; Q, \xi) \rangle db / \pi b_1^2, \quad (\text{B4})$$

and where the total rate of stars with impact parameter $b < b_1$ is

$$\Gamma(b_1) = \int_0^{b_1} 2\pi b \frac{d\Gamma}{db} db. \quad (\text{B5})$$

It should be noted that the step function approximation implies that the periape-averaged energy extracted per star should not depend strongly on the mode of loss cone replenishment, whether it is in the empty loss cone regime, where stars diffuse into the loss cone from its boundary ($r_p \sim a$), or whether it is in the full loss cone regime, where the orbits span the entire range $0 \leq r_p \leq a$. This behavior is indeed seen indirectly in the simulations of Merritt & Szell (2006, Fig. 2), where the mass ejection rate remains nearly constant as the system transits from the full to the empty loss cone regime.

Q96 does not quote the simulation results in terms of $\langle \Delta E \rangle$ directly, but rather in terms of a related dimensionless quantity H_1 , which expresses the rate at which energy is extracted from the BMBH by an ambient background of stars with mass density ρ and velocity v at infinity, $d(1/a)/dt = H_1 G \rho / v$. Hills (1983) and Q96 express the extracted energy in a dimensionless form,

$$C \equiv M_{12} \Delta E / 2M_* E_{12} = a \Delta \varepsilon / G \mu, \quad (\text{B6})$$

where $\Delta \varepsilon = \Delta E / M_*$ is the specific energy extracted by the star, and $\mu = M_1 M_2 / M_{12}$ is the reduced mass ($C = 1$ corresponds to the case where the specific energy carried by the star equals twice that of the BMBH). In terms of C , equation (B4) can be written as

$$\bar{C}_1 = \int_0^{b_1} 2\pi b \langle C(b; Q, \xi) \rangle db / \pi b_1^2. \quad (\text{B7})$$

The quantity H_1 is related to the orbitally averaged $\langle C \rangle$ in terms of the dimensionless impact parameter x by (Q96, eq. [11])

$$H_1(Q, \xi) = 8\pi \int_0^\infty x \langle C(x; Q, \xi) \rangle dx = 4\pi \int 2\pi b \langle C \rangle db / \pi b_0^2. \quad (\text{B8})$$

A comparison of equations (B7) and (B8) shows that \bar{C}_1 is related to the values of H_1 quoted by Q96 through the relation

$$\bar{C}_1(Q, \xi) = H_1(Q, \xi) (b_0 / b_1)^2 / 4\pi. \quad (\text{B9})$$

Let $r_{p1} = y_1 a$ be the periape that corresponds to the effective impact parameter b_1 . It then follows that

$$\bar{C}_1(Q, \xi) = H_1(Q, \xi) / [4\pi y_1 (1 + y_1 \xi^2 / 2)]. \quad (\text{B10})$$

Q96 suggests an analytic fit to the behavior of H_1 as function of Q and ξ (Q96, eq. [16] and Table 1),

$$H_1(Q, \xi) = \frac{H_0(Q)}{\sqrt{1 + [\xi / w_0(Q)]^4}}, \quad (\text{B11})$$

whereas here we use a slightly different notation from Q96, $w_0 = w_{Q96} / V_{12}$, so that the values of $w_0(Q)$ are the numeric values in the third column of Table 1 in Q96, or are given by the analytic fit formula (Q96, eq. [17])

$$w_0(Q) \simeq 0.85 \sqrt{M_2 / M_{12}} = 0.85 \sqrt{Q / (1 + Q)}. \quad (\text{B12})$$

The tabulated values of $H_0(Q)$ (Q96, Table 1, second column) are nearly independent of Q , with $\bar{H}_0 = 21.1_{-3.2}^{+1.4}$ over the range $Q = 1/256$ to $Q = 1$ (the lower values corresponding to larger Q).

For a distribution of velocities characterized by a one-dimensional velocity dispersion σ , the effective H is given in terms of $\zeta = \sigma / V_{12}$ by (Q96, eq. [18])

$$H(Q, \zeta) = H_1(Q, \sqrt{3}\zeta) \left(\sqrt{2/\pi} + \log \left\{ 1 + \alpha [\zeta / w_0(Q)]^\beta \right\} \right), \quad (\text{B13})$$

where $\alpha = 1.16$ and $\beta = 2.40$. This can then be approximately related to the mean ejection energy as in equation (B10) by

$$\bar{C}(Q, \zeta) = H(Q, \zeta) / [4\pi y_1 (1 + y_1 \zeta^2 / 2)]. \quad (\text{B14})$$

The nature of the approximation here is that the translation between b and r_p is done for a representative velocity, assuming Keplerian motion. For the purpose of numeric calculations, we assume $y_1 = 1$.

The relevant scale for MPs is $r_{\text{MP}} \gtrsim 2r_h$, which encloses $>4 M_\bullet$ in stars. On that scale, the potential is dominated by the stars. For a r^{-2} stellar density distribution far from the MBH, the velocity dispersion is $\sigma^2(r) \simeq GM_*(<r)/r \simeq \text{const}$. Here we represent the typical initial stellar velocity by the circular velocity $v = \sqrt{2}\sigma$. This velocity needs to be corrected for the fact that the star is accelerated by the galactic potential as it falls toward the MBH. In the fictitious three-body system (the BMBH and the star), its effective hardness

parameter, $\zeta_{\text{eff}}(r) > \zeta$, depends on the star's point of origin (see Appendix B2). Thus, the BMBH total decay rate is given by integrating over the contribution of stars originating from all radii, with the loss cone size expressed in terms of the periaapse,

$$\frac{d \log a}{dt} = -2 \frac{M_*}{M_{12}} \int \bar{C}[Q, \zeta_{\text{eff}}(r; a)] \frac{d\Gamma(<v_1 a)}{dr} dr. \quad (\text{B15})$$

Note that the “hard limit,” $d(1/a)/dt = \text{const}$, is recovered when the cross section for interacting with the BMBH is dominated by the gravitational cross section term ($\zeta \rightarrow 0$, $\bar{C} = \text{const}$, eq. [B14]), and $\Gamma \propto a$ (full loss cone regime, eq. [2]).

B2. DEPENDENCE ON THE GALACTIC POTENTIAL

The extracted energy (eq. [B14]) depends on the hardness of the encounter ζ . In the soft encounter limit ($\zeta \rightarrow 0$), the interaction with the BMBH is strong and independent of ζ (eqs. [B10] and [B11]). The hardness of the encounter depends on the star's point of origin. The farther away it starts from the center, the more it will be accelerated by the galactic potential, and the faster it will be when it approaches the BMBH. Since MPs typically deflect stars into the loss cone from large distances, the effect of the galactic potential in making the encounters harder and less efficient cannot be neglected (Fig. 3).

The three-body scattering experiments of Q96 took into account only the potential of the BMBH. To relate the energy extraction to that of a star falling in the combined potential of the BMBH and the galaxy, it is necessary to calculate the corresponding effective initial velocity the star should have in the fictitious three-body system containing only the BMBH and the star.

The gravitational potential in a spherical stellar system with mass density $\rho(r)$ surrounding a central BMBH of mass M_{12} is

$$\phi(r) = -4\pi G \left[\frac{1}{r} \int_0^r \rho(x) x^2 dx + \int_r^\infty \rho(x) x dx \right] - \frac{GM_{12}}{r}. \quad (\text{B16})$$

For a power-law mass density profile between r_1 and r_2 , where $r_1 \ll r_2$,

$$\rho(r) = \rho_0 \left(\frac{r}{r_0} \right)^{-\alpha}, \quad (\text{B17})$$

the enclosed stellar mass is ($\alpha \neq 3$, $r \gg r_1$)

$$M(<r) \simeq \frac{4\pi}{3-\alpha} \rho_0 r_0^3 \left(\frac{r}{r_0} \right)^{3-\alpha}. \quad (\text{B18})$$

The potential at $r_1 < r < r_2$ is

$$\phi(r) = -\frac{GM_{12}m(r)}{r} - 4\pi G \int_r^\infty \rho(x) x dx = -\frac{GM_{12}m(r)}{r} - 4\pi G \rho_0 r_0^\alpha \begin{cases} \ln(r_2/r), & \alpha = 2 \\ \frac{1}{2-\alpha} (r_2^{2-\alpha} - r^{2-\alpha}), & \alpha \neq 2 \end{cases}, \quad (\text{B19})$$

where $m(r) = 1 + M(<r)/M_{12}$ is the total mass up to radius r relative to the BMBH mass.

Suppose a star starts falling toward the BMBH with velocity v from an initial radius r down to a radius r_1 , which is close enough to the BMBH so that $M(<r_1) \rightarrow 0$. The specific orbital energy of the star, ε , is conserved:

$$\varepsilon = \frac{1}{2} v^2 + \phi(r) = \frac{1}{2} v_1^2 + \phi(r_1). \quad (\text{B20})$$

Taking the velocity of this star at r_1 as the velocity it would have if it began falling from the same distance in the fictitious three-body system, we can find what the *effective* velocity, v_{eff} , should be at a distance r from the BMBH:

$$\varepsilon' = \frac{1}{2} v_{\text{eff}}^2 + \phi'(r) = \frac{1}{2} v_1^2 + \phi'(r_1), \quad (\text{B21})$$

where

$$\phi'(r) = -\frac{GM_{12}}{r}. \quad (\text{B22})$$

The effective velocity is then

$$v_{\text{eff}}^2 = v^2 + 2[\phi'(r_1) - \phi'(r) + \phi(r) - \phi(r_1)] = v^2 + 2GM_{12} \left[-\frac{1}{r_1} + \frac{1}{r} - \frac{m(r)}{r} + \frac{m(r_1)}{r_1} + \frac{4\pi G}{M_{12}} \int_{r_1}^r \rho(x) x dx \right]. \quad (\text{B23})$$

Since $m(r_1) \rightarrow 1$,

$$v_{\text{eff}}^2 = v^2 + 2G \left[-\frac{M(<r)}{r} + 4\pi \int_{r_1}^r \rho(x) dx \right]. \quad (\text{B24})$$

For the $\alpha = 2$ power law assumed here ($r \gg r_1$),

$$v_{\text{eff}}^2 \simeq v^2 + 8\pi G \rho_0 r_0^2 \left[\ln \left(\frac{r}{r_1} \right) - 1 \right]. \quad (\text{B25})$$

The effective hardness parameter is then $\zeta_{\text{eff}}(r) = v_{\text{eff}}/V_{12}$, which is used to evaluate the mean extracted energy (eq. [B14]).

REFERENCES

- Ashman, K. M., & Zepf, S. E. 1998, *Globular Cluster Systems* (Cambridge: Cambridge Univ. Press)
- Backer, D. C., & Sramek, R. A. 1999, *ApJ*, 524, 805
- Bailey, M. E. 1983, *MNRAS*, 204, 603
- Barnes, J. E., & Hernquist, L. E. 1991, *ApJ*, 370, L65
- . 1992, *ARA&A*, 30, 705
- . 1996, *ApJ*, 471, 115
- Begelman, M. C., Blandford, R. D., & Rees, M. J. 1980, *Nature*, 287, 307
- Bender, R., & Saglia, R. P. 1999, in *ASP Conf. Ser. 182, Galaxy Dynamics*, ed. D. R. Merritt, M. Valluri, & J. A. Sellwood (San Francisco: ASP), 113
- Berczik, P., Merritt, D., & Spurzem, R. 2005, *ApJ*, 633, 680
- Berczik, P., Merritt, D., Spurzem, R., & Bischof, H.-P. 2006, *ApJ*, 642, L21
- Blaes, O., Lee, M. H., & Socrates, A. 2002, *ApJ*, 578, 775
- Borisova, J., Ivanov, V. D., Minniti, D., Geisler, D., & Stephens, A. W. 2005, *A&A*, 435, 95
- Capuzzo-Dolcetta, R. 1993, *ApJ*, 415, 616
- Christopher, M. H., Scoville, N. Z., Stolovy, S. R., & Yun, M. S. 2005, *ApJ*, 622, 346
- Cullen, H., Alexander, P., Green, D. A., & Sheth, K. 2007, *MNRAS*, 376, 98
- Dehnen, W. 1993, *MNRAS*, 265, 250
- Dotti, M., Colpi, M., Haardt, F., & Mayer, L. 2007, *MNRAS*, 379, 956
- Downes, D., & Solomon, P. M. 1998, *ApJ*, 507, 615
- Downes, D., Solomon, P. M., & Radford, S. J. E. 1993, *ApJ*, 414, L13
- Ebisuzaki, T., et al. 2001, *ApJ*, 562, L19
- Enoki, M., Inoue, K. T., Nagashima, M., & Sugiyama, N. 2004, *ApJ*, 615, 19
- Escala, A., Larson, R. B., Coppi, P. S., & Mardones, D. 2005, *ApJ*, 630, 152
- Evans, A. S., Mazzarella, J. M., Surace, J. A., & Sanders, D. B. 2002, *ApJ*, 580, 749
- Ferrarese, L., & Merritt, D. 2000, *ApJ*, 539, L9
- Ferrarese, L., et al. 2006, *ApJS*, 164, 334
- Figer, D. F., Kim, S. S., Morris, M., Serabyn, E., Rich, R. M., & McLean, I. S. 1999, *ApJ*, 525, 750
- Figer, D. F., Rich, R. M., Kim, S. S., Morris, M., & Serabyn, E. 2004, *ApJ*, 601, 319
- Figer, D. F., et al. 2002, *ApJ*, 581, 258
- Frank, J., & Rees, M. J. 1976, *MNRAS*, 176, 633
- Friel, E. D. 1995, *ARA&A*, 33, 381
- Gebhardt, K., et al. 2003, *ApJ*, 583, 92
- Gnedin, O. Y., Lee, H. M., & Ostriker, J. P. 1999, *ApJ*, 522, 935
- Gnedin, O. Y., & Prieto, J. L. 2006, preprint (astro-ph/0606169)
- Graham, A. W. 2004, *ApJ*, 613, L33
- Güsten, R., & Philipp, S. D. 2004, in *The Dense Interstellar Medium in Galaxies*, ed. S. Pfalzner et al. (Berlin: Springer), 253
- Haehnelt, M. G. 1994, *MNRAS*, 269, 199
- Haehnelt, M. G., Davies, M. B., & Rees, M. J. 2006, *MNRAS*, 366, L22
- Hänninen, J., & Flynn, C. 2002, *MNRAS*, 337, 731
- Henkel, C., Baan, W. A., & Mauersberger, R. 1991, *Astron. Astrophys. Rev.*, 3, 47
- Hills, J. G. 1981, *AJ*, 86, 1730
- . 1983, *AJ*, 88, 1269
- Hoffman, L., & Loeb, A. 2006, *ApJ*, 638, L75
- . 2007, *MNRAS*, 377, 957
- Ivanov, P. B., Papaloizou, J. C. B., & Polnarev, A. G. 1999, *MNRAS*, 307, 79
- Iwasawa, M., Funato, Y., & Makino, J. 2006, *ApJ*, 651, 1059
- Jenkins, A., & Binney, J. 1990, *MNRAS*, 245, 305
- Kim, S. S., & Morris, M. 2001, *ApJ*, 554, 1059
- Knapp, G. R. 1999, in *ASP Conf. Ser. 163, Star Formation in Early-Type Galaxies*, ed. P. Carral & J. Cepa (San Francisco: ASP), 119
- Koda, J., Okuda, T., Nakanishi, K., Kohno, K., Ishizuki, S., Kuno, N., & Okumura, S. K. 2005, *A&A*, 431, 887
- Komossa, S. 2006, *Mem. Soc. Astron. Italiana*, 77, 733
- Komossa, S., Burwitz, V., Hasinger, G., Predehl, P., Kaastra, J. S., & Ikebe, Y. 2003, *ApJ*, 582, L15
- Kravtsov, A. V., & Gnedin, O. Y. 2005, *ApJ*, 623, 650
- Lacey, C. G. 1984, *MNRAS*, 208, 687
- Larsen, S. S. 2006, preprint (astro-ph/0606252)
- Leitherer, C. 2001, in *ASP Conf. Ser. 245, Astrophysical Ages and Times Scales*, ed. T. von Hippel, C. Simpson, & N. Manset (San Francisco: ASP), 390
- Li, Y., Mac Low, M.-M., & Klessen, R. S. 2004, *ApJ*, 614, L29
- Lightman, A. P., & Shapiro, S. L. 1977, *ApJ*, 211, 244
- Magain, P., Letawe, G., Courbin, F., Jablonka, P., Jahnke, K., Meylan, G., & Wisotzki, L. 2005, *Nature*, 437, 381
- Maillard, J. P., Paumard, T., Stolovy, S. R., & Rigaut, F. 2004, *A&A*, 423, 155
- Makino, J., & Ebisuzaki, T. 1994, *ApJ*, 436, 607
- Mamon, G. A. 2006, preprint (astro-ph/0607482)
- Mandushev, G., Staneva, A., & Spasova, N. 1991, *A&A*, 252, 94
- Merritt, D. 2006, *ApJ*, 648, 976
- Merritt, D., Mikkola, S., & Szell, A. 2007, *ApJ*, 671, 53
- Merritt, D., & Milosavljević, M. 2005, *Living Rev. Relativ.*, 8, 8
- Merritt, D., Storch-Bergmann, T., Robinson, A., Batcheldor, D., Axon, D., & Cid Fernandes, R. 2006, *MNRAS*, 367, 1746
- Merritt, D., & Szell, A. 2006, *ApJ*, 648, 890
- Meylan, G., & Mayor, M. 1991, *A&A*, 250, 113
- Miller, M. C., & Hamilton, D. P. 2002, *MNRAS*, 330, 232
- Milosavljević, M., & Merritt, D. 2003, *ApJ*, 596, 860
- Milosavljević, M., Merritt, D., Rest, A., & van den Bosch, F. C. 2002, *MNRAS*, 331, L51
- Miocchi, P., Capuzzo Dolcetta, R., Di Matteo, P., & Vicari, A. 2006, *ApJ*, 644, 940
- Myers, P. C., Dame, T. M., Thaddeus, P., Cohen, R. S., Silverberg, R. F., Dwek, E., & Hauser, M. G. 1986, *ApJ*, 301, 398
- Oka, T., Hasegawa, T., Sato, F., Tsuboi, M., Miyazaki, A., & Sugimoto, M. 2001, *ApJ*, 562, 348
- Perets, H. B., Hopman, C., & Alexander, T. 2007, *ApJ*, 656, 709 (Paper I)
- Peters, P. C. 1964, *Phys. Rev.*, 136, 1224
- Portegies Zwart, S. F., Makino, J., McMillan, S. L. W., & Hut, P. 2002, *ApJ*, 565, 265
- Portegies Zwart, S. F., McMillan, S. L. W., & Gerhard, O. 2003, *ApJ*, 593, 352
- Prieto, J. L., & Gnedin, O. Y. 2006, preprint (astro-ph/0608069)
- Quinlan, G. D. 1996, *NewA*, 1, 35 (Q96)
- Ravindranath, S., Ho, L. C., & Filippenko, A. V. 2002, *ApJ*, 566, 801
- Rodríguez, C., Taylor, G. B., Zavala, R. T., Peck, A. B., Pollack, L. K., & Romani, R. W. 2006, *ApJ*, 646, 49
- Rupen, M. P. 1997, in *ASP Conf. Ser. 116, The Nature of Elliptical Galaxies*, ed. M. Arnaboldi, G. S. Da Costa, & P. Saha, 322
- Sakamoto, K., Ho, P. T. P., & Peck, A. B. 2006, *ApJ*, 644, 862
- Sakamoto, K., Okumura, S. K., Ishizuki, S., & Scoville, N. Z. 1999, *ApJS*, 124, 403
- Sanders, D. B., & Mirabel, I. F. 1996, *ARA&A*, 34, 749
- Saslaw, W. C., Valtonen, M. J., & Aarseth, S. J. 1974, *ApJ*, 190, 253
- Sawada, T., Hasegawa, T., Handa, T., & Cohen, R. J. 2004, *MNRAS*, 349, 1167
- Sesana, A., Haardt, F., & Madau, P. 2006, *ApJ*, 651, 392
- . 2007, *ApJ*, 660, 546
- Sesana, A., Haardt, F., Madau, P., & Volonteri, M. 2004, *ApJ*, 611, 623
- Shields, G. A., Gebhardt, K., Salviander, S., Wills, B. J., Xie, B., Brotherton, M. S., Yuan, J., & Dietrich, M. 2003, *ApJ*, 583, 124
- Spitzer, L. J., & Schwarzschild, M. 1951, *ApJ*, 114, 385
- . 1953, *ApJ*, 118, 106

- Villumsen, J. V. 1983, *ApJ*, 274, 632
———. 1985, *ApJ*, 290, 75
Wada, K. 2001, *ApJ*, 559, L41
Wada, K., & Norman, C. A. 2001, *ApJ*, 547, 172
Wang, J., & Merritt, D. 2004, *ApJ*, 600, 149
Wiklund, T., Combes, F., Henkel, C., & Wyrowski, F. 1997, *A&A*, 323, 727
Young, J. S., & Scoville, N. Z. 1991, *ARA&A*, 29, 581
Young, P. J. 1977, *ApJ*, 215, 36
Yu, Q. 2002, *MNRAS*, 331, 935
Zhang, Q., & Fall, S. M. 1999, *ApJ*, 527, L81
Zhao, H., Haehnelt, M. G., & Rees, M. J. 2002, *NewA*, 7, 385
Zier, C. 2006, *MNRAS*, 371, L36
———. 2007, *MNRAS*, 378, 1309

Chapter 4

Dynamical and evolutionary constraints on the nature and origin of hypervelocity stars

Perets

The Astrophysical Journal, Volume 690, Issue 1, pp. 795-801 (2009)

DYNAMICAL AND EVOLUTIONARY CONSTRAINTS ON THE NATURE AND ORIGIN OF HYPERVELOCITY STARS

HAGAI B. PERETS

Weizmann Institute of Science, P.O. Box 26, Rehovot 76100, Israel; hagai.perets@weizmann.ac.il

Received 2007 December 23; accepted 2008 September 9; published 2008 December 1

ABSTRACT

In recent years, several hypervelocity stars (HVSs) have been observed in the halo of our Galaxy. Such stars are thought to be ejected through dynamical interactions near the massive black hole (MBH) in the Galactic center (GC). Three scenarios have been suggested for their ejection: binary disruption by an MBH, scattering by inspiraling intermediate mass black hole (IMBH) and scattering by stellar black holes (SBHs) close to MBH. These scenarios involve different stellar populations in the GC. Here we use observations of the GC stellar population together with dynamical and evolutionary arguments to obtain strong constraints on the nature and origin of HVSs. We show that the IMBH inspiral scenario requires too many $\mathcal{O}(10^3)$ main-sequence B stars to exist close to the MBH (< 0.01 pc) at the time of inspiral, where current observations show $\mathcal{O}(10)$ such stars. Scattering by SBHs also require too many B stars to be observed in the GC, but may contribute a small fraction of the currently observed HVSs. The binary disruption scenario is still consistent with current observations. In addition, it is shown that recently suggested signatures for HVSs origin such as hypervelocity binaries and slow rotating HVSs are much weaker than suggested and require too large statistics. In addition, we show that due to the conditions close to the MBH most binary star systems are not expected to survive for long in this region. Consequently, unique stellar populations that require long evolution in binaries are not expected to be ejected as HVSs in the SBHs scattering mechanisms (this may also be related to the recently observed asymmetry in the velocity distribution of HVSs).

Key words: black hole physics – galaxies: nuclei – stars: kinematics

Online-only material: color figures

1. INTRODUCTION

In recent years several hypervelocity stars (HVSs) have been observed in the halo of our Galaxy, some of them unbound to the Galaxy (Brown et al. 2007b). Most of the observed HVSs are B-type stars (Brown et al. 2005, 2006a, 2006b, 2007a, 2007b; Edelmann et al. 2005), implying a Galactic population of 96 ± 10 such unbound HVSs (closer than ~ 120 kpc to the Galactic center (GC); Brown et al. 2007b). Given the color selection of the targeted survey for these stars (Brown et al. 2006a), such stars could be either main-sequence (MS; or blue straggler) B stars or hot blue horizontal branch (BHB) stars. Only four of the observed B-type stars have stellar-type identification, and were found to be B-type MS stars (Edelmann et al. 2005; Fuentes et al. 2006; Przybilla et al. 2008; Lopez-Morales & Bonanos 2008). In addition, a single subdwarf O HVS has been observed (Hirsch et al. 2005). More recently, a new HVSs survey of A-type stars have detected additional HVSs (Brown et al. 2008). We also note that more HVSs may be detected in the future in M31 (Sherwin et al. 2008) and other galaxies.

Extreme velocities as found for these stars most likely suggest a dynamical origin from an interaction with the massive black hole (MBH) in the GC. Several scenarios have been suggested for ejection of HVSs: a disruption of a stellar binary by the MBH in the GC (Hills 1988; Yu & Tremaine 2003; Perets et al. 2007; hereafter the binary disruption scenario), an interaction of a single star with an intermediate mass black hole (IMBH) that inspirals to the GC (Hansen & Milosavljević 2003; Yu & Tremaine 2003; Levin 2006; hereafter the IMBH inspiral scenario), or interaction with stellar black holes (SBHs) in the GC (Yu & Tremaine 2003; Miralda-Escudé & Gould 2000; O’Leary & Loeb 2007; hereafter the SBH kicks scenario). The later two scenarios scatter HVSs mostly from regions very close

to the MBH (< 0.01 pc) whereas the binary disruption scenario mostly ejects HVSs that evolved in binaries much farther from the MBH ($\gtrsim 2$ pc). The IMBH inspiral scenario is a discrete event, which does not occur continuously (although a sequence of several IMBH inspirals may eject HVSs semicontinuously; Löckmann & Baumgardt 2007) whereas the binary disruption or SBH kicks are continuous processes leading to a constant rate of HVS ejection. The different stellar populations involved in the different scenarios, the importance of binarity in the binary disruption scenario, and the dynamical history of HVS ejection could thus help to constrain the nature and origin of HVSs.

Recently, several methods were suggested for discriminating between the HVS ejection mechanisms. These include the differences in the velocity and directional distribution of HVSs (Levin 2006; Baumgardt et al. 2006; Sesana et al. 2007), the binarity of HVSs (Lu et al. 2007), and the rotational velocities of HVSs (Hansen 2007). Brown et al. (2007b), Svensson et al. (2008), and Kenyon et al. (2008) discussed the propagation of observed HVSs and the asymmetric distribution of ingoing and outgoing HVSs (with negative and positive radial velocities, respectively, in Galactocentric coordinates) in regard to their nature (MSB stars or hot BHB stars).

Here we use the current observations of HVSs, observations of the stellar population in the GC, and dynamical arguments to further constrain the possible scenarios for the origin of HVSs. We show that the population of B-type MS stars required by the IMBH inspiral scenario and the SBH kicks scenario is too large to be consistent with current observations. We then discuss some unique stellar populations that require long evolution in binaries, and suggest that they are not likely to be ejected as HVSs in the SBH kicks or IMBH inspiral scenarios, since their binary progenitors are not likely to survive in the harsh environment close to the MBH. We also discuss the implications of the short

survival time of binaries to the distribution of HVS rotational velocities and show that these are not likely to serve as good discriminators for HVSs' origin. Finally, we shortly discuss how these arguments may be related to the recently observed asymmetric velocity distribution of observed HVSs (Brown et al. 2007b).

2. CONSTRAINTS FROM THE YOUNG STELLAR POPULATION IN THE GALACTIC CENTER

In each of the HVS ejection scenarios, the unbound HVSs reflect only a fraction of the total number of stars ejected from the GC. Many more stars are ejected at lower velocities, but high enough to escape the close environment of the MBH. Given the inferred number of B-type HVSs from current observations, one can obtain the total number of such ejected stars. Therefore, we can infer the number of such stars that have existed in the appropriate environment of the GC during the time period of HVS ejection. In the following subsections, we discuss the constraints on the HVS scenarios suggested by such considerations. We assume a total number of unbound HVSs to be ~ 100 (Brown et al. 2007b). This is probably only a lower limit for the total number of HVSs, since many of them might have had higher velocities and propagated beyond the ~ 120 kpc currently observed; therefore, the constraints suggested here might be more stringent.

2.1. The IMBH Inspiral Scenario

In the IMBH inspiral scenario (Hansen & Milosavljević 2003; Yu & Tremaine 2003), an IMBH inspirals to the GC through dynamical interactions with stars. In the late stages of the inspiral, when the IMBH is already close to the MBH in the GC (< 0.01 pc or even less, depending on the IMBH mass), it may closely interact with stars and scatter them at very high velocities, thus producing HVSs (Levin 2006; Baumgardt et al. 2006; Löckmann & Baumgardt 2007; Sesana et al. 2008). Consequently, the population of HVSs ejected by an IMBH in the GC should be strongly correlated with the stellar population in the central 0.01 pc of the GC.¹ In this scenario, the stellar type of the stars (and hence their mass) only negligibly affect the possibility of their ejection as HVSs. Therefore, any star in the close region of the MBH may become an HVS in this case.

Results of N -body simulations (Baumgardt et al. 2006; Löckmann & Baumgardt 2007; Sesana et al. 2008) show that only a fraction of the stars are ejected as HVSs, and most are ejected at lower velocities. Sesana et al. (2008) find a total number of 500 (2500) HVSs ejected for an IMBH of mass $\sim 5 \times 10^3 M_\odot$ ($\sim 1.5 \times 10^4 M_\odot$). They find the total number of stars ejected during the inspiral to be about 10^4 (3.5×10^4). These numbers indicate that a fraction of $f_{\text{HVS}} \sim 0.05$ (0.07) of all ejected stars during the IMBH inspiral are HVSs. Current observations infer ~ 100 unbound B-type HVSs exist in the galaxy and, therefore, $\sim 100/f_{\text{HVS}} \sim 2000$ (1400) B-type stars must have existed at a distance of 0.001 (0.01) pc from the MBH during the short time of IMBH inspiral. Current observations show ~ 1 (30) B-type stars at 0.001 (0.01) pc

from the MBH (Eisenhauer et al. 2005; Ghez et al. 2005); less luminous B-type stars might be missed so this could get a factor of 3–8 times larger.² One may suggest that the stellar population in the GC at the time of inspiral (up to $\sim 10^8$ yr ago) is significantly different than currently observed; however, the possibility of so many B-type stars existing in this small region of the GC is highly unlikely, and would require a yet unknown process for producing such overabundance of B-type stars. Given our theoretical understanding of this process, the current observations of the GC, and the inferred number of HVSs, the IMBH inspiral scenario is unlikely to be the main origin for the ejection of currently observed HVSs.

2.2. The SBH Kicks Scenario

In the SBH kicks scenario (Miralda-Escudé & Gould 2000; O'Leary & Loeb 2007), SBHs in the close environment of the MBH (mostly less than 0.01 pc or even less than 0.001 pc; O'Leary & Loeb 2007) strongly interact with stars and scatter them at high velocities thus producing HVSs. Consequently, and similar to the IMBH scenario, the population of HVSs ejected by an IMBH in the GC should be strongly correlated with the stellar population in the central 0.01 pc of the GC. In this scenario, the stellar type of the stars (and hence their mass) affects the possibility of their ejection as HVSs, but not strongly for the B MS stars of 3–4 M_\odot currently observed.

Results of analytical calculations by O'Leary & Loeb (2007) indicate that only a fraction of the stars are ejected as HVSs, and most are ejected at lower velocities. They find that the ejection rate of stars at velocities lower than required for HVSs ($\lesssim 800 \text{ km s}^{-1}$) is given by $(v_{\text{ej}}/800 \text{ km s}^{-1})^{-2.5}$. For the 100 unbound HVSs inferred from observations, about $\sim 100 \times (100/800)^{-2.5} \simeq 1.8 \times 10^4$ B-type stars have been ejected from the central 0.01 pc with velocities greater than 100 km s^{-1} , i.e., for the lifetime of such 3–4 M_\odot stars, a star formation rate of at least $\sim (2 \times 10^4)/(2 \times 10^8) = 10^{-4}$ B stars per year is required. Given that most of the stars are not scattered outside the GC region, this is only a lower limit on the required star-formation rate, and at least as many stars should have been left over in this region.

It is unlikely that regular star formation could have formed such stars so close to the MBH, given the tidal forces in this region (that would disrupt a progenitor molecular cloud). These stars might have formed continuously through a fragmentation of a gaseous disk, although so close to the MBH even such star formation would most likely be prohibited or be inefficient given the required Toomre criteria in this region (Levin 2007). Nevertheless, these stars could have formed at some larger distance such as the young stars observed at less than 0.5 pc scale stellar disk in the GC (Paumard et al. 2006) and continuously migrated close to the MBH (Levin 2007). Such a scenario would require the star formation rate in this region (most likely below 0.5 pc) to be greater than 10^{-4} yr^{-1} ,

¹ One could suggest that the ejected stars do not belong to the cusp population near the MBH, but have inspiraled in the cluster accompanying the IMBH, and have been scattered during the inspiral. However, simulations of such scenario show that the young stars are stripped from the cluster much before the IMBH reaches the central 0.01 pc (see e.g., Levin et al. 2005; Berukoff & Hansen 2006; see also observational evidence against the IMBH inspiral origin for the young stars in the GC, Paumard et al. 2006) from which region HVSs can be ejected in this scenario.

² Assuming a present-day mass function, and assuming the B stars to have masses between 3 M_\odot and 15 M_\odot , the relative fractions of the observed (more luminous) B stars in the overall population of B stars can be estimated. The fraction of such stars f_{4-15} or f_{5-15} with masses between $4 M_\odot < m < 15 M_\odot$ or $5 M_\odot < m < 15 M_\odot$, respectively, is $f_{4-15} = 0.31$ and $f_{5-15} = 0.13$, i.e., up to ~ 3 –8 times more B stars than observed (with lower masses) could be missed in these regions. In these calculations, we assumed star formation at a constant rate with a Miller–Scalo initial mass function (IMF; Miller & Scalo 1979), and used a stellar population synthesis code (Sternberg et al. 2003) with the Geneva stellar evolution tracks (Schaller et al. 1992) to estimate the present-day number fraction of stars in the S-star mass range. Using an initial mass function instead gives a smaller factor of only 2–3 times undetected B stars.

and would also require an efficient mechanism for transferring a large fraction of these formed stars to the central 0.01 pc within short times. The relaxation time in the GC is much longer than the lifetime of such stars and, therefore, some other migration mechanism would be required (e.g., migration in a gaseous disk; Levin 2007). The central region of the GC probably contains $\lesssim 5 \times 10^2$ B-type stars similar to the observed HVSs (F. Eisenhauer 2006, private communication) and, therefore, implies a star formation rate of less than $5 \times 10^2 / 2 \times 10^8 = 2.5 \times 10^{-6}$ or so B stars per year. This rate is much smaller than the minimally required rate of $\sim 10^{-4} \text{ yr}^{-1}$ we found above for explaining the inferred number of HVSs in this scenario. More simply put we would have expected to observe $\sim 10^4$ B stars in the GC region where only ~ 500 are observed (or even less in the central 0.01 pc), suggesting that this scenario is unlikely to be the main origin for the ejection of currently observed HVSs, although it could explain a fraction of them.

2.3. The Binary Disruption Scenario

In the binary disruption scenario (Hills 1988), binaries are disrupted by the MBH in the GC if they come closer than the tidal radius. One star is captured by the MBH where the other is ejected at high velocity thus producing HVSs. The fraction of ejected stars with velocities lower than those of HVSs is strongly dependent on the semimajor axis distribution of the binaries (where higher velocity stars are ejected from disruption of closer binaries; Hills 1991; Bromley et al. 2006), which is unknown in the GC. The velocity of an ejected star was found in numerical simulations (Hills 1988; Bromley et al. 2006) to scale as 1

$$v_{\text{BH}} = 892 \text{ km s}^{-1} \left(\frac{a}{1 \text{ AU}} \right)^{-1/2} \left(\frac{M_{\text{bin}}}{8 M_{\odot}} \right)^{1/3} \left(\frac{M_{\text{BH}}}{3.7 \times 10^6} \right)^{1/6}. \quad (1)$$

To reproduce the high HVS velocities we consider binaries with $a < 0.95 \text{ AU}$. These are tidally disrupted at $r_t < 3.8 \times 10^{-4} \text{ pc}$ and eject an unbound HVS with $v_{\text{BH}} \gtrsim 920 \text{ km s}^{-1}$, which could be observed as an HVS with velocity greater than 450 km s^{-1} at 55 kpc from the GC, given estimated Galactic potential difference between the center and 55 kpc of $v_{55} \sim 800 \text{ km s}^{-1}$ (Carlberg & Innanen 1987).

For the semimajor axis distribution of massive binary stars, which is strongly biased toward close binaries, a large fraction of all binaries ($f_{\text{bin}} \sim 0.3\text{--}0.9$) have semimajor axis short enough ($\lesssim \text{AU}$; Garmany et al. 1980; Abt 1983; Kobulnicky & Fryer 2008) such that the binary disruption by the MBH would lead to a ejection of HVS. Therefore, given the ~ 100 HVSs inferred from observations one would require $\sim 330/(f_{\text{bin}}/0.3)$ binaries to be disrupted. This does not constrain the stellar population from which the binaries originate (most originate from the central 10 pc of the GC where $\sim 10^4$ such binaries exist), but may constrain the number of captured stars (Perets et al. 2007). In each binary disruption, the companions to the ejected stars are captured by the MBH. The capture semimajor axis distance to the MBH is linearly dependent on the semimajor axis of the original stellar binary (Hills 1991), which is $\lesssim 0.02 \text{ pc}$ for the companion of a HVS and, therefore, 100–300 such stars should be captured near the MBH during the last $\sim 10^8 \text{ yr}$ in this region. This is generally consistent with current observations of ~ 100 massive B stars at less than 0.04 pc from the MBH, where the number of less massive (less luminous) B stars may be a few times larger (see Footnote 2).

Although less likely, the initial semimajor axis distribution of B MS binaries in the GC environment may behave like that of lower mass stars (Duquennoy & Mayor 1991). Most binaries with large semimajor axis would not survive for long in the central regions of the GC ($< 10 \text{ pc}$; from which most disrupted binaries originate; see Figure 1), and so only the closer binaries (about half of the primordial population) survive. In this case, the fraction of disrupted binaries that lead to ejection of HVSs (binaries closer than $\lesssim \text{AU}$) is ~ 0.16 . Therefore, we obtain a total number of $\sim 100/0.16 = 625$ stars captured by the MBH during the last $\sim 10^8 \text{ yr}$. However, many of these captured stars would be captured at much larger distances than the companions of HVSs and would be distributed up to distances of $\sim \text{pc}$ from the MBH; i.e., the constrain we have is of ~ 625 B-type stars (more likely a few times more, if both stars are captured, and also taking into account the larger impact parameter for wider binaries) in the central pc. This is still marginally consistent with current observations in this region, but might be excluded in future observations. We conclude that the scenario of HVS ejection from binary disruption is consistent with current observations of B stars in the GC given a binary distribution of B stars binaries similar to that observed in the solar neighborhood, and marginally consistent if the binary distribution is similar to that of lower mass stars in the solar neighborhood.

3. CONSTRAINTS FROM THE EVOLUTION OF BINARY SYSTEMS IN THE GALACTIC CENTER

Stellar evolution in binary systems can be very different than the evolution of isolated stars. In such systems, the binary components may interact in many ways, whether through mass transfer, tidal forces, winds, radiation, or other ways. Such interaction can considerably change the evolution of the stars and lead to unique characteristics of stars that are different or not even accessible to stars evolved in isolation. Some of these effects require long-term evolution in binaries. Other effects are related to the formation process of a binary system (e.g., stars in binary systems show lower average rotational velocities than single stars, irrespective of their age; Abt & Boonyarak 2004). Observationally, several peculiar stellar populations are observed mostly or only in binaries (Abt 1983).

The different evolution of stars in binaries can be used for discriminating between ejection scenarios of HVSs and helping to understand and predict their characteristics. Recently, two such discriminators have been suggested. The binary disruption scenario, by definition, involves the ejection of a single star which evolved in a binary. It was pointed out that binary components have lower average rotational velocities (Abt & Boonyarak 2004) and, therefore, HVSs from such a scenario should similarly be slow rotators (Hansen 2007). In the inspiraling IMBH scenario, both single and binary stars could be ejected as HVSs. The latter possibility of a binary HVS has been suggested as a unique signature of the IMBH inspiral scenario (Lu et al. 2007). In the following, we generalize the use of binary evolution as a signature of HVS ejection scenarios (and predictors for their nature), and suggest additional signatures. However, we also show that the dynamics of binaries in the GC usually make this type of signatures only weak signatures at most, and would probably require large statistics to be useful discriminators in most cases. Nevertheless, these may better constrain the characteristics of HVSs ejected from the GC and may help explain the asymmetric velocity distribution of observed HVSs.

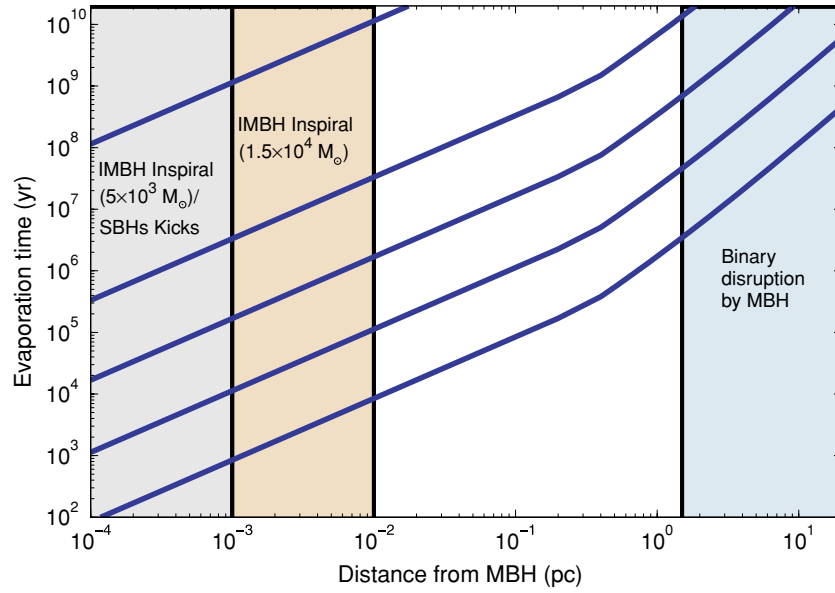


Figure 1. Evaporation time of binaries in the GC for binaries with different semimajor axis; 0.01 AU (contact binaries), 0.1 AU, 1 AU, 10 AU, and 100 AU (from top to bottom). The shaded regions show the distance range from which most HVSs are ejected in the IMBH inspiral scenario (IMBH masses of $1.5 \times 10^4 M_\odot$ and $5 \times 10^3 M_\odot$; Sesana et al. 2008), the SBH kick scenario (O’Leary & Loeb 2007), and the binary disruption scenario (Perets et al. 2007).

(A color version of this figure is available in the online journal.)

We note that all of the arguments given below are predictors not only for the characteristics of HVSs, but also for stars observed close to the MBH, that were either formed close by (e.g., in the recently observed stellar disk; Paumard et al. 2006) or captured through the binary disruption mechanism (Perets et al. 2007).

3.1. Binary Survival in the Galactic Center

Binaries may survive for a Hubble time unless destroyed due to stellar evolutionary processes (e.g., merger or disruption due to mass transfer or mass loss) or subjected to dynamical interactions. In dense environments, the latter possibility may play an important role in the evolution of binary systems. In such environments binaries (soft binaries; Heggie 1975) may gradually evaporate due to perturbations from encounters with other single stars if

$$|E|/m_{\text{bin}}\sigma^2 < 1, \quad (2)$$

where $E = -Gm_1m_2/2a$ is the orbital energy of a binary with component masses m_1 and m_2 and separation a , $m_{\text{bin}} = m_1 + m_2$ is the binary mass, and σ is the velocity dispersion of stars in the system. Due to the high-velocity dispersions in the GC, all but the closest (contact) binaries are soft binaries. Hard, close binaries can become harder due to interactions with other stars, i.e., become even closer. However the hardening changes the orbital energy of these binaries at a rate of less than $\sim 20\%$ per relaxation time for marginally hard binaries, and even less for harder binaries (see, e.g., Equations (8)–(113) in Binney & Tremaine 1987). This would only slightly change the distribution of periods of close binaries. Given the uncertainties in the distribution of binaries in the GC this effect is negligible and does not contribute much to the processes of binary evolution in the GC. Most of the binary population in the GC is in soft binaries. The evaporation time of such binaries is

given by (Binney & Tremaine 1987)

$$t_{\text{evap}} = \frac{m_{12}}{m} \frac{\sigma}{16\sqrt{\pi}\rho a \ln \Lambda}, \quad (3)$$

where ρ is the stellar density, m is the typical mass of a star in this region, and $\ln \Lambda$ is the Coulomb logarithm. In the GC, σ is dependent on r ; $\sigma \sim \sqrt{GM(<r)}/r$, where $M(>r)$ is the enclosed mass up to distance r from the MBH. Figure 1 shows the evaporation time for binaries with different semimajor axis (10^{-2} – 10^2 AU) in the central regions in the GC, taking $\rho(r) = \rho_0(r/r_0)^{-\alpha}$, where $r_0 = 0.4$ pc, $\rho_0 = 1.2 \times 10^6 M_\odot \text{ pc}^{-3}$, $\alpha = 1.4$ for $r < r_0$, and $\alpha = 2$ for $r > r_0$ (Genzel et al. 2003). The binary mass ratio is assumed to be 1 ($m_{12} = 2m$).

Typical low mass ($< 3 M_\odot$) binaries have a log normal distribution of semimajor axis centered around ~ 30 AU (Duquennoy & Mayor 1991). As can be clearly seen in Figure 1 most such binaries cannot survive for long close to the MBH. Many of the peculiar properties of stars evolved in binaries are due to their long-term evolution in such systems (Abt 1983). Since binaries close to the MBH are disrupted in very short time scales, the component stars in these binaries would become single stars, and effectively evolve as isolated stars. Consequently, peculiar stellar populations that require long-term evolution in binaries are not expected to form in these regions. As discussed earlier, the scenarios of HVS ejection by SBHs or by an IMBH are most efficient at close distances of ~ 0.001 – 0.01 pc from the MBH and, therefore, most HVSs are ejected from these regions in these scenarios (O’Leary & Loeb 2007; Sesana et al. 2008). At such distances from the MBH the velocity dispersion is of the order of a few 10^2 – 10^3 km s $^{-1}$, and even the closest binaries are soft and would be disrupted in less than 10^7 yr (see Figure 1), i.e., shorter than the MS lifetimes of most stars. Consequently, the hypervelocity binaries that were suggested as a possible signature of the IMBH inspiral scenario (Lu et al. 2007) and peculiar stellar populations evolved and observed mainly in binaries, are not expected to be ejected

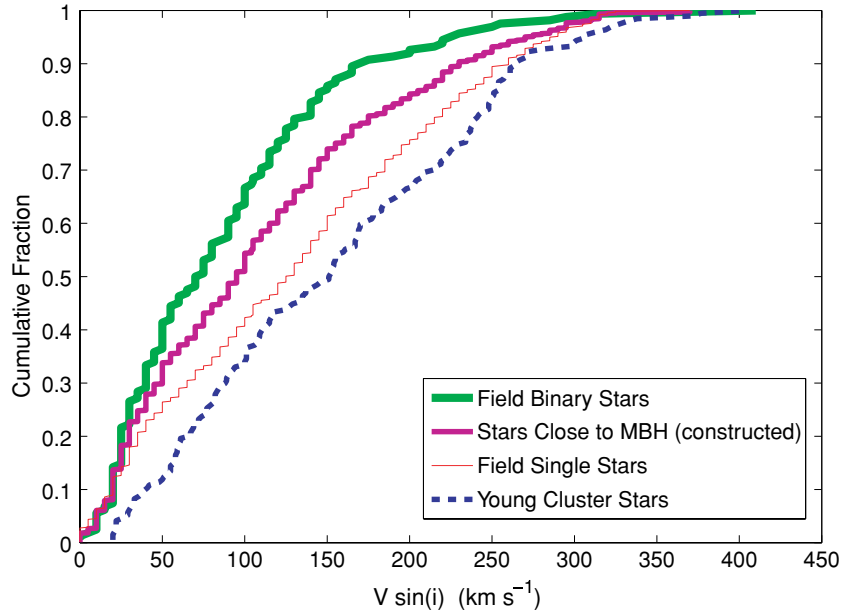


Figure 2. Cumulative distribution of the rotational velocities of massive B stars of different environments or populations. From top to bottom, field stars in binaries (Abt & Boonyarak 2004; thick solid line), constructed distribution close to the MBH (see the text; intermediate solid line), isolated field stars (Abt et al. 2002; thin solid line), and young cluster stars (*h* and χ Persei, Strom et al. 2005; dashed line).

(A color version of this figure is available in the online journal.)

as HVSSs in these scenarios (see also Löffmann & Baumgardt 2007). Other stellar populations include, for example, subdwarf B (sdB) stars (Maxted et al. 2001; Han et al. 2003), Am stars (see also Hansen 2007), and BY Dra stars (see Abt 1983 for a review).

In the binary disruption scenario for ejection of HVSSs a different picture arises. In this case, most binaries disrupted by the MBH come from much larger distances from the MBH ($\gtrsim 2$ pc; Perets et al. 2007) than HVSSs ejected in the SBH kick or IMBH inspiral scenarios. At these distances binaries could survive longer (Figure 1). However, a HVS is ejected following the disruption of the binary, destroying the possible progenitor of any binary-evolved peculiar star. Consequently, only stars that already evolved in a binary to become peculiar prior to the disruption of the binary could be ejected as peculiar-type HVSSs. Unfortunately the lifetime of many peculiar stars at this phase are usually much shorter than their lifetime on the MS (e.g., the lifetime of sdB stars is of the order of 10^8 to 2×10^8 yr; Dorman et al. 1993; whereas their progenitor MS lifetimes could be a few Gyr) and, therefore, fine tuning would be required for the ejection of HVSSs in this case (i.e., they need to be ejected within the short time after they become peculiar, and before they end their life at this phase) and they would be rare. Nevertheless, if observed, they are expected to be single stars, which would be a strong signature of their binary disruption origin, since such stellar populations are expected to be and usually observed as binary stars.

Some stellar populations do not exist in binaries, or exist only in long-period binaries. In the binary disruption scenario, such stellar populations are not (or rarely) expected to be ejected as HVSSs. For example, Be-type stars and A4-F2-type stars are usually observed with large semimajor axis, and their binary fraction at smaller semimajor axis ($< \sim 1$ AU) is low (Abt 1983; Abt & Cardona 1984). Statistics of this type of stars in HVSSs observations (or of stars very close to the MBH in the GC, where they could have been captured in the binary disruption mechanism; see, e.g., Gould & Quillen 2003; Perets et al. 2007),

could give a measure of this possible signature for the HVSSs origin from binary disruptions.

3.2. Rotational Velocities of Hypervelocity Stars

Recently, it was suggested that the rotational velocity of HVSSs can serve as a signature for their origin (Hansen 2007). Observations show that field A- and B-type MS stars that evolve in binaries have lower average rotational velocities than isolated stars (Abt et al. 2002; Abt & Boonyarak 2004). If HVSSs origin is from the binary disruption scenario, they are expected to form in binaries and, therefore, be slower rotators on average. Lower rotational velocities have been observed even for relatively young MS stars in binaries, suggesting that the low rotations are related to their formation in a binary and are not a consequence of their later evolution in that system (Abt & Boonyarak 2004). Consequently, stars formed in binaries should show this signature even if their binaries have been disrupted in a short time.

We point out that the rotational velocity distribution of stars both isolated and in binaries is very wide spread (see Figure 2) and, therefore, some statistics are required to test this signature and the rotational velocity of a single star, which cannot pinpoint to its origin as a single or a binary star (many of the stars formed in isolation are quite slow rotators, Abt & Boonyarak 2004, where as some of the binary evolved stars are very fast rotators). Using a Kolmogorov–Smirnov test we find out that $\gtrsim 25$ B MS HVSSs are required, on average, to be able to differentiate between these distributions with a $\geq 95\%$ confidence level, if all these HVSSs are taken from the same distribution (either all evolved in binaries or all evolved in isolation).

Binaries formed close to the MBH in the GC are soft binaries and would shortly after be disrupted due to perturbing encounters with other stars. Consequently, the binary components, now single stars, should also have lower rotational velocities, on average, similar to other stars formed in binaries. Since the binary fractions of stars are high (e.g., greater than 70% for B stars in

young clusters; Kobulnicky & Fryer 2008; Kouwenhoven et al. 2007), many, probably most, of the A and B MS stars in the GC are expected to have formed in binaries as slow rotators, and later on become single stars. If HVSs were ejected due to the SBH or IMBH kick scenarios, most of them are therefore expected to be relatively slower rotators. Still, a non-negligible fraction of the stars are formed as isolated stars and will possibly be faster rotators.

We can construct the rotational velocity distribution of the currently single-star populations close to the MBH (< 0.01 pc). The stellar population in this region is composed of single stars formed in isolation and of single stars originally formed in binaries that have evaporated (with the appropriate fractions). The constructed rotational velocities distribution is the combination of the single stars' and binary stars' rotational velocities with the appropriate weights that depend on the binary fraction in the population. To be conservative we take a lower limit on the initial binary fraction of $\sim 35\%$ (Abt 1983) where one should recall that each evaporated binary contributes two stars to the combined single-star population. In other words, any star chosen from our constructed rotational velocities distribution in the GC has a $35 \cdot 2 / (35 \cdot 2 + 65) = 0.51$ probability to originally form in a binary and, therefore, have a rotational velocity chosen from the binary stars distribution, although it is currently a single star. Again using a Kolmogorov–Smirnov test, we find out that $\gtrsim 100$ B MS HVSs are required, on average, to be able to differentiate between these distributions with a $\geq 95\%$ confidence level, if all these HVSs are taken from the same distribution (either all from the constructed distribution for the stellar population in the close environment of the MBH, or all evolved in binaries). Given the small number of HVSs observed and inferred to exist, such a signature for the HVSs origin is unfortunately quite weak (even weaker if a higher binary fraction is assumed).

Recently, Strom et al. (2005) and Wolff et al. (2007) have shown that the rotational velocity distribution in denser environments lack the cohort of slow rotators, thus showing very different rotational velocity distribution than field stars. Given these observations and our poor knowledge of the star formation environments in the GC (both close to the MBH and further out), it would be difficult to use the rotational velocities of HVSs as a tracer for their ejection scenario. We conclude that the rotational velocities of A and B MS HVSs are strongly dependent on the formation environment of these stars, but are most likely not good tracers for the ejection scenario of HVSs. Data on the rotational velocity distribution of stars close to the MBH and further away, may be an important clue for our understanding of their ejection mechanism, but even in that case too large statistics may be required for them to be used as a signature for the HVS ejection scenario.

3.3. On the Asymmetric Velocity Distribution of Observed Hypervelocity Stars

Current observation of HVSs detect B-type stars of limited magnitude. Such HVSs could either be MS B stars ($3\text{--}4 M_{\odot}$; possibly blue stragglers) or hot BHB stars. The velocity distribution of HVSs shows a marked asymmetry between HVSs, with many more HVSs with positive Galactocentric radial velocities than HVSs with negative ones (Brown et al. 2007b). This was suggested to infer that the observed HVSs have short lifetimes and, therefore, bound HVSs are too short lived to be observed returning with negative radial velocities (Brown et al. 2007b;

Kollmeier & Gould 2007; Svensson et al. 2008; Perets et al. 2008).

If HVSs are ejected continuously, such as in the ejection scenarios of the binary disruption by a MBH or scattering by SBHs, then bound HVSs ejected at earlier times could now be observed returning with negative radial velocities. In this cases, no asymmetry in the HVSs velocity distribution should be observed (up to the escape velocity from the galaxy, above which no returning stars are expected at any time). Consequently, the observations of asymmetry may raise a grave problem for these scenarios, unless there is a special physical reason for ejecting stars with short lifetimes. One explanation could be related to the survival probability of binaries in the GC.

Hot BHB stars have been suggested to form through evolution in binaries and may have high binary fraction, similar to sdB stars (Peterson & Green 2002; Peterson et al. 2002). If this is the case, then the fast evaporation of binaries close to the MBH in the GC would exclude the formation of such stars (as well as sdB stars) and no such BHB HVS would be ejected in the SBH kick or IMBH inspiral scenarios (see the discussion in Section 3.1). In this case, hot BHB stars would be very rare in the population of HVSs, and therefore all or most of the observed HVSs will be B MS stars that naturally have short lifetimes consistent with the asymmetric velocity distribution of observed HVSs. Alternatively, even if some of the HVSs are hot BHB stars (e.g., from the binary disruption scenario, see Section 3.1), they had to be ejected only after they evolved to this stage, and therefore their propagation time as HVSs is limited to their lifetime at this phase, which is short (a few 10^8 yr) and comparable to that of MS B stars. In both cases, an asymmetric velocity distribution of the HVSs would be expected.

HVSs could also be blue straggler stars (which would possibly give them longer propagation times, and therefore different observable velocity asymmetry). In this case, the same arguments could be introduced as for the hot BHB stars. Since the evolution of blue stragglers is also through mass transfer in binaries (or stellar collisions, however, this would not happen for an ejected star), and most if not all of the field blue stragglers are in binaries (Carney et al. 2001; note, however, that these refer to lower mass blue stragglers), we may expect to see only blue straggler HVSs that have been already ejected after they evolved to this phase. Such stars are practically indistinguishable from regular MS stars, and their lifetime at this stage is as short.

Another possibility for explaining HVSs velocity asymmetry is the case of a limited time span for the ejection of HVSs, such as expected during an IMBH inspiral in the GC; i.e., a short-lived discrete event, and not long-lived continuous process such as discussed above. In this case, stars are expected to be ejected only during the limited and relatively short timescale at which the IMBH could eject HVSs (unless several such inspiral events happened). Such a timescale could be as large as 10^8 yr (Löckmann & Baumgardt 2007), which could marginally fit the observed ejection time span of the unbound HVSs (Figure 8 in Brown et al. 2007b)³.

Recently, the possibility of rare massive binary encounter in dense young clusters (Gvaramadze et al. 2008) has been suggested for ejection of HVSs. Such a process is also a continuous process which should have similarly lead to a symmetric velocity distribution. However, in this scenario mostly massive stars (and hence short lifetimes) are expected to be ejected, which

³ Note, however, that scattering of stars by massive perturbers such as giant molecular clouds and clumps could shorten the inspiral time of the IMBH considerably (Perets & Alexander 2008).

could explain the lack or high velocity of returning stars. However, it is not at all clear whether the necessary conditions in such young clusters exist, and whether the frequency of such rare strong encounters could, to begin with, explain the observed population of HVSSs (and especially unbound HVSSs; see Perets 2008 for a short discussion on this).

We conclude that the currently observed B-type HVSSs are most likely MS B stars, and suggest that hot BHB HVSSs could only be produced in the binary disruption scenario. However, even in the latter scenario these are not expected to be frequent.

4. SUMMARY

In this study, we have explored some dynamical and evolutionary constraints on the nature and origin of HVSSs and of the stellar population in the GC. Hypervelocity stars are thought to be ejected through dynamical interactions near the MBH in the GC. Three scenarios have been suggested for their ejection: a disruption of a binary star by the MBH, scattering by an intermediate mass BH, which inspirals to the MBH, or scattering by stellar BHs in the close region of the MBH. In the binary disruption scenario, HVSSs originate only from binaries, where most of them evolved far from the MBH (> 2 pc). In the scattering scenarios by an intermediate mass or stellar BHs most HVSSs are single stars scattered from a close region near the MBH (< 0.01 pc from it). Given the differences between them, the ejection scenarios of HVSSs are expected to involve different stellar populations in the GC. We have used dynamical and evolutionary arguments together with current observations regarding the stellar population in the GC to constrain the nature and origin of HVSSs. We have shown that the IMBH inspiral scenario requires too many MS B stars to exist close to the MBH (< 0.01 pc). Scattering by SBHs are also not likely to be consistent with the observed population of B stars in the GC, although this scenario can still be compatible with observations under extreme conditions. The binary disruption scenario is still consistent with current observations.

Due to the conditions close to the MBH most binary star systems are not expected to survive for long in this region. Consequently, unique stellar populations that require a long evolution in a binary, such as sdB (and possibly hot BHB) stars, blue stragglers, Am stars, and other populations are not expected to be ejected as HVSSs in the SBH kicks or IMBH inspiral scenarios. In the binary disruption scenarios, the involved binaries originate much further from the MBH where they could survive longer, and therefore HVSSs of these unique stellar population are not excluded, although their rates might be quenched because of their shortened evolution in the binary systems. Conversely, stellar populations that are not frequently observed in close binaries, such as required in the binary disruption scenario (e.g., Be stars, A4-F2-type stars), are not expected to be ejected as HVSSs, or to be captured close to the MBH in this case, but they can still possibly be ejected in the SBH kicks scenarios. We also show that these arguments suggest that signatures for HVSSs origin such as hypervelocity binaries and slow rotating HVSSs may be much weaker than expected and may require large statistics.

I thank Warren Brown, Brad Hansen, Tal Alexander, and Uli Heber for helpful discussions and references. I also thank the Israeli Commercial & Industrial Club for their support through the Ilan Ramon scholarship. H.B.P. is supported by ISF grant 928/06.

REFERENCES

- Abt, H. A. 1983, *ARA&A*, **21**, 343
 Abt, H. A., & Boonyarak, C. 2004, *ApJ*, **616**, 562
 Abt, H. A., & Cardona, O. 1984, *ApJ*, **285**, 190
 Abt, H. A., Levato, H., & Grosso, M. 2002, *ApJ*, **573**, 359
 Baumgardt, H., Gualandris, A., & Portegies Zwart, S. 2006, *MNRAS*, **372**, 174
 Berukoff, S. J., & Hansen, B. M. S. 2006, *ApJ*, **650**, 901
 Binney, J., & Tremaine, S. 1987, *Galactic Dynamics* (Princeton, NJ: Princeton Univ. Press)
 Bromley, B. C., et al. 2006, *ApJ*, **653**, 1194
 Brown, W. R., et al. 2005, *ApJ*, **622**, L33
 Brown, W. R., et al. 2006a, *ApJ*, **640**, L35
 Brown, W. R., et al. 2006b, *ApJ*, **647**, 303
 Brown, W. R., et al. 2007a, *ApJ*, **660**, 311
 Brown, W. R., et al. 2007b, *ApJ*, **671**, 1708
 Brown, W. R., et al. 2008, in press, arXiv:0808.2469
 Carlberg, R. G., & Innanen, K. A. 1987, *AJ*, **94**, 666
 Carney, B. W., et al. 2001, *AJ*, **122**, 3419
 Dorman, B., Rood, R. T., & O'Connell, R. W. 1993, *ApJ*, **419**, 596
 Duquennoy, A., & Mayor, M. 1991, *A&A*, **248**, 485
 Edelmann, H., et al. 2005, *ApJ*, **634**, L181
 Eisenhauer, F., et al. 2005, *ApJ*, **628**, 246
 Fuentes, C. I., et al. 2006, *ApJ*, **636**, L37
 Garmany, C. D., Conti, P. S., & Massey, P. 1980, *ApJ*, **242**, 1063
 Genzel, R., et al. 2003, *ApJ*, **594**, 812
 Ghez, A. M., et al. 2005, *ApJ*, **620**, 744
 Gould, A., & Quillen, A. C. 2003, *ApJ*, **592**, 935
 Gvaramadze, V. V., Gualandris, A., & Portegies Zwart, S. 2008, *MNRAS*, **385**, 929
 Han, Z., et al. 2003, *MNRAS*, **341**, 669
 Hansen, B. 2007, *ApJ*, **671**, L133
 Hansen, B. M. S., & Milosavljević, M. 2003, *ApJ*, **593**, L77
 Heggie, D. C. 1975, *MNRAS*, **173**, 729
 Hills, J. G. 1988, *Nature*, **331**, 687
 Hills, J. G. 1991, *AJ*, **102**, 704
 Hirsch, H. A., et al. 2005, *A&A*, **444**, L61
 Kenyon, S. J., Bromley, B. C., Geller, M. J., & Brown, W. R. 2008, *ApJ*, **680**, 312
 Kobulnicky, H. A., & Fryer, C. L. 2008, *ApJ*, **670**, 747
 Kollmeier, J. A., & Gould, A. 2007, *ApJ*, **664**, 343
 Kouwenhoven, M. B. N., et al. 2007, *A&A*, **474**, 77
 Levin, Y. 2006, *ApJ*, **653**, 1203
 Levin, Y. 2007, *MNRAS*, **374**, 515
 Levin, Y., Wu, A., & Thommes, E. 2005, *ApJ*, **635**, 341
 Löckmann, U., & Baumgardt, H. 2008, *MNRAS*, **384**, 323
 Lopez-Morales, M., & Bonanos, A. Z. 2008, *ApJ*, **685**, L47
 Lu, Y., Yu, Q., & Lin, D. N. C. 2007, *ApJ*, **666**, L89
 Maxted, P. f. L., et al. 2001, *MNRAS*, **326**, 1391
 Miller, G. E., & Scalo, J. M. 1979, *ApJS*, **41**, 513
 Miralda-Escudé, J., & Gould, A. 2000, *ApJ*, **545**, 847
 O'Leary, R. M., & Loeb, A. 2007, *MNRAS*, **383**, 1076
 Paumard, T., et al. 2006, *ApJ*, **643**, 1011
 Perets, H. B. 2008, arXiv:0802.1004
 Perets, H. B., & Alexander, T. 2008, *ApJ*, **677**, 146
 Perets, H. B., Hopman, C., & Alexander, T. 2007, *ApJ*, **656**, 709
 Perets, H. B., et al. 2008, arXiv:0809.2087
 Peterson, R. C., & Green, E. M. 2002, in IAU Symp. 187, *Cosmic Chemical Evolution*, ed. K. Nomoto & J. W. Truran (Dordrecht: Kluwer), 97
 Peterson, R. C., et al. 2002, in ASP Conf. Ser. 265, *Omega Centauri, A Unique Window into Astrophysics*, ed. F. van Leeuwen, J. D. Hughes, & G. Piotto (San Francisco, CA: ASP), 255
 Przybilla, N., et al. 2008, *A&A*, **488**, L51
 Schaller, G., Schaerer, D., Meynet, G., & Maeder, A. 1992, *A&AS*, **96**, 269
 Sesana, A., Haardt, F., & Madau, P. 2007, *MNRAS*, **379**, L45
 Sesana, A., Haardt, F., & Madau, P. 2008, *ApJ*, **686**, 432
 Sherwin, B. D., Loeb, A., & O'Leary, R. M. 2008, *MNRAS*, **386**, 1179
 Sternberg, A., Hoffmann, T. L., & Pauldrach, A. W. A. 2003, *ApJ*, **599**, 1333
 Strom, S. E., Wolff, S. C., & Dror, D. H. A. 2005, *AJ*, **129**, 809
 Svensson, K. M., Church, R. P., & Davies, M. B. 2008, *MNRAS*, **383**, L15
 Wolff, S. C., et al. 2007, *AJ*, **133**, 1092
 Yu, Q., & Tremaine, S. 2003, *ApJ*, **599**, 1129

Chapter 5

Runaway and hypervelocity stars in the Galactic halo: Binary rejuvenation and triple disruption

Perets

The Astrophysical Journal, in press (2009; arXiv:0802.1004)

RUNAWAY AND HYPERVELOCITY STARS IN THE GALACTIC HALO: BINARY REJUVENATION AND TRIPLE DISRUPTION

HAGAI B. PERETS¹

Weizmann Institute of Science, POB 26, Rehovot 76100, Israel

Draft version May 28, 2009

Abstract

Young stars observed in the distant Galactic halo are usually thought to have formed elsewhere, either in the Galactic disk or perhaps the Galactic center, and subsequently ejected at high velocities to their current position. However, some of these stars have apparent lifetimes shorter than the required flight time from the Galactic disk/center. We suggest that such stars have evolved in close runaway or hypervelocity binaries. Stellar evolution of such binaries can drive them into mass transfer configurations and even mergers. Such evolution could then rejuvenate them (e.g. blue stragglers) and extend their lifetime after their ejection. The extended lifetimes of such stars could then be reconciled with their flight times to the Galactic halo. We study the possibilities of binary runaway and hypervelocity stars and show that such binaries could have been ejected in triple disruptions and other dynamical interactions with stars or with massive black holes. We show that currently observed “too young” star in the halo could have been ejected from the Galactic disk or the Galactic center and be observable in their current position if they were ejected as binaries. Specifically it is shown that the hypervelocity star HE 0437-5439 could be such a rejuvenated star. Other suggestions for its ejection from the LMC are found to be highly unlikely. Moreover, it is shown that its observed metallicity is most consistent with a Galactic origin and a Galactic center origin can not currently rule out. In addition, we suggest that triple disruptions by the massive black hole in the Galactic center could also capture binaries in close orbits near the MBH, some of which may later evolve to become more massive rejuvenated stars.

Subject headings: black hole physics — galaxies: nuclei — stars: kinematics

1. INTRODUCTION

Young massive OB stars are usually observed close to their birth place in young stellar clusters or associations (e.g. Hoogerwerf et al. 2000). Some of them, however, are observed in isolation, far from any star forming region. Observations of such stars in the Galactic halo are especially puzzling given the unfavorable conditions for regular star formation in such regions. Formation of massive stars usually requires special conditions such as the the existence of molecular clouds with dense cores that could collapse to form massive stars. Such gas reservoirs do not exist at large distances in the Galactic halo (Savage & de Boer 1981; Sembach & Danks 1994). Nevertheless, young OB stars are observed there. These halo young stars are usually observed to have high peculiar velocities ($> 40 \text{ km s}^{-1}$), and are thought to have been ejected from their birth place and acquire their high velocity through some dynamical process. Due to their high velocities they could propagate to their currently observed remote location, even during their short lifetimes. Such high velocity stars are thought to be dynamically ejected in stellar binary interactions or through a binary supernova explosions (so called runaway stars; Blaauw e.g. 1961; Poveda et al. e.g. 1967; Martin e.g. 2006, and references there in). Young stars with even higher velocities, so called Hypervelocity stars (HVSs; with velocities $> 300 \text{ km s}^{-1}$; Hills 1988; Brown et al. 2005; Hirsch et al. 2005; Brown et al. 2007b, and references there in), are most likely ejected from the Galactic center (GC) through some interaction with the massive black hole (MBH) known to exist there (Hills 1988; Yu & Tremaine 2003). However, in some cases even the high velocities of these runaway/hypervelocity stars are not sufficient to explain their remote locations, so far from any star forming region.

In those cases it appears that flight times of these the young stars from their birthplace in the Galactic disk (or the GC) to their current location is longer than their main sequence (MS) lifetimes.

In the following we suggest that such discrepancy could be solved if these stars were ejected as runaway or hypervelocity binaries. A combination of dynamical and evolutionary processes could then explain the existence of these “too young” halo stars. Following their ejection and propagation in the Galaxy, the ejected runaway/hypervelocity binaries could evolve and rejuvenate through mass between (or merger of) the binary stellar components. Such rejuvenation could extend the main sequence lifetime of these stars and resolve the discrepancy between their apparent lifetimes and estimated flight times. We first shortly overview the observations of Galactic halo young stars in §2. We then discuss the possible dynamical scenarios for the ejection of runaway and hypervelocity binaries that can serve as progenitors of rejuvenated halo stars (§3). The rejuvenation scenario is presented in §4, followed by the discussion (§5) and summary.

2. YOUNG STARS IN THE GALACTIC HALO

In many cases dynamical processes can eject massive stars from their original birth place at high velocities. These so called ‘runaway’ stars (Blaauw 1961; for a short overview see Hoogerwerf et al. 2001) constitute a considerable fraction of the early O and B star population in the galaxy; $\sim 30 - 40\%$ of the O stars and $5 - 10\%$ of the B stars (Stone 1991, and refs. within). Such stars have large peculiar velocities of $40 \leq v_{pec} \leq 200 \text{ km s}^{-1}$ (Gies 1987; Hoogerwerf et al. 2001) or even higher (Martin 2006). Besides their relatively high velocities, runaway stars are also distinguished from the normal early-type stars by their much lower ($< 10\%$) multiplicity compared with the binary fraction of normal early-type

Electronic address: hagai.perets@weizmann.ac.il

TABLE 1
TOO YOUNG STARS IN THE GALACTIC HALO

Name	Mass (M_{\odot})	T_{evol} (Myrs)	T_{ej} (Myrs)	References
Hypervelocity Stars				
HE 0437-5439	9	29	90 ± 10	Edelmann et al. 2005
Runaway stars				
BD +38 2182	6.6	60	53 ± 8	Martin 2006
BD +36 2268	6.9	51	50 ± 2	"
HD 140543	22	8	23 ± 3	"
HD 188618	9.7	26	38 ± 8	"
HD 206144	9.7	26	25 ± 2	"
PG 0122+214	6.7	35 ± 6	51 ± 24	Ramspeck et al. 2001
PG 1610+239	5.8	54 ± 10	> 62	"
PHL 159	8	28 ± 2	31	"
PHL 346	9.9	19 ± 2	27 ± 7	"
SB 357	7.4	26 ± 4	61	"
HS 1914+7139	6.2	39 ± 6	91	"
PG 0914+001 ^a	5.8 (4.7)	79 (116)	199 (109)	Lynn et al. 2004
PG 1209+263 ^a	6.3 (5)	62 (91)	272 (170)	"
PG 2219+094 ^a	7.5 (6.5)	41 (53)	53 (52)	"
PG 2229+099 ^a	5.8 (5.4)	49 (63)	63 (58)	"

^aNumbers in parentheses show lower/upper limits on the timescales that could minimize the time discrepancies (from Lynn et al. 2004).

stars ($> 50\%$ and up to 100% ; Garmany et al. 1980; Mason et al. 1998; Kobulnicky & Fryer 2007; Kouwenhoven et al. 2007). An additional class of stars with even higher velocities have been discovered in recent years, with the observations of several HVSs ($> 300 \text{ km s}^{-1}$) in the Galactic halo (Brown et al. 2005; Edelmann et al. 2005; Brown et al. 2007b).

In most cases observed OB runaways and HVSs are found to have kinematics consistent with an ejection from a star forming region in the Galactic disk of from the GC (Hoogerwerf et al. 2001; Martin 2006; Brown et al. 2007b). However, some of the young stars observed at large distances in the Galactic halo can not be regular runaway or hypervelocity stars. The flight times of these stars, required in order to reach their current position after being ejected from their birth place, are longer than their lifetimes (given their observed positions and velocities). Table 1 shows a list of such candidate stars, collected from the literature, where we list stars with calculated propagation times which could potentially be larger than their evolutionary time, given the uncertainties. We caution that the uncertainties in the radial and/or proper motion velocities exist for some of these stars, and their travel time and evolutionary times may be in fact consistent (this is true for 10 of the 16 stars in the table). Nevertheless, we show all of the halo stars that potentially have travel time and life time inconsistencies, not excluded by current observations. Several other stars suggested in the literature to have such inconsistencies, were later found to be closer/older or faster stars in later observations (Ramspeck et al. 2001; Lynn et al. 2004; Martin 2006). Such stars were excluded from the list.

Such 'too young' halo stars have been suggested to possibly form in situ in the halo (see Keenan 1992 and references there in). However, as we suggest below, it is far more likely that these stars have been ejected as binaries and then became blue stragglers by rejuvenating through mass transfer from (or merger with) their binary companion.

3. DYNAMICAL EJECTION OF RUNAWAY AND HYPERVELOCITY BINARIES

3.1. Runaway binaries

Two mechanisms are thought to contribute to the ejection of runaway stars, both involve binarity (or higher multiplicity). In the binary supernova scenario (Blaauw 1961) a runaway star receives its velocity when the primary component of a massive binary system explodes as a supernova (SN). When the SN shell passes the secondary, the gravitational attraction of the primary reduces considerably, and the secondary starts to move through space with a velocity comparable to its original orbital velocity. In the dynamical ejection scenario (Poveda et al. 1967) runaway stars are formed through gravitational interactions between stars in dense, compact clusters. Simulations show that such encounters may produce runaways with velocities up to 200 km s^{-1} (Mikkola 1983; Leonard & Duncan 1990; Leonard 1991; Gualandris et al. 2004). These scenarios suggest that many of the early OB stars formed in young clusters could be ejected from their birth place and leave the cluster at high velocity.

Theoretical studies suggest that binary stars could also be ejected at high velocities, although at smaller fraction of ~ 0.1 of all the runaway stars (Leonard & Duncan 1988, 1990; Portegies Zwart 2000). Such runaway binaries have indeed been observed (Gies & Bolton 1986; Mason et al. 1998; Martin 2006; Lockman et al. 2007; McSwain et al. 2007b,a), with fractions of ~ 0.1 in the runaway stars samples. The periods of the runaway binaries were found to be typically short (< 5 days; Gies & Bolton 1986; Mason et al. 1998; Martin 2003) as expected from the dynamical ejection scenario. Some of the binaries were found to be with larger period (~ 20 days) and relatively eccentric orbits (> 0.4) and are thought to be ejected due to a SN explosion (Lockman et al. 2007; McSwain et al. 2007b,a), in which case rejuvenation is not possible.

3.2. Hypervelocity binaries

Extreme velocities as found for HVSs most likely suggest a different dynamical origin than that of runaway stars. Several scenarios have been suggested for ejection of HVSs, all of them require an interaction with the MBH. These include a disruption of a stellar binary by a MBH (Hills 1988; Yu & Tremaine 2003; Ginsburg & Loeb 2006; Perets et al. 2007), an interaction of a single star with an intermediate mass black hole (IMBH) which inspirals to the GC (Hansen & Milosavljević 2003; Yu & Tremaine 2003; Levin 2006; Baumgardt et al. 2006; Lockmann & Baumgardt 2007; Sesana et al. 2007), or interaction with stellar black holes (SBHs) in the GC (Yu & Tremaine 2003; Miralda-Escudé & Gould 2000; O'Leary & Loeb 2007). In such scenarios stars could be ejected from the GC with velocities of hundreds and even a few thousands km s^{-1} possibly extending much beyond the escape velocity from the galaxy.

Recently it was suggested that binary stars could also be ejected as hypervelocity binaries during the inspiral of an IMBH (Lu et al. 2007; Sesana et al. 2008), and could serve as evidence for the binary MBH ejection scenario. It was noted that the other scenarios for hypervelocity ejection are not likely to eject hypervelocity binaries. Specifically the probability for a binary ejection in a triple disruption by a MBH is negligibly small. The later claim may well be correct for the low mass hypervelocity stars discussed in Lu et al. paper, however, as we show in the following, a non-negligible number of massive hypervelocity binaries could be ejected through a triple disruption by the MBH in the GC. Young massive binaries may also be ejected by an inspiraling IMBH as suggested by Lu et al. for low mass binaries. However, the

fraction of surviving binaries close to the MBH, where they could be ejected as HVSBs by an inspiraling IMBH is small, since most would be disrupted through dynamical interactions with other stars in this hostile environment; see Perets (2009) for detailed discussion. Moreover, it is likely that the most if not all of the observed young HVSBs in the Galactic halo were not ejected in such a scenario, given the observational constraints on the number of young stars observed close to the MBH in the GC (Perets 2009). In the following we discuss the triple disruption scenario.

3.2.1. Triple disruption by a MBH

A close pass of a binary star near a massive black hole results in an exchange interaction, in which one star is ejected at high velocity, while its companion is captured by the MBH and is left bound to it. Such interaction occurs because of the tidal forces exerted by the MBH on the binary components. Typically, a binary (with mass, $M_{bin} = M_e + M_c$ and semi-major axis, a_{bin}), is disrupted when it crosses the tidal radius of the MBH (with mass M_{BH}), given by

$$r_t = \left(\frac{M_{BH}}{M_{bin}} \right)^{1/3} a_{bin} \quad (1)$$

and one of the stars (with mass M_c) is captured close to the MBH and the other (with mass M_e) is ejected at high velocity of about (Hills 1991; Bromley et al. 2006)

$$v_{BH} = 1800 \text{ km s}^{-1} \times \left(\frac{a_{bin}}{0.1 \text{ AU}} \right)^{-1/2} \left(\frac{M_e + M_c}{2M_\odot} \right)^{1/3} \times \left(\frac{M_{BH}}{4 \times 10^6 M_\odot} \right)^{1/6} \left(\frac{2M_c}{M_e + M_c} \right)^{(1/2)}. \quad (2)$$

The same scenario could be extended to a triple disruption by a MBH. Triple stars have a stable configuration if the semi major axis of the outer binary, a_o is much larger than the semi major axis of the inner binary, a_i (i.e. $a_i \ll a_o$). In such hierarchical triples, the outer binary could be disrupted by the MBH while the inner closer binary is kept bound. In this case a triple disruption could produce a hypervelocity binary, or alternatively a captured binary star near the MBH. The ejection velocity in Eq. 2 is strongly dependent on the semi major axis of the binary (the outer binary in the triple case) and on the mass of the stellar binary (triple in this case). Both of these parameters vary by much between the population of low mass stars and high mass stars.

For low mass stars ($M_{triple} \sim 3 M_\odot$, for equal mass stars) such as studied by Lu et al. (2007), one requires $a_{bin} = a_o \sim 0.4 \text{ AU}$ for ejection of a hypervelocity binary at $\sim 900 \text{ km s}^{-1}$. Such close binaries are infrequent (only a few percents of the binary population; Duquennoy & Mayor 1991), and the fraction of low mass triples with such close outer binaries is negligibly small (Tokovinin et al. 2006).

For higher mass stars such as the observed young B-type hypervelocity stars in the Galactic halo, $m_* \sim 2 - 4 M_\odot$ corresponding to a triple mass of $M_{triple} \sim 6 - 12 M_\odot$ (assuming equal mass stars). In this case even a semi major axis of $a_o \sim 0.6 - 1 \text{ AU}$ is sufficient for the ejection of a hypervelocity binary. High mass binary stars are known to have higher binary fraction (probably $f_{bin} > 0.8$, e.g. Abt et al. 1990; Mason et al. 1998; Kobulnicky & Fryer 2007)

and different semi-major axis distribution than low mass stars, with a large fraction of them ($f_{cbin} \sim 0.4$) in close binaries ($a_{bin} < 1 \text{ AU}$, e.g. Abt 1983; Morrell & Levato 1991). The triple fraction and distribution of massive stars is still uncertain, but it is strongly suggestive of a high triple fraction among binaries. Evans et al. (2005) find that most if not all of the massive binaries they observed (in Cepheids) are likely to be triple systems. Some $f_{triple} \sim 0.8$ of the wide visual binaries in stellar associations are in fact hierarchical triple systems, where typically the more massive of the binary components is itself a spectroscopic or even eclipsing binary pair (Zinnecker 2005). Fekel (1981) compared the properties of close multiple stars. He finds a fraction $f_{\frac{1}{2} \text{ yr}} \sim 0.2$ of the more massive systems (we choose systems with total mass of $> 6 M_\odot$) to have outer binary periods shorter than half a year, corresponding to $a_o \lesssim 1 \text{ AU}$, i.e. with characteristics allowing for the ejection of hypervelocity binary, if they were disrupted by a MBH. The fraction of close triples (such as those in Fekel 1981) out of the total triple population is unknown. In the lack of better estimate we assume this fraction to follow the the fraction of close binaries¹, i.e. we take the fraction of close triples out of the full triple population to be $f_{ctriple} = f_{cbin} \cdot f_{\frac{1}{2} \text{ yr}} = 0.4 \times 0.2 = 0.08$ (note that the fraction of close triples might in fact be higher, since f_{cbin} is taken for binaries with $a_{bin} < 1 \text{ AU}$ where as Fekel's sample also contain triples with wider outer binaries). Taken together we can estimate the triple fraction of hypervelocity binary potential progenitors to be $f_{prog} = f_{bin} \cdot f_{triple} \cdot f_{ctriple} \simeq 0.05$ (taking a binary fraction of 0.8 of which 0.8 are triples, and 0.08 of those have outer binaries with period $< 0.5 \text{ yr}$). We note that there is some weak trend for more massive stars to have higher multiplicity, however, more observational data is required for a better resolution of the mass dependence of the multiplicity, and the quoted values are assumed to represent all main sequence B-stars.

Note that very few studies on observed massive triples have been done, and therefore we also try to estimate the appropriate triple fraction differently, based only on the better known characteristics of massive binaries, where we follow the method used by Fabrycky & Tremaine (2007). Again, we assume that the orbital and stellar characteristics of the third component in a given triple could be chosen from the same distributions of the binaries¹. We pick a sample of randomly chosen triple systems taken from the appropriate binary distributions. For our sample we choose many triples with initial orbital distributions such that both their inner and outer binaries are taken from the best fit observed distributions of Kobulnicky & Fryer (2007). Each given triple has an inner binary with semi major axis a_i and masses m_1 and m_2 ; and an outer companion with mass m_3 in an orbit with semi major axis a_o . The period is chosen from a distribution of orbital separations which is flat in log space, $f(\log p) \propto \text{Const}$, corresponding to $f(r) \propto 1/r$ (i.e., Öpik's law). The minimum value for the for the appropriate semi-major axis is taken to be twice the radii of the binary stars, i.e. separation of a contact binary which does not immediately merge. The maximal value is

¹ This is a reasonable assumption since the difference in the dynamics of a star due to the interaction with a companion single mass or a very close binary (i.e. the inner binary) are very small, especially when discussing the surviving triples that are hierarchical. Nevertheless, we emphasize that this is an assumption. Future observations of triple systems, when available, should be used to produce more accurate and not assumption dependent estimates of triples distributions.

taken to be 1000 AU, following the best fit distribution found by Kobulnicky & Fryer (2007). The mass ratio, q , is chosen from a power law distribution ($f(q) \propto q^{-0.4}$); we also tried other distributions suggested in the literature and found only minor effects on the final calculated fraction. The mass of the tertiary companion, m_3 , was determined by choosing $q = m_3/m_1 + m_2$ from the same mass ratio distribution. This approach implies that the mass of the third star was correlated with the mass of the inner binary, but we do not believe that this correlation has any significant effect on our results.

Two periods and eccentricities were picked in the same manner discussed in Fabrycky & Tremaine. The smaller (larger) period was assigned to the inner (outer) orbit. The semi major axes were computed from these masses and periods assuming non interacting Keplerian orbits. The mutual inclination distribution of the tertiary is assumed to be isotropic with respect to the inner binary. After these parameters were selected, we used the empirical stability criterion used in Fabrycky & Tremaine (2007; see their Eq. (37) originally formulated in Mardling & Aarseth 2001) to determine whether the system is hierarchical or if it will disrupt in a small number of dynamical times. If the semi major axes obeyed this criterion then we accepted the triple as stable, otherwise, we assumed it disrupted. We then found the fraction of stable triples, such that their disruption by the MBH in the GC could eject a hypervelocity binary, i.e. have outer semi-major axis small enough for the ejection velocity to be high.

From a large sample of triples (10^5) we find that about 0.03 of potentially formed triples are stable triples that could serve as hypervelocity binaries progenitors, where this results is not very sensitive to the prime mass m_1 of the inner binary component. This is generally consistent with the observation based estimates given before. We conclude that $\sim 0.03 - 0.05$ of all massive hypervelocity stars could have been ejected with a binary companion or have left a close binary captured in an orbit very close to the MBH.

4. REJUVENATION AND EVOLUTION IN HIGH VELOCITY CLOSE BINARIES

Binaries ejected at high velocities are relatively close binaries. For both runaway and hypervelocity binaries the closer the binary is, the higher is its probability to be ejected at high velocity (see e.g. Eq. 2). In the case of binaries evolving in triples (e.g. hypervelocity binaries from triple disruptions), dynamical evolution could be very efficient in producing very close inner binaries. A large fraction of such triples evolve through Kozai oscillations (Kozai 1962), in which the inner binary is periodically driven into high eccentricities. When the eccentricity of the inner binaries are high enough the binary components tidally interact, and dissipate the orbital energy. This mechanism of Kozai cycles and tidal friction (KCTF) was shown to drive the inner binary into close configuration and circularization at periods of a few days (Kiseleva et al. 1998; Eggleton & Kiseleva-Eggleton 2001; Fabrycky & Tremaine 2007), at relatively short times (\sim Myr), much shorter than the MS lifetime of the stars (Fabrycky, private communication; 2007). In fact it is quite plausible that most of the observed contact binaries are produced through evolution in triple stars (D’Angelo et al. 2006; Pribulla & Rucinski 2006; Fabrycky & Tremaine 2007). We conclude that most if not all runaway and hypervelocity binaries should be ejected as close (period of up to a few tens of days) or even contact binaries.

During the evolution of close binaries in the triples they

can closely interact through mass transfer and even mergers (citeper+09). Such interaction could lead to rejuvenation of one the binary components (see e.g. Dray & Tout 2007; Vanbeveren et al. 1998), and even to its “reincarnation” as higher mass star. Such rejuvenated stars, also known as blue stragglers (although this term usually refers to low mass rejuvenated stars) could appear much younger than their real age (Vanbeveren et al. 1998). For high velocity stars such extended lifetimes could potentially be translated into much larger propagation distances from their birth place. Consequently, such high velocity massive blue stragglers could be observed to have flight times longer than their apparent lifetime (see table 1).

We used the population synthesis program SeBa², as described in detail in Portegies Zwart & Verbunt (1996) and Portegies Zwart & Yungelson (1998), to study the possible outcomes from the evolution of close runaway and hypervelocity binaries. In this module stars are evolved via the time dependent mass-radius relations for solar metallicities given by Eggleton et al. (1989) with corrections by Eggleton et al. (1990) and Tout et al. (1996). These equations give the radius of a star as a function of time and the initial mass of the star (on the zero-age main-sequence). The mass of the stellar core and the rate of mass loss via a stellar wind (not specified in this prescription) were included using the prescriptions of Portegies Zwart & Verbunt (1996).

We have focused on the evolution of the possible binary progenitors of the rejuvenated OB stars, such as currently observed in the Galactic halo (table 1). For this purpose we generated a grid of initial conditions for the periods (in the range 1 – 100 days) and eccentricities (0 – 0.99) of the binaries. Observations of massive binaries show that the components mass ratios are usually large (Kobulnicky & Fryer 2007). We have studied binaries with different masses and/or mass ratios. For each possibility we followed the binaries evolution for any initial condition in our grids, until both the binary components (or single component in case of a merger) have finished their evolution on the MS. We then recorded the total evolution time and the binary characteristics (component masses, period, and eccentricity). Here we show the results of two representative masses for the prime binary component (4.8 and $9.6 M_\odot$) and two possible mass ratios ($q = 0.9, 0.5$). Similar results have been found for other masses and mass ratios.

The binary evolution scenarios in our grid which produce rejuvenated stars correspond to different types of mass transfer scenarios, namely type A and type B mass transfer (Paczynski (1971)). We find three main outcomes for the evolution of such close binaries; merger, strong mass transfer and weak mass transfer (see Fig. 1). When the two components are very close (i.e. small periods of a few days for circular orbits, or longer period binaries with higher eccentricities), the binary components merge to form a single star containing almost all of the total initial binary mass. These mass transfer scenarios are all basically subtypes of type A mass transfer (see Nelson & Eggleton (2001) for detailed description). The time until merger varies between almost immediate merger up to the MS lifetime of the more massive component. A mass transfer and/or merger evolution may lead to some observational signatures, such as possibly high rotational velocity (Leonard 1995, and references there in); or chemical anomalies, such as CNO abundances anomalies citepsar+96,che+04,fer+06. For our rejuvenated stars candi-

² <http://www.ids.ias.edu/~starlab/seba/>

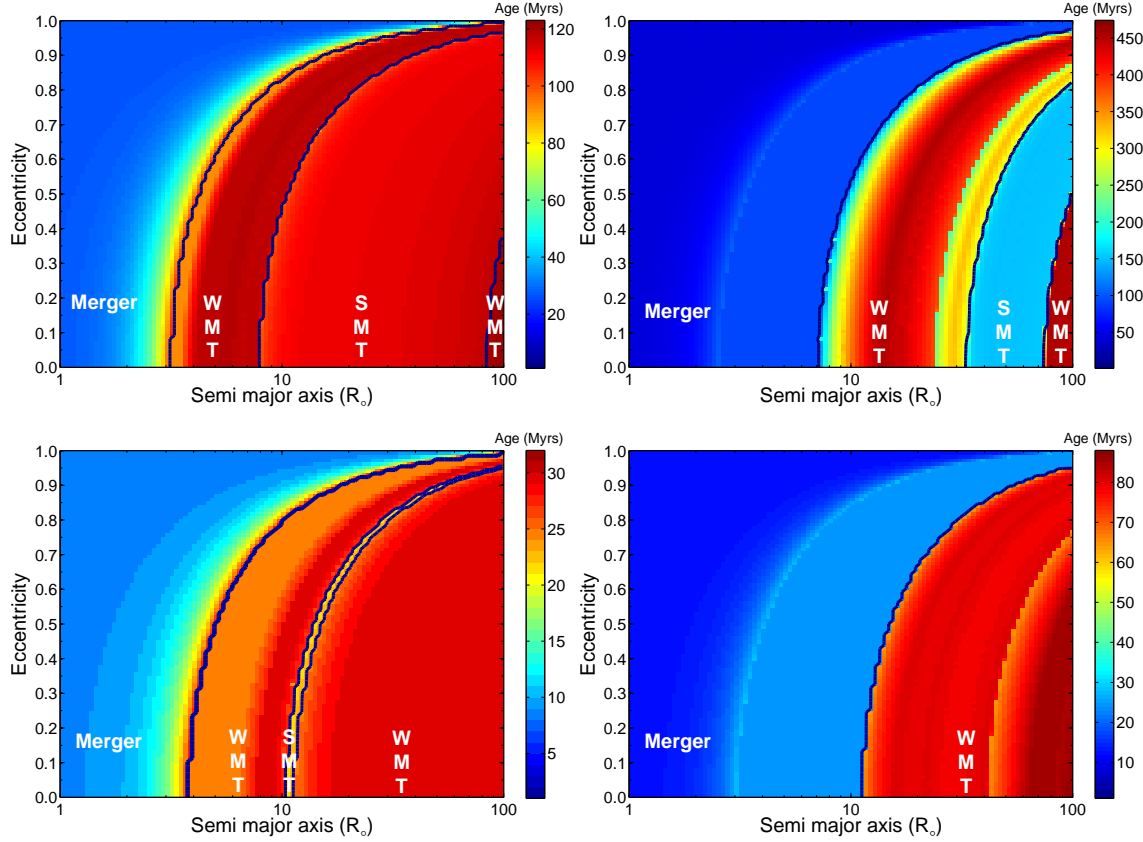


FIG. 1.— Evolutionary time scale for close binaries with a range of initial conditions (semi-major axis and eccentricity). Colors (in Myrs) indicate the evolutionary time after which both binary components end their life on the main sequence. Black lines separate the different evolutionary regimes; full merger, weak mass transfer (WMT) and strong mass transfer (SMT). Four cases are shown corresponding to binaries with prime masses of $4.8 M_{\odot}$ (upper figs.) and $9.6 M_{\odot}$ (lower figs.), and mass ratios of 0.9 (left figs.) and 0.5 (right figs.). The masses of the rejuvenated binary component are $m_{rej} > 0.95$ times the initial total binary mass m_{bin} in the merger case (single star); $0.8 m_{bin} < m_{rej} < 0.9 m_{bin}$ in the SMT case; and $0.4 m_{bin} < m_{rej} < 0.6 m_{bin}$ in the WMT case.

date sample we find that high rotational velocities are possibly observed in PG 1209+263, HS 1914+7139; PG 0914+001 (Ramspeck et al. 2001). Large chemical anomalies are observed in HS 1914+7139; Lynn et al. 2004). However, such peculiarities are not likely to be strong signatures, since they do not necessarily arise only due to mass transfer processes, and may not even be produced in the majority of rejuvenated stars to begin with. We conclude that given the weak observational signature of the rejuvenation process on the appearance of the rejuvenated stars, observations of the chemical or rotational properties can not serve to directly trace their binary origin.

In longer period binaries (and/or smaller eccentricities) strong mass transfer occurs when the more massive binary components leave the MS. The massive component then shed most of its mass to its companion. This scenario usually produces a massive MS star containing $0.8 - 0.9$ of the initial total binary mass with a low mass companion. Such scenario corresponds to type B mass transfer (see e.g. Paczyński (1971) for details). These binaries have typical periods of $few \times 10 - 200$ days. The timescale for the production of the accreting massive components is typically the MS lifetime of the initial prime component of the binary. In a smaller part of the phase space explored in our grids, a weak mass transfer occurs where only a small fraction of the mass from the prime

component is accreted by its companion. In these cases, the rejuvenation of the companion is negligible.

5. DISCUSSION

Young stars have been observed in the Galactic halo since the 1970's (e.g. Greenstein & Sargent 1974). Such stars are found well away from any star-forming region and are remote from any high density interstellar gas pockets where they could have potentially formed. The origin of these young stars in the Galactic halo have been extensively studied (see Keenan 1992 for a review), and many of them could be understood in terms of ejection mechanisms. They could have formed in the Galactic disk and then be ejected at high velocities due to dynamical interactions, and travel to their current position in the halo. However, some of these young halo stars have apparent evolutionary age shorter than the flight time from any star forming region in the Galactic disk or the GC (cf. table 1).

In situ star formation in the Galactic halo could potentially explain the existence of young halo stars. However, the very low gas density in the halo (e.g. Savage & de Boer 1981; Sembach & Danks 1994) make this possibility seem difficult. Dyson & Hartquist (1983) suggested that star formation could occur during collisions between cloudlets within high velocity clouds at high galactic latitudes, but Christodoulou et al.

(1997) have shown that such events are much too rare. Martos et al. (1999) suggested that spiral density waves in the disk could trigger star formation above the Galactic plane up to a kpc, but this seems unlikely for higher distances, where many of the young halo stars are observed. Both of these mechanisms would produce a few or up to tens of young stars with correlated velocities whereas formation of isolated stars is unlikely. In one case Lynn et al. (2002) have studied the environment of the halo young star PHL 346, but found no evidence for similarly young stars in its vicinity.

Rejuvenation scenarios of runaway stars have been discussed in the literature, but in a different context, dealing with mass accretion onto a star following a supernova explosion (Martin 2003), and the possible formation of a Thorne-Zytkow object (Leonard et al. 1993). These scenarios dealt either with a specific observed runaway (Martin 2003), or with more rare cases than the scenario discussed here. They also discussed interaction of a compact object with its companion rather than the rejuvenation due to mass transfer in the post-main sequence evolution stages of binaries.

In the following we discuss the status of the candidate runaway and hypervelocity stars in the Galactic halo and the implications of the binary rejuvenation and the triple disruption scenarios for the young stellar population in the GC. We suggest that all of the currently observed young Halo stars could have been ejected from the Galactic disk or the GC, when the binary rejuvenation scenario is taken into account. We also expand our discussion on the origin of the hypervelocity star HE 0437-5439, which was recently discussed in the literature. We show that an ejection origin by an IMBH or through interactions in a massive cluster in the LMC (Gualandris & Portegies Zwart 2007; Gvaramadze et al. 2007) are highly unlikely to be the origin of this star and suggest this HVS as a candidate rejuvenated HVS ejected as a binary from the GC, which later on merged to form a more massive HVS. We also show that its observed low metallicity is a consistent with a Galactic origin and a GC origin can not be ruled out.

5.1. Rejuvenated runaway stars

In table 1 we have listed young stars observed in the Galactic halo that have estimated propagation times which could potentially be larger than their evolutionary time, given the uncertainties. As we have shown in section 4, the rejuvenation in binaries can extend the travel time of the runaway stars as main sequence stars. Following the rejuvenation, in both the full merger and the strong mass transfer cases discussed above, we find that the newly rejuvenated massive star, with mass m_{rej} , contains most of the mass of the initial binary. The typical formation timescale is of the order of the MS lifetime of the prime binary component, t_{m_1} . If such binaries are ejected as runaway or hypervelocity stars they could propagate for as long as t_{m_1} before producing the newly formed massive star. The MS lifetime of this rejuvenated star, t_{mrej} , could then be much smaller than the propagation time, $t_{mrej} < t_{prop} \leq t_{m_1}$, thus producing an apparent discrepancy between the flight time and the lifetime of this star.

Such rejuvenation scenarios provide a maximal flight time for a given star of $t_{prop} = t_{m_1} + t_{mrej}$. Since the mass of the prime component in the binary progenitor is at least half the mass of the rejuvenated star we find the maximal propagation time to be $t_{prop}^{max} = t_{\frac{1}{2}mrej} + t_{mrej}$, where $t_{\frac{1}{2}mrej}$ is the MS lifetime of a star with half the mass of the observed halo star. We find that all of the candidate stars in table 1 have $t_{flight} < t_{prop}^{max}$, and could be rejuvenated stars.

5.2. Rejuvenated hypervelocity stars and the case for HE 0437-5439 and US 708

Currently ~20 HVSs have been observed in the Galactic halo (Brown et al. 2005; Hirsch et al. 2005; Edelmann et al. 2005; Brown et al. 2007a,b). The kinematics and ages of most of these stars are consistent with their possible origin from the GC. A discrepancy between the kinematics and the ages of a few of the bound HVSs might exist (Brown et al. 2007a), making them possible candidate rejuvenated stars. However, more observations are required to confirm that these stars are truly early B-type stars, and not halo extreme horizontal branch stars.

The hypervelocity star HE 0437-5439 was spectroscopically identified to be a genuinely young B2 III-IV halo star with mass of $\sim 9 \pm 0.8 M_{\odot}$ (Edelmann et al. 2005; Bonanos et al. 2008; Przybilla et al. 2008). Its apparently short lifetime and the large distances from the GC and the Galactic disk make it too young to have traveled from these regions during its lifetime, even with its very high velocity (723 km s^{-1} ; Edelmann et al. 2005)³. It was therefore suggested to be either ejected from the large Magellanic cloud (LMC) or rejuvenated in a binary ejected by an IMBH inspiral to the GC (Edelmann et al. 2005). In the following we discuss the possible evidence for the origin of this star (metallicity), and its dynamical history. We show that the suggested dynamical origins of this star from the LMC require improbable dynamical scenarios, and as an alternative we suggest it is a rejuvenated star ejected as a hypervelocity binary in a triple disruption by the MBH in the GC. We also show that the chemical abundances of HE 0437-5439 suggested as evidence for an LMC origin of the HVS, do not rule out its possible Galactic center origin, and could be consistent with such a scenario. In addition we shortly discuss the possible rejuvenation origin of the low mass old HVS US 708.

5.2.1. Ruling out some possible dynamical origins of HE 0437-5439 from the LMC

Given the observed high velocity of HE 0437-5439, a dynamical scenario for this star would most likely require an interaction with a MBH. Gualandris & Portegies Zwart (2007) have suggested that a tidal disruption of a binary by an IMBH in a young stellar cluster in the LMC could produce hypervelocity star such as HE 0437-5439 at a rate of $5 \times 10^{-8} \text{ yr}^{-1}$. We note that such IMBH have not yet been observed in the LMC (or elsewhere). Moreover, Gualandris & Portegies Zwart (2007) have not taken into account a few important considerations. (1) The travel time from the LMC to our galaxy for such a HVS is about 20 Myrs, very close to the ages of the clusters they suggested as possible hosts of an IMBH. For these clusters the HVS should have been ejected immediately after the formation of the IMBH (assuming the IMBH have formed quickly enough in the cluster to begin with), probably during less than 1 Myrs, in order to achieve its current position. Given the calculated ejection rates, only $N_{eject} \sim 10^6 \times 5 \times 10^{-8} = 0.05$ HVSs could have been ejected, on average, in the relevant time. (2) The stellar mass function has not been taken into account by Gualandris & Portegies Zwart (2007). The fraction of stars as massive as $8.5 M_{\odot}$ or more (the estimated mass of HE 0437-5439) is very small, only a fraction of $f_{IMF} \sim 0.01$ of the stellar

³ Recently, and after this study was done, another HVS was found suggesting an origin outside the GC (Heber et al. 2008). We do not discuss this interesting star in the current paper and leave it to future study.

population is in such massive stars (and likely even smaller, as most of these more massive stars were likely to fuel the growth of the IMBH). (3) The ejection of HVSSs is isotropic, and therefore only a fraction of them $f_{MW} < 0.1$ would be directed to the Milky Way galaxy. Taking together the average number of observable massive ($> 8.5 M_{\odot}$) HVSSs from the LMC (similar to HE 0437-5439) should be about $N_{eject} \times f_{imf} \times f_{MW} = 5 \times 10^{-5}$, making this possibility highly unlikely.

Recently it was suggested that HVSSs might be produced through binary-binary dynamical interactions of massive binaries in a dense cluster (Gvaramadze et al. 2007). Leonard (1991) have studied such encounters. He found that the lowest mass star participating in the interaction could attain the highest velocity. Such velocity would be comparable to the escape velocity from the the most massive star participating in the encounter. If HE 0437-5439 was ejected from the LMC, it would require an ejection velocity of $> 900 \text{ km s}^{-1}$ in order to acquire its current position during its lifetime (Gualandris & Portegies Zwart 2007; Przybilla et al. 2008). For this to happen HE 0437-5439 would need to encounter stars more massive than itself. Even then the fraction of encounters where such velocity could be attained by this star is $f_{high} \sim 10^{-4}$ (4×10^{-4} , 2×10^{-3} ; see Leonard 1991) for encounters where the masses of the other stars are larger than $15 M_{\odot}$ ($30 M_{\odot}$, $60 M_{\odot}$; respectively). Since binary-binary encounters usually lead to the disruption of one of the binaries, one would require $\sim 1/f_{high}$ such binaries to exist in order for one of them to potentially be ejected at such high velocity. Such conditions, i.e. the existence of hundreds (thousands) of $> 30 M_{\odot}$ ($> 15 M_{\odot}$) stars in a super dense cluster core are not known to exist in any young cluster in the Galaxy or in the LMC. We conclude that the scenario for ejection of HE 0437-5439 through a dynamical interaction with massive stars in a cluster is highly unlikely.

5.2.2. The metallicity of HE 0437-5439 does not rule out a Galactic center origin

Recently Bonanos et al. (2008) and Przybilla et al. (2008) have found the metallicity of the HVS HE 0437-5439 to be low relative to solar metallicity. They suggested this as a possible evidence for an LMC origin of this star rather than a Galactic origin. However, an LMC origin would be difficult to explain dynamically, as discussed above. Moreover, in the following we show that the current metallicity measurements do not rule out a Galactic (and Galactic center) origin for HE 0437-5439.

It is known that the observed abundances of some elements in Galactic B stars are depressed relative to the established solar values (see e.g. Martin 2004, 2006 and the appendix). Therefore, one should compare the metallicity of B type stars such as HE 0437-5439 with large surveys of similar B type stars. Przybilla et al. (2008) made a comparison with a single galactic B star and a single LMC B star that may not representative of the large scatter in the abundances shown in larger samples. Bonanos et al. (2008) made a comparison with a large B stars survey in the LMC, but for the comparison with the Galactic abundances they took the solar abundances rather than Galactic B stars surveys. Fig. 2 show the spread in the measured chemical abundances for different samples of stars (LMC, milky way and the Galactic center stars) found in the literature (see caption of fig. 2). For small samples (with 10 stars or less) the data for each of the stars is shown rather than the mean abundance, since given the very small samples the

mean may not be a good representative of the underlying distribution of abundances. For the larger samples the 1σ spread around the mean (i.e. where 68 percents of the measured values are found) is shown⁴. We can use these data samples and compare them with the chemical abundances of HE 0437-5439. The results by Przybilla et al. (2008) have systematically smaller error bars, and also contain the abundances for more elements (*C*, *N*, *O*, *Mg*, *Si* and *Fe*) compared with the results obtained by Bonanos et al. (2008) (which do not show the Fe abundance), and are therefore used in the comparison. Nevertheless, given the large differences that exist between the chemical abundances obtained by Przybilla et al. (2008) and those found by Bonanos et al. (2008), the latter results are also shown in fig. 2 for completeness.

Comparison of the chemical abundances of HE 0437-5439 as found by Przybilla et al. (2008) to those found in surveys of B type stars throughout the Galaxy (Daflon et al. 2001) show that its metallicity is highly consistent with their metallicities⁵. Most (>50 percents) of the stars in the sample have more extreme elemental abundances than that of HE 0437-5439 (for each of the elemental abundances observed; see fig. 2, bottom panel), showing that the elemental abundances of HE 0437-5439 are quite typical of the Milky Way chemical abundances.

Although a galactic origin is most consistent with the metallicities of HE 0437-5439, its high velocity would require an interaction with a MBH, currently known to exist only in the GC. Therefore, its metallicities should be compared to the metallicities of similar unevolved B stars in the GC. Unfortunately, metallicity measurements of stars in the GC region exist only for a small number of stars, none of which are similar to HE 0437-5439 (although some of these GC stars have similar masses, they are at a very different evolutionary stage; Cunha et al. 2007). Therefore, given the current data, drawing conclusions on the origin of HE 0437-5439 based on metallicity comparisons with GC stars is premature. Nevertheless, we shortly discuss such metallicity comparison, but caution that this should not be taken as evidence for the origin of HE 0437-5439, but at most as a possible clue until further measurements of the metallicity of GC stars are available.

The chemical abundances of stars in the GC are known mostly for cool evolved stars (Cunha et al. 2007). Data on two additional highly massive ($\sim 150 M_{\odot}$) LBV stars exists (Najarro et al. 2008), but given their very different stellar type and evolution, comparing their abundances with that of HE 0437-5439 is not justified, and we do not use their data. The number of data points (stars) for each element are 10, 7, 6 and 5 for the elements *Fe*, *O*, *C* and *N*, respectively. The *C*, *O* and *Fe* abundances of HE 0437-5439 are found to be consistent with GC values (see fig. 2⁶), but the *N* abundance is not (with **all**

⁴ Notice that the specific Fe abundance for each of the LMC stars is not given by Hunter et al. (2007), and we therefore quote the mean and uncertainty given by them in this case.

⁵ Even in such surveys large uncertainties exist; in the appendix we show the chemical abundances of B stars found both in the Galaxy and the LMC in several different surveys, enabling a more detailed comparison. Fig. 2 shows only the results from the survey of Daflon et al. 2001, nevertheless, this survey includes B stars from different regions in the Galaxy, and it is generally consistent with the other samples (see appendix). One could also compare the values obtained for HE 0437-5439 to those of other young halo stars showing that its metallicities are not unusual for such objects.

⁶ Przybilla et al. (2008) have shown a somewhat similar plot, however the data shown by Przybilla et al. (2008) for the GC stars did not include IRS 8 (Geballe et al. 2006) and some of the elemental abundances for IRS 7 (Carr et al. 2000), that show a larger scatter in the element abundances. They also used, with no justification, the data from the GC LBV stars.

5 stars in the GC sample have higher abundances than those found for HE 0437-5439). We note that better agreement is observed for those elements for which more data exist. The N abundance of HE 0437-5439 is lower than those of the GC stars. However, since CNO cycle mixing can convert these elements in the GC stars (see e.g. Carr et al. 2000; Cunha et al. 2007) and in HE 0437-5439, one should be careful and also check the sum of these elements and not only compare each of these elements by itself. We find that the sum of these elements is consistent with that of the GC sample stars, i.e. not even the N abundance of HE 0437-5439 could be interpreted as an evidence against a GC origin. Moreover, given the low statistics of the GC sample, the lower N abundance is not statistically significant, even by itself. Given the wide range of abundances found in different Galactic B-type stars surveys (see appendix), it is possible that this specific HVS B star may have lower abundances of these specific element.

The middle panel of fig. 2 shows the comparison of the elements abundances of HE 0437-5439 to those found in the LMC. The metallicities of B stars in the LMC were found by several groups (the largest samples by Korn et al. 2002; Hunter et al. 2007), where we show the values obtained by Hunter et al., for which a large sample exists (30), whereas the sample by Korn et al. contain only 4 stars). The comparison shows much poorer agreement with LMC abundances than with the Milky way abundances. The N , Fe and the Si abundances of HE 0437-5439 are found to be consistent with LMC values, but the C , O and Mg abundances are not (all 30 stars in the LMC samples have higher abundances than those found for HE 0437-5439 for these elements). We do note, however, that the metallicities of HE 0437-5439 obtained by Bonanos et al. (2008) are consistent with those of the LMC for all elements. In addition the results of Przybilla et al. (2008) are better consistent with LMC values found by Korn et al. which are systematically higher).

These comparisons show that the metallicities obtained by Przybilla et al. (2008) are more consistent with the GC abundances than the LMC abundances shown here (and best consistent with a Galactic origin). However, we caution again that the small statistics and the different type of stars included in the GC sample of stars, the large differences inferred for the metallicities of HE 0437-5439 by different authors (Bonanos et al. 2008; Przybilla et al. 2008); and the different analysis methods used by different groups, suggest that it is still too early to draw conclusions from such metallicity comparisons. It is clear from the above discussion, however, that none of the suggested origins for HE 0437-5439, including the Galactic disk, the LMC and the GC can be ruled out based upon current metallicity data.

5.2.3. The possibility of HE 0437-5439 as a rejuvenated star from the Galactic center

As discussed in the previous sections, young halo stars such as HE 0437-5439 could have evolved from two lower mass members of ejected hypervelocity binaries. The binary components either merge completely, or may evolve through a strong mass transfer from the more massive binary component to its initially lower mass companion, which becomes a rejuvenated massive star. The later possibility would give a strong observable signature in the form of a high mass ratio binary with a period of tens of days. The observations of Przybilla et al. (2008) and Bonanos et al. (2008) rule out the possibility of such a binary, and therefore if this HVS is a rejuvenated star its binary progenitor fully merged. As can

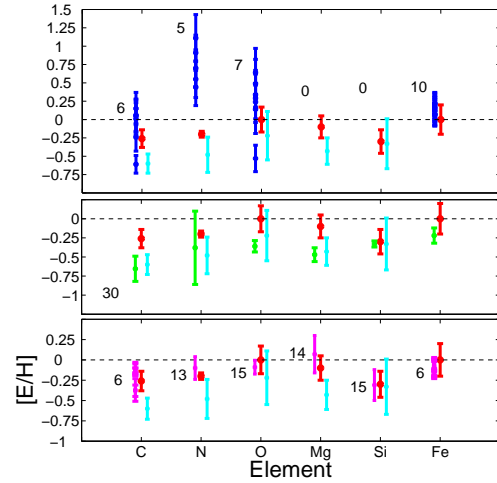


FIG. 2.— Comparison of the metal abundances of the hypervelocity star HE 0437-5439 (Przybilla et al. 2008 middle red bars and Bonanos et al. 2008 right cyan bars) to those of the Galactic center (top panel, left blue bars), LMC B stars (middle panel, left green bars) and Galactic B stars (bottom panel, left magenta bars). Galactic B stars metallicities are taken from Daflon et al. (2001), LMC B stars metallicities are taken from Hunter et al. (2007). Galactic center metallicities are taken from Carr et al. 2000; Geballe et al. 2006; Cunha et al. 2007; Najaro et al. 2008. All values are given relative to solar abundances (dashed lines; Grevesse et al. 2007). Note that the GC metallicity values are shown for each of the stars in those samples containing ten or less stars (see text), whereas for larger sample sizes the median metallicity values and the 1σ spread around the median are shown. The number of stars from which the range of abundance values were obtained is denoted beside the bars (the LMC samples includes 30 values for all the elements beside Fe , see text).

be seen in fig. 1, a binary progenitor with 4.8 and 4.3 M_{\odot} components, for example, could have propagated for more than 60 – 80 Myrs and then merge to form a 9 M_{\odot} star, consistent with the required travel time from the GC (Edelmann et al. 2005). We note that binaries with other high mass ratio components (not shown here), but with a total binary mass of $\sim 9 M_{\odot}$ could also produce such a merged star with the appropriate evolutionary time scales. Given the tendency of massive binaries to have high mass ratios, it is likely that most ejected binaries should have mass ratios in the relevant parameter space as to produce a merged star similar to HE 0437-5439. All the hypervelocity binaries have initial semi-major axis smaller than $\sim 0.2 AU$ ($4-5 R_{\odot}$), since they were originally part of the inner binaries in close stable triples. In addition, the KCTF mechanism in triples (see section 4) can evolve such inner binaries into even closer contact configuration at a very short timescale (Myr). It is therefore expected that most hypervelocity binaries would be at very tight orbits or a few R_{\odot} separations, such as those required to eventually form a merged star like HE 0437-5439 (see fig. 1). In other words the rejuvenation scenario is a likely scenario for the formation and ejection of HE 0437-5439. The estimate in section 3.2.1 suggests $f_{prog} = 3 - 5\%$ of the HVSs could be ejected as close hypervelocity binaries or leave a binary star close to the MBH. The fraction of rejuvenated HVSs is therefore $f_{rej} = f_{prog} \cdot f_{inner} \cdot f_{merged} \cdot f_{lifetime}$ where f_{inner} is the fraction of disrupted triples that eject the inner binary, f_{merged} is the probability the binary merges, $f_{lifetime}$ is the fractional lifetime of the merger remnant to the original stars lifetime. Simulations of binary disruptions by a MBH (Miller et al. 2005; Bromley et al. 2006) suggest that there is

no preference for the primary or the secondary in the binary to be ejected, i.e. they have equal ejection probability, I therefore take $f_{\text{inner}} = 0.5$. Estimating the probability of binary merger is very uncertain. Taking the observed triples sample of Fekel (1981), I find that the inner binaries in the HVSs binaries possible progenitors have periods of a few days, which together with the binary stellar evolution simulations (see fig. 1) suggest that > 0.75 of them would merge due to stellar evolution. I therefore take $f_{\text{merger}} = 0.75$. The question of f_{lifetime} is more complicated. The merger remnant has a lifetime of t_{mrej} as discussed in section 5.1, and the maximal lifetime of its progenitor is at most $t_{\frac{1}{2}\text{mrej}}$. A rejuvenated star therefore has a fractional life time to the original stars of $t_{\text{mrej}}/t_{\frac{1}{2}\text{mrej}}$. Taking the stellar evolution main sequence lifetimes from the Geneva stellar evolution tracks (Schaller et al. 1992), I find this to be approximately 0.2. However, on average, the HVSs are ejected after half their lifetime. In addition, the ejected stars are observed only after their propagation for $t_{\text{prop}} = f_{\text{ew}} \times 10^7 - 10^8$ yrs (the flight time to distances of 10 – 100 kpc from the GC where they are currently observed), the fraction of the merger remnant lifetime to the time spent by the progenitor at observable regions is $t_{\text{mrej}}/(0.5 \cdot t_{\frac{1}{2}\text{mrej}} + t_{\text{prop}}) > 0.4$. A reasonable estimate is therefore $f_{\text{lifetime}} = 0.2 - 0.6$. Taken together, we find $f_{\text{rej}} \simeq 0.003 - 0.012^7$. Given the current estimate of $N_{\text{HVS}} \sim 100 - 650$ $3 - 4 M_{\odot}$ B type HVSs in the galactic halo Brown et al. (2007b); Perets et al. (2008), we may expect to find $N_{\text{HVS}} \cdot f_{\text{rej}} = 0.25 - 8$ rejuvenated (more) massive HVSs in a full sky survey (compare with the value of 5×10^{-5} massive stars expected to originate from the LMC in the IMBH scenario, if such IMBH indeed exist there in a young massive cluster).

We summarize this section by concluding that current suggestions for the hypervelocity ejection of HE 0437-5439 from the LMC (either by an IMBH or through interactions with other massive stars) are highly unlikely, and suggest that HE 0437-5439 was ejected from our GC (where we stress that this scenario is not ruled out by current metallicity comparisons) in a hypervelocity binary following a triple disruption by the MBH.

5.2.4. The possibility of US 708 as a rejuvenated star from the Galactic center

We note that the hypervelocity star US 708, which is not a young star but an evolved sdO star, was suggested to evolve from a merger of a close binary (Hirsch et al. 2005). In that respect we find that when the evolution of close binaries such as studied here is followed to later times (not shown here) such white dwarfs are indeed formed in some cases. It is therefore possible that US 708 was also ejected as a binary star from a triple disruption that later on evolved and merged to form an sdO star, in a similar way to the rejuvenated young halo star studied here (as suggested by W. Brown, private communication). However, the unique evolution and the a merger of two white dwarfs is only poorly followed in the evolutionary code used here, and further studies should be made to check this possibility.

⁷ One could also discuss the probability of getting a metallicity distribution such as observed for HE 0437-5439 given the metallicities observed in the GC. As discussed above, its metallicity is consistent with the GC metallicities of similar massive stars. However, current data can not be reliably used regarding this point, since these stars are at different evolutionary stages and are not comparable to HE 0437-5439.

5.3. Binaries in the S-stars cluster in the Galactic center

In recent years high resolution observations have revealed the existence of many young OB stars in the GC near the MBH. Most of the young stars are observed in the central 0.5 pc around the MBH. The young stars population in the inner 0.04 pc (the 'S-stars') contain only young B-stars, in apparently isotropic distribution around the MBH (Eisenhauer et al. 2005; Ghez et al. 2005). The young stars outside this region contain many O-stars in a disk like structure and were probably formed from the fragmentation of a gaseous disk (Levin & Beloborodov 2003; Paumard et al. 2006). However, the origin of the S-stars is difficult to explain by this process. It was suggested that the S-stars with their very different properties migrated from the stellar disk through a planetary migration like process (Levin 2007). This interesting possibility has not yet been studied quantitatively. Another possibility is that these stars have a different origin, possibly from the disruption of young binaries and the following capture of one of their components (Gould & Quillen 2003). It was recently shown that such a scenario could be consistent with the current knowledge regarding the number of the observed S-stars and their orbital properties (Perets et al. 2007). In case of a triple disruption, a binary could be captured at a close orbit near the MBH. We therefore suggest that some of the observed S-stars may be binaries. Such binaries may not survive for long in this environment due to interactions with other stars (See Perets 2009, for a detailed discussion on binaries survival in the GC). Such interactions could also change the orbits of the disrupted binary components near the MBH. Still, the closest binaries could survive for longer times (Perets 2009) and may be observed. Interestingly, observations of wider S-stars binaries would suggest more recent capture, i.e. the binary period may serve to estimate the time a binary spent in the close by regions of the MBH. In addition such S-star binaries could rejuvenate to form more massive S-stars, possibly explaining the occurrence of the most massive S-stars such as S-2.

6. SUMMARY AND CONCLUSIONS

In this paper we have studied a possible explanation for the existence of young stars far in the Galactic halo. Such stars are usually thought to have formed elsewhere, either in the Galactic disk or the Galactic center, and later on ejected at high velocities into their current position. However, some of these stars have apparent lifetimes shorter the required flight time from the Galactic disk/center. Here we suggested that such stars have evolved in close runaway or hypervelocity binaries. We found that stellar evolution of such binaries can drive them into mass transfer configurations and even mergers. Such evolution could then rejuvenate them (similar to the cases of lower mass blue stragglers) and extend their lifetimes after ejection. The extended lifetimes of such stars could then be reconciled with their flight times to the Galactic halo, and the travel times could be extended up to 3-4 times relative to their apparent lifetimes.

Three typical scenarios were found for the binaries evolution. (1) In case of a full merger of the binary progenitor components, a single halo star would be observed. Unless the binary merger lead to peculiar characteristics of the merged star, such as possibly high rotational velocity, or chemical peculiarities, observation of such stars could not directly trace their binary origin. Nevertheless, we predict that in such cases the calculated propagation time of the star from its birthplace would be limited to approximately the main sequence lifetime of its binary progenitor components (at most the main

TABLE A2
CHEMICAL ABUNDANCES OF B STARS

Name	<i>C</i>	<i>N</i>	<i>O</i>	<i>Mg</i>	<i>Si</i>	<i>Fe</i>	
LMC B1-2 stars	7.73	6.88	8.33	7.06	7.19	7.23	Hunter et al. (2007)
LMC B V stars	8.06	7.01	8.37	7.37	7.1	7.33	Korn et al. (2002)
Solar	8.39	7.78	8.66	7.53	7.51	7.45	Grevesse et al. (2007)
MW B1-2 III/IV stars	7.82	7.38	8.68	7.09	7.14	–	Vrancken et al. (2000)
MW B IV/V stars	8.22	7.78	8.52	7.38	6.81	–	Kilian 1992
“	8.20	7.81	8.68	–	7.58	7.72	Gies & Lambert 1992
“	8.24	7.69	8.6	7.65	7.25	7.35	Daflon et al. 2001
MW B stars	8.21	7.98	8.55	7.56	7.36	7.4	Martin 2004
	8.29	7.9	–	–	–	–	Nieva & Przybilla 2006, 2007
HE 0437-5439 (B2 III-IV star)	8.13 ± 0.12	7.58 ± 0.04	8.66 ± 0.17	7.43 ± 0.15	7.21 ± 0.16	7.45 ± 0.2	Przybilla et al. (2008)
HE 0437-5439	7.79 ± 0.13	7.3 ± 0.24	8.44 ± 0.33	7.1 ± 0.18	7.18 ± 0.34	–	Bonanos et al. (2008)
BD +38 2182	–	–	–	–	7.02 ± 0.04	–	Martin 2004
BD +36 2268	7.14 ± 0.19	7.89 ± 0.2	8.27 ± 0.37	–	6.6 ± 0.2	–	“
HD 140543	–	8.18	8.76 ± 0.46	–	8.74 ± 0.43	–	“
HD 188618	–	7.93 ± 0.00	8.51 ± 0.23	–	7.71 ± 0.35	–	“
HD 206144	–	7.86	8.58 ± 0.33	–	7.56 ± 0.15	6.99	“
PHL 159	8.17 ± 0.26	7.85 ± 0.18	8.72 ± 0.16	7.28 ± 0.2	7.34 ± 0.2	7.33 ± 0.09	“
PHL 346	8.14 ± 0.32	8.04 ± 0.19	8.54 ± 0.28	7.14	7.47 ± 0.08	7.38 ± 0.16	“
PG 1209+263	–	–	–	5.03	8.31 ± 0.04	7.22 ± 0.56	Lynn et al. 2004
PG 2219+094	7.82	–	–	7.16	–	–	Rolleston et al. 1999
PG 2229+099	8.15 ± 0.1	7.94 ± 0.31	8.99 ± 0.06	7.1 ± 0.62	7.36	5.63	“

sequence lifetime of a star with half the mass of the observed halo star). (2) In the case of a strong mass transfer, one of the binary progenitor component have accreted most of the mass of its companion. In such a case the evolved binary could be observable as a high mass ratio binary, with typical periods of 10 – 200days. (3) In the case of a weak mass transfer, only a small fraction of the mass of the binary progenitor component is accreted by its companion, leading to negligible or mild rejuvenation. This third evolutionary route would not produce “too young” halo stars, albeit they could produce marginal cases. However, such halo young binaries (that have already been observed) can confirm the scenario of runaway binaries that, for different orbital parameters of the binary, could have produced rejuvenated high velocity stars.

We studied the possibilities of binary runaway and hypervelocity stars and showed that such binaries could have been ejected in triple disruptions and other dynamical interactions with stars or with massive black holes. Consequently, currently observed “too young” star in the halo could have been ejected from the Galactic disk or the Galactic center and be observable in their current position if they were ejected as binaries (whereas other suggestions such as ejection from the LMC are shown to be highly unlikely). The calculated propagation times of these stars are indeed consistent with the evo-

lutionary lifetimes in rejuvenated binaries. We suggest to look for binary companions that may exist for some of these stars, thus directly confirming the binary rejuvenation scenario (HD 188618 in table 1 has already been suggested as binary candidate; Martin 2006). We also specifically discuss the hypervelocity star HE 0437-5439 in that respect, and show that it could be a rejuvenated HVS from the GC (where we also discuss its recently observed metallicity, showing that a Galactic center origin can not be currently ruled out, contrary to recent suggestions).

Finally, we also suggest that triple disruptions by the massive black hole in the Galactic center could capture binaries in close orbits near the MBH, some of which may later evolve to become more massive rejuvenated stars. Future observations might be able to study these binaries.

I would like to thank Warren Brown, Uli Heber, Clovis Hopman, Tal Alexander, Mercedes Lopez-Morales and the anonymous referee for helpful comments and suggestions on this manuscript. I would also like to thank Daniel Fabrycky for using his code for producing stable triples for my calculations of the hypervelocity binaries fraction, and Ben Davies for helpful correspondence.

APPENDIX

A. CHEMICAL ABUNDANCES OF YOUNG B STARS AND HALO STARS

Following section 5.2.2 we supplement in this appendix a table in which the detailed chemical abundances of B stars found in Galactic and LMC surveys are shown, in order to give better and broader perspective on their scatter and uncertainties. These show the typically lower measured metallicities characterizing B stars, in comparison with the solar abundances. Also shown are the chemical abundances found for HE 0437-5439 by Bonanos et al. (2008) and Przybilla et al. (2008). In addition we detail the metallicities of other candidate rejuvenated halo stars from table 1 (for which measurements are available), showing that the metallicities of HE 0437-5439 are not unusual. The quoted mean abundances in the surveys have typical 0.1 – 0.2 dex uncertainties in the measurements. The specific uncertainties for single stars is given specifically for each star.

REFERENCES

- Abt, H. A. 1983, *ARA&A*, 21, 343
- Abt, H. A., Gomez, A. E., & Levy, S. G. 1990, *ApJS*, 74, 551
- Baumgardt, H., Gualandris, A., & Portegies Zwart, S. 2006, *MNRAS*, 372, 174
- Blaauw, A. 1961, *Bull. Astron. Inst. Netherlands*, 15, 265
- Bonanos, A. Z. et al. 2008, *ApJ*, 675, L77
- Bromley, B. C. et al. 2006, *ApJ*, 653, 1194
- Brown, W. R. et al. 2005, *ApJ*, 622, L33
- . 2007a, *ApJ*, 660, 311
- . 2007b, *ArXiv:0709.1471*
- Carr, J. S., Sellgren, K., & Balachandran, S. C. 2000, *ApJ*, 530, 307
- Chen, X., & Han, Z. 2004, *MNRAS*, 355, 1182
- Christodoulou, D. M., Tohline, J. E., & Keenan, F. P. 1997, *ApJ*, 486, 810
- Cunha, K., Sellgren, K., Smith, V. V., Ramirez, S. V., Blum, R. D., & Terndrup, D. M. 2007, *ApJ*, 669, 1011
- Daflon, S. et al. 2001, *ApJ*, 552, 309
- D'Angelo, C., van Kerkwijk, M. H., & Rucinski, S. M. 2006, *AJ*, 132, 650
- Dray, L. M. & Tout, C. A. 2007, *MNRAS*, 376, 61
- Duquennoy, A. & Mayor, M. 1991, *A&A*, 248, 485
- Dyson, J. E. & Hartquist, T. W. 1983, *MNRAS*, 203, 1233
- Edelmann, H. et al. 2005, *ApJ*, 634, L181
- Eggleton, P. P., Fitchett, M. J., & Tout, C. A. 1990, *ApJ*, 354, 387
- Eggleton, P. P. & Kiseleva-Eggleton, L. 2001, *ApJ*, 562, 1012
- Eggleton, P. P., Tout, C. A., & Fitchett, M. J. 1989, *ApJ*, 347, 998
- Eisenhauer, F. et al. 2005, *ApJ*, 628, 246
- Evans, N. R. et al. 2005, *AJ*, 130, 789
- Fabrycky, D. & Tremaine, S. 2007, *ApJ*, 669, 1298
- Fekel, Jr., F. C. 1981, *ApJ*, 246, 879
- Ferraro, F. R., et al. 2006, *ApJ*, 647, L53
- Garmany, C. D., Conti, P. S., & Massey, P. 1980, *ApJ*, 242, 1063
- Geballe, T. R. et al. 2006, *ApJ*, 652, 370
- Ghez, A. M. et al. 2005, *ApJ*, 620, 744
- Gies, D. R. 1987, *ApJS*, 64, 545
- Gies, D. R. & Bolton, C. T. 1986, *ApJS*, 61, 419
- Gies, D. R. & Lambert, D. L. 1992, *ApJ*, 387, 673
- Ginsburg, I. & Loeb, A. 2006, *MNRAS*, 368, 221
- Gould, A. & Quillen, A. C. 2003, *ApJ*, 592, 935
- Greenstein, J. L. & Sargent, A. I. 1974, *ApJS*, 28, 157
- Grevesse, N., Asplund, M., & Sauval, A. J. 2007, *Space Science Reviews*, 130, 105
- Gualandris, A. & Portegies Zwart, S. 2007, *MNRAS*, 376, L29
- Gualandris, A., Portegies Zwart, S., & Eggleton, P. P. 2004, *MNRAS*, 350, 615
- Gvaramadze, V. V., Gualandris, A., & Portegies Zwart, S. 2007, *ArXiv: astro-ph/0702735*
- Hansen, B. M. S. & Milosavljević, M. 2003, *ApJ*, 593, L77
- Heber, U. et al. 2008, *A&A*, 483, L21
- Hills, J. G. 1988, *Nature*, 331, 687
- . 1991, *AJ*, 102, 704
- Hirsch, H. A. et al. 2005, *A&A*, 444, L61
- Hoogerwerf, R., de Bruijne, J. H. J., & de Zeeuw, P. T. 2000, *ApJ*, 544, L133
- . 2001, *A&A*, 365, 49
- Hunter, I. et al. 2007, *A&A*, 466, 277
- Keenan, F. P. 1992, *QJRAS*, 33, 325
- Kilian, J. 1992, *A&A*, 262, 171
- Kiseleva, L. G., Eggleton, P. P., & Mikkola, S. 1998, *MNRAS*, 300, 292
- Kobulnicky, H. A. & Fryer, C. L. 2007, *ApJ*, 670, 747
- Korn, A. J. et al. 2002, *A&A*, 385, 143
- Kouwenhoven, M. B. N. et al. 2007, *ArXiv: 0707.2746*
- Kozai, Y. 1962, *AJ*, 67, 591
- Leonard, P. J. T. 1991, *AJ*, 101, 562
- . 1995, *MNRAS*, 277, 1080
- Leonard, P. J. T. & Duncan, M. J. 1988, *AJ*, 96, 222
- . 1990, *AJ*, 99, 608
- Leonard, P. J. T., Hills, J. G., & Dewey, R. J. 1993, in *Astronomical Society of the Pacific Conference Series*, Vol. 45, *Luminous High-Latitude Stars*, ed. D. D. Sasselov, 386–4
- Levin, Y. 2006, *ApJ*, 653, 1203
- . 2007, *MNRAS*, 374, 515
- Levin, Y. & Beloborodov, A. M. 2003, *ApJ*, 590, L33
- Lockman, F. J., Blundell, K. M., & Goss, W. M. 2007, *MNRAS*, 381, 881
- Löckmann, U. & Baumgardt, H. 2007, *ArXiv:0711.1326*
- Lu, Y., Yu, Q., & Lin, D. N. C. 2007, *ApJ*, 666, L89
- Lynn, B. B. et al. 2002, *MNRAS*, 336, 1287
- . 2004, *MNRAS*, 349, 821
- Mardling, R. A. & Aarseth, S. J. 2001, *MNRAS*, 321, 398
- Martin, J. C. 2003, *PASP*, 115, 49
- . 2004, *AJ*, 128, 2474
- . 2006, *AJ*, 131, 3047
- Martos, M., Allen, C., Franco, J., & Kurtz, S. 1999, *ApJ*, 526, L89
- Mason, B. D. et al. 1998, *AJ*, 115, 821
- McSwain, M. V. et al. 2007a, *ApJ*, 655, 473
- . 2007b, *ApJ*, 660, 740
- Mikkola, S. 1983, *MNRAS*, 205, 733
- Miller, M. C., Freitag, M., Hamilton, D. P., & Lauburg, V. M. 2005, *ApJ*, 631, L117
- Miralda-Escudé, J. & Gould, A. 2000, *ApJ*, 545, 847
- Morrell, N. & Levato, H. 1991, *ApJS*, 75, 965
- Najarro, F. et al. 2008, *ApJ*, 675, 1011
- Nelson, C. A., & Eggleton, P. P. 2001, *ApJ*, 552, 664
- Nieva, M. F. & Przybilla, N. 2006, *ApJ*, 639, L39
- . 2007, *ArXiv e-prints*, 712
- O'Leary, R. M. & Loeb, A. 2007, *MNRAS*, 376, 1076
- Paumard, T. et al. 2006, *ApJ*, 643, 1011
- Perets, H. B. 2009, *ApJ*, 690, 795
- Perets, H. B., Hopman, C., & Alexander, T. 2007, *ApJ*, 656, 709
- Perets, H. B. et al. 2008, *ArXiv:0809.2087*
- Perets, H. B., & Fabrycky, D. C. 2009, *arXiv:0901.4328*
- Paczynski, B. 1971, *ARA&A*, 9, 183
- Portegies Zwart, S. F. 2000, *ApJ*, 544, 437
- Portegies Zwart, S. F. & Verbunt, F. 1996, *A&A*, 309, 179
- Portegies Zwart, S. F. & Yungelson, L. R. 1998, *A&A*, 332, 173
- Poveda, A., Ruiz, J., & Allen, C. 1967, *Boletín de los Observatorios Tonantzintla y Tacubaya*, 4, 86
- Pribulla, T. & Rucinski, S. M. 2006, *AJ*, 131, 2986
- Przybilla, N. et al. 2008, *ArXiv: 0801.4456*, *A&A*, in press, 801
- Ramspeck, M., Heber, U., & Moehler, S. 2001, *A&A*, 378, 907
- Rolleston, W. R. J., Hambly, N. C., Keenan, F. P., Dufton, P. L., & Saffer, R. A. 1999, *A&A*, 347, 69
- Sarna, M. J., & de Greve, J.-P. 1996, *QJRAS*, 37, 11
- Savage, B. D. & de Boer, K. S. 1981, *ApJ*, 243, 460
- Schaller, G., Schaerer, D., Meynet, G., & Maeder, A. 1992, *A&AS*, 96, 269
- Sembach, K. R. & Danks, A. C. 1994, *A&A*, 289, 539
- Sesana, A., Haardt, F., & Madau, P. 2007, *ArXiv:0710.4301*
- Sesana, A., Madau, P., & Haardt, F. 2008, *ArXiv e-prints*
- Stone, R. C. 1991, *AJ*, 102, 333
- Tokovinin, A. et al. 2006, *A&A*, 450, 681
- Tout, C. A. et al. 1996, *MNRAS*, 281, 257
- Vanbeveren, D., De Loore, C., & Van Rensbergen, W. 1998, *A&A Rev.*, 9, 63
- Vrancken, M., Lennon, D. J., Dufton, P. L., & Lambert, D. L. 2000, *A&A*, 358, 639
- Yu, Q. & Tremaine, S. 2003, *ApJ*, 599, 1129
- Zinnecker, H. 2005, in *Multiple Stars across the H-R Diagram*, ed. S. Hubrig, M. Petr-Gotzens, & A. Tokovinin, 265–280

Chapter 6

The Galactic potential and the asymmetric distribution of hypervelocity stars

Perets et al.

The Astrophysical Journal, Volume 697, Issue 2, pp. 2096-2101 (2009)

THE GALACTIC POTENTIAL AND THE ASYMMETRIC DISTRIBUTION OF HYPERVELOCITY STARS

HAGAI B. PERETS¹, XUFEN WU², HONGSHENG ZHAO^{2,3}, BENOIT FAMAËY⁴, GIANFRANCO GENTILE^{4,5}, AND TAL ALEXANDER¹

¹ Weizmann Institute of Science, P.O. Box 26, Rehovot 76100, Israel; hagai.perets@weizmann.ac.il

² Scottish University Physics Alliances, University of St. Andrews, KY16 9SS, UK

³ Sterrewacht, Leiden University, Niels Bohrweg 2, 2333 CA, Leiden, Netherlands

⁴ Institut d’Astronomie et d’Astrophysique, Université Libre de Bruxelles, Boulevard du Triomphe, B-1050 Bruxelles, Belgium

⁵ Sterrenkundig Observatorium, Ghent University, Krijgslaan 281, S9, B-9000 Ghent, Belgium

Received 2008 September 11; accepted 2009 March 31; published 2009 May 18

ABSTRACT

In recent years several hypervelocity stars (HVSs) have been observed in the halo of our Galaxy. Such HVSs have possibly been ejected from the Galactic center and then propagated in the Galactic potential up to their current position. The recent survey for candidate HVSs show an asymmetry in the kinematics of candidate HVSs (position and velocity vectors), where more outgoing stars than ingoing stars (i.e., positive Galactocentric velocities versus negative ones) are observed. We show that such kinematic asymmetry, which is likely due to the finite lifetime of the stars and Galactic potential structure, could be used in a novel method to probe and constrain the Galactic potential, identify the stellar type of the stars in the survey and estimate the number of HVSs. Kinematics-independent identification of the stellar types of the stars in such surveys (e.g., spectroscopic identification) could further improve these results. We find that the observed asymmetry between ingoing and outgoing stars favors specific Galactic potential models. It also implies a lower limit of $\sim 54 \pm 8$ main-sequence HVSs in the survey sample ($\gtrsim 648 \pm 96$ in the Galaxy), assuming that all of the MS stars in the survey originate from the GC. The other stars in the survey are likely to be hot blue horizontal branch stars born in the halo rather than stars ejected from the GC.

Key words: black hole physics – galaxies: nuclei – stars: kinematics

Online-only material: color figures

1. INTRODUCTION

Hypervelocity stars (HVSs) are stars with extremely high peculiar velocities relative to the velocity distribution of their parent population. In recent years several HVSs have been observed in the Galactic halo, some of them unbound to the Galaxy (with velocities beyond the escape velocity; Brown et al. 2007b). From these a Galactic population of 96 ± 10 such HVSs was inferred (Brown et al. 2007b), up to the 100 kpc distance limit of the survey. Many similar bound HVSs (with velocities lower than the escape velocity) have been observed at larger numbers. Most of the observed HVSs are B-type stars (Brown et al. 2005, 2006a, 2006b, 2007a, 2007b; Edelmann et al. 2005; future observations of HVSs of other stellar types are discussed in Kollmeier & Gould 2007; Brown et al. 2009; Kenyon et al. 2008). Given the color selection of the targeted survey for these stars (Brown et al. 2006a), such stars could be either main-sequence (MS; or blue straggler) B stars or hot blue horizontal branch (BHB) stars. Currently, only three of the stars in the survey have specific unambiguous identification and were found to be MS stars (Fuentes et al. 2006; Lopez-Morales & Bonanos 2008; Przybilla et al. 2008a).

Extreme velocities as found for these stars most likely suggest a dynamical origin from an interaction with or close to the massive black hole (MBH) in the Galactic center (GC; Hills 1988; Yu & Tremaine 2003; Levin 2006; O’Leary & Loeb 2007; Perets et al. 2007). In the following we discuss only HVSs ejected from the GC⁶ and observed in the Galactic halo, >10

kpc from the GC, which would require ejection velocities from the GC of $\gtrsim 800 \text{ km s}^{-1}$. Such HVSs could serve as probes of the GC environment, stellar population and dynamics (see, e.g., Sesana et al. 2007; Kenyon et al. 2008; Perets 2009b) and serve as an independent evidence for the existence of an MBH in the GC (Hills 1988). Most of the B-type stars observed through the HVSs survey have lower velocities and are either bound HVSs (Brown et al. 2007a) or are just halo stars. The survey shows an asymmetry in the kinematics of the stars, where more stars have positive radial velocities in Galactocentric coordinates (i.e., outgoing stars) than negative ones (ingoing or returning stars). As we show this asymmetry is dependent on both the absolute velocity and the distance of the stars from the GC, and could be used in a novel method to probe and constrain the Galactic potential, identify the stellar type of the stars in the survey and estimate the number of HVSs.

This paper is organized as follows. We first briefly describe the HVSs survey (Section 2), and then suggest a novel method to probe the Galactic potential using such surveys (Section 3). In Section 4, we use a similar analysis to infer the statistics of the stellar type of stars in the HVSs survey and estimate a lower limit to the number of HVSs in the Galaxy.

2. THE VELOCITY–DISTANCE DISTRIBUTION OF HVSs

HVSs of almost any stellar type could theoretically be observed, since the currently suggested scenarios for the origin of HVSs give rise to only limited number of constraints on their stellar characteristics (e.g., Hansen 2007; Perets 2009b). However, given their relatively small numbers in the Galaxy, it is practically impossible to find HVSs close by. For this reason, following the discovery of the first HVSs in the Galactic halo (Brown et al. 2005; Hirsch et al. 2005; Edelmann et al. 2005); Brown et al. (2006b) have issued a survey of HVSs extending to large distances. They have searched for HVSs among color

⁶ Note that recent observations possibly suggest a different origin for two of HVSs observed serendipitously (Bonanos et al. 2008; Przybilla et al. 2008b; Heber et al. 2008, but see Perets 2009a). Throughout this paper, we assume that most (if not all) of the MS stars in the HVSs survey sample have a GC origin. We note however that the methods we describe here to constrain the Galactic potential could similarly be used, in principle, for the analysis of high-velocity stars ejected from the Galactic disk.

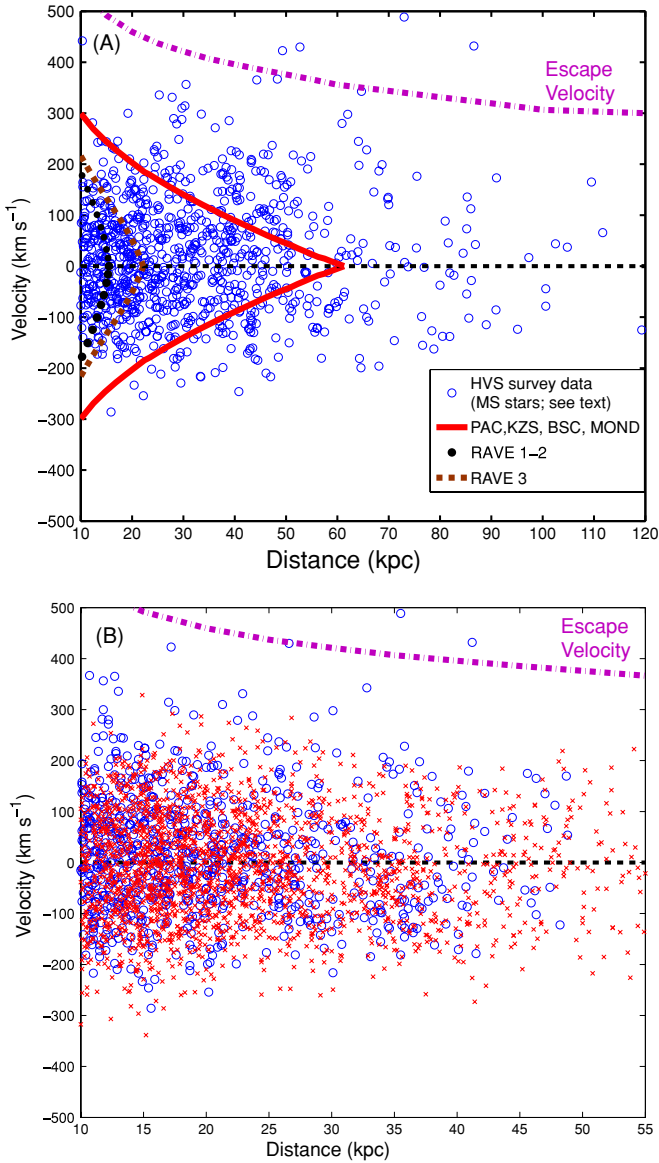


Figure 1. Distance–velocity distribution of Halo B-type stars from Brown et al. (2007b) observations (blue circles). (a) The observed stars are assumed to be MS stars. The lines represent the critical asymmetry lines (see the text) for various potentials (see legend), for propagation up to the maximal lifetime of such stars ($\sim 4 \times 10^8$ yr). (b) The same, but now assuming all the stars are hot BHB stars, and therefore less distant. The velocity–distance distribution of regular halo BHB stars (\times marks; taken from Xue et al. 2008), is shown for comparison. Dashed middle line in both panels separates between outgoing and ingoing stars. The escape velocity (in the KZS model) is also shown for comparison in both panels.

(A color version of this figure is available in the online journal.)

selected B-type halo stars of limited magnitude (a more recent survey also searches for A type stars; Brown et al. 2009; not included in our analysis). Such stars are luminous enough to be observed at large distances in the Galactic halo where the relative frequency of HVSSs is much higher, and are less likely to be contaminated by the disk and halo stellar population. These stars could be either MS B stars (or blue stragglers) with masses of $3\text{--}4 M_{\odot}$ and short lifetimes ($(1\text{--}4) \times 10^8$ yr) or hot BHB stars also with short lifetimes (few $\times 10^8$ yr on the horizontal branch), but long progenitor lifetime. The absolute magnitudes of observed stars and hence their inferred distances depend on their stellar type. Any analysis of the distribution of HVSSs should take both possibilities into account.

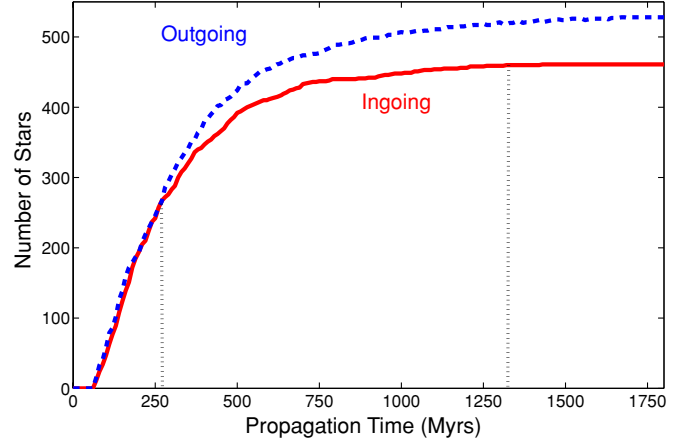


Figure 2. Asymmetric distribution of outgoing vs. ingoing stars. The curves show the integrated number of outgoing vs. ingoing stars below (or above, respectively) the critical asymmetry lines (PAC model), corresponding to the range of propagation times in the Galactic potential. The asymmetry begins at propagation times of $\sim 2.5 \times 10^8$ yr (see the left dotted vertical line). No ingoing stars are observed to correspond to propagation times beyond $\sim 1.3 \times 10^9$ yr.

(A color version of this figure is available in the online journal.)

Figure 2 in Brown et al. (2007b) shows a definite asymmetry in the distribution of ingoing and outgoing HVSSs, where the velocities of ingoing stars do not extend beyond 300 km s^{-1} . Given that the escape velocity at these distances is much higher, one would expect to see bound HVSSs returning at velocities up to the escape velocity, in striking contrast with observations. In order to study this behavior, we turn to the velocity–distance distribution of these stars. In Figure 1, we show the radial velocity–distance distribution (relative to the GC) for all of the observed B-type stars in the Brown et al. (2007b) survey, assuming they are either MS stars (and are therefore more luminous and more distant; Figure 1(a)), or hot BHB stars (and therefore closer; Figure 1(b)).

3. PROBING THE GALACTIC POTENTIAL USING HYPERVELOCITY STARS

Many studies have been done to constrain the Galactic potential at large distances through observations (see, e.g., Fich & Tremaine 1991; Battaglia et al. 2005; Smith et al. 2007; Xue et al. 2008, and references therein). Some of these studies use the velocity dispersion of observed objects to constrain the Galactic potential (e.g., Battaglia et al. 2005; Xue et al. 2008), however these suffer from uncertainties regarding the velocity anisotropy and the behavior of the stellar halo density at very large distances, and require some a priori assumptions regarding these parameters, which may lead to large uncertainties (see, for example, discussion in Dehnen et al. 2006). In addition, many objects are needed in order to obtain the velocity dispersion at a given distance from the GC. Other studies explore the local escape velocity from the Galaxy through observations of high-velocity stars (Smith et al. 2007). However, such analysis contains degeneracies and depends on the unknown structure of the tail of the velocity distribution of the high-velocity stars. Consequently, specific assumptions must be taken for the velocity distribution, which could be strongly affected by the small number statistics of the observed highest velocity stars in the distribution tail. Moreover, the assumptions used for the stellar velocities depend on their being extended up to the escape velocity from the Galaxy. Although large surveys may help solve this problem, very high velocity stars are quite rare in the Galaxy,

and would be difficult to find especially in surveys limited to relatively close environment of the solar neighborhood.

Gnedin et al. (2005) and Yu & Madau (2007) suggested to use the kinematics of HVSs in order to probe the Galactic potential using the position and velocity vectors of HVSs at large Galactocentric distances. Under the assumption that HVSs were ejected from the GC they suggest to measure the slight departure from purely radial orbits of these HVSs, due to the (possible) triaxiality of the Galactic potential. These methods require the accurate distance and three-dimensional velocity of HVSs, and focus on the triaxiality of the Galactic potential, which is important in the context of hierarchical, cold dark matter (CDM) models of structure formation (e.g., Hayashi et al. 2007), although we note this should be interesting also in respect to modified Newtonian dynamics (MOND) theories (Milgrom 1983). Recently, Kenyon et al. (2008) have studied the propagation of HVSs in the Galactic potential and showed that it could depend strongly on the Galactic potential at the central regions of the Galaxy (200 pc). They also showed the dependence of the HVSs radial distributions on the stellar type, and their observational implications.

In the following, we suggest a method which is more general in nature and more useful in constraining and distinguishing between different Galactic mass distributions which are required by the different Galactic potential models at large distances (although it could also be relevant to probing the triaxiality of the Galactic potential). This can also be used in order to discriminate between different CDM Galactic potential models and/or between Galactic potentials in MOND theories. This method makes use of the asymmetry in velocity distributions of ingoing and outgoing HVSs (see also related discussion in Kenyon et al. 2008). We begin with a naive description of the method, assuming one could observe even the oldest bound HVSs (i.e., those that could not leave the Galaxy, and could have gone through the Galaxy a few times). We then continue with a more realistic treatment which takes into account the finite lifetime of stars observable in the halo, given the limited observational capabilities.

3.1. Long-Lived, Observable Hypervelocity Stars

Let us assume that HVSs have been continuously ejected from the GC with some distribution of velocities, which would produce both bound and unbound HVSs. Unbound stars eventually leave the galaxy. Bound stars reach the apo-apse point of their orbit and then return back to the GC with negative radial velocity (in Galactocentric coordinates). The Galactocentric distance–velocity distribution of ingoing stars would then have a cutoff, which would correspond to the escape velocity of these stars at a given distance from the GC. Such a cutoff is distance dependent and thus more distant HVSs would have lower absolute velocities. At the same time, we should see that the distribution of outgoing HVSs extends to much higher absolute velocities, since this population includes the unbound stars, on their way out of the galaxy. Consequently, a clear asymmetry should be observed between the distribution of ingoing and outgoing stars. This asymmetry or cutoff in the distance–velocity distribution would map the escape velocity of stars from the galaxy at any given distance where HVSs are observed, and serve as a direct probe of the galactic potential. Note, however, that very different galactic potential may have escape velocities which are quite similar at a wide range of distances from the GC (Wu et al. 2008). In such cases, observations of more distant HVSs (i.e., wider distance range) may be required to distinguish between

such potentials. Since such stars would be fainter, this would be more difficult observationally.

The use of ingoing and outgoing halo HVSs has three advantages over methods used to probe the local escape velocity from the Galaxy. First, there is a clear natural separation between bound and unbound stars, and the latter cannot contaminate the sample of ingoing high-velocity bound stars which are used to calculate the escape velocity. Second, there is no required assumption regarding the structure of the velocity distribution and its tail. Third, the HVSs are observed over a large distance range, and could thus map the Galactic potential in this full range, and not only at the local scale as have been done with high-velocity stars in surveys such as the Rave survey (Smith et al. 2007).

3.2. Realistic Short-Lived Hypervelocity Stars

In reality, observable stars in the HVSs targeted survey may not have an unlimited propagation time, as was our naive assumption. This may result either because of their short lifetimes (after which they evolve to a different stellar type, which cannot be observed at such distances with current instruments) or due to their possible origin from a burstlike event, which ejected HVSs only over a limited short time, and not as a continuous process occurring over the lifetime of the Galaxy (see Perets 2009b).⁷ Nevertheless, the general method prescribed above could still be applicable, with some modifications. In fact, as we the limited propagation time of HVSs may prove to be more advantageous in some respects).

Assuming some finite propagation time for HVSs, we would still expect an asymmetry in the ingoing and outgoing HVSs distance–velocity distributions. However, in this case the cutoff in the ingoing HVSs distribution would be at much lower velocities than the escape velocity. This cutoff corresponds to the maximal return velocity of HVSs which could still be observed coming back during their short propagation time. Assuming a maximal propagation time for the HVSs (its lifetime), this cutoff could thus be used as a probe of the Galactic potential in the same way as the naive method outlined above. Moreover, the short propagation time of stars can be advantageous for our purposes. Stars of different stellar types have different maximal lifetimes and would produce different distance–velocity cutoffs. Consequently, these different populations can supply us with several independent probes of the Galactic potential, that, combined together, would further assist in constraining the Galactic potential. A higher velocity at a given distance implies a longer travel time (as the travel time depends on the potential out to the apo-apse of the orbit), ingoing HVSs provide information not only on the escape velocity at the point where they are observed today, but even further away. Furthermore, up to the distance–velocity cutoff the distribution of outgoing and ingoing stars (with lower velocities than the cutoff velocity at their position) could be compared.^{7,8} in terms of the number of stars; the two-dimensional distance–(absolute) velocity distribution and the stellar types (if known) or color–color distributions of the samples of outgoing and ingoing stars. Any difference between these distributions is due to the further propagation in the Galactic potential of the ingoing HVSs to the apocenter of their

⁷ In such a case, for example, the highest velocity bound HVSs may never be observed as ingoing HVSs, since a longer propagation time is required for them to reach the apo-apse point of their orbit and become ingoing HVSs.

⁸ This, however, is true only under the assumption of a continuous and constant ejection rate, which is not the case for burst ejection of HVSs by an inspiralling IMBH (Levin 2006; Baumgardt et al. 2006; Löckmann & Baumgardt 2008; Sesana et al. 2008).

orbit and back. Different Galactic potential models give different return times that are also highly sensitive to the velocity of the HVSSs. Consequently, the statistical correlation between the ingoing and outgoing distance–velocity distributions could serve as a quantitatively sensitive method for discriminating between models for the Galactic potential than just the population of the highest velocity ingoing HVSSs.

3.3. Discriminating Between Galactic Potential Models

Currently, only three HVSSs in the HVSSs survey have an unambiguous stellar-type identification, and the analysis suggested here for probing the Galactic potential cannot be used directly. The clear cutoff in the ingoing stars distribution would not be observed, as it would be smeared by the existence of hot BHB stars contaminating the sample. Nevertheless, we still expect a statistical asymmetry between the number of ingoing versus outgoing stars in the sample, which should be observable beyond the theoretical cutoff. As an illustrative example we show the critical asymmetry lines for propagation of MS B stars HVSSs up to a maximal lifetime of 4×10^8 . In Figure 1(a), we show the critical asymmetry lines for such time-limited propagation in different models for the Galactic potential. The different models we use include five dark matter (CDM) potentials and one MOND potential. Beside the Paczynski (1990) model (hereafter PAC) all models are described in detail in Wu et al. (2008), where the same reference names are used (KZS, BSC, RAVE 1–3, and MOND). The PAC, KZS, BSC, and the MOND models are almost indistinguishable in this range of distances, whereas the RAVE 1–2 (indistinguishable in this range) and RAVE 3 models show very different behavior (see Appendix A for a short discussion on the differences between these Galactic potential models). We look for asymmetry by counting the numbers of outgoing versus ingoing stars in the sample, for the different potentials, i.e., counting the number of stars above and below the positive and negative velocity lines of the critical asymmetry curves shown in Figure 1(a). We look for the best fit model, which should show the largest asymmetry. We find a total of 166 outgoing stars versus 112 ingoing stars for the PAC, KZS, BSC and MOND models (the probability for getting such an asymmetric distribution from an a priori symmetric distribution is $p = 10^{-3}$) and 378 (452) outgoing stars versus 319 (388) ingoing stars for the RAVE 3 (RAVE 1–2) models ($p = 0.025$ (0.027)). Although all models show asymmetric distributions, the stars counted for the RAVE models contain the contribution from the PAC/KZS/BSC/MOND models. When subtracting this contribution, we find that the RAVE models do not show any additional asymmetry (212 (286) outgoing vs. 207 (276) ingoing stars; $p = 0.8$ (0.67)). Therefore, the HVSSs sample favors the PAC, KZS, BSC and MOND models over the RAVE models.

As we have shown even the contaminated sample of HVSSs could already constrain Galactic potential models. Future identification of the stellar types of the stars in the survey which could purify it could give even stronger constraints on these and other Galactic potential models. In Appendix B, we give a simple example for the use of such future data, using mock simulated data of ejected HVSSs. We also note that stars with longer MS lifetimes could probe larger distance range during their propagation and still return during their MS lifetimes to be observed as ingoing HVSS.⁹ Such stars could therefore serve

as observable probes of the Galactic potential at even larger distances not accessible in any other ways (and could possibly discriminate between CDM and MOND models that differ only at these distance ranges). This would require the identification of later-type HVSSs among halo stars (e.g., Brown et al. 2009, not analyzed here).

4. PROPAGATION IN THE GALACTIC POTENTIAL AND THE LIFETIMES OF OBSERVED HYPERVELOCITY STARS

The method described above uses the finite lifetimes of stars and their kinematics to constrain the Galactic potential. A very similar approach could also be used to constrain the number of the HVSSs and their lifetimes, given a specific Galactic potential. Making use of this approach we show that most of the stars in the HVSSs survey, especially with ingoing velocities, are likely to be halo hot BHB stars and have not been ejected from the GC (see also Kollmeier & Gould 2007; Yu & Madau 2007; Brown et al. 2007b; Kenyon et al. 2008, for related discussions), but nevertheless the number of HVSSs ejected from the GC could be much higher than previously thought.

In the previous section, we described the critical distance–velocity asymmetry lines. For a given Galactic potential and a given propagation time of an HVS, one could find the critical line outside which no such ingoing stars should be observed. In other words any ingoing star beyond this line cannot be an HVS from the GC with such (or shorter) lifetime. We can therefore identify at least some of the HVSSs sample stars as stars that are not MS stars ejected from the GC using this criteria (see Svensson et al. 2007 for a related discussion). Moreover, since the distribution of such stars should be symmetric (as observed for other samples of halo objects, such as regular halo BHB stars) any asymmetry beyond the critical lines is due to the outgoing MS HVSSs from the GC (or from the Galactic disk,¹ a possibility which we do not discuss here).

Assuming the PAC model (or the KZS and BSC model that give similar results) and a maximal propagation time of 4×10^8 yr (lifetime of a $3 M_{\odot}$ MS B star) we find an overabundance of $166 - 112 = 54$ outgoing stars, where an asymmetry of eight stars correspond to the 1σ probability level. We therefore give a lower limit estimate for the number of HVSSs beyond the critical line of $\gtrsim 54 \pm 8$ HVSSs, from which we infer, following the calculations by Brown et al. (2007b), that a total number of $\gtrsim 648 \pm 96$ such stars (MS B stars of $3-4 M_{\odot}$ at distances of $10 \text{ kpc} \lesssim r \lesssim 100 \text{ kpc}$ ejected from the GC) exist in the Galaxy. We expect that most if not all of the ingoing stars beyond the critical line are hot BHB stars, where outgoing stars beyond the line could be both hot BHB stars or MS stars, with a ratio of 2 to 1 ($166 - 54 = 112$ versus 54). These large estimated number of HVSSs may suggest a different contamination from high-velocity stars ejected from the Galactic disk that could also produce an asymmetric distribution due to finite MS lifetimes of the stars. Here we do not address this possibility, which requires a more detailed study and would be addressed in another paper.

In this calculation, we assumed a specific maximal propagation time for the GC HVSSs. Instead, we can look at the asymmetric distributions for stars that propagated in the Galactic potential for shorter propagation times. Such stars could be either more massive MS B stars with shorter MS lifetimes, or MS stars ejected from the GC only after evolving for some time in the GC (or ejected more recently from the GC). Since the frequency of more massive stars is small, the latter possibilities are

⁹ In fact, rejuvenated blue straggler stars could therefore contaminate the sample of the HVSSs, however this population is not expected to be large (Perets 2009a).

more likely to apply. One would therefore expect to see an asymmetric distribution even at times shorter than the MS lifetime of $3 M_{\odot}$ B MS star (4×10^8 yr), likely of the order of half this time ($\sim 2 \times 10^8$ yr), assuming a continuous ejection rate of HVSSs. In Figure 2, we show the number of outgoing versus ingoing stars for a range of propagation times. For the PAC potential model we used, the distribution begins to become asymmetric at propagation times of 2.5×10^8 yr, in good agreement with our expectations.

For completeness, we discuss the possibility that the HVSSs are not MS stars but hot BHB stars ejected from the GC. In this case their absolute magnitude is different from that of MS stars, and the inferred distances change accordingly (see Figure 1(b)). Again we can look for the typical propagation time at which we see an asymmetric distribution of these stars assuming they were ejected from the GC. We find this to be at a few 10^8 yr. This time is comparable, but longer, than the lifetime of hot BHB stars at this phase. It is also much shorter than the lifetime of hot BHB progenitors, which could extend up to a few Gyr. Both of these inconsistencies, together with the dynamical constraints against the ejection of hot BHB HVSSs (Perets 2009b), suggest a different identification of these stars. Furthermore, comparing their velocity–distance distribution to that of regular BHB stars in the halo (Xue et al. 2008) show very similar distribution (see Figure 1(b)), i.e., the observed cutoff in the distribution is not related to the critical lines we described, but due to the limit of the symmetric distribution of halo objects.

Another possibility is that asymmetries in the HVSSs candidates sample are not due to the population of HVSSs, but due to stellar streams located at specific regions of the Galactic halo, which could have correlated velocities, and not an isotropic distribution as we assumed. To check this, we repeated the asymmetry calculations described above, but this time for several different and distinct regions in the Galactic halo (different Galactic longitudes). Although some differences in the strength of the asymmetry are observed, all regions showed a clear asymmetry bias toward outgoing stars.

5. SUMMARY

In this paper, we studied the characteristics, the origins, and the use of stars observed in the survey for HVSSs in the Galactic halo. The kinematics of currently observed HVSSs ejected from the GC depend strongly on their lifetimes and their propagation in the Galactic potential. We suggest a novel method to probe the Galactic potential up to large distances using the kinematics and the spectral identification of HVSSs. We also use a reverse method, where a specific Galactic potential model is assumed, to give lower limit estimates on the number of HVSSs ejected from the GC. Future observations of HVSSs in M31 (Sherwin et al. 2008) and in other galaxies could have a similar use for studies of galactic structures and potentials.

We thank Warren Brown for helpful discussions and for supplying us with the data on the kinematics of the stars in the HVSSs sample. H.B.P. thanks the Israeli Commercial & Industrial Club for their support through the Ramon scholarship. B.F. is a postdoctoral researcher of the FNRS (Belgium). G.G. is a postdoctoral fellow with the National Science Fund (FWO-Vlaanderen). T.A. is supported by ISF grant 928/06 and ERC Starting Grant 202996. X.W. acknowledges support of SUPA studentship.

APPENDIX A

GALACTIC POTENTIAL MODELS

In the following, we shortly discuss the Galactic potential models used in Section 3.3 (KZS, BSC, RAVE 1–2, PAC, and MOND models) and the differences between them. For CDM models, we test Klypin et al. (2002) B1 model (KZS model), with a double-exponential disk for baryons and an NFW profile (Navarro et al. 1996) for a dark matter halo. We also replace baryons with the Besancon model together with the same CDM component in KZS B1 (BSC model). After that we adopt two of the models appeared in RAVE survey (Smith et al. 2007). In both RAVE models we apply Miyamoto & Nagai (1975) disk and Hernquist bulge (Hernquist 1990) for baryons, while for CDM, one of the models is uncontracted NFW (RAVE 1 model) and the other has a Wilkinson & Evans (1999) profile (RAVE 3). The PAC model uses Miyamoto & Nagai (1975) potential for the disk, bulge and halo components parameterized to match observations (see Paczynski 1990 for details).

The KZS and BSC models we use have the same NFW dark matter profile, but they differ in the distribution of their baryonic component. However, the propagation of the HVSSs is mostly dominated by the CDM halo far in the halo, and is therefore quite similar in these different models, as well as to the PAC model. The RAVE 1 model also uses the NFW profile, but with a different set of parameters (see Smith et al. 2007 for details). In this model, the dark matter halo is much more concentrated than the KZS/BSC (Klypin et al. 2002) models and the virial mass is almost twice as large as the virial mass in the KZS/BSC. The RAVE-3 model has a steeper distribution toward the center ($\rho \propto r^{-2}$), and a sharp cutoff at large radii. The MOND model uses the same baryon density of BSC but the potential in MOND is deeper than any of the CDM models (with the strength of external field $0.01 a_0$). When the external field is stronger, up to $0.03 a_0$ (corresponding to the upper limit from the constraints of the RAVE survey), the MONDian potential becomes very similar to the KZS/BSC models up to the distances of the observed HVSSs, and differ significantly only at larger radii. Due to the similarity between some of the models at the distances of the observed HVSSs, it is difficult to discriminate between the potentials of the KZS/BSC, PAC, and MOND using the critical asymmetry lines we present.

APPENDIX B

CONSTRAINING THE GALACTIC POTENTIAL: EXAMPLE OF SIMULATED DATA

In the following, we use a simple example of mock simulated data of HVSSs to show the way in which galactic potentials could be constrained by future HVSSs data. Using Monte Carlo simulations of HVSSs propagating in various galactic potential models, we produce distance–velocity plots of their expected distributions. This mock data are then compared with the critical asymmetry lines corresponding to the different models.

In this example, we assume the HVSSs were ejected from the GC following binary disruption by the MBH. We make use of the same methods described by Bromley et al. (2006) and Kenyon et al. (2008) to simulate the HVSSs ejection velocities, assuming the progenitor binaries of the HVSSs were $3 + 3 M_{\odot}$ binaries. For each ejected star we choose a random ejection time during its lifespan, and a random ejection time during the last 4×10^8 yr (the lifespan of $3 M_{\odot}$ stars; no such star could survive to current day if it were ejected earlier). We reject those

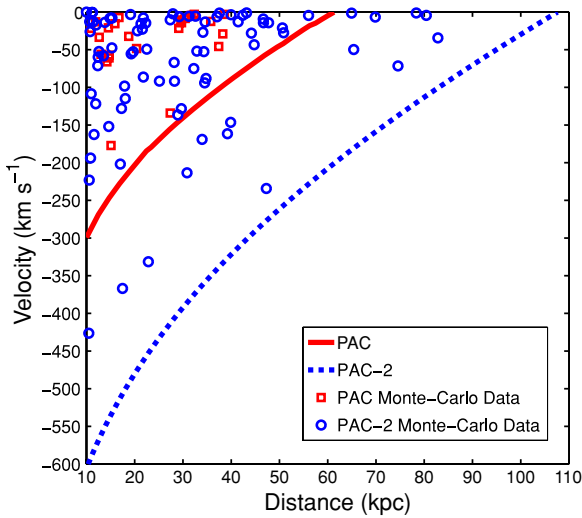


Figure 3. Distribution of incoming simulated HVSSs. The squares represent HVSSs propagating in the PAC model, and the circles represent HVSSs propagating in the PAC-2 model (see the text). The critical asymmetry lines are shown for both Galactic potential models, PAC (solid line) and PAC-2 (dashed line).

(A color version of this figure is available in the online journal.)

stars which would end their lifespan on the MS before current day, i.e., they would not have been observable today. Each of the potentially observable HVSSs is then propagated in a given Galactic potential until the current day. For simplicity, we show the results for the propagation of HVSSs in two Galactic potential models, which differ in only one parameter. We use the PAC model which is parameterized by eight parameters (see details in Paczynski 1990), to produce two potentials. The first (PAC) is the Galactic potential as originally parameterized in Paczynski (1990), and the second (PAC-2) differs only in the halo core radius, r_c , which is taken to be $r_c = 2$ kpc instead of $r_c = 6$ kpc in the original PAC model. The number of simulated stars was chosen such that the total number of HVSSs with velocity greater than 450 km s^{-1} observable in the Galactic halo would be ~ 100 , i.e., the total number of such HVSSs estimated to exist in the Galaxy based on current surveys.

The distance–velocity distribution of incoming simulated HVSSs is shown in Figure 3, together with the critical asymmetry lines for the two models. As can be seen in the figure, HVSSs propagating in the PAC-2 model obtain distance–velocity position beyond the critical asymmetry line of the PAC model, i.e., the PAC model would be directly excluded, independently of the detailed distribution of the HVSSs. HVSSs propagating in the PAC model could never get beyond the critical asymmetry line of the PAC-2 model and therefore can never totally exclude

this model. Nevertheless, the probability for not observing even a single HVSS beyond the PAC critical asymmetry line, assuming that the HVSSs did propagate in the PAC-2 model is ~ 0.007 (one would expect to see five such stars in the sample of 25 ingoing HVSSs, given the PAC-2 model data, but none is observed), i.e., rejecting the PAC-2 model at high confidence.

REFERENCES

- Battaglia, G., et al. 2005, *MNRAS*, **364**, 433
 Baumgardt, H., Gualandris, A., & Portegies Zwart, S. 2006, *MNRAS*, **372**, 174
 Bonanos, A. Z., et al. 2008, *ApJ*, **675**, L77
 Bromley, B. C., et al. 2006, *ApJ*, **653**, 1194
 Brown, W. R., Geller, M. J., & Kenyon, S. J. 2009, *ApJ*, **690**, 1639
 Brown, W. R., et al. 2005, *ApJ*, **622**, L33
 Brown, W. R., et al. 2006a, *ApJ*, **640**, L35
 Brown, W. R., et al. 2006b, *ApJ*, **647**, 303
 Brown, W. R., et al. 2007a, *ApJ*, **660**, 311
 Brown, W. R., et al. 2007b, *ApJ*, **671**, 1708
 Dehnen, W., McLaughlin, D. E., & Sahanian, J. 2006, *MNRAS*, **369**, 1688
 Edelmann, H., et al. 2005, *ApJ*, **634**, L181
 Fich, M., & Tremaine, S. 1991, *A&A*, **29**, 409
 Fuentes, C. I., et al. 2006, *ApJ*, **636**, L37
 Gnedin, O. Y., et al. 2005, *ApJ*, **634**, 344
 Hansen, B. 2007, *ApJ*, **671**, L133
 Hayashi, E., Navarro, J. F., & Springel, V. 2007, *MNRAS*, **377**, 50
 Heber, U., et al. 2008, *A&A*, **483**, L21
 Hernquist, L. 1990, *ApJ*, **356**, 359
 Hills, J. G. 1988, *Nature*, **331**, 687
 Hirsch, H. A., et al. 2005, *A&A*, **444**, L61
 Kenyon, S. J., et al. 2008, *ApJ*, **680**, 312
 Klypin, A., Zhao, H., & Somerville, R. S. 2002, *ApJ*, **573**, 597
 Kollmeier, J. A., & Gould, A. 2007, *ApJ*, **664**, 343
 Levin, Y. 2006, *ApJ*, **653**, 1203
 Löckmann, U., & Baumgardt, H. 2008, *MNRAS*, **384**, 323
 Lopez-Morales, M., & Bonanos, A. Z. 2008, *ApJ*, **685**, L47
 Milgrom, M. 1983, *ApJ*, **270**, 365
 Miyamoto, M., & Nagai, R. 1975, *PASJ*, **27**, 533
 Navarro, J. F., Frenk, C. S., & White, S. D. M. 1996, *ApJ*, **462**, 563
 O’Leary, R. M., & Loeb, A. 2007, *MNRAS*, **383**, 86
 Paczynski, B. 1990, *ApJ*, **348**, 485
 Perets, H. B. 2009a, *ApJ*, in press (arXiv:0802.1004)
 Perets, H. B. 2009b, *ApJ*, **690**, 795
 Perets, H. B., Hopman, C., & Alexander, T. 2007, *ApJ*, **656**, 709
 Przybilla, N., Nieva, M. F., Tillich, A., Heber, U., Butler, K., & Brown, W. R. 2008a, *A&A*, **488**, L51
 Przybilla, N., et al. 2008b, *A&A*, **480**, L37
 Sesana, A., Haardt, F., & Madau, P. 2007, *MNRAS*, **379**, L45
 Sesana, A., Haardt, F., & Madau, P. 2008, *ApJ*, **686**, 432
 Sherwin, B. D., Loeb, A., & O’Leary, R. M. 2008, *MNRAS*, **386**, 1179
 Smith, M. C., et al. 2007, *MNRAS*, **379**, 755
 Svensson, K. M., Church, R. P., & Davies, M. B. 2007, *MNRAS*, **383**, L15
 Wilkinson, M. I., & Evans, N. W. 1999, *MNRAS*, **310**, 645
 Wu, X., et al. 2008, *MNRAS*, **386**, 2199
 Xue, X., et al. 2008, *ApJ*, **684**, 1143
 Yu, Q., & Madau, P. 2007, *MNRAS*, **379**, 1293
 Yu, Q., & Tremaine, S. 2003, *ApJ*, **599**, 1129

Chapter 7

Dynamical evolution of the young stars in the Galactic center: N-body simulations of the S-stars

Perets, Gualandris, Kupi, Merritt, & Alexander

The Astrophysical Journal, in press (2009; arXiv:0903.2912)

DYNAMICAL EVOLUTION OF THE YOUNG STARS IN THE GALACTIC CENTER:
N-BODY SIMULATIONS OF THE S-STARSHAGAI B. PERETS¹, ALESSIA GUALANDRIS², GABOR KUPI¹, DAVID MERRITT² AND TAL ALEXANDER¹*Draft version March 20, 2009*

Abstract

We use N -body simulations to study the evolution of the orbital eccentricities of stars deposited near ($\lesssim 0.05$ pc) the Milky Way massive black hole (MBH), starting from initial conditions motivated by two competing models for their origin: formation in a disk followed by inward migration; and exchange interactions involving a binary star. The first model predicts modest eccentricities, lower than those observed in the S-star cluster, while the second model predicts higher eccentricities than observed. The N -body simulations include a dense cluster of $10M_{\odot}$ stellar black holes (SBHs), expected to accumulate near the MBH by mass segregation. Perturbations from the SBHs tend to randomize the stellar orbits, partially erasing the dynamical signatures of their origin. The eccentricities of the initially highly eccentric stars evolve, in 20 Myr (the S-star lifespan), to a distribution that is consistent at the $\sim 95\%$ level with the observed eccentricity distribution. In contrast, the eccentricities of the initially more circular orbits fail to evolve to the observed values in 20 Myr, arguing against the disk migration scenario. We find that 20%–30% of the S-stars are tidally disrupted by the MBH over their lifetimes, and that the S-stars are not likely to be ejected as hypervelocity stars outside the central 0.05 pc by close encounters with stellar black holes.

Subject headings: black hole physics — galaxies: nuclei — stars: kinematics

1. INTRODUCTION

In recent years, high resolution observations have revealed the existence of many young OB stars in the Galactic center (GC). Accurate measurement of the orbital parameters of these stars gives strong evidence for the existence of a massive black hole (MBH) which dominates the dynamics in the GC (Ghez et al. 1998; Eisenhauer et al. 2005; Gillessen et al. 2008). Most of the young stars are observed in the central 0.5 pc around the MBH. The young star population in the inner 0.05 pc (the “S-stars”) consists exclusively of B-stars, in an apparently isotropic distribution around the MBH, with relatively high eccentricities ($0.3 \lesssim e \lesssim 0.95$; Gillessen et al. 2008). The young stars outside this region comprise O-stars in one or two disks, and present markedly different orbital properties (Levin & Beloborodov 2003; Bartko et al. 2008; Lu et al. 2009).

Since regular star formation in the region near the MBH is inhibited by tidal forces, many suggestions have been made regarding the origin of the S-stars. Many of these are probably ruled out by observations and/or by theoretical arguments (see Alexander 2005; Paumard et al. 2006, for a review). The various scenarios for the origin of the S-stars predict very different distributions for their orbits, which in principle could be constrained by observations. However, it is not clear to what extent relaxation processes can produce changes in the distribution of orbital parameters after the stars have been deposited near their current locations. Here we try to resolve this question. We use N -body simulations to follow the evolution of stellar orbits around the GC MBH for 20 Myr, starting from various initial conditions that were motivated by different models for the origin of the S-stars. However, we do not discuss here the possibility that an intermediate mass black hole was involved in the production and/or evolution

of the S-stars, which is discussed in details elsewhere (see Merritt et al. 2009, and references therein). We find our N -body results to be consistent with our analytical predictions, and compare them with current observations. We then discuss the implications for the validity of the models for the production of the S-stars. In addition we study the possible ejection of the S-stars outside the inner 0.05 pc and the contribution of such ejected stars to the population of hypervelocity stars (as suggested by O’Leary & Loeb (2007)) and to the isotropic population of B-stars observed at distances of up to 0.5 pc from the MBH (i.e. at distances similar to those of the young O/WR stellar disks, but outside of these disks at high inclinations).

In §2 we summarize the different models for the origin of the S-stars and the predictions that they make for the stellar orbits at the time when the stars are first deposited near the MBH. §3 describes the N -body simulations we carried out to follow the S-star orbital evolution starting from these initial conditions. §4 and §5 present the results of these simulations and discusses the implications for the origin of the stellar populations of B-stars in the GC and for the population of hypervelocity stars observed in the Galactic halo. §6 sums up.

2. MODELS FOR THE S-STARS ORIGIN

Many solutions have been suggested for the origin of the S-stars, but many of these have been effectively excluded (see Alexander 2005; Paumard et al. 2006 for a review). Here we focus on two basic models which differ substantially in their predictions for the initial orbital distribution of the S-stars and/or the time passed since their arrival/formation at their current location. These are (1) formation of the S-stars in a stellar disk close to the MBH, followed by transport through a planetary-migration-like scenario to their current positions (Levin 2007); (2) formation of the S-stars in binaries far from the MBH followed by scattering onto the MBH by massive perturbers (e.g. giant molecular clouds) and tidal disruption of the binaries (Perets et al. 2007; Perets & Alexander 2007), leaving a captured star in a tight orbit around the

¹ Weizmann Institute of Science, POB 26, Rehovot 76100, Israel

² Department of Physics and Center for Computational Relativity and Gravitation, Rochester Institute of Technology, Rochester, NY 14623
Electronic address: hagai.perets@weizmann.ac.il

MBH. Binary disruption scenarios similar to (2) have been proposed, in which the S-stars formed in a stellar disk (either the currently observed 6 Myr old disk, or an older, currently not observed disk) and later changed their orbits due to coherent torques through an instability of eccentric disks (Madigan et al. 2008); or through the Kozai mechanism resulting from the presence of two disks (Löckmann et al. 2008). The latter alternative is unlikely since the Kozai mechanism is quenched in the presence of a massive enough cusp of stars such as exists in the GC (Chang 2008; Madigan et al. 2008). In any case, all the binary-disruption scenarios imply very similar initial distributions for the captured S-stars, and may differ only in their relevant timescales.

In the following, we briefly discuss the initial distribution of the eccentricities and inclinations of the S-stars expected from the different scenarios for their production. The models are summarized in Table 1.

2.1. Binary disruption by a massive black hole

A close pass of a binary star near a massive black hole results in an exchange interaction, in which one star is ejected at high velocity, while its companion is captured by the MBH and left on a bound orbit. Such interaction occurs because of the tidal forces exerted by the MBH on the binary components. Typically, a binary (with mass, M_{bin} , and semi-major axis, a_{bin}), is disrupted when it crosses the tidal radius of the MBH (of mass M_\bullet), given by $r_t = a_{bin}(M_\bullet/M_{bin})^{1/3}$. One of the binary components is captured by the MBH (Gould & Quillen 2003) on a wide and eccentric orbit while the companion is ejected with high velocity (Hills 1988).

The capture probability and the semi-major axis distribution of the captured stars were estimated by means of numerical simulations, showing that most binaries approaching the MBH within the tidal radius $r_t(a_{bin})$ are disrupted (Hills 1991, 1992; Gualandris et al. 2005; Bromley et al. 2006). The harmonic mean semi-major axis for 3-body exchanges with equal mass binaries was found to be (Hills 1991)

$$\langle a_{cap} \rangle \simeq 0.56 \left(\frac{M_\bullet}{M_{bin}} \right)^{2/3} a_{bin} \simeq 0.56 \left(\frac{M_\bullet}{M_{bin}} \right)^{1/3} r_t, \quad (1)$$

where a_{bin} is the semi-major axis of the infalling binary and a_{cap} that of the captured star (the MBH-star “binary”). Most values of a_{cap} fall within a factor 2 of the mean. This relation maps the semi-major axis distribution of the infalling binaries to that of the captured stars: the harder the binaries, the more tightly bound the captured stars. The periastron of the captured star is at r_t , and therefore its eccentricity is very high (Hills 1991; Miller et al. 2005),

$$e = 1 - r_t/a_{cap} \simeq 1 - 1.8(M_{bin}/M_\bullet)^{1/3} \simeq 0.94 - 0.99 \quad (2)$$

for values typical of B-type main sequence binaries and the MBH in the GC ($M_{bin} = 6 - 30 M_\odot$; $M_\bullet = 3.6 \times 10^6 M_\odot$; $a_{cap} = 0.5 - 2 \times \langle a_{cap} \rangle$). Therefore, in order to study the evolution of S-stars from the binary disruption scenarios we assume that the initial eccentricities of S-stars are in the range $0.94 - 0.99$ (where most are close to the mean value of 0.98).

In principle the binary disruption scenario has specific predictions for the semi-major axis distribution of the captured stars, which could also be used for constraining the model. However such distribution is highly sensitive to differences in the (unknown) binary distribution in the GC region. The prediction of high eccentricities for the captured S-stars, instead,

is robust and has only a weak dependence on the mass of the binary.

The inclinations of the captured S-stars in the massive perturbers scenario (Perets et al. 2007) are likely to be distributed isotropically since the stars originate in an isotropic cusp. Although in the disk instability scenario (Madigan et al. 2008) the progenitors of the captured stars form in the stellar disk, their original inclinations could be excited to higher inclinations than the typical inclinations observed in the stellar disk (Y. Levin, private communication), and may resemble a more isotropic distribution.

2.2. Planetary like migration from the young stellar disk(s)

Levin (2007) suggested that the S-stars could have formed in the currently observed stellar disk in the GC (Bartko et al. 2008; Lu et al. 2009), and then migrated inward in a way similar to planetary migration. The migration time scale expected from such a scenario could be as short as 10^5 yr (for type I migration), which could be comparable to (although possibly larger than; Nayakshin et al. (2007)) the lifetime of the gaseous disk. Recent analytic work (Ogilvie & Lubow (2003); Goldreich & Sari (2003); and references therein) has shown that eccentricity is likely to be damped during migration, unless eccentricity excitation occurs, which requires the opening of a clean gap in the disk. In the latter case the migration timescale might be larger (Levin 2007), possibly inconsistent with the lifetime of the gaseous disk (Nayakshin et al. 2007). It is therefore more likely that the eccentricities of the stars are damped during the migration. Even eccentricity excitation, if such took place, is unlikely to excite very high eccentricities. The mean eccentricity of the observed stars in the stellar disk is 0.34 ± 0.06 . Therefore, in order to study the evolution of the S-stars following their formation in a stellar disk, we assume them to have low eccentricities, or, being conservative, moderately high eccentricities ($e_{max} = 0.5$; where we use a thermal distribution of eccentricities, cut off at e_{max}). These simulations include the less likely (Levin 2007) possibility that the stellar disk extended inward to the current region of the S-stars, in which case the S-stars were formed in-situ and did not migrate.

3. THE N-BODY SIMULATIONS

To test these competing models, we carried out N -body simulations of the inner Milky Way bulge using models containing a realistic number of stars. All integrations were carried out on the 32-node GRAPE cluster gravitySimulator at the Rochester Institute of Technology which adopts a parallel setup of GRAPE accelerator boards to efficiently compute gravitational forces. The direct-summation code ϕ GRAPE was used (Harfst et al. 2007). The simulations used a softening radius of $\sim 4 R_\odot$ comparable to the radius of the S-stars r_\star , so as to be able to follow even the closest encounters between stars.

Our initial conditions were based on a collisionally evolved model of a cusp of stars and stellar remnants around the GC MBH (Hopman & Alexander 2006b, hereafter HA06; see also Freitag et al. 2006). HA06 evolved the multi-mass isotropic Fokker-Planck equation representing the stellar distribution in the region extending to ~ 1 pc from the MBH; in their models the contribution to the gravitational potential from the distributed mass is ignored. HA06 fixed the relative numbers of objects in each of four mass bins by assuming a mass function consistent with continuous star formation. The $10 M_\odot$ stellar-mass black holes (SBHs) were found to follow

TABLE 1
MODELS FOR THE S-STARS ORIGIN

#	Origin	Initial Eccentricity	Time (Myr)	Model Probability ^a	Survival Fraction ^b	Refs. ^c
1	Capture following binary disruption due to disk instability in the currently observed disk	High ($0.94 \leq e \leq 0.99$)	6	0.26	0.8	1
2	Capture following binary disruption due to massive perturbers or to disk instability in an old non-observed disk	High ($0.94 \leq e \leq 0.99$)	20	0.93	0.7	2
3	Disk formation + planetary like migration (currently observed disk)	Low ($e \leq 0.5$)	6	8×10^{-3}	0.9	3
4	Disk formation + planetary like migration (possible old disk)	Low ($e \leq 0.5$)	20	0.06	0.8	3

^aProbability for the samples of the observed and simulated S-stars to be randomly chosen from the same distribution (see text).
^bFraction of S-stars not disrupted by the MBH during the simulation (see text).
^c(1) Madigan et al. (2008) (2) Perets et al. (2007) (3) Levin (2007)

a steep, $n(r) \sim r^{-2}$ density profile near the MBH while the lower-mass populations (main-sequence stars, white dwarfs, neutron stars) had $n \sim r^{-\alpha}$, $1.4 \lesssim \alpha \lesssim 1.5$. The SBHs were found to dominate the mass density inside ~ 0.01 pc.

Based on this model, we constructed an N -body realization containing a total of 1200 objects within 0.3 pc of the MBH: 200 “stars,” with masses of $3 M_{\odot}$, and 1000 “black holes” with masses $10 M_{\odot}$, around a MBH of $3 \times 10^6 M_{\odot}$. We set $\alpha = 2$ for the SBHs and $\alpha = 1.5$ for the lower-mass stars, and each density component was tapered smoothly to zero beyond 0.1 pc when computing the corresponding $f(E)$. Since the S-stars may have masses as high as $\sim 10 M_{\odot}$, the higher mass stars in our simulations could also be treated as S-stars. We did not see any major differences in the evolution of the more massive and the less massive stars, and we discuss the evolution of both together.

The number of SBHs contained within a radius r in our N -body models was

$$N(< r) \approx 600 \left(\frac{r}{0.1 \text{ pc}} \right) \quad (3)$$

implying a distributed mass within 0.1 pc of $\sim 10^4 M_{\odot}$. This is somewhat ($\sim 2 - 3\times$) lower than the mass in SBHs in the HA06 or similar (Morris 1993; Miralda-Escudé & Gould 2000; Freitag et al. 2006) models at the same radius, and a factor ~ 5 lower than the *total* mass (mostly in main-sequence stars) in the Fokker-Planck models. In this sense, the rates of evolution that we infer below can be considered to be conservative.

On the other hand, we note that the late-type (old) stars that dominate the number counts in this region have a much flatter density profile than predicted by the HA06 models, possibly even exhibiting a central “hole” (Figer et al. 2003; Zhu et al. 2008). Only the B-type stars in the nuclear star cluster show a steeply-rising number density, $\alpha = 1.1 \pm 0.3$ (Schödel et al. 2007; Gillessen et al. 2008) but they presumably constitute a negligible fraction of the total mass in this region, and in any case are far too young to have reached a collisional steady state around the MBH. While the origin of this discrepancy between models and observations is currently unresolved, it may imply that the other contributors to the distributed mass around the MBH, including the SBHs, also have a lower density than in the Fokker-Planck models. For instance, relaxation times at the GC may be too long for collisionally relaxed steady states to have been established in the last 10 Gyr (Merritt & Szell 2006).

Modeling of the stellar proper motion data (Trippe et al. 2008; Schoedel et al. 2009) implies a distributed mass within 1 pc of $0.5 - 1.5 \times 10^6 M_{\odot}$, but these data are consistent with both rising and falling mass densities within this region and the distributed mass in the inner 0.1 pc is essentially unconstrained (Schoedel et al. 2009).

Because of these uncertainties, we discuss below how our results would vary if different numbers of SBHs were assumed.

As discussed in the previous section, we studied two basic sets of initial conditions for the S-stars. In the first model we assumed that the S-stars were captured by the MBH as in the binary disruption scenario (Gould & Quillen 2003), which leaves the captured stars in highly eccentric orbits ($> 0.94 - 0.99$; cf. section 2.1). Under these assumptions, the stars evolved for 6 Myr (if formed in the stellar disk) or longer (if the S-stars formed outside the central pc, i.e. not in the young stellar disk). We evolved the models for up to 20 Myr, which is comparable to the lifetime of the observed S-stars (although some may have longer lifespans). In the second scenario we assumed that the S-stars formed in a gaseous disk and then migrated inwards (or formed in situ in a disk extending close to the MBH). For this case we assumed the S-stars to have low eccentricities (< 0.5), as typical of disk formation models, and to evolve for 6 Myr (the lifetime of the observed stellar disk). In order to check both scenarios we selected the stars with initially high eccentricity orbits ($0.94 \leq e \leq 0.99$) and low eccentricity orbits ($e \leq 0.5$) and followed their evolution for a time appropriate to their presumed origin.

In addition to these evolutionary scenarios we also studied the possibility of ejection of S-stars as hypervelocity stars, following a close encounter with a SBH in the vicinity of the MBH, as suggested by O’Leary & Loeb (2007). Our high resolution simulations can accurately follow close encounters between stars, and therefore track any resulting high velocity ejections of stars. Motivated by recent observations of B-type main sequence stars outside the inner 0.05 pc of the Galaxy, which show evidence of random orientations similar to those of the S-stars, we also looked for stars scattered to larger distances by gravitational encounters. In other words, we considered whether captured S-stars could dynamically evolve to become the extended B-type stars population observed outside the central 0.05 pc.

Although some binaries could exist in the close regions near the MBH (Perets 2008, 2009), these are likely to be rapidly disrupted and not play an important role in the dynamical

evolution of the S-stars (Perets 2009). We therefore do not include any binaries in our initial conditions for the S-stars and SBHs evolution.

4. RESULTS

4.1. Simulations vs. theory: resonant relaxation

We applied the correlation curve method Eilon et al. (2008) to our simulations to identify the relaxation process responsible for the dynamical evolution of the stars (Fig. 1). The method is able to detect and measure relaxation in nearly Keplerian N -body systems. In the isotropic system considered here, the angular momentum of the stars, J , evolves both due to the slow stochastic two-body relaxation (e.g. Binney & Tremaine 1987) and to the rapid resonant relaxation (RR) (Rauch & Tremaine 1996; Rauch & Ingalls 1998; Hopman & Alexander 2006a; Gürkan & Hopman 2007; Eilon et al. 2008). Two-body relaxation changes J in a random walk fashion, $|\Delta J|/J_c = \sqrt{\tau/\tau_{NR}}$ over the long two-body relaxation time-scale $\tau_{NR} \sim Q^2/(N \log Q)$, where J_c is the maximal (circular orbit) angular momentum for a given energy, $Q = M_\bullet/M_*$, N is the number of enclosed stars on the distance scale of interest, and time $\tau = t/P$ is measured in terms of the orbital period on that scale. Resonant relaxation occurs when the symmetries of the potential act to constrain the stellar orbits (e.g. closed ellipses in a Kepler potential, or planar rosettes in a spherical one). As long as the symmetry is approximately maintained on the coherence timescale t_w , the stars experience coherent torques, and $\Delta J/J_c \sim (\sqrt{N}/Q)\tau$. In a nearly Keplerian potential, as is the case in the inner parsec of the GC, RR can change both the magnitude of J (“scalar RR”) and its direction (“vector RR”). In the Newtonian context, the coherence of scalar RR is limited by the precession of the apoapse due to the enclosed stellar mass, on a time-scale $\tau_M \sim Q/N$. On timescales $\tau > \tau_M$, the coherent change $\Delta J(\tau_M)$ becomes the mean free path in J -space for a rapid random walk, $|\Delta J|/J_c = \sqrt{\tau/\tau_{sRR}}$, where $\tau_{sRR} \sim Q \ll \tau_{NR}$. The coherence of vector RR is self-limited by the change in the orbital orientation due to RR, and is even faster, $|\Delta \mathbf{J}|/J_c = \sqrt{\tau/\tau_{vRR}}$, where $\tau_{vRR} \sim Q/\sqrt{N}$.

Figure (1) shows the rms change in the scalar and vector angular momentum of the stars in the simulation, as a function of the time lag τ (correlation curves), up to the maximal time lag for which the simulation can still be analyzed with high statistical confidence, $\tau_{\max} \sim 10^4$. In our simulation³, the scalar RR coherence time expected from theory is $\tau_M \sim 283$ and the scalar RR timescale is $\tau_{sRR} \sim 3.1 \times 10^5$. The behavior of the scalar correlation curve clearly indicates that RR dominates relaxation in our GC model. The turn from the coherent phase to the random-walk phase of RR is seen at $\tau \sim 300$, close to the predicted value of τ_M . The random-walk growth continues up to full randomization and saturation at $\sim \tau_\phi$, as expected (Eilon et al. 2008). The scalar RR timescale can be estimated directly from the simulated data by $\tau_{RR} = \tau/(|\Delta J|/J_c)^2$; substituting $|\Delta J|/J_c \sim 0.15$ at $\tau \sim \tau_\phi/2 \sim 5000$ yields $\tau_{sRR} \sim 2.2 \times 10^5$, in good agreement with the predicted value.

Furthermore, since $J/J_c = \sqrt{1 - e^2}$, the RR-driven eccentricity evolution relates the final eccentricity, e_f , after time

³ For a spectrum of masses, $\tau_M \sim Q/N \langle M_* \rangle$ and $\tau_{sRR} \sim M_\bullet/M_{\text{eff}}$, where $\langle M_* \rangle = 8.8 M_\odot$ and $M_{\text{eff}} = \langle M_*^2 \rangle / \langle M_* \rangle$. $M_{\text{eff}} \simeq 9.7 M_\odot$ for our simulation.

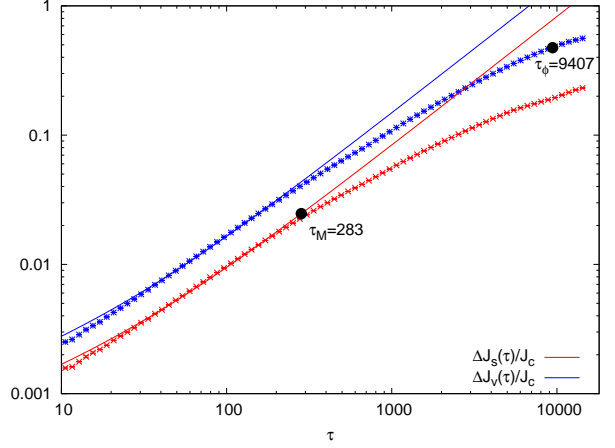


FIG. 1.— The correlation curves $|\Delta J|/J_c$ and $|\Delta \mathbf{J}|/J_c$ as a function of the time lag τ for all the stars in the simulation. The simulation data (points) are compared to the best fit theoretical curves (lines). Four regimes are seen (Eilon et al. 2008, see text and also). At very short timescales, non-resonant two-body relaxation ($\propto \sqrt{\tau}$) dominates over RR ($\propto \tau$); At $\tau < \tau_M$ the curves display a coherent, linear rise; At $\tau_M < \tau < \tau_\phi$, the curves display a random-walk growth and at $\tau > \tau_\phi$ they begin to saturate.

lag τ to the initial eccentricity, e_i . We therefore expect the eccentricities at some given time lag to have a typical spread, $e^-(\tau) \lesssim e_f(\tau) \lesssim e^+(\tau)$, where

$$e^\pm(\tau) = \left[1 - \left(\sqrt{1 - e_i^2} \mp \sqrt{\frac{\tau}{\tau_{RR}}} \right)^2 \right]^{1/2}. \quad (4)$$

The magnitude of the predicted change in eccentricity agrees well with that observed in the simulations. For example, an S-star initially captured by a tidal exchange event on a $P = 500$ yr ($a \sim 0.04$ pc), $e_i = 0.97$ orbit can evolve by RR to an $e_f = 0.80$ orbit in 20 Myr. The short vector RR timescale $\tau_{vRR} \sim 10^4$ ($t_{vRR} = 5 \times 10^6$ yr at 0.04 pc) implies full randomization of the orbital planes after 6 Myr, throughout the S-cluster volume, as is observed in the simulation. We therefore conclude that RR is the dominant mechanism responsible for the dynamical evolution of the S-stars and other stars close to the MBH in the GC.

4.2. S-star eccentricities and inclinations

In Figure 2 we show the final cumulative eccentricity distribution of the S-stars for the different origin models (Table 1). These are compared to the the orbits of the observed S-stars (taken from Gillessen et al. 2008). The probabilities for the samples of the observed and simulated S-stars to be randomly chosen from the same distribution (calculated using a two-sample χ^2 test) are given in Table 1. We find that the binary disruption model taking place at least 20 Myr ago is much favored over all other models tested here. We find 93% chance for the observed S-stars and the simulated stars in such model to originate from the same distribution (with the shorter timescale of 6 Myr consistent at the 26% level). In contrast, the disk migration scenarios seem to be excluded (for the given assumptions), since they have major difficulties in explaining the large fraction of eccentric orbits observed for the S-stars in the GC.

We find that the inclination distribution of the captured stars, initialized with the same inclination, is rapidly isotropized, to resemble a random distribution of inclinations

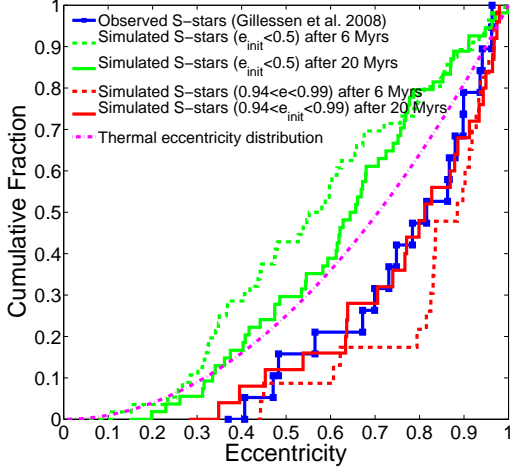


FIG. 2.— Cumulative distribution of observed and simulated S-stars eccentricities, for various models (see legend).

(consistent with random at the $\sim 65\%$ and $\sim 20\%$ level, after evolution of 20 and 6 Myr, respectively). This is expected from the RR process, as discussed in the previous section (see also fig. 1). We conclude that the observed isotropic distribution of the S-stars angular momentum direction is consistent with all the S-stars production models studied here, and can not be used to discriminate between them, although it constrains the lifetime of the S-stars system to be at least ~ 4 Myr at the 95% level, assuming all S-stars were initially put on the same plane.

4.3. Survival of the S-stars: tidal disruption, ejection and hypervelocity stars

As already discussed above, the S-stars can change their orbits due to their dynamical evolution. A star could therefore be scattered very close to the MBH and be disrupted by it, if its pericenter distance from the MBH becomes smaller than the tidal radius of the star $r_t = r_*(M_\bullet/m_*)^{1/3}$. Many of the S-stars could therefore not survive for long close to the MBH. We followed the orbits of stars in our simulations and calculated the fraction of stars that have been disrupted. For the tidal disruption calculations all stars were assumed to have the typical main sequence radius according to their mass. We consider a star as being disrupted if its pericenter became smaller than twice the tidal radius during the simulation (i.e., when it is strongly affected by the MBH tidal forces or even totally disrupted in one pericenter passage). We find that most of the S-stars survived to current times in all the models (see survival fractions in 1). The S-stars population in the GC therefore gives a good representation of all the S-stars formed/captured in this region. The production rate of the S-stars required to explain current observations is therefore only slightly higher (1.2–1.3 times higher) than that deduced from current number of S-stars observed.

In principle the S-stars could be ejected by strong encounters to orbits with larger semi-major axes, putting them outside the 0.05 pc region near the MBH (Miralda-Escudé & Gould 2000), or even ejecting them as unbound hypervelocity stars (O’Leary & Loeb 2007). The softening radius used in our simulation was $r_{soft} = 4R_\odot$, comparable to the radius of observed S-stars, allowing us to

follow even very close encounters. Nevertheless, we find that only $\sim 10\%$ of the stars were ejected outside of the central 0.05 pc, and even those had maximal semi-major axis in the end of the simulation not extending beyond 0.1 pc. We therefore conclude that such ejected S-stars can not explain recent observations of many B-type stars outside the central 0.05 pc (H Bartko, private communication). Moreover, none of the $3 M_\odot$ stars in our simulations have been ejected as a hypervelocity star, suggesting that ejection of hypervelocity stars through encounters with SBHs is not an efficient mechanism (see also Perets 2009 for the related constraints on this mechanism). We note that since our simulations can be rescaled, we can probe much higher stellar densities and smaller softening radius (see next section). When such rescaling is used, in which all the 1200 stars are distributed between 3×10^{-4} pc to 0.1 pc (rescaling the radii by half), we find 5 stars ejected beyond 0.1 pc (to have final semi-major axis of 0.1, 0.16, 0.16, 0.21 and 0.37 pc), but none ejected as hypervelocity stars or even as slow unbound stars.

5. DEPENDENCE OF THE RESULTS ON THE ASSUMED DENSITY OF SBHS

As discussed above, the density of the SBHs that are responsible for the evolution in our N -body models is not well determined. Scaling the N -body results to different assumed values of N is complicated by the fact that scalar resonant relaxation has two regimes, coherent and random walk. In our models, the transition occurs at

$$t_M \simeq QP/N \sim 3 \times 10^4 \left(\frac{N_{SBH}}{10^3} \right)^{-1} \left(\frac{P}{100 \text{ yr}} \right) \text{ yr}, \quad (5)$$

where the N_{SBH}^{-1} scaling is for scattering by SBHs of a given mass.

In the coherent regime, $\Delta t \lesssim t_M$, orbital angular momenta grow as

$$\frac{\Delta J}{J_c} \sim 10^{-4} \left(\frac{N_{SBH}}{10^3} \right)^{1/2} \frac{\Delta t}{P}. \quad (6)$$

In the diffusive regime, $\Delta t \gtrsim t_M$,

$$\left| \frac{\Delta J}{J_c} \right| \sim \sqrt{\frac{\tau}{\tau_{sRR}}} \approx 2 \times 10^{-3} \sqrt{\frac{\Delta t}{P}}, \quad (7)$$

independent of N_{SBH} .

We are interested in the orbital evolution of the S-stars over timescales of $\Delta t \sim O(10^7)$ yr. In our simulations and those with larger N , $\Delta t \gg t_M$. In this large- N regime, changes in eccentricity are dominated by the diffusive relation and are therefore expected to be nearly independent of N for time scales of interest, at least up to N -values of $\sim 10^5$ where the distributed mass begins to approach the mass of the MBH and resonant relaxation is no longer effective. Only for $N_{SBH} \lesssim 10$ does t_M approach 10^7 yr and our results start depending significantly on N_{SBH} . However, such a small number of SBHs in the volume of interest is highly unlikely, and therefore our results are robust to the details of the SBH cusp model.

The N -body simulations can also trivially be rescaled by

$$r \rightarrow Ar, \quad t \rightarrow A^{3/2}t \quad (8)$$

at fixed mass. This corresponds to placing the same number of SBHs into a smaller (larger) region and integrating for a shorter (longer) time. For instance, if we rescale our simulations to three times smaller distances (in which case the stars are distributed between 3×10^{-4} and 0.05 pc), the integration time becomes ~ 5 Myr.

6. SUMMARY

The approximately thermal eccentricity distribution of the S-stars near the massive black hole (MBH) in the galactic center (GC), $N(< e) \propto e^2$, is not naturally predicted by either of the two leading models for their production: migration of stars formed in a gaseous disk; or capture of stars following binary disruption by the MBH. The former model predicts eccentricities that are too low, the latter too high. In this paper, we followed the dynamical evolution of orbits of various eccentricities near the GC MBH, including for the first time the cluster of stellar-mass black holes (SBHs) that is expected to form around the MBH via mass segregation. We found that perturbations from the SBHs can reduce the eccentricities of initially very eccentric orbits ($0.94 \leq e_{\text{init}} \leq 0.99$) into a distribution that is consistent with the observed one, in a time of approximately 20 Myr, comparable to S-star lifespans; some of the stars change their eccentricities by more than 0.5 to values as low as $e_{\text{final}} = 0.2 - 0.4$. We confirmed these N -body results via a theoretical analysis of the relaxation process, and used that analysis to argue that our results are not strongly dependent on the (unknown) normalization of the SBH density near the MBH. The same mechanism is unable to convert initially low-eccentricity orbits into very eccentric ones on the

same time scale, arguing against the validity of the disk migration model for the origin of the S-stars. We also found that most S-stars are not disrupted by the MBH during their lifetime, and very few are ejected outside the central 0.05 pc near the MBH, and none having a semi-major axis beyond 0.1 pc. We did not find any hypervelocity star ejected in our simulation.

Evolution toward a thermal eccentricity distribution is a natural consequence of random gravitational encounters with a population of massive perturbers. In this paper, we considered the effect of a background of SBHs, which are expected on the basis of very general arguments to contribute a total mass of $\sim 10^4 M_\odot$ in the inner 0.1 pc around the MBH. We showed that they were effective at moderating the eccentricities of initially highly eccentric orbits. These results strengthen models in which the S-stars form from disrupted binaries, and disfavor models in which the S-stars are formed with low eccentricities.

This work was supported by grants NASA NNX07AH15G, NSF AST-0821141, and NSF AST-0807810 to D. M., and by ISF grant 928/06 and Starting Grant 202996 to T. A.

REFERENCES

- Alexander, T. 2005, *Phys. Rep.*, 419, 65
 Bartko, H. et al. 2008, *ApJ*, in press (arXiv:0811.3903)
 Binney, J. & Tremaine, S. 1987, *Galactic Dynamics* (Princeton, NJ: Princeton University Press)
 Bromley, B. C. et al. 2006, *ApJ*, 653, 1194
 Chang, P. 2008, arXiv:0811.0829
 Eilon, E., Kupi, G., & Alexander, T. 2008, arXiv:0807.1430
 Eisenhauer, F. et al. 2005, *ApJ*, 628, 246
 Figier, D. F. et al. 2003, *ApJ*, 599, 1139
 Freitag, M., Amaro-Seoane, P., & Kalogera, V. 2006, *ApJ*, 649, 91
 Ghez, A. M. et al. 1998, *ApJ*, 509, 678
 Gillessen, S. et al. 2008, arXiv:0810.4674
 Goldreich, P. & Sari, R. 2003, *ApJ*, 585, 1024
 Gould, A. & Quillen, A. C. 2003, *ApJ*, 592, 935
 Gualandris, A., Portegies Zwart, S., & Sipior, M. S. 2005, *MNRAS*, 363, 223
 Gürkan, M. A. & Hopman, C. 2007, *MNRAS*, 379, 1083
 Harfst, S. et al. 2007, *New Astronomy*, 12, 357
 Hills, J. G. 1988, *Nature*, 331, 687
 —. 1991, *AJ*, 102, 704
 —. 1992, *AJ*, 103, 1955
 Hopman, C. & Alexander, T. 2006a, *ApJ*, 645, 1152
 —. 2006b, *ApJ*, 645, L133
 Levin, Y. 2007, *MNRAS*, 374, 515
 Levin, Y. & Beloborodov, A. M. 2003, *ApJ*, 590, L33
 Löckmann, U., Baumgardt, H., & Kroupa, P. 2008, *ApJ*, 683, L151
 Lu, J. R. et al. 2009, *ApJ*, 690, 1463
 Madigan, A.-M., Levin, Y., & Hopman, C. 2008, arXiv:0812.3395
 Merritt, D., Gualandris, A., & Mikkola, S. 2009, *ApJ*, 693, L35
 Merritt, D. & Szell, A. 2006, *ApJ*, 648, 890
 Miller, M. C. et al. 2005, *ApJ*, 631, L117
 Miralda-Escudé, J. & Gould, A. 2000, *ApJ*, 545, 847
 Morris, M. 1993, *ApJ*, 408, 496
 Nayakshin, S., Cuadra, J., & Springel, V. 2007, *MNRAS*, 379, 21
 Ogilvie, G. I. & Lubow, S. H. 2003, *ApJ*, 587, 398
 O’Leary, R. M. & Loeb, A. 2007, *MNRAS*, 1076
 Paumard, T. et al. 2006, *ApJ*, 643, 1011
 Perets, H. B. 2008, arXiv: 0802.1004
 —. 2009, *ApJ*, 690, 795
 Perets, H. B. & Alexander, T. 2007, arXiv: 0705.2123
 Perets, H. B., Hopman, C., & Alexander, T. 2007, *ApJ*, 656, 709
 Rauch, K. P. & Ingalls, B. 1998, *MNRAS*, 299, 1231
 Rauch, K. P. & Tremaine, S. 1996, *New Astronomy*, 1, 149
 Schödel, R. et al. 2007, *A&A*, 469, 125
 Schoedel, R., Merritt, D., & Eckart, A. 2009, arXiv:0902.3892
 Trippe, S. et al. 2008, *A&A*, 492, 419
 Zhu, Q. et al. 2008, *ApJ*, 681, 1254

Chapter 8

Conclusions

In this thesis we explored the dynamics of stars near MBHs and the relaxation processes which govern their dynamical evolution. We have shown that in these environments relaxation processes beyond the two-body relaxation play a major role. Such processes affect the distribution of stars and compact remnants, lead to close interactions between them and the MBH, and may be related to the unusual stellar populations that are observed in the GC. These are of relevance because of the very high quality stellar data coming from our own Galactic nucleus, which harbors a MBH, as well as the relevance for the dynamics in other galactic nuclei and in galactic mergers.

Two processes beyond minimal two-body relaxation were discussed here: accelerated relaxation and loss-cone replenishment by MPs and rapid RR. Evidence was presented that these processes operate and may even dominate relaxation and its consequences in the GC, such as the production of the S-stars and HVSs in our Galaxy ; RR appears to play a major role in the redistribution orbital parameters of the S-stars following their initial production and binary heating contributes to the evolution of the stellar disk in the GC. There are also cosmic implications: MPs enable the efficient merger of binary MBHs, and boost the rates of white dwarf EMRIs captured near the MBH by tidal disruptions of stellar binaries.

An important part of this thesis dealt with the ejection of hypervelocity stars from the close environment of the MBH due to the interactions of single stars or binaries with the MBH (or binary MBH). These processes were studied analytically and through simulations, and made use of observational data to constrain the origin of HVSs. In addition a novel method was suggested for the use of HVSs as probes of the Galactic potential and its dark matter component.

We use the theoretical framework, that we developed, together with the simulations, numerical analysis and observations to study several different astrophysical phenomena. Our main findings can be summarized as follows:

Efficient relaxation processes in galactic nuclei --- Our studies [96, 93] indicate that massive perturbers such as giant molecular clouds or stellar clusters, frequently observed in galactic nuclei, play a major role in the dynamics of stars in these regions. We find that their effects could dominate over other relaxation processes which are typically considered, even when their total mass is much smaller than the mass of

the stars in these regions. In addition such efficient relaxation processes are highly important in scattering stars into the MBH, leading to high rates of close encounters between stars and MBHs and their various outcomes.

Coalescence of binary MBHs — Following galactic mergers, MBHs sink to the center of the newly formed galaxy. Such binary MBHs could scatter stars. In such binary MBH-star encounters orbital energy is transferred from the binary to the stars, which are ejected at high velocities. We show, similar to previous studies, that the rate of such encounters could be very low. Such low rate induced by two-body stellar relaxation process, can not induce the orbital decay and final coalescence of the binary MBHs during a Hubble time. However, when MPs are considered the encounter rates could be boosted by orders of magnitude leading to fast evolution and final coalescence of the binary MBHs in times much shorter than a Hubble time.

Production of the S-stars and hypervelocity stars and their dynamical evolution — We find that the high scattering rate of binaries on to the MBH in the GC, induced by MPs, lead to the capture of a large number of stars close to the MBH. Such capture processes followed by the dynamical evolution of these stars, could produce the population of young B-stars (the S-stars) and their observed characteristics, as well as the population of HVSSs observed in the outskirts of the Galaxy; possibly solving the puzzle regarding their origin.

Constraints on the nature and origin of HVSSs — We have shown that observations of the populations of hypervelocity stars and young stars in the GC, could be used together with theoretical arguments, in order to strongly constrain the possible origin of HVSSs from the GC. We used this method in addition to N-body simulations to exclude the IMBH inspiral and SBHs scenarios for ejection of HVSSs from the GC, leaving the binary disruption model as the only viable scenario for the GC origin of HVSSs currently suggested in the literature. We have also shown that binary HVSSs could be ejected from the GC following triple disruption, possibly leading to the formation of rejuvenated ('blue straggler') HVSSs, with extended lifetimes.

Probing the Galactic potential using hypervelocity stars — We have developed a novel method of probing the Galactic potential through the analysis of the distance-velocity distribution of observed HVSSs, which could be used to probe Galactic potential models up to large distances.

Gravitational wave sources — We have shown that capture of COs near MBHs following binary disruptions could lead to a large increase in the rates of close encounters between the COs and the MBH and the emission of GWs, observable through GW EMRIs in galactic nuclei. In addition the accelerated mergers of binary MBHs due to massive perturbers also leads to high rates of high mass ratio GW inspirals and the emission of strong GWs signal observable by the planned LISA mission.

Finally, my main studies during my PhD focused on the dynamics of stars near MBHs as presented above. In addition to these studies, I have explored several other directions, both in astrophysics and in quantum optics, including the formation of blue stragglers in triple systems, the evolution of binary minor planets, the discovery of a new type of stellar explosions and the realization of quantum walk processes using optical waveguide lattices. These works, which are only loosely, or not at all, related to the main theme of this thesis are not discussed here, but they are included in the appendix, for the full presentation of my PhD studies and their results. In addition to these

works I have contributed to several additional studies, but not as first author. These studies are not presented in this thesis and can be found in the following references: 118, 120, 12, 7.

The Road Not Taken

TWO roads diverged in a yellow wood,
And sorry I could not travel both
And be one traveler, long I stood
And looked down one as far as I could
To where it bent in the undergrowth;

Then took the other, as just as fair,
And having perhaps the better claim
Because it was grassy and wanted wear;
Though as for that, the passing there
Had worn them really about the same,

And both that morning equally lay
In leaves no step had trodden black.
Oh, I marked the first for another day!
Yet knowing how way leads on to way
I doubted if I should ever come back.

I shall be telling this with a sigh
Somewhere ages and ages hence:
Two roads diverged in a wood, and I,
I took the one less traveled by,
And that has made all the difference.

Robert Frost

Part I

Appendix

Chapter 9

Molecular hydrogen formation on amorphous silicates under interstellar conditions

Perets et al.

The Astrophysical Journal, Volume 661, Issue 2, pp. L163-L166 (2007)

MOLECULAR HYDROGEN FORMATION ON AMORPHOUS SILICATES UNDER INTERSTELLAR CONDITIONS

H. B. PERETS,¹ A. LEDERHENDLER,² O. BIHAM,² G. VIDALI,³ L. LI,³ S. SWORDS,³ E. CONGIU,^{3,4,5} J. ROSER,⁶
 G. MANICÓ,⁵ J. R. BRUCATO,⁷ AND V. PIRRONELLO⁵

Received 2007 March 11; accepted 2007 April 16; published 2007 May 14

ABSTRACT

Experimental results on the formation of molecular hydrogen on amorphous silicate surfaces are presented for the first time and analyzed using a rate equation model. The energy barriers for the relevant diffusion and desorption processes are obtained. They turn out to be significantly higher than those obtained earlier for polycrystalline silicates, demonstrating the importance of grain morphology. Using these barriers, we evaluate the efficiency of molecular hydrogen formation on amorphous silicate grains under interstellar conditions. It is found that unlike polycrystalline silicates, amorphous silicate grains are efficient catalysts of H₂ formation within a temperature range that is relevant to diffuse interstellar clouds. The results also indicate that the hydrogen molecules are thermalized with the surface and desorb with low kinetic energy. Thus, they are unlikely to occupy highly excited states.

Subject headings: dust, extinction — ISM: molecules — molecular processes

Online material: color figures

1. INTRODUCTION

H₂ is the most abundant molecule in the interstellar medium (ISM). It plays a crucial role in the initial cooling of clouds during gravitational collapse and is involved in most reaction schemes that produce other molecules (Duley & Williams 1984). It is widely accepted that H₂ formation in the ISM takes place on dust grains (Gould & Salpeter 1963). In this process, H atoms that collide with a grain and adsorb on its surface quickly equilibrate and diffuse either by thermal activation or tunneling. They may encounter each other and form H₂ molecules (Williams 1968; Hollenbach & Salpeter 1970) or desorb thermally in atomic form.

In recent years, we have conducted a series of experiments on the formation of molecular hydrogen on dust grain analogs such as polycrystalline silicates (Pirronello et al. 1997a, 1997b), amorphous carbon (Pirronello et al. 1999), and amorphous water ice (Manico et al. 2001; Roser et al. 2002, 2003; Perets et al. 2005), under astrophysically relevant conditions. In these experiments, the surface was irradiated by beams of H and D atoms. The production of HD molecules was measured during the irradiation and during a subsequent temperature programmed desorption (TPD) experiment. To disentangle the process of diffusion from the one of desorption, separate experiments were carried out in which molecular species were irradiated on the sample and were later induced to desorb. Related studies were done on amorphous ice surfaces (Hornekaer et al. 2003, 2005; Dulieu et al. 2005; Perets et al. 2005; Amiaud et al. 2006; Williams et al. 2007).

The results were analyzed using rate equation models, and the energy barriers for the relevant diffusion and desorption processes were obtained (Katz et al. 1999; Cazaux & Tielens 2004; Perets et al. 2005). Using these parameters, the conditions for efficient H₂ formation on different astrophysically relevant surfaces were found. In particular, the formation of H₂ on

polycrystalline silicates was found to be efficient only in a narrow temperature window below 10 K. Since the typical dust grain temperature in diffuse interstellar clouds is higher than 10 K, these results indicated that polycrystalline silicate grains cannot be efficient catalysts for H₂ formation in most diffuse clouds.

In this Letter we present, for the first time, experiments on molecular hydrogen formation on *amorphous* silicates and analyze the results using a suitable rate equation model (Perets et al. 2005). Using the parameters that best fit the experimental results, the efficiency of hydrogen recombination on grains is obtained for a range of conditions pertinent to diffuse interstellar clouds. It is found that unlike the polycrystalline silicate grains, amorphous silicate grains, which are the main silicate component in interstellar clouds (Tielens 2005) are efficient catalysts for H₂ formation within a broad temperature window that extends at least up to about 14 K.

2. EXPERIMENTAL METHODS AND RESULTS

The apparatus consists of an ultrahigh vacuum chamber housing the sample holder and a detector. The sample can be cooled by liquid helium to ~5 K, as measured by a calibrated silicon diode and thermocouple placed in the back of the sample. A heater in the back of the sample is used to maintain a set temperature between 5 and 30 K during the irradiation phase of the experiment. The sample and detector can rotate around the vertical axis. Prior to a series of measurements, the sample is heated to 380–400 K. During a series of measurements, the sample is taken periodically to 200–250 K to desorb condensables. Hydrogen and deuterium gases are dissociated in two radio-frequency dissociation sources, with dissociation efficiency of 80%–90% and are sent into the sample chamber via two triple differentially pumped beam lines (Vidali et al. 2004).

In the experiments reported here, we used beams of low fluxes and short dosing times. Using the standard Langmuir-Hinshelwood analysis, plotting the total yield of HD versus the exposure time (Biham et al. 2001), we estimated the coverage to be a small fraction (a few percent) of a monolayer (ML). This is still far from interstellar values but is within the regime in which results can be safely extrapolated to diffuse cloud conditions (Katz et al. 1999; Perets et al. 2005). The interstellar dust analogs we used are amor-

¹ Faculty of Physics, Weizmann Institute of Science, Rehovot 76100, Israel.

² Racah Institute of Physics, Hebrew University, Jerusalem 91904, Israel.

³ Physics Department, Syracuse University, Syracuse, NY 13244.

⁴ Università di Cagliari, Dipartimento di Fisica, Cagliari, Italy.

⁵ Università di Catania, DMFCI, 95125 Catania, Sicily, Italy.

⁶ NASA Ames, Mail Stop 245-6, Moffett Field, CA, 94035.

⁷ INAF-Osservatorio Astronomico di Capodimonte, Napoli, Italy.

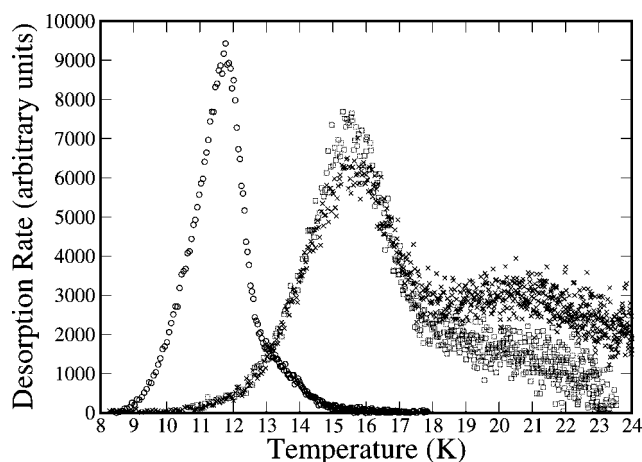


FIG. 1.—TPD curves of HD desorption after irradiation of HD molecules (crosses) and H+D atoms (squares) on amorphous silicate. Also shown, for comparison, is HD desorption after irradiation with H+D atoms on polycrystalline silicate (circles). [See the electronic edition of the Journal for a color version of this figure.]

phous silicate samples, $(\text{Fe}_x, \text{Mg}_{1-x})_2\text{SiO}_4$, prepared by one of us (J. R. B.) by laser ablation (wavelength 266 nm) of a mixed MgO, FeO, and SiO₂ target in an oxygen atmosphere (10 mbar). The optical and stoichiometric characterization of samples produced with this technique is given elsewhere (Brucato et al. 2002). The results reported here are for a sample with $x = 0.5$.

The experiment consists of adsorbing hydrogen atoms onto the surface while monitoring the amount of hydrogen molecules that are formed. To increase the signal-to-noise ratio, hydrogen and deuterium atoms are used and the formation of HD is monitored. The measurement of HD formation is done in two steps. First, we record the amount of HD that forms and comes off the surface while the sample is being dosed with H and D atoms (the “irradiation phase”). Next, after dosing is completed, in a TPD experiment, the surface temperature is raised rapidly and the rate of HD desorption is measured (the “TPD phase”). By far, the main contribution comes from the TPD phase.

Irradiations with beams of H and D (hereafter H+D) were done on an amorphous silicate surface in order to explore the formation processes of HD molecules. The H+D irradiation runs were performed with different irradiation times (15, 30, 60, 120, and 240 s), at a surface temperature of $T_0 \approx 5.6$ K. In a separate set of experiments, beams of HD molecules were irradiated on the same surface. During the TPD runs, the sample temperature was monitored as a function of time. The temperature ramps $T(t)$ deviate from linearity but are highly reproducible (see Fig. 2, inset).

The desorption rates of HD molecules versus surface temperature during the TPD runs are shown in Figure 1, for H+D irradiation on polycrystalline silicate (circles) and amorphous silicate (squares) surfaces, with irradiation times of 120 s. The TPD curve following irradiation of HD molecules on an amorphous silicate surface is also shown (crosses). The results of current experiments of H+D irradiation on amorphous silicates clearly differ from those of earlier experiments on polycrystalline silicates. The desorption curves from amorphous silicates contain two wide peaks, located at a significantly higher temperatures than the single narrow peak obtained for the polycrystalline silicate. The higher peak temperatures indicate that the relevant energy barriers are larger, while their large width reflects a broader distribution of the energy barriers of the HD desorption sites. The TPD curve of HD desorption from amor-

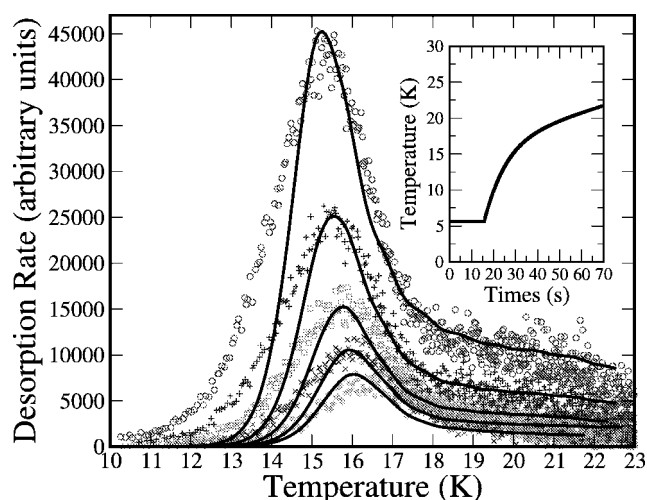


FIG. 2.—TPD curves of HD desorption after irradiation with H+D atoms on amorphous silicate with irradiation times of 15 (asterisks), 30 (crosses), 60 (squares), 120 (plus signs) and 240 (circles) s. The solid lines are fits obtained using the rate equation model. The temperature ramps (shown in the inset) are identical for all the runs. [See the electronic edition of the Journal for a color version of this figure.]

phous silicates, after irradiation with HD molecules (Fig. 1, crosses), is qualitatively similar to the curve obtained for H+D irradiation. In particular, the peak temperatures are the same. The relative weights of the high temperature peaks versus the low temperature peaks are somewhat different. Also, in similar experiments with higher values of T_0 , a third peak was observed at higher temperatures. We attribute this behavior to diffusion of HD molecules, which gradually migrate from shallow into deep adsorption sites (Perets et al. 2005; Dulieu et al. 2005; Amiaud et al. 2006).

In Figure 2 we present a series of TPD curves for HD desorption after irradiation with H+D atoms on an amorphous silicate surface with different irradiation times. Each curve exhibits a large peak at a lower temperature and a broader peak (or a shoulder) at a higher temperature. The position of the high temperature peak is found to be independent of the irradiation time, indicating that this peak exhibits first-order kinetics. The low temperature peak shifts to the right as the irradiation time is reduced. Since in the low-coverage regime studied here, the activation energies and the pre-exponential factor are not expected to depend on the coverage, these results indicate that the low temperature peak exhibits second-order kinetics. This is unlike the case of irradiation with HD molecules, where the lower temperature peak does not shift, showing first-order kinetics.

3. ANALYSIS OF THE EXPERIMENTAL RESULTS

In the model used here, there is no distinction between the H and D atoms, namely, the same diffusion and desorption barriers are used for both isotopes. Hydrogen atoms that stick to the surface hop as random walkers and may either encounter each other and form molecules, or desorb from the surface. As the sample temperature is raised, both the diffusion and desorption rates quickly increase. If a large fraction of the energy released when two H atoms recombine is transformed into kinetic energy of the formed molecule, it would immediately desorb from the grain surface in a high rovibrational state and with large translational energy. However, both our experiments on ice (Perets et al. 2005) and the current experiments indicate that such prompt desorption does not occur on amorphous sur-

TABLE 1
ENERGY BARRIERS FOR DIFFUSION AND DESORPTION

Material	$E_{\text{H}}^{\text{diff}}$ (meV)	$E_{\text{H}}^{\text{des}}$ (meV)	$E_{\text{HD}}^{\text{des}}$ (meV)
Polycrystalline silicate	25	32	27
Amorphous silicate	35	44	35, 53

faces (but see Perry and Price 2003, Tine et al. 2003, and Creighan et al. 2006 for other, more ordered, surfaces). Instead, the newly formed molecules dissipate their energy, probably through multiple collisions with the rough surface or internal pores. These molecules thermalize with the surface and become trapped in adsorption sites before they thermally desorb. Consequently, the desorbed molecules are not highly excited and desorb only with a thermal energy comparable with the grain surface temperature. Therefore, in our model it is assumed that the newly formed molecules do not promptly desorb but are trapped in adsorption sites with a range of potential barriers.

The experimental results were fitted using the rate equation model described in Perets et al. (2005). The parameters for the diffusion and desorption of hydrogen atoms and molecules on the amorphous silicate surface were obtained. These include the energy barrier $E_{\text{H}}^{\text{diff}}$ for the diffusion of H atoms and the barrier $E_{\text{H}}^{\text{des}}$ for their desorption. The value obtained for the desorption barrier should be considered only as a lower bound, because the TPD results are insensitive to variations in $E_{\text{H}}^{\text{des}}$, as long as it is higher than the reported value. The desorption barriers of HD molecules adsorbed in shallow (lower temperature peak) and deep (higher temperature peak) sites are given by $E_{\text{H}_2}^{\text{des}}(j)$, where $j = 1, 2$, respectively.

The rate equation model is integrated using a Runge-Kutta stepper. For any given choice of the parameters, one obtains a set of TPD curves for the different irradiation times used in the experiments. The actual temperature curve of the sample, recorded during the experiment, is used in the analysis (see Fig. 2, *inset*). In the first step, the barriers $E_{\text{H}_2}^{\text{des}}(j)$, $j = 1, 2$, for the desorption of molecules are obtained using the results of the experiments in which HD molecules are irradiated on the surface. To obtain better fits, we incorporate suitable Gaussian distributions of energy barriers around these two values. In the second step, the barriers for diffusion and desorption of H atoms are obtained, using the model to fit the results of H+D irradiation experiments (Table 1).

The second-order behavior of the low temperature peak in the H+D irradiation experiments can be explained as follows. Most HD molecules are formed only when the surface temperature is sufficiently high to enable significant mobility of H and D atoms. At this temperature, the shallow adsorption sites cannot retain the newly formed molecules adsorbed in these sites, which quickly desorb from the surface by thermal activation. However, those newly formed molecules that are trapped in deeper sites do not desorb yet and remain on the surface until its temperature increases further. Thus, the high temperature peak exhibits first-order kinetics and is located at the same temperatures in both HD and H+D irradiation experiments. Note that we cannot exclude the possibility that some fraction of the molecules desorbed in the high temperature peak are formed during irradiation and remain trapped in deep adsorption sites until the temperature becomes sufficiently high for them to desorb.

At longer H+D irradiation times, more atoms are adsorbed on the surface, and they find each other more easily. The low temperature peak (corresponding to HD desorption from shallower sites) shifts to lower temperatures with longer irradiation

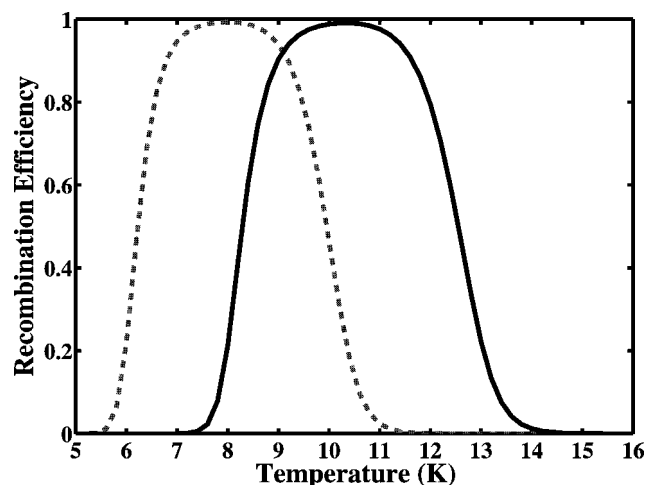


FIG. 3.—Calculated recombination efficiency of hydrogen at steady state on amorphous silicate (solid line) and polycrystalline silicate (dashed line) vs. temperature, using the parameters obtained from the TPD experiments. [See the electronic edition of the Journal for a color version of this figure.]

times, thus showing second-order behavior. This behavior must saturate with even longer irradiation times, when the temperature needed for HD formation becomes lower than the temperature needed for thermal desorption from the shallower HD adsorption sites. The HD molecules then form at low temperatures but are trapped in the shallow sites. They then await until the temperature is further increased, much like the adsorbed HD molecules in the HD irradiation experiments. Therefore, at longer irradiation times the low temperature peak should saturate into first-order-like behavior and the TPD curves of the H+D and HD irradiation experiments should become more similar. This behavior is confirmed by the TPD curves for H+D and HD irradiation shown in Figure 1.

Using the parameters obtained from the experiments, we now calculate the recombination efficiency of hydrogen on amorphous silicate surfaces under interstellar conditions. The recombination efficiency is defined as the fraction of hydrogen atoms adsorbed on the surface that come out as molecules. In Figure 3 we present the recombination efficiency versus surface temperature for the amorphous silicate sample under flux of 5.2×10^{-10} ML s $^{-1}$. This flux is within the typical range for diffuse interstellar clouds, where bare amorphous silicate grains are expected to play a crucial role in H $_2$ formation. This flux corresponds to a gas density of 10 atoms cm $^{-3}$, gas temperature of 100 K, and density of 7×10^{14} adsorption sites per cm 2 on the surface, obtained using the procedure described in Biham et al. (2001).

A window of high-recombination efficiency is found between 8 and 13 K, compared to 6–10 K for polycrystalline silicate under similar conditions. For a gas density of 100 atoms cm $^{-2}$, the high-efficiency window for the amorphous silicates surface shifts to 9–14 K. At higher temperatures atoms desorb from the surface before they have sufficient time to encounter each other. At lower temperatures diffusion is suppressed, and the Langmuir-Hinshelwood mechanism is no longer efficient. Saturation of the surface with immobile H atoms might render the Eley-Rideal mechanism more efficient in producing some recombination (Katz et al. 1999; Perets et al. 2005). Our results thus indicate that recombination efficiency of hydrogen on amorphous silicates is high in this temperature range, which is relevant to interstellar clouds. Therefore, amorphous silicates seem to be good candidates for interstellar grain components on which hydrogen recombines with high efficiency.

4. DISCUSSION AND SUMMARY

The analysis of the TPD curves from amorphous silicate surfaces shows that the relevant energy barriers on these surfaces are significantly higher than on polycrystalline silicates (Katz et al. 1999; Cazaux & Tielens 2004). A similar trend was observed in amorphous and porous ice surfaces (Williams et al. 2007). These results confirm the effect of surface morphology on the distribution of energy barriers. This effect can be parameterized using a model that provides a quantitative connection between the roughness and the energy barriers (Cuppen & Herbst 2005). Our results are consistent with this model and can be used to quantitatively constrain its parameters. More specifically, we find a 1.4–1.5 times increase in the energy barriers of the amorphous silicate versus the polycrystalline silicate surface. This gives rise to shifting and broadening of the temperature window in which H_2 formation is efficient, by a similar factor. Scanning electron microscope images show that the morphology of the amorphous silicate samples is very rough (H. Cuppen 2006, private communication). These samples are made of a broad (lognormal-like) distribution of spheres and agglomerates, from several nanometers up to a micron size. It is safe to conclude that our present results, together with those on amorphous carbon (Pirronello et al. 1999; Katz et al. 1999), show that amorphous silicate and carbon grains are efficient catalysts for the formation of molecular hydrogen in diffuse clouds. However, the results indicate that surface roughness is unlikely to extend the window of efficient recombination to temperatures of the order of 30–50 K observed in photodissociation regions (PDRs). We thus conclude that surface roughness, by itself, does not explain the high abundance of H_2 in PDRs.

In the model used here, it is assumed that H_2 molecules do not desorb immediately on formation. Instead, they stay trapped in the adsorption sites or hop between them until thermal desorption takes place. Consequently, one needs to consider mechanisms for the dissipation of the excess energy acquired from the recombination process in order to prevent prompt desorption. For amorphous, porous ice surfaces it was shown, using time-of-flight (TOF) measurements, that the kinetic energy of the desorbed molecules is small (≈ 3 meV), namely, the excess energy is absorbed by the surface (Roser et al. 2003; Hornekaer et al. 2003, 2005). Although we do not have direct measurements of the TOF of the HD molecules desorbed from the amorphous silicate surface, the similarity between the TPD curves obtained after HD and H+D irradiations indicates that

newly formed HD molecules reside and then desorb from the same adsorption sites as HD molecules irradiated on the surface. In light of the results on both ice and amorphous silicates, it is likely that H_2 molecules formed on realistic interstellar dust would have low kinetic energy and would probably not occupy excited vibrational or rotational states.

In summary, we have analyzed a set of TPD experiments on molecular hydrogen formation and desorption from amorphous silicate surfaces under conditions relevant to interstellar clouds. Fitting the TPD curves by rate equation models, the essential parameters of H_2 formation on amorphous silicate surfaces were obtained. These parameters include the energy barrier for diffusion of H atoms as well as their barrier for desorption (considered as a lower bound). The distribution of barriers for desorption of H_2 molecules is also obtained. Interestingly, a single type of adsorption site for hydrogen atoms is identified, versus two types of sites for molecules. The fraction of the adsorption sites, which belong to each of the two types is also evaluated. The rate equation model provides a unified description of several first- and second-order processes. It enables us to extrapolate the production rate of H_2 molecules from laboratory conditions to astrophysical conditions. It thus provides a quantitative evaluation of the efficiency of amorphous silicate surfaces as catalysts in the formation of H_2 molecules in interstellar clouds. We find that the recombination efficiency strongly depends on the surface temperature. In particular, the amorphous silicate sample studied here exhibits high efficiency within a range of surface temperatures that is relevant to diffuse interstellar clouds. The comparison of the current results with earlier ones on polycrystalline silicate surfaces shows the importance of surface morphology in molecular hydrogen formation. The results are in agreement with theoretical predictions on the effects of surface roughness (Cuppen & Herbst 2005). The results also indicate that on amorphous surfaces, newly formed H_2 molecules are thermalized on the surface and do not promptly desorb. Consequently, H_2 molecules formed on and desorbed from realistic *amorphous* interstellar dust are expected to have very low kinetic energy and would probably not occupy excited vibrational or rotational states.

This work was supported by the Adler Foundation for Space Research and the Israel Science Foundation (O. B.), by NASA grants NAG5-11438 and NAG5-9093 (G. V.), and by the Italian Ministry for University and Scientific Research grant 21043088 (V. P.).

REFERENCES

- Amiaud, L., et al. 2006, *J. Chem. Phys.*, 124, 094702
 Biham, O., Furman, I., Pirronello, V., & Vidali, G. 2001, *ApJ*, 553, 595
 Brucato, J. R., Mennella, V., Colangeli, L., Rotundi, A., & Palumbo, P. 2002, *Planet. Space Sci.*, 50, 829
 Cazaux, S., & Tielens, A. G. G. M. 2004, *ApJ*, 604, 222
 Creighan, S. C., et al. 2006, *J. Chem. Phys.*, 124, 114701
 Cuppen, H. M., & Herbst, E. 2005, *MNRAS*, 361, 565
 Duley, W. W., & Williams, D. A. 1984, *Interstellar Chemistry* (London: Academic Press)
 Dulieu, F., et al. 2005, *Chem. Phys. Lett.*, 404, 187
 Gould, R. J., & Salpeter, E. E. 1963, *ApJ*, 138, 393
 Hollenbach, D., & Salpeter, E. E. 1970, *J. Chem. Phys.*, 53, 79
 Hornekaer, L., Baurichter, A., Petrunin, V. V., Field, D., & Luntz, A. C. 2003, *Science*, 302, 1943
 Hornekaer, L., Baurichter, A., Petrunin, V. V., Luntz, A. C., Kay, B. D., & Al-Halabi, A. 2005, *J. Chem. Phys.*, 122, 124701
 Katz, N., Furman, I., Biham, O., Pirronello, V., & Vidali, G. 1999, *ApJ*, 522, 305
 Manicò, G., Ragunì, G., Pirronello, V., Roser, J. E., & Vidali, G. 2001, *ApJ*, 548, L253
 Perets, H. B., Biham, O., Manicò, G., Pirronello, V., Roser, J., Swords, S., & Vidali, G. 2005, *ApJ*, 627, 850
 Perry, J. S. A., & Price, S. D. 2003, *Ap&SS*, 285, 769
 Pirronello, V., Biham, O., Liu, C., Shen, L., & Vidali, G. 1997a, *ApJ*, 483, L131
 Pirronello, V., Liu, C., Roser, J. E., & Vidali, G. 1999, *A&A*, 344, 681
 Pirronello, V., Liu, C., Shen, L., & Vidali, G. 1997b, *ApJ*, 475, L69
 Roser, J. E., Manicò, G., Pirronello, V., & Vidali, G. 2002, *ApJ*, 581, 276
 Roser, J. E., Swords, S., Vidali, G., Manicò, G., & Pirronello, V. 2003, *ApJ*, 596, L55
 Tielens, A. G. G. M. 2005, *The Physics and Chemistry of the Interstellar Medium* (Cambridge: Cambridge Univ. Press)
 Tiné, S., Williams, D. A., Clary, D. C., Farebrother, A. J., Fisher, A. J., Meijer, A. J. H. M., Rawlings, J. M. C., & Davis, C. J. 2003, *Ap&SS*, 288, 377
 Vidali, G., Roser, J. E., Manicò, G., & Pirronello, V. 2004, *J. Geophys. Res.*, 109, E07S14
 Williams, D. A. 1968, *ApJ*, 151, 935
 Williams, D. A., Brown, W. A., Price, S. D., Rawlings, J. M. C., & Viti, S. 2007, *Astron. Geophys.*, 48, 25

Chapter 10

Realization of quantum walks with negligible decoherence in waveguide lattices

Perets et al.

Physical Review Letters, , vol. 100, Issue 17, id. 170506 (2008)

Realization of Quantum Walks with Negligible Decoherence in Waveguide Lattices

Hagai B. Perets,^{1,*} Yoav Lahini,¹ Francesca Pozzi,² Marc Sorel,² Roberto Morandotti,³ and Yaron Silberberg¹

¹*Faculty of Physics, The Weizmann Institute of Science, 76100 Rehovot, Israel*

²*Department of Electronics & Electrical Engineering, University of Glasgow, Glasgow G12 8QQ, Scotland, United Kingdom*

³*Institute National de la Recherche Scientifique, Université du Québec, Varennes, Québec J3X 1S2, Canada*

(Received 24 September 2007; published 2 May 2008)

Quantum random walks are the quantum counterpart of classical random walks, and were recently studied in the context of quantum computation. Physical implementations of quantum walks have only been made in very small scale systems severely limited by decoherence. Here we show that the propagation of photons in waveguide lattices, which have been studied extensively in recent years, are essentially an implementation of quantum walks. Since waveguide lattices are easily constructed at large scales and display negligible decoherence, they can serve as an ideal and versatile experimental playground for the study of quantum walks and quantum algorithms. We experimentally observe quantum walks in large systems (~ 100 sites) and confirm quantum walks effects which were studied theoretically, including ballistic propagation, disorder, and boundary related effects.

DOI: [10.1103/PhysRevLett.100.170506](https://doi.org/10.1103/PhysRevLett.100.170506)

PACS numbers: 03.67.Lx, 05.40.Fb, 42.25.Dd, 42.50.Xa

In classical random walks, a particle starting from an initial site on a lattice randomly chooses a direction, and then moves to a neighboring site accordingly. This process is repeated until some chosen final time. This simple random walk scheme is known to be described by a Gaussian probability distribution of the particle position, where the average absolute distance of the particle from the origin grows as the square root of time. First suggested by Feynman [1] the term *quantum* random walks was defined to describe the random walk behavior of a quantum particle. The coherent character of the quantum particle plays a major role in its dynamics, giving rise to markedly different behavior of quantum walks (QWs) compared with classical ones. For example, in periodic systems, the quantum particle propagates much faster than its classical counterpart, and its distance from the origin grows linearly with time (ballistic propagation) rather than diffusively [2]. In disordered systems, the expansion of the quantum mechanical wave-function can be exponentially suppressed even for infinitesimal amount of disorder, while such suppression does not occur in classical random walks.

In recent years QWs have been extensively studied theoretically [2] and have been used to devise new quantum computation algorithms [3]. Both discrete and continuous time QWs (DQWs; CQWs) [4–6] have been studied. In DQWs the quantum particle hops between lattice sites in discrete time steps, while in CQW the probability amplitude of the particle leaks continuously to neighboring sites. Experimentally, many methods have been suggested for the implementation of DQWs (see [2]), but only a small scale system consisting of a few states was implemented, using linear optical elements [7]. For CQWs, a few suggestions have been made [8,9], yet only one experimental method have been implemented by realizing a small scale cyclic system (4 states) using a nuclear magnetic resonance system [10]. Such systems are difficult

to scale to much larger configurations. Moreover, even at these very small scales, errors attributed to decoherence have been observed.

Here we suggest a very different implementation of CQWs using optical waveguide lattices. These systems have been studied extensively in recent years [11], but not in the context of QWs and quantum algorithms. We show that these systems can serve as a unique and robust tool for the study of CQWs. For this purpose we demonstrate three fundamental QW effects that have been theoretically analyzed in the QW literature. These include ballistic propagation in the largest system reported to date (~ 100 sites), the effects of disorder on QWs, and QWs with reflecting boundary conditions (related to Berry's "particle in a box" and quantum carpets [12,13]). Waveguide lattices can be easily realized with even larger scales than shown here (10^2 – 10^4 sites with current fabrication technologies), with practically no decoherence. The high level of engineering and control of these systems enable the study of a wide range of different parameters and initial conditions. Specifically it allows the implementation and study of a large variety of CQWs and show experimental observations of their unique behavior.

The CQW model was first suggested by Farhi and Gutmann [6], where the intuition behind it comes from continuous time classical Markov chains. In the classical random walk on a graph, a step can be described by a matrix M which transforms the probability distribution for the particle position over the graph nodes (sites). The entries of the matrix $M_{j,k}$ give the probability to go from site j to site k in one step of the walk. The idea was to carry this construction over to the quantum case, where the *Hamiltonian* of the process is used as the generator matrix. The system is evolved using $U(t) = \exp(-iHt)$. If we start in some initial state $|\Psi_{\text{in}}\rangle$, evolve it under U for a time T and measure the positions of the resulting state, we obtain a

probability distribution over the vertices of the graph. This is described by

$$i \frac{\partial \psi_j}{\partial t} = -d_j \gamma \psi_j + \gamma_{j,j+1} \psi_{j+1} + \gamma_{j,j-1} \psi_{j-1}, \quad (1)$$

where ψ_j is the wave function at site j , d_j is the number of sites connected to site j ($d_j = 2$ in the 1D nearest neighbor case), and $\gamma_{i,j}(= \gamma_{j,i})$ is the probability per unit time for the transition between neighboring [14,15]. This mathematical formulation is effectively identical to the well known discrete Schrödinger equation used in the tight-binding (Bloch ansatz) formalism in solid state physics [15]. It is used to describe the evolution of a wave function on a periodic potential, which is essentially the propagation of a quantum particle on a lattice [16,17].

An immediate implication for the correspondence between QWs and these processes is that many of the experiments in solid state physics described by the tight-binding model could serve as implementations of QWs. However, such experiments deal with the macro-physics of the system and with overall observables such as conductance or transmission. Therefore, one cannot measure the specific spatial and temporal distribution of the electrons or photons wave functions and the microphysics of the system cannot be directly observed. Moreover, solid state systems contain many electrons which interact nontrivially and thus cannot be described by the evolution equation of a single particle usually studied in QWs. Consequently, a qualitatively different experimental approach is needed in order to study QWs. Here we report such an approach using waveguide lattices.

Recently, a new technique has been developed for the experimental investigation of periodic systems using optics. The salient feature of these experiments is that evolution of waves in time is also spread out in space, making it much easier to observe. This is achieved by using waveguide structures which are periodic on one dimension [x axis; see Fig. 1(a)], but are homogeneous along the other (z axis). In this way the wave propagation along the z axis is free and corresponds to the evolution in time [11]. Under appropriate conditions light is guided inside the waveguides and can coherently tunnel between them. The ex-

perimental setup and typical lattice parameters are described elsewhere [18].

Light propagating in weakly coupled, single mode waveguides, can be described by [19]:

$$i \frac{n}{c} \frac{\partial A_j}{\partial t} = i \frac{\partial A_j}{\partial z} = \beta_j A_j + C_{j,j+1} A_{j+1} + C_{j,j-1} A_{j-1}. \quad (2)$$

Here A_j is the wave amplitude at site j , β_j is the on-site eigenvalue, $C_{i,j}$ is the coupling constant or tunneling rate between two adjacent sites i and j (for a periodic lattice $C_{i,j} \equiv C$ is constant), and z is the longitudinal space coordinate. The description by Eq. (2) is completely analogous to the quantum description of noninteracting electrons in a solid crystal in the tight-binding approximation, i.e., the discrete Schrödinger equation. The main differences are that (i) the spatial modulation of the index of refraction in the x direction now plays the role of the tight-binding potential, and the β_j s represent the propagation-constant eigenvalues of each waveguide in the lattice (ii) the evolution at a given time can be observed by measuring the intensity distribution at the corresponding position in the z axis [11], since $z = ct/n$, where c/n is the speed of light in the medium. The advantage of this system is the possibility to control the exact initial conditions for the light propagating inside the lattice. This is done by setting the width, the phase and the position across the lattice of the beam injected into the structure. In addition, this approach enables direct observation of the resulting wave function by measuring the distribution of light intensity at the sample's output [Fig. 1(b)]. Furthermore, the temporal evolution of the wave function can be observed by changing the sample length, or the initial conditions (e.g., [13,20]).

One of the hallmarks of QWs on ordered lattices is their ballistic propagation [2]. In order to observe this behavior, coherent light is injected into a single site in the lattice and the output intensity is measured. In Fig. 2 we compare the theoretical and the measured output distribution. The signature of ballistic propagation is clearly observed both at short and long propagation times [Fig. 2(a)]. Note that decoherence effects are negligible even after relatively long evolution in time, maintaining the detailed interference pattern predicted by theory [Fig. 2(b)]. Similar results, studied in a different context, were observed as early as in 1973 by Somekh *et al.* [21] on small scales in structures similar to the ones described above. The propagating photons tunnel from the origin site to an adjacent site, and immediately start tunneling to the next neighboring site. Through the tunneling between sites the photons accumulate a $\pi/2$ phase, and an additional phase is accumulated continuously in each lattice site j , at a rate given by β_j . The interference of all these waves depends on the phase accumulated in each possible path, and gives rise to the observed intensity distribution. This description is practically identical to the description of the QW, where the light intensity corresponds to the probability distribu-

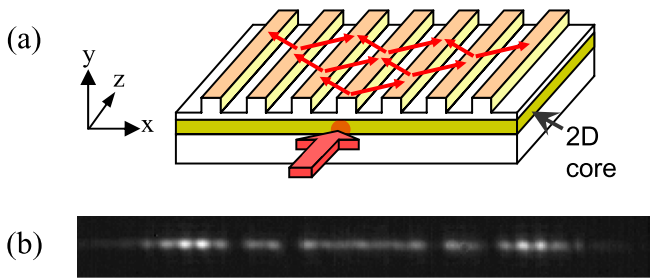


FIG. 1 (color online). (a) Schematic view of the optical waveguide lattice used in the experiments (see text). (b) Image of the output light distribution as recorded in the infrared camera, when the light is injected to a single lattice site at the input.

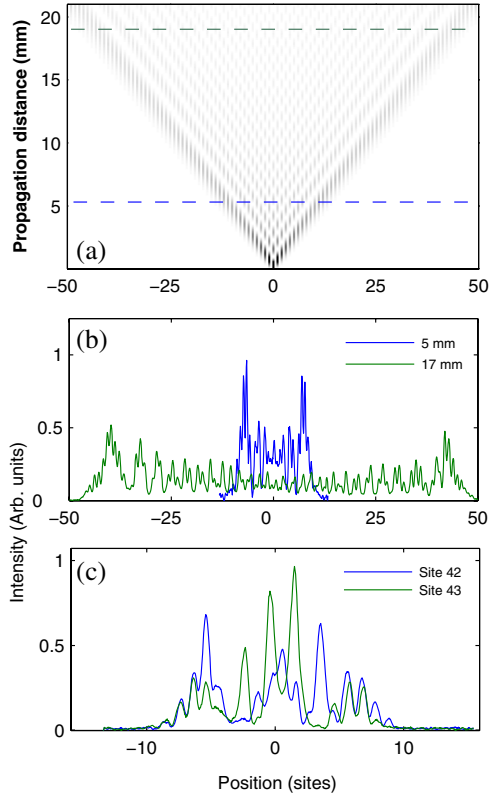


FIG. 2 (color online). (a) The theoretical prediction showing the ballistic evolution of the probability distribution of a CQW. The dashed lines correspond to the experimental measurements in (b). (b) The observed output pattern of light intensity after short (blue) and long (green) propagation in a periodic lattice. This well-known pattern is one of the hallmarks of the ballistic propagation of QWs. (c) Output patterns of light intensity resulting from injection of light into two adjacent single waveguides (sites 42 and 43) of a disordered lattice. The different patterns observed demonstrate the high sensitivity of the QW to the initial conditions in this case.

tion of the quantum particle. Since the single photon and many photon problems are described by the same probability distribution, experiments measuring light intensity are equivalent to performing a series of single photon experiments, from which the probability distribution is obtained. The propagation of more complex quantum states can be studied using correlated or entangled photons (see, for example, [22]). In this case the particle characteristics of the quantum walkers can be revealed by measuring two-photon correlation functions.

When disordered lattices are used [23,24], a different behavior is observed. Accumulated random phases of the random walker lead to destructive interferences that increase with distance from the origin. As a result, after a short ballistic propagation, the tails of the distribution are exponentially suppressed leaving the probability distribution exponentially localized to a small regime. This phenomena should be distinguished from a disordered related decoherence. Decoherence is related to temporal disorder, which induces a loss of phase coherence and results in a

transition into classical diffusion, characterized by an expanding Gaussian probability distribution [25,26]. Spatial disorder such as used here leads to an exponential (Anderson) localization (e.g., [27,28]), which is a coherent interference effect. In the context of CQWs, such behavior was found to be important for the efficiency of quantum algorithms [17,26,29].

QWs in disordered lattices are highly sensitive to the initial conditions. Figure 2(c) shows two output patterns of light intensity resulting from the injection of light into a single waveguide of a lattice and similar injection to an adjacent site of the same lattice. The different patterns observed demonstrate the high sensitivity of the QW to the exact initial conditions. This serves as a unique signature of the coherent nature of the QW, which is not present in the classical case. In addition these results demonstrate the effect of disorder on QWs, where in this case the disorder was introduced through randomizing the tunneling rate between sites (off-diagonal disorder). The tails of the distribution still show the ballistic component of the regular QW. However, additional strong peaks now appear near the origin. At later times these peaks evolve (on average) into an exponentially localized distribution, while the ballistic side lobes are suppressed (see [24] for detailed discussion).

Several theoretical studies have been done on QWs with boundary conditions [30,31], that give rise to complex self-interference patterns. In Fig. 3 we show experimental results of a QW with one reflecting boundary condition, compared with the theoretical analysis. A series of measurements is shown (horizontal cross sections), where in each measurement light was injected closer to the boundary. The observed pattern results from the self-interference of the incoming and reflected photons near the boundary, in agreement with theoretical predictions [30,32]. Although these are limited observations showing results of a short time propagation, longer waveguide lattices could be used

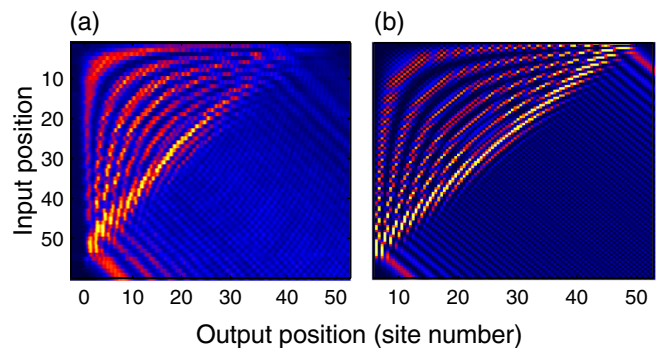


FIG. 3 (color online). (a) Measurements of the self-interference patterns of QWs near a reflecting boundary. Horizontal cross sections show the left half of the probability distribution of the QW, at decreasing input site position (vertical axis), where position 0 marks the lattice left boundary. (b) Comparison to the theoretical analysis using the method of images [32].

to study the more complex evolution at later times. For example, such behavior of a two boundary conditions system can be used for studying quantum carpets containing fractal patterns [12,29].

As an implementation of QWs, waveguide lattices carry some important advantages over other possible schemes. First, the technologies available for their fabrication or induction have reached a peak in recent years, enabling full control of every lattice parameters in one and two dimensions [18,33], or limited yet real time control of lattice parameters in two dimensions [34]. Second, waveguide lattices have excellent structural stability; thus, in practice decoherence due to noise is negligible. The optical wavelength in our experiments (using AlGaAs wafers) is around $1.5\ \mu\text{m}$, the standard communication wavelength, and losses at these wavelengths are extremely small. This is highly important for quantum computational tasks where coherency is essential. Third, effects arising from the interactions between different random walkers in other possible implementations are eliminated here, due to the bosonic, noninteracting nature of photons.

In recent years, several quantum algorithms based on QWs have been suggested [35]. For realistic use of such algorithms one requires exponentially large systems. We note that as long as entanglement is not introduced, our system is limited to large but not exponentially large scale functionality. The lack of entanglement limits the number of the states of the system, which scales linearly with the number of waveguides. Our system, even without entanglement, can potentially implement QW algorithms, since quantum entanglement is not required for the algorithm implementation or its improved efficiency. Its only role in this case is to allow for a larger number of states (see, for example the discussion in [36]. Some of the suggested QW algorithms have been shown to provide polynomial or even exponential speed up [37,38]. Unfortunately, in all of the algorithms suggested so far the speed up of quantum over classical algorithms is achieved only when applied to high dimensional systems. Nevertheless, our system can still be used to implement and study these algorithms in lower dimensions.

In summary, we have demonstrated the strong correspondence between QWs and light propagation in waveguide lattices. This correspondence can be used to extend and interchange ideas and knowledge acquired in both fields (e.g., nonlinear behavior [11] in CQWs or entanglement effects [39,40] in waveguide lattices). The high level of control, the accuracy, and the low decoherence rates achieved in waveguide lattices experiments provide a powerful tools for the study of QWs, and may prove useful in the implementation of QWs-based algorithms.

This work was supported by the German-Israeli Project Cooperation (DIP), NSERC and CIPI (Canada), and EPSRC (UK). Y.L. is supported by the Israeli Academy of Sciences and Humanities. H.P. and Y.L. thank the members of the WIS PIRATE club in which this study

was initiated.

*hagai.perets@weizmann.ac.il

- [1] A. Feynman and R.P. Hibbs, *Quantum Mechanics and Path Integrals* (McGraw-Hill, New-York, 1965).
- [2] J. Kempe, *Contemp. Phys.* **44**, 307 (2003).
- [3] V. Kendon, *Phil. Trans. R. Soc. A* **364**, 3407 (2006).
- [4] S. Godoy and S. Fujita, *J. Chem. Phys.* **97**, 5148 (1992).
- [5] Y. Aharonov, L. Davidovich, and N. Zagury, *Phys. Rev. A* **48**, 1687 (1993).
- [6] E. Farhi and S. Gutmann, *Phys. Rev. A* **58**, 915 (1998).
- [7] B. Do *et al.*, *J. Opt. Soc. Am. B* **22**, 499 (2005).
- [8] R. Côté *et al.*, *New J. Phys.* **8**, 156 (2006).
- [9] O. Mülken *et al.*, *Phys. Rev. Lett.* **99**, 090601 (2007).
- [10] J. Du *et al.*, *Phys. Rev. A* **67**, 042316 (2003).
- [11] D.N. Christodoulides, F. Lederer, and Y. Silberberg, *Nature (London)* **424**, 817 (2003).
- [12] M.V. Berry, *J. Phys. A* **29**, 6617 (1996).
- [13] R. Iwanow *et al.*, *Phys. Rev. Lett.* **95**, 053902 (2005).
- [14] R. Feynman, *The Feynman Lectures on Physics* (Addison-Wesley, Boston, 1963), Vol. 3.
- [15] N.W. Ashcroft and D.N. Mermin, *Solid State Physics* (Brooks Cole, Belmont, MA, 1976).
- [16] O. Mülken and A. Blumen, *Phys. Rev. E* **71**, 036128 (2005).
- [17] J.P. Keating *et al.*, *Phys. Rev. A* **76**, 012315 (2007).
- [18] H.S. Eisenberg *et al.*, *Phys. Rev. Lett.* **81**, 3383 (1998).
- [19] A. Yariv, *Quantum Electronics* (Wiley, New-York, 1989).
- [20] R. Morandotti *et al.*, *Phys. Rev. Lett.* **83**, 4756 (1999).
- [21] S. Somekh *et al.*, *Appl. Phys. Lett.* **22**, 46 (1973).
- [22] A. Politi *et al.*, arXiv:0802.0136.
- [23] T. Schwartz *et al.*, *Nature (London)* **446**, 52 (2007).
- [24] Y. Lahini *et al.*, *Phys. Rev. Lett.* **100**, 013906 (2008).
- [25] V. Kendon, *Math. Struct. Comp. Sci.* **17**, No. 6, 1169 (2007).
- [26] Y. Yin, D.E. Katsanos, and S.N. Evangelou, *Phys. Rev. A* **77**, 022302 (2008).
- [27] P.W. Anderson, *Phys. Rev.* **109**, 1492 (1958).
- [28] P. Sheng, *Introduction to Wave Scattering, Localization, and Mesoscopic Phenomena* (Springer, New-York, 1989).
- [29] O. Mülken, V. Bierbaum, and A. Blumen, *Phys. Rev. E* **75**, 031121 (2007).
- [30] E.J. Amanatidis, D.E. Katsanos, and S.N. Evangelou, *Phys. Rev. B* **69**, 195107 (2004).
- [31] A.J. Bessen, arXiv:quant-ph/0609128.
- [32] K.G. Makris and D.N. Christodoulides, *Phys. Rev. E* **73**, 036616 (2006).
- [33] A. Szameit *et al.*, *Opt. Express* **13**, 10 552 (2005).
- [34] J.W. Fleischer *et al.*, *Nature (London)* **422**, 147 (2003).
- [35] A. Ambainis, arXiv:quant-ph/0403120.
- [36] N. Bhattacharya, H.B. van Linden van den Heuvell, and R.J. Spreeuw, *Phys. Rev. Lett.* **88**, 137901 (2002).
- [37] A.M. Childs *et al.*, in *Proc. of STOC 2003* (2003), p. 59.
- [38] A.M. Childs and J. Goldstone, *Phys. Rev. A* **70**, 022314 (2004).
- [39] I. Carneiro *et al.*, *New J. Phys.* **7**, 156 (2005).
- [40] G. Abal *et al.*, *Phys. Rev. A* **73**, 042302 (2006).

Chapter 11

On the triple origin of blue stragglers

Perets & Fabrycky

The Astrophysical Journal, Volume 697, Issue 2, pp. 1048-1056 (2009)

ON THE TRIPLE ORIGIN OF BLUE STRAGGLERS

HAGAI B. PERETS¹, AND DANIEL C. FABRYCKY^{2,3}

¹ Weizmann Institute of Science, Rehovot 76100, Israel; hagai.perets@weizmann.ac

² Harvard-Smithsonian Center for Astrophysics, 60 Garden St, MS-51, Cambridge, MA 02138, USA

Received 2009 January 27; accepted 2009 March 17; published 2009 May 8

ABSTRACT

Blue straggler stars (BSSs) are stars observed to be hotter and bluer than other stars with the same luminosity in their environment. As such they appear to be much younger than the rest of the stellar population. Two main channels have been suggested to produce such stars: (1) collisions between stars in clusters or (2) mass transfer between, or merger of, the components of primordial short-period binaries. Here we suggest a third scenario, in which the progenitors of BSSs are formed in primordial (or dynamically formed) hierarchical triple stars. In such configurations, the dynamical evolution of the triples through the Kozai mechanism and tidal friction can induce the formation of very close inner binaries. Angular momentum loss in a magnetized wind or stellar evolution could then lead to the merger of these binaries (or to mass transfer between them) and produce BSSs in binary (or triple) systems. We study this mechanism and its implications and show that it could naturally explain many of the characteristics of the BSS population in clusters, most notably the large binary fraction of long-period BSS binaries; their unique period–eccentricity distribution (with typical periods > 700 days); and the typical location of these BSSs in the color–magnitude diagram, far from the cluster turnoff point of their host clusters. We suggest that this scenario has a major (possibly dominant) role in the formation of BSSs in open clusters and give specific predictions for the BSSs population formed in this manner. We also note that triple systems may be the progenitors of the brightest planetary nebulae in old elliptical galaxies, which possibly evolved from BSSs.

Key words: binaries: close – binaries: general – blue stragglers – open clusters and associations: general – stellar dynamics

Online-only material: color figures

1. INTRODUCTION

Blue Straggler Stars (BSSs) are stars that appear to be anomalously young compared to other stars of their population. In particular, BSSs lie along an extension of the main sequence (MS) in the color–magnitude diagram, a region from which most of the stars of equal mass and age have already evolved. Such stars appear to be brighter and bluer than the turnoff point of the stellar population in which they were observed. Their location in the color–magnitude diagram suggests that BSSs have typical masses of $1.2\text{--}1.5 M_{\odot}$, that are significantly larger than those of normal stars in old stellar systems such as old open clusters (OCs) or globular clusters (GCs). Thus, they are thought to have increased their mass during their evolution. Two main mechanisms have been proposed for their formation: (1) the merger of two stars induced by stellar collision (Hills & Day 1976) and (2) coalescence or mass-transfer between two companions in a binary system (McCrea 1964). The roles of each of these mechanisms in producing the observed BSSs populations are still debated, as each of these scenarios were found to be successful in explaining some of the BSSs observations, but fail in others (e.g., Bailyn 1995). In fact, even when both these mechanisms are taken into account (e.g., in N -body simulations including stellar evolution), they have major difficulties explaining the observations, especially those of binary BSSs (Leonard 1996; Hurley et al. 2005): the period–eccentricity distribution of BSSs binaries produced through these mechanisms is in poor agreement with the observed distribution of BSS binaries (Section 4.1.3). Moreover, typical BSS binaries produced in combined N -body and stellar

evolution simulations are produced in the inner regions of a cluster core (Hurley et al. 2005), whereas observations show many of the BSS binaries in clusters to exist much farther out (Geller et al. 2008; A. M. Geller et al. 2009, in preparation).

In the binary merger scenario for BSS formation, close binaries with periods shorter than 5–6 days evolve into mass transfer configuration or merger in less than 10 Gyr, thus producing a rejuvenated star (Andronov et al. 2006). As we point out in this work theoretical studies and observations suggest that most such close binaries form as the inner binaries in triple systems (Kiseleva et al. 1998; Eggleton & Kiseleva-Eggleton 2006; Tokovinin et al. 2006; Fabrycky & Tremaine 2007). A straightforward conclusion is that BSSs formed in close binaries are most likely to be (or to have been) members of triple systems. Such a scenario has strong implications on the properties of BSSs, their multiplicity and their orbital parameters. Here we raise this basic conclusion and follow its implications. We suggest a third mechanism for the origin of BSSs in which the progenitors of blue stragglers are formed in primordial (and also in dynamically formed) hierarchical triple stars. The inner binary in such triples can be rapidly driven into close or even contact configurations, due to the combined effects of Kozai cycles and tidal friction (KCTF mechanism: Kiseleva et al. 1998; Eggleton & Kiseleva-Eggleton 2001; Fabrycky & Tremaine 2007), as we discuss below. Such close binaries could then evolve through mass transfer or merger and produce BSSs. We show that such a scenario could explain and predict the characteristics of the BSS population in clusters, and could naturally explain the large fraction of long-period binary BSSs, their unique period–eccentricity distribution, and their location in the color–magnitude diagram, whereas previously proposed mechanisms cannot. This mechanism has some additional predictions that

³ Michelson Fellow.

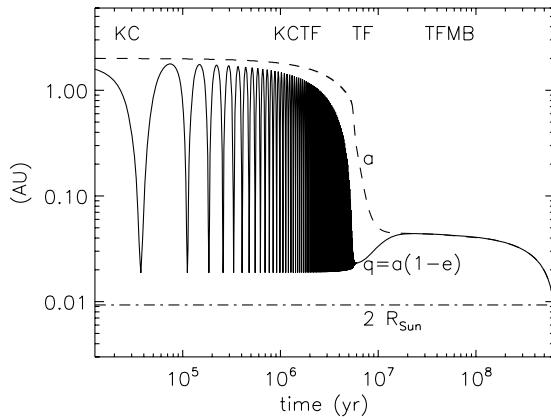


Figure 1. Merger of the two stars of an inner binary, accomplished by a combination of Kozai cycles (KC), tidal friction (TF), and magnetic braking (MB).

could discriminate it from other models for BSSs formation: (1) BSSs could have long-period *main-sequence* binary companions, (2) the spin axes of such BSSs are likely to be misaligned in a specific way from the orbital axes of the binary orbits, and (3) they may exist in regions where collisions between stars are unlikely; additional implications are discussed below. Such predictions differ from those of the previously suggested mechanisms for BSSs formation and could serve to further support and confirm the novel model suggested here.

We note that although triples have been suggested before to play a role in BSSs formation, they were not considered to have a major contribution to the BSSs population (Leonard 1996; Ivanova 2008), and the role of primordial triples has not been discussed. Here we study the triple origin scenario for BSSs and its general implications in detail. We show that current observations strongly support this model and confirm its predictions where other models fail.

In this paper, we begin with an overview of the dynamics of Kozai cycles and tidal friction in triples (Section 2). Then we compare the timescales for the KCTF mechanism and for binary disruption in different environments (Section 3) and describe the theoretical and observational implications of this formation mechanism for various environments (Section 4). We then summarize in Section 5.

2. TRIPLE DYNAMICS, KOZAI CYCLES, AND TIDAL FRICTION

To be stable for many orbital periods, triple systems usually require a hierarchical configuration in which two stars orbit each other in a relatively tight “inner binary,” and the third star and the inner binary orbit their common center of mass as a wider “outer binary.” Although such triples do not disrupt, their orbits may change shape and orientation on timescales much longer than the dynamical time. A particularly important change was discovered by Kozai (1962), who studied the orbital changes of asteroids due to the weak interactions with Jupiter (where the asteroid–Sun system serves as an inner binary in the Sun–Jupiter–asteroid triple). He found that if the asteroid’s initial inclination relative to Jupiter’s orbit is high enough, secular torques will cause its eccentricity and inclination to fluctuate out of phase with one another: these are called “Kozai oscillations.” Lidov (1962) independently studied a similar process effecting the motion of artificial satellites of the Earth as they are perturbed by the Sun and Moon, and he noted the possibility of collision

between a satellite and the Earth if the satellite’s eccentricity becomes large enough.

Collisions were also prominent in the first application of these dynamical concepts to triple stars. Harrington (1968) noted that large initial inclination ($i_c \lesssim i \lesssim 180^\circ - i_c$, for a “Kozai critical angle” of $i_c \approx 40^\circ$) leads to large eccentricities, which could cause a tidal interaction, mass loss, or even collision of the members of the inner binary. Thus, Harrington reasoned that a triple star system with an inner binary mutually perpendicular to the outer binary should not exist for many secular timescales. However, as was noted by Mazeh & Shaham (1979), the inner binary stars coming close to one another will not merge immediately; instead, the tidal dissipation between them shortens the semimajor axis of the inner binary during these eccentricity cycles. They suggested that such inner binaries could therefore attain a very close configuration, in which mass transfer and accretion could occur, possibly forming cataclysmic variables or binary X-ray sources. Eggleton & Kiseleva-Eggleton (2006) discussed binary stellar evolution, including mergers, following KCTF. Recently, Ivanova (2008) discussed the possibility of forming BSSs in dynamically formed triples in dense clusters, showing that such newly formed triples may explain as much as 10% of the BSSs in such clusters.

The equations of motion from the equilibrium tide model, with arbitrary eccentricity of a binary system and arbitrary spin obliquities of its components, were coupled to triple star dynamics by Eggleton et al. (1998). This analysis led to further fruitful studies (Kiseleva et al. 1998; Eggleton & Kiseleva-Eggleton 2001), suggesting that a large percentage of close binaries may have become close through KCTF. Several observational studies verified that close binaries very often have tertiary components (Tokovinin 2004; Pribulla & Rucinski 2006; D’Angelo et al. 2006; Rucinski et al. 2007), showing a strong correlation between the binary period and the existence of a third companion (Tokovinin et al. 2006). In fact it was found that nearly all ($\sim 96\%$) closest binaries ($P < 3$ days) have distant tertiary components (Tokovinin et al. 2006). Recently, Fabrycky & Tremaine (2007) used the equations of Eggleton et al. (1998) to verify that the observational results of Tokovinin et al. (2006) are consistent with KCTF acting on a population of triples. They found that the population of close binaries could be explained through evolution in triples, even if no such primordial binaries (with $P < 6$ days) exist. They also noticed that although eccentricity will have damped during the tightening of the close binary, the mutual inclination between inner and outer binaries should very often finish at either $i \approx 40^\circ$ or $i \approx 140^\circ$.

The connection to BSS comes when the inner binary merges to become a single, more massive star. We put the whole scenario together in Figure 1, assuming the mechanism for close binary merger is angular momentum loss through magnetized stellar winds. The initial system is an inner binary of two solar mass stars, at low eccentricity and $a = 2$ AU, orbited by a $0.5 M_\odot$ star on a circular orbit at 50 AU with a mutual inclination of 84° . On short timescales, the eccentricity of the inner binary fluctuates (Kozai cycles; KC). On millions of year timescales, tidal friction seals in a large eccentricity (KCTF), then damps the binary at constant orbital angular momentum (TF). Lastly, on a timescale of ~ 1 Gyr, magnetic braking (MB) of the stellar spins drains the orbital angular momentum because the spins stay tidally locked, causing the binary to come into contact. After a contact evolutionary phase (Andronov et al. 2006), the binary would merge to form a BSS accompanied by a main-sequence star in a very wide orbit. The contact phase may be rapid for low-mass

ratio binaries ($q \leq 0.6$), but could extend to a few 10^8 – 10^9 yr for binaries with higher mass ratios, before the final merger and the formation of a BSS (Nelson & Eggleton 2001).

In this figure, we have used the equations and parameters for KCTF found in Fabrycky & Tremaine (2007) and the magnetic braking prescription of Eggleton (2006, Section 4.4), in which angular momentum is extracted from the spin Ω_i of each star $i = 1, 2$ at a rate

$$\frac{d\Omega_i}{dt} = -|\dot{M}_i| \left(\frac{2}{3} R_i^2 + R_{A,i}^2 \right) \Omega_i, \quad (1)$$

where $\dot{M}_i = 10^{-12} M_\odot \text{ yr}^{-1}$ are the mass-loss rates from each component, $R_i = R_\odot$ are the stellar radii, and $R_{A,i} = 10 R_\odot$ are the Alfvén radii. This expression corresponds to a saturated magnetic field (Andronov et al. 2006), which is valid for quick rotation. In reality, the stars lose a small amount of mass which directly carries away a small amount of *orbital* angular momentum, but we have not explicitly computed those two effects.

3. TRIPLE-FORMED BLUE STRAGGLERS INTERACTING WITH CLUSTER MEMBERS

Before discussing the implications of the triple BSS progenitor model and its predictions for the BSSs properties, we need to insure that such a scenario is viable for OCs or GCs where the triple’s evolution could be affected by encounters with other stars. One should also note that close binaries may also be formed through tidal capture encounters in the densest regions of GCs, i.e., in some cases they may not be formed from triples.

The studies of KCTF evolution of triples have usually dealt with isolated triples. Triples evolving in clusters may be influenced by encounters with other stars in the cluster (Aarseth & Mardling 2001; Ivanova et al. 2008). Several scenarios are then possible: (1) an encounter destroys the triple before an inner close binary forms; (2) an encounter occurs before an inner close binary forms, but only perturbs the triple and does not destroy it; (3) KCTF evolution produces an inner close binary before an encounter occurs, and then an encounter destroys the outer binary of the triple, leaving a close binary; (4) KCTF evolution produces an inner close binary before an encounter occurs, and then either the triple evolves as if it was isolated or it is perturbed but not destroyed.

In the first scenario, the fraction of BSS progenitors is reduced relative to their fraction in a similar population of isolated triples, since in this case the destroyed triples could not form close inner binaries.

The second scenario, however, suggests an interesting possibility. In this case, perturbed triples change their orbital parameters in a chaotic way due to the encounter (see, e.g., Heggie 1975; Hut 1983; Binney & Tremaine 1987 for the behavior in binary encounters), but are not destroyed. These could be thought of as new triples. These new triples are now subjected to the same possible scenarios as the primordial triples, i.e., some of them could now form close inner binaries, while others are perturbed or destroyed beforehand.

The third scenario would produce close inner binary progenitors of BSSs. Such binaries are very hard (i.e., have orbital energy $E \ll m\sigma^2$; where σ is the velocity dispersion in the cluster, and m is the mass of the binary system; Heggie 1975), and are not likely to suffer from further perturbations, and therefore effectively evolve in isolation, and contribute to the fraction of close binaries and the fraction of BSSs in the cluster. Though

hard, these binaries did not contribute their orbital energy to the energy budget of the cluster to affect its dynamical evolution as a whole; rather, the energy was deposited as tidal heat and radiated away, as for tidally captured binaries. Binaries formed in this way are expected to be observed as close binaries or even contact binaries, without a triple companion and therefore reduce the fraction of such binaries with tertiary companions (which is close to unity for close binaries in the field; Tokovinin et al. 2006). A BSS formed in such binaries is likely to do so through coalescence and is therefore likely to be observed as a single BSS. Nevertheless, in some cases, they may be observed as very close binaries during a mass transfer epoch before coalescence. The observable predictions from such a scenario may be difficult to disentangle from the case of tidally formed binaries. However, tidally captured binaries are expected to form only in the densest regions of cluster cores, whereas the triple scenario could produce such binaries even in OCs or the outskirts of GCs, since triples may suffer encounters in these regions, but the rates of tidal captures are negligibly small.

The fourth scenario is maybe the most intriguing in terms of the observable implications. In this case, KCTF evolution produces a close inner binary in a system that survives as a triple in the cluster. The close inner binaries may form a BSS, either by angular momentum loss through magnetized winds, or by the primary evolving to its Roche lobe, prompting mass transfer and coalescence. Such systems would therefore be observable as long-period BSS binaries (or a triple if the inner binary has transferred mass but not yet coalesced), with period–eccentricity distribution similar to that of the outer binaries in triples. If the triple is later perturbed, a companion star is still predicted by the model, but the orbital configuration of the outer binary is not predictable by KCTF alone (as in Fabrycky & Tremaine 2007).

In order to estimate the importance of the different scenarios, we can compare the typical timescales of the isolated KCTF evolution and the typical timescales between encounters. In order to do so, we used the methods described in detail by Fabrycky & Tremaine (2007) to evolve a large population of triple systems in isolation. We ran a Monte Carlo simulation of the evolution of primordial triples drawn from appropriate distributions (as described in Fabrycky & Tremaine 2007, where all inner binaries were assumed to have initial periods of $P > 6$ days) and the triples were checked for stability using the criterion of Mardling & Aarseth (2001). About 40% of the selected triples failed to fulfill the condition. A total of 5×10^4 stable systems were then integrated in time up to 10 Gyr, while neglecting stellar evolution or angular momentum loss through magnetized stellar winds. In Figure 2, we show the typical timescale for the KCTF mechanism to form close inner binaries from triples of different periods. This timescale is defined as the median time close inner binaries take to become “close” (defined as $P_{\text{in}} < 6$ days, where magnetic braking may become important). The feature apparent at $P_{\text{out}} = 10^3$ – 10^4 days is a combination of (1) the assumed eccentricity distribution of outer binaries switches from a Raleigh distribution (moderate eccentricities) to a thermal distribution (generally large eccentricities) there (Duquennoy & Mayor 1991; Fabrycky & Tremaine 2007), and (2) inner binaries with companions at $P < 10^3$ days must be initially rather close to satisfy dynamical stability anyway, so they do not have far to travel before magnetic braking becomes important. Also shown are the typical encounter timescales for triples at different periods, calculated for several cases; typical conditions in GCs, OCs, GC cores, or OCs cores. The encounter timescale

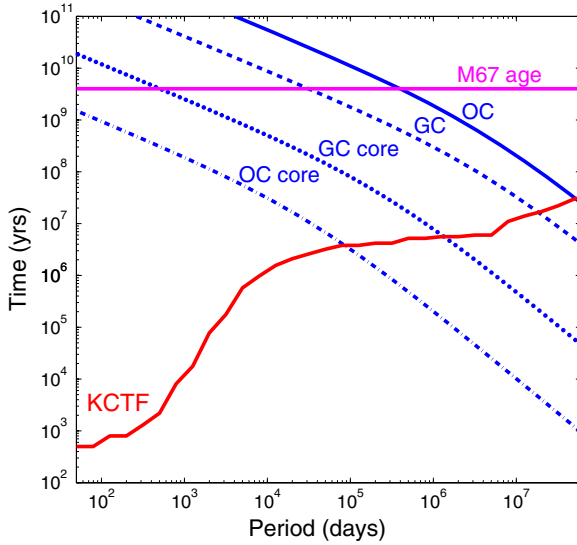


Figure 2. Timescales for encounters and Kozai cycles with tidal friction (KCTF) evolution of triples in clusters. The typical encounter time of triples of different outer periods is shown for different environments; OCs (upper solid), OC cores (dashed line), GCs (dotted line), GCs cores (dash-dotted line). The typical KCTF evolution time (see text) of triples with a range of outer period is also shown (lower solid line). The typical age of GCs and the age of the old OC M67 are denoted by vertical lines.

(A color version of this figure is available in the online journal.)

is given by (e.g., Ivanova et al. 2008)

$$t_{\text{enc}} = 8.5 \times 10^{12} \text{yr} \times P_{\text{out}}^{-4/3} M_{\text{tri}}^{-2/3} n_5^{-1} \sigma_{10}^{-1} \times \left[1 + 913 \frac{M_{\text{tri}} + \langle M \rangle}{2 P_{\text{out}}^{2/3} M_{\text{tri}}^{1/3} \sigma_{10}^2} \right]^{-1}, \quad (2)$$

where P_{out} is the outer binary's period in days, M_{tri} is the total triple mass in M_{\odot} , $\langle M \rangle$ is the mass of an average single star in M_{\odot} , σ_{10} is the velocity dispersion $\sigma_{10} = \sigma / (10 \text{ km s}^{-1})$, and n_5 is the stellar density in units of 10^5 pc^{-3} . For simplicity, we assumed all triples have equal masses of $M_{\text{tri}} = 3$ with the average mass of stars $\langle M \rangle = 1$. This timescale is for encounters between a single star and a binary (outer binary of a triple in our case). In binary–binary encounters, the cross section for the encounter is determined by the wider binary. In the following section, we compare the KCTF timescale to the encounter timescale in a variety of environments, allowing us to establish predictions for the observations.

4. IMPLICATIONS OF THE TRIPLE ORIGIN OF BSSs IN VARIOUS ENVIRONMENTS

4.1. Low-density Environments (OCs and GC Outskirts)

In relatively low-density environments such as OCs or at the outskirts of GCs, the timescales for close encounters are larger than the Hubble time (and could be much larger than the typical age of OCs). In these clusters, the triples effectively evolve in isolation. The only caveat is for very long outer period triples ($P_{\text{out}} \gtrsim 5 \times 10^4 - 5 \times 10^5$ for the conditions in OCs). Such triples can form close inner binaries in $\sim 10^7$ yr that evolve into a BSS, but the outer binary may still encounter other stars in the cluster later on and therefore change its configuration. In particular, triples for which the KCTF mechanism was inefficient may be perturbed into a different configuration which is more favorable for KCTF evolution. Since the timescale for the Kozai cycles,

when those occur (i.e., $40^\circ \lesssim i \lesssim 140^\circ$), is usually much shorter than the time between dynamical encounters, encounters are not likely to interfere with KCTF evolution and destroy potential BSSs progenitors. Encounters can, however, contribute to the formation of new BSSs progenitors. For example, if a triple is initially coplanar, it cannot evolve through KCTF evolution to form a close inner binary. However, if an encounter excites its mutual inclination sufficiently, then KCTF will rapidly operate before the next encounter. If the companion stays bound, it has a better chance of causing KCTF evolution. Therefore, encounters that do not destroy the triple tend to make KCTF evolution more likely (for a similar discussion in the context of the KCTF mechanism in dense environments, see Perets & Naoz 2008). Since tidally captured close binaries are not expected to form in these low-density regions, we can conclude that the majority of close binaries should be part of triple systems, and in particular, the majority of BSSs produced in close binaries should be part of triple systems. Such a conclusion has many implications for BSSs properties, some of which can be compared with currently available observations to test the triple scenario, while others can be checked by future observations. In the following, we list these implications and compare them with observations, when available. The triple origin of BSSs has many implications and direct falsifiable predictions.

4.1.1. BSS Fraction

The BSSs formed in the triple scenario mostly form through the merger of the inner close binary in a triple. As discussed above, it is likely that nearly all close binaries (defined as $P < 6$ days) are formed in triples. The BSS fractions we expect to be produced are therefore similar to those predicted in the close binaries merger scenario, where the only difference is that we expect the produced BSSs to have companions (see below). Andronov et al. (2006) studied the BSS fractions from mergers of close binaries. Their results for the BSS fractions, applicable also to the triple scenario, are that the expected BSS fractions are consistent with observations. Note, however, that such results require a relatively high fraction of close binaries to be assumed. Such caveat applies in general to other theoretical predictions in the literature (e.g., Hurley et al. 2005 that also assumed high fraction of close binaries). In the triple scenario such high fraction of close binaries is the result of KCTF evolution, and need not be primordial. This is important since it is not clear how can binaries with $\lesssim 6$ days period form primordially, as the protostars of the binaries components are of comparable size to the size of such short binaries (Fabrycky & Tremaine 2007). Binary distributions containing large fractions of close binaries are indeed observed in very young clusters and are therefore reasonable assumptions (see the extended discussions in Hurley et al. 2005 and Andronov et al. 2006). Note however, that the field distribution of binaries in the binaries sample of Duquennoy & Mayor (1991) shows smaller fractions of close binaries than those observed in very young clusters, which is perhaps the signature of their merger.

4.1.2. BSS Binaries Fraction

BSSs formed following the merger of the inner binary of a triple should still have a companion following the merger. Although such binaries could later be destroyed through encounters with other stars, this is likely to happen mainly for very large period binaries (soft binaries). The binary fraction of BSSs should therefore be higher than the overall binary fraction

in the environment where they are observed. Current observations of spectroscopic BSS binaries (Geller et al. 2008; A. M. Geller et al. 2009, in preparation; Latham 2007) could only detect binaries with periods of $\lesssim 3000$ days to a good level of completeness, due to the finite duration of the surveys. Longer period binaries would be observed as single BSSs and could therefore lower the *observed* BSSs binary fraction. Nevertheless, hard BSS binaries with an initial $P_{\text{out}} > 3000$ days could be affected by encounters and harden to become closer, and thus observable, binaries (since BSSs are more massive than other cluster stars, they are more likely to survive in binaries even in exchange encounters). In any case, the BSS binary fraction is expected to much exceed the general binary fraction (of all stars) in the cluster environment. Since the hardening of binaries is dependent on the age of the cluster and its density, we may expect the (detection limited) *observations* of BSS binary fraction to show higher fractions in older and/or denser environments, as long as the period detection limit is smaller than the expected final hardening period (Hills 1984). For example, for the typical conditions in NGC 188, hard binaries should harden down to periods of $\lesssim 10^4$ days (see Equation (5) in Hills 1984), this period is close to the detection limit of the binary periods, and therefore most of the BSS binaries should be observed as such, and the observed BSS binary fraction is expected to be high (> 0.5), as indeed confirmed by observations (e.g., a binary fraction $> 76\%$ for BSS binaries in NGC 188, Geller et al. 2008). M67 is a younger and less dense cluster and, therefore, the expected BSS binary fraction is expected to be lower than that in NGC 188, but still higher than the general binary fraction in the cluster.

We expect some specific correlations between BSSs fraction and cluster properties in the triple KCTF scenario. The primordial triple fraction is expected to be directly related to the binary fraction, and we should therefore expect a correlation between the binary fraction in clusters and the BSSs fraction. Since close encounters do not have important effects on the BSSs formation in the triple KCTF scenario, the BSSs fraction should be related to the unperturbed evolution of triples, similar to scenarios of unperturbed evolution of binary stars, which is consistent with recent analysis of the correlations between cluster properties and BSS fractions (Davies et al. 2004; Sollima et al. 2008; Knigge et al. 2009).

4.1.3. The Period–Eccentricity Distribution of BSS Binaries

The triple origin scenario implies that the period and eccentricity distribution of the BSS binaries should be the same as that of the outer binaries of triple systems (observed in the field) that have close inner binaries. In Figure 3(d), we show such a sample of such triples. The inner binaries in such field triples with $P_{\text{in}} < 6$ days should be directly comparable with BSSs progenitors, although we may miss some of the closest inner binaries in the field which may have already merged via magnetic winds. Systems seen as triples with close inner binaries now are likely to become BSS in binaries later. We therefore also show the sample of triples with larger inner periods ($P_{\text{in}} \lesssim 10$ days), which is also likely to be comparable, and could add to our statistics. We choose an upper cutoff of 3000 days, comparable to the detection limit of binaries in the observations of M67 and NGC 188. All the triples were chosen from the multiple stars catalog. Only low-mass triples, i.e., triples not containing stars with masses larger than $\sim 3 M_{\odot}$ were chosen. Higher mass stars would evolve off the MS on short timescales and not contribute to the BSSs in older clusters such as M67 and NGC 188.

The period–eccentricity distribution of the outer binaries in the triples discussed above is in good agreement with the observed BSS binaries distribution in the OC M67 (see Figure 3(d)) and NGC 188 (full data will be available in A. M. Geller et al. 2009, in preparation). Although the triples sample is not large, one can still observe some very unique characteristics that would be expected for BSS binaries in the triple origin scenario; note that the general binary distribution in Figure 3(b) clearly shows a different behavior than that of the BSS binaries in Figure 3(a). In particular, we expect BSS binaries from the triple scenario to usually have large periods, typically with $P \gtrsim 700$ days (also true for the larger NGC 188 sample, where 12 out of 15 BSS binaries have periods longer than this cutoff A. M. Geller et al. 2009, in preparation).⁴ Such a lower cutoff for the period of the outer binaries in triples could be the result of their formation process. Closer triples may have formed with correlated angular momentum. In such a case, the relative inclination between the inner and outer binaries in the triple may be low or even close to zero, which will quench KCTF evolution. These triples could not then produce close inner binaries. Note also that the stability of the triples may also play a role in biasing against the formation of close triples (Tokovinin et al. 2006). We also note that observed BSS binaries with $P < 10$ days are more likely to be the inner binaries of triples in which the BSSs were rejuvenated through mass transfer and not through a full merger (similar to the close BSS binaries produced in Hurley et al. 2005 simulations). Since the rejuvenated BSSs have only accreted some of their companions’ mass, such close BSS binaries are likely to have lower masses (and be fainter) than the typical BSSs observed in the cluster. Even within the triple scenario, then, it is no surprise that some short-period BSS binaries do not match the $P - e$ diagram of *outer* binaries; the scenario predicts that a third, yet unseen star orbits each of these binaries.

Regarding the eccentricity distribution of BSSs produced by the triple scenario, we note that the eccentricities of outer binaries are consistent with the distributions of regular binaries in the field (Duquennoy & Mayor 1991): generally low ($\lesssim 0.4$) eccentricities for period of $P \lesssim 1000$ days and a wider distribution up to high eccentricities for periods of $P > 1000$ days (again also consistent with the larger sample in A. M. Geller et al. 2009, in preparation). For the triple to be initially dynamically stable, the periastron of the outer binary must not pass too close to the inner binary, and this constraint translates to an upper limit on the eccentricity of the outer binary (which becomes the BSS binary), although for individual systems this limit is difficult to evaluate as the orbit of the original inner binary is not known.

The unique properties of the outer binaries in triples which are consistent with the behavior of BSS binaries are difficult to reproduce by either the collisional or the binary mass transfer scenarios for BSSs formation, even when combined together with the full dynamics of the system (see Figure 3(c); high eccentricities are mainly due to exchange encounters). The observations of BSS binaries therefore serve as a good discriminator between different formation scenarios, and current observations clearly favor the triple scenario as the major formation route of BSSs.

⁴ Interestingly, higher mass triples do show outer binary periods much shorter than ~ 700 days, which suggest very different characteristics of massive versus low-mass triples (see also Geller et al. 2008, Section 3.2.1, in this respect), which may suggest a very different BSS binary period distribution in very young OCs.

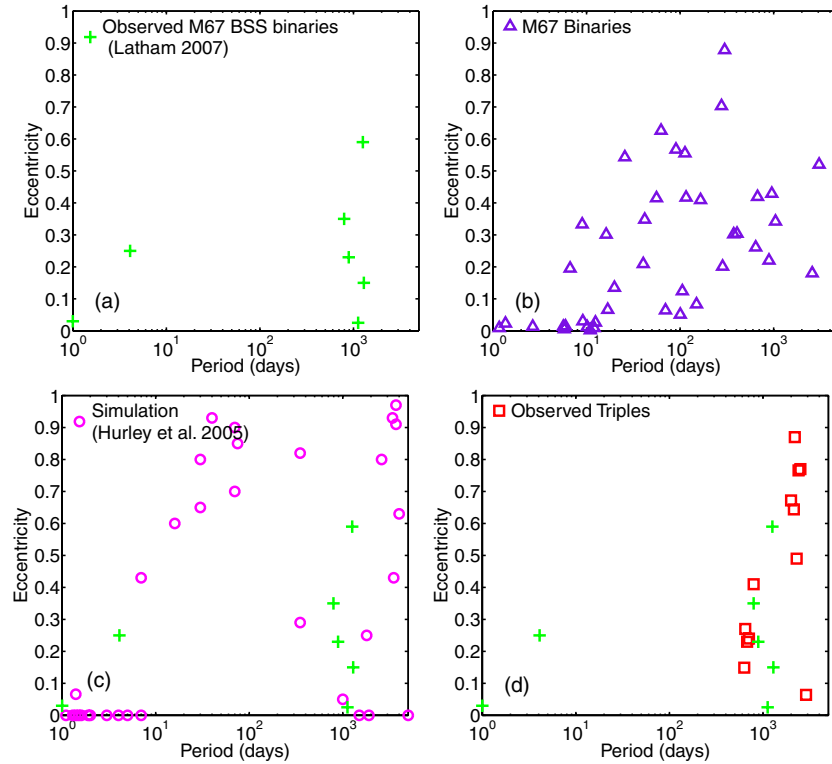


Figure 3. Period–eccentricity distribution of observed BSS binaries. (a) The period–eccentricity distribution of BSS binaries in M67 (+; Latham 2007), note that the larger sample of BSS binaries in NGC 188 (not shown; A. M. Geller 2009, in preparation) show similar behavior to that of M67 BSS binaries. (b) The period–eccentricity distribution of regular (non-BSS) binaries observed in M67 (Δ ; Latham 2007). (c) The period–eccentricity distribution of BSS binaries produced in N -body simulations of M67 (\circ ; Hurley et al. 2005) compared with the observed BSS binaries. (d) The period–eccentricity distribution of outer binaries in triple systems with close inner binaries (\square ; taken from the multiple stars catalog (Tokovinin 1997)) compared with the observed BSS binaries. Only binaries with periods shorter than 3000 days are shown (approximately the radial-velocity detection limit for the periods of the BSS binaries in the clusters). The good agreement between the distribution of outer binaries of triples to that of BSS binaries is evident. The comparison of BSS binaries to the other distributions (regular binaries in the same cluster or simulated BSS binaries in Hurley et al. 2005 simulation) is poor.

(A color version of this figure is available in the online journal.)

4.1.4. The Companions of Blue Straggler

The binary companions of long-period BSSs could be MS stars in the triple scenario (see also Eggleton & Kisseleva-Eggleton 2006, 2008 for a related discussion, and possible observations of such cases), which could not be the case for long-period BSS binaries produced following the post MS evolution of their companion, that are expected to be white dwarfs (WDs) at this stage. Another interesting discrimination method in this respect might be the comparison to CH stars found in clusters (which have low eccentricities and long periods, consistent with post-MS evolution in binaries; e.g., McClure 1997). If the triple KCTF scenario is the dominant mechanism for BSSs formation, one would expect very different distribution of CH binary stars and BSSs binaries, but very similar distribution if the mass transfer scenario is the dominant mechanism, and the former is apparently the case.

Since higher multiplicity systems are abundant (e.g., quadruples are 1/3 as abundant as triples), one may find a similar fraction of the BSSs binaries to be in triple (or higher multiplicity) systems. In particular, two binaries in a double–double quadruple system (see, e.g., the doubly eclipsing light curves of Pilecki & Szczygiel 2007) could produce a long-period binary system containing two BSSs. This could happen if both inner binaries merged. Similarly a triple (or quadruple) system containing two BSSs could form in this way if one (or both) of the inner binaries transferred mass, but has not merged, yielding

BSSs in the inner binaries. We therefore expect multiple systems containing more than one BSS to be observed.⁵

4.1.5. The Masses of Blue Stragglers and Their Location in Color–Magnitude Diagrams

Mass transfer in long-period binaries ($P > 700$ days, such as the BSS binaries observed) is highly inefficient. The total mass transferred from the post-MS companion to the formed BSS is likely to be small ($< 0.3 M_{\odot}$; and typically even lower) in this case, producing BSSs with masses not much larger than the turnoff mass of the cluster (i.e., $M_{\text{BSS}} \lesssim M_{\text{turnoff}} + 0.3 M_{\odot}$). The triple scenario can produce a much more massive BSS, as it is the sum of the inner components of the triple ($M_{\text{BSS}} \lesssim 2M_{\text{turnoff}}$). Such a higher mass would therefore discriminate them from those formed through mass transfer. The latter binaries are expected to be composed of a low-mass (fainter) BSS with a WD companion at an intermediate period of a few hundred days as observed for field BSS binaries (see Preston & Sneden 2000 and Section 4.3.1). Such BSSs would be located close to the turnoff mass in the color–magnitude diagram of a given

⁵ Interestingly, a triple containing two BSSs, one with a close companion, is observed in M67 (van den Berg et al. 2001; Sandquist et al. 2003). Such system could be formed, in principle, through the quadruple evolution we discuss. However, the large masses of s1082 components inferred from the orbital solution (Sandquist et al. 2003; but note the discrepancy with the position in the color–magnitude diagram) would require such system to be much younger (age of 1–1.5 Gyr) than the age of M67 (4 Gyr).

cluster, whereas the BSSs from the triple scenario can be distributed much further, typically far from the turnoff point of the cluster. Note that most BSSs in both NGC 188 and M67 are far from the turnoff point in the color–magnitude diagrams of the clusters (Geller et al. 2008; Liu et al. 2008), consistent with the predictions of the triples scenario and at odds with the binary mass transfer origin.

In case a close BSS binary did not fully merge, i.e., a close companion could still be detected, the BSS product should be less massive than the product of a full merger, as mentioned before, and would be observed closer to the turnoff point of the cluster than a merged BSS. The binary companion of such BSSs is likely to be an evolved star, and the system could be a close or even contact binary (possibly an Algol-like system, e.g., Jeon et al. 2006; Kaluzny et al. 2007). The frequency of such BSS Algols and other close BSS binaries is still unknown, but is likely to be small (Tian et al. 2006). In addition, one should then expect to find a triple companion, as is observed in close binary systems in the field (see Sepinsky et al. 2000 for possible observation of such systems).

In some cases, the companion of the KCTF-formed BSS may evolve off the MS during the lifetime of the BSS, in which case the BSS may accrete some of its mass, and become a more massive BSS, possibly even extending beyond twice the turnoff mass of the cluster. This could possibly explain the existence of some overmassive BSSs observed in clusters. In such cases, we might expect the binary companion to be a WD, probably on a rather circular orbit.

4.1.6. Spin–Orbit Correlation in BSS Binaries

In their theoretical analysis, Fabrycky & Tremaine (2007) found that the distribution of the relative inclination between the inner and outer binary orbits of KCTF triples should be in the range 30° – 150° , with peaks at 40° and 140° . This distribution is therefore expected for BSS triples with nonfully merged inner close binaries. If the inner binaries did merge, it is likely that the angular momentum of the premerged inner binary would leave its signature on the spin of the merged BSS. It is therefore possible that the typical relative inclination distribution found by Fabrycky & Tremaine could still be detectable in relative inclination between the *spin* of the BSS and the binary orbit (i.e., the *obliquity* of the BSS), which is observationally accessible (although currently only through an overall statistical analysis; e.g., Hale 1994).

4.1.7. Radial Distribution of BSSs in Clusters

Since our triple scenario suggests the same progenitors for BSSs and close binaries, we expect the radial distribution (from the cluster center) of BSSs in clusters to be similar to that of close binaries. This prediction may seem natural also in the scenario of BSS production from primordial close binaries not evolved in triples; however, there are few differences between the two predictions. In principle, triple systems are likely to be more massive than binary systems, and therefore be somewhat more mass segregated in clusters, and possibly have different formation efficiency in different parts of a cluster, than that of binaries. These could possibly make a priori differences in the radial distribution of BSSs compared with regular binaries, although it is not clear whether enough statistics exist for making such a signature significant. In addition, in the triple scenario, we would also expect BSS binaries with long periods (i.e., with the inner binaries fully merged, see Section 4.1.3) to have a similar radial distribution to that of regular (non-BSS) close

binaries in the cluster. If short- and long-period binaries have different radial distributions, the BSSs distribution should also reflect this.

Possible differences in the radial distribution may also serve as good discriminators between the triple scenario and the combined effects of all other suggested scenarios such as studied in *N*-body simulations (Hurley et al. 2005), since the latter suggest that BSSs and especially BSS binaries form only in the inner regions of the cluster, whereas the triple scenario could also form BSSs and BSS binaries in the outskirts of clusters⁶.

4.1.8. A General Relation Between BSSs and Close Binaries

A more general prediction of the triple KCTF scenario is the close relation between close binaries and the BSSs population. This relation suggests that the predictions and implications described in the previous points regarding BSSs should be applicable also to the general population of close binaries in clusters (e.g., eclipsing binaries, contact binaries W UMa binaries, etc.) which may also be expected to have third companions in many cases. We note however that some close binaries populations such as X-ray binaries and cataclysmic variables were likely to form in a different route. In such populations, the close binaries form only after the main-sequence evolution of the compact object progenitor, and the binary separation must have been large during this time (e.g., Ritter 2008 and references therein), i.e., excluding the possibility of KCTF evolution in which the binaries must have a very small pericenter distance during their evolution.

4.2. High-density Environments (GCs Cores)

As can be seen in Figure 2, the timescales for close encounters with triples are larger than the typical KCTF time even in the dense environments of GCs, and therefore close binaries could form through KCTF even in such environments. Therefore, the primordial triples (and dynamically formed triples; see Ivanova 2008; Ivanova et al. 2008; Trenti et al. 2008) should be taken into account when studying BSSs formation scenarios in GCs. Nevertheless, given the high encounter rates in GCs, even close KCTF-formed binaries may be involved in close encounters which could destroy them, change their configuration or cause collisions, and possibly forming BSSs. The outer binaries in such triples are even more likely to be involved in several encounters at some stage during the GC evolution, which may even disrupt the triple, if the outer binary's periastron sinks too close to the inner binary (see, e.g., Heggie 1975; Hills 1984; Aarseth 2004). Given that the BSSs that do form would have a long-period binary companion, they are most likely to be involved in many encounters, following which they are still expected to be in relatively wide binaries (for the hard triples), even in the case of an exchange. According to Trenti et al. (2008), $\sim 1\%$ of binaries have tertiary companions at any given time by dynamical formation, but this population continually evolves, so up to $\sim 10\%$ of binaries have a chance to evolve through KCTF. The complex dynamics of high-density environments (see, e.g., de La Fuente Marcos et al. 1997; Aarseth 2004)

⁶ Note that observation of a bimodal radial distribution of close binaries in a cluster would be highly interesting, since such a distribution is usually thought to be quite unique for BSSs. Following this prediction, we searched the literature for any evidence of such bimodal radial distribution of close binaries in clusters, and indeed found two examples for such a distribution in the clusters ω Centauri and Tuc 47 (Weldrake et al. 2004, 2007, this is by no means a complete list, and many others may exist). The analysis of this phenomena is, however, beyond the scope of this paper and will be discussed elsewhere.

and the need to include stellar evolution in old system such as GCs make it difficult to make clear predictions for the BSSs population without more elaborate dynamical analysis and/or N -body simulations; it is beyond the scope of this work.

In addition, given the old ages of GCs, BSSs formed from primordial triples in the triple scenario may already evolve off the MS in these clusters (see also the following section), and possibly only the dynamically formed triples could then directly form BSSs at later stages of the cluster evolution (see also Ivanova 2008; Ivanova et al. 2008). In this case, BSS binaries observed in GCs would have a different distribution than that of BSS binaries in lower density environments, with likely more eccentric and shorter period orbits.

4.3. Halo Environment

Now we discuss BSS formation, including the triple scenario, within the old populations of the halo of the Milky Way and of early-type galaxies, which have properties similar to old OCs and the outskirts of GCs.

4.3.1. Field BSSs

In the galactic halo, the stellar population is expected to be very old, so apparently younger stars are conspicuously blue; these are called Field BSSs (Preston & Sneden 2000; Carney et al. 2001, 2005). Such a noncluster stellar population is expected to evolve in isolation, and therefore field BSSs are not expected to form through collisions. Field BSSs could be explained by the binary stellar evolution of isolated binaries with periods of at most a few thousands days which evolve through mass transfer to form binaries with typical periods of a few hundred days (100–800; McCrea 1964). In such binaries, one of the components would evolve and expand, leading to a mass transfer to its companion which could become a BSS. Such stellar evolution would usually lead to circularization of the binary orbit and its shrinkage and leave a WD companion to the BSS. The field BSSs identified by Preston & Sneden (2000) and Carney et al. (2001) are single-lined spectroscopic binaries, so the companions are consistent with being WDs, and the orbital period distribution is consistent with that expected from mass transfer in evolved binaries. One may ask whether triple systems could also contribute to the formation of field BSSs.

When it operates, the KCTF mechanism leads to a rapid formation ($\lesssim 10^7$ yr) of a close inner binary. Stellar evolution of such a close binary is likely followed by its merger.⁷ A merger product is usually much more massive than a star which accreted some mass from its companion (see Section 4.1.5). Therefore, such a rejuvenated star is very likely to evolve off the MS relatively early, and not be currently observed as a field BSS. When evolved such a star may transfer mass to its long-period companion (originally the star in the outer period of the triple), forming a low-mass BSS (i.e., at $M_{\text{BSS}} \lesssim M_{\text{turnoff}} + 0.3 M_{\odot}$). Such a scenario may still show a weak signature on the BSS binary.

Since the outer period of triples is usually larger than ~ 700 days (see Section 4.1.3), field BSS binaries from triples may have larger periods, on average (although these may be

somewhat shortened during the mass transfer evolution). The more massive BSSs may also produce more massive WDs, on average. Combined together we might observe wider period field BSS binaries to have more massive WD companions (see O'Brien et al. 2001 for a related scenario). The most massive (and luminous) field BSSs could be the product of a full merger of the inner binary in triples with very long KCTF timescales. Observation of a field BSS binary with a main-sequence companion could serve as a strong evidence for a triple origin in this noncollisional environment, where an exchange scenario for the MS star origin is not possible. Such a BSS is likely to be one of the brightest, most massive field BSSs. Nevertheless, the signature of triple-formed field BSSs is not strong, and it is possible that in most cases triple-formed BSS binaries would be indistinguishable from the other field BSS binaries produced in binaries. We conclude that triples may contribute to the formation of field BSS binaries, but their contribution is not likely to be dominant, and would leave only a weak signature, unless very massive BSSs are observed ($\geq 2 M_{\odot}$).

4.3.2. Bright Planetary Nebulae

Ciardullo et al. (2005) suggested that the progenitors of bright planetary nebulae (PNe) observed in old stellar population are BSSs formed in close binaries, since the progenitor mass of these bright PNe is thought to be larger than $2 M_{\odot}$. Such high mass is much beyond the turnoff mass of stars in old stellar populations, such as in early-type galaxies and in galactic halos. Moreover, high-mass BSSs are likely to form only through mergers or strong mass transfer (see Section 4.1.5) which are only produced in close binaries or in collisions in dense environments. Since in the triple origin for BSSs we suggest such close binaries and their merged BSS product are formed in triples, a straightforward conclusion is that the progenitors of bright PNe are also triple stars. We therefore predict that such PNe may still have a long-period binary companion after the inner binary in the triple produced the BSS which evolved to become a PN. The further evolution of the BSS to a PN could affect the binary orbit, possibly circularizing it, due to low-mass transfer from the evolved BSS to its companion. Likewise, the presence of the binary companion could affect the morphology of the nebula. The details of such evolutionary process are beyond the scope of this work.

5. SUMMARY

In this paper, we have studied the possible formation scenario of BSSs in primordial and dynamically formed triple systems and its implications for the evolution and observations of BSSs. The direct relation between triple stars and BSSs in this scenario suggests a strong connection between BSSs properties and those of triples stars. Many specific predictions for the BSSs populations are implied by this relation and described mainly in Section 4, some of which are unique predictions that can discriminate it from the two other BSSs formation scenarios: stellar collisions and mass transfer in or merger of binaries. Possibly the strongest signature expected from this scenario is the expected high binary fraction of long-period BSS binaries and their unique period–eccentricity distribution with its strong bias toward long-period orbits (> 700 days). This distribution is not likely to be produced by any other single scenario for BSSs formation, and not even through their combined effect as studied in N -body simulations with stellar evolution. We showed

⁷ We do caution, however, that for wide systems for which the TF timescale is too long initially, stellar evolution can play an important role in the KCTF evolution, leading to a complicated interplay of mass transfer and eccentricity driving. The analysis of such combined KCTF and stellar evolution processes, however, is beyond the scope of this work. See Iben & Tutukov (1999) for foundational considerations on this subject.

that the recent observations of the BSS binaries population in the open clusters M67 and NGC 188 (the only clusters for which we have a wealth of data on BSSs binaries) could naturally be explained by the triple scenario, where all other currently suggested scenarios for BSS formation and evolution encounter major difficulties (see Figure 3). The triple scenario is likely to play a more minor role in the formation of field BSSs and in other low density *old* stellar populations, but could be important for the production of the most massive BSSs in these environments. The brightest planetary nebulae observed could be the product of such massive field BSSs, and may therefore have long-period binary companions as expected for BSSs in this scenario. In the cores of globular clusters, the interplay between triple evolution and other dynamical effects may become more complex, and both processes are likely to play a role in the BSSs formation. However, in open clusters, the triple origin scenario is possibly the most dominant mechanism for the formation of blue stragglers and currently the only model explaining the BSS binary properties in these environments.

We thank Bob Mathieu and Aaron Geller for helpful discussions and for supplying us with their prepublished data on BSS binaries in NGC 188. We thank Scott Tremaine and the referee Peter Eggleton for helpful comments and discussions. H.B.P. is supported by ISF grant 928/06 and gratefully acknowledges support from a Michelson Fellowship, which is supported by the National Aeronautics and Space Administration and administered by the Michelson Science Center.

REFERENCES

- Aarseth, S. J. 2004, *RevMexAA Conf. Ser.*, **21**, 156
- Aarseth, S. J., & Mardling, R. A. 2001, in *ASP Conf. Ser. 229, Evolution of Binary and Multiple Star Systems*, ed. P. Podsiadlowski et al. (San Francisco, CA: ASP), 77
- Andronov, N., Pinsonneault, M. H., & Terndrup, D. M. 2006, *ApJ*, **646**, 1160
- Bailyn, C. D. 1995, *ARA&A*, **33**, 133
- Binney, J., & Tremaine, S. 1987, *Galactic Dynamics* (Princeton, NJ: Princeton Univ. Press)
- Carney, B. W., Latham, D. W., & Laird, J. B. 2005, *AJ*, **129**, 466
- Carney, B. W., Latham, D. W., Laird, J. B., Grant, C. E., & Morse, J. A. 2001, *AJ*, **122**, 3419
- Ciardullo, R., Sigurdsson, S., Feldmeier, J. J., & Jacoby, G. H. 2005, *ApJ*, **629**, 499
- D'Angelo, C., van Kerkwijk, M. H., & Rucinski, S. M. 2006, *AJ*, **132**, 650
- Davies, M. B., Piotto, G., & de Angeli, F. 2004, *MNRAS*, **349**, 129
- de La Fuente Marcos, R., et al. 1997, in *Astrophysics and Space Science Library, Visual Double Stars: Formation, Dynamics and Evolutionary Tracks*, Vol. 223, ed. J. A. Docobo, A. Elipe, & H. McAlister (Dordrecht: Kluwer), 165
- Duquennoy, A., & Mayor, M. 1991, *A&A*, **248**, 485
- Eggleton, P. 2006, *Evolutionary Processes in Binary and Multiple Stars* (Cambridge: Cambridge Univ. Press)
- Eggleton, P. P., Kiseleva, L. G., & Hut, P. 1998, *ApJ*, **499**, 853
- Eggleton, P. P., & Kiseleva-Eggleton, L. 2001, *ApJ*, **562**, 1012
- Eggleton, P. P., & Kiseleva-Eggleton, L. 2006, *Ap&SS*, **304**, 75
- Eggleton, P. P., & Kiseleva-Eggleton, L. 2008, in *Multiple Stars Across the H-R Diagram*, ed. S. Hubrig, M. Petr Gotzens, & A. Tokovinin (Berlin: Springer), 1
- Fabrycky, D., & Tremaine, S. 2007, *ApJ*, **669**, 1298
- Geller, A. M., et al. 2008, *AJ*, **135**, 2264
- Hale, A. 1994, *AJ*, **107**, 306
- Harrington, R. S. 1968, *AJ*, **73**, 190
- Heggie, D. C. 1975, *MNRAS*, **173**, 729
- Hills, J. G. 1984, *AJ*, **89**, 1811
- Hills, J. G., & Day, C. A. 1976, *Astrophys. Lett.*, **17**, 87
- Hurley, J. R., et al. 2005, *MNRAS*, **363**, 293
- Hut, P. 1983, *ApJ*, **268**, 342
- Iben, I. J., & Tutukov, A. V. 1999, *ApJ*, **511**, 324
- Ivanova, N. 2008, in *Multiple Stars Across the H-R Diagram*, ed. S. Hubrig, M. Petr-Gotzens, & A. Tokovinin (Berlin: Springer), 101
- Ivanova, N., et al. 2008, *MNRAS*, **386**, 553
- Jeon, Y.-B., Kim, S.-L., Lee, M. G., Lee, H., & Lee, J. W. 2006, *ApJ*, **636**, L129
- Kaluzny, J., Thompson, I. B., Rucinski, S. M., Pych, W., Stachowski, G., Krzeminski, W., & Burley, G. S. 2007, *AJ*, **134**, 541
- Kiseleva, L. G., Eggleton, P. P., & Mikkola, S. 1998, *MNRAS*, **300**, 292
- Knigge, C., Leigh, N., & Sills, A. 2009, *Nature*, **457**, 288
- Kozai, Y. 1962, *AJ*, **67**, 591
- Latham, D. W. 2007, *Highlights Astron.*, **14**, 444
- Leonard, P. J. T. 1996, *ApJ*, **470**, 521
- Lidov, M. L. 1962, *Planet. Space Sci.*, **9**, 719
- Liu, G. Q., Deng, L., Chávez, M., Bertone, E., Davo, A. H., & Mata-Chávez, M. D. 2008, *MNRAS*, **390**, 665
- Mardling, R. A., & Aarseth, S. J. 2001, *MNRAS*, **321**, 398
- Mazeh, T., & Shaham, J. 1979, *A&A*, **77**, 145
- McClure, R. D. 1997, *PASP*, **109**, 536
- McCrea, W. H. 1964, *MNRAS*, **128**, 147
- Nelson, C. A., & Eggleton, P. P. 2001, *ApJ*, **552**, 664
- O'Brien, M. S., Bond, H. E., & Sion, E. M. 2001, *ApJ*, **563**, 971
- Perets, H. B. 2009, *ApJ*, in press (arXiv:0802.1004)
- Perets, H. B., & Naoz, S. 2008, arXiv:0809.2095
- Pilecki, B., & Szczygiel, D. M. 2007, *Inf. Bull. Var. Stars*, 5768, 1
- Preston, G. W., & Sneden, C. 2000, *AJ*, **120**, 1014
- Pribulla, T., & Rucinski, S. M. 2006, *AJ*, **131**, 2986
- Ritter, H. 2008, arXiv:0809.1800
- Rucinski, S. M., Pribulla, T., & van Kerkwijk, M. H. 2007, *AJ*, **134**, 2353
- Sandquist, E. L., Latham, D. W., Shetrone, M. D., & Milone, A. A. E. 2003, *AJ*, **125**, 810
- Sepinsky, J. F., et al. 2000, *BAAS*, **32**, 740
- Sollima, A., et al. 2008, *A&A*, **481**, 701
- Tian, B., Deng, L., Han, Z., & Zhang, X. B. 2006, *A&A*, **455**, 247
- Tokovinin, A. 2004, in *RevMexAA Conf. Ser. 27, IAU Coll. 191, Environment and Evolution of Double and Multiple Stars*, ed. C. Allen & C. Scarfe (México, D.F.: Instituto de Astronomía), 7
- Tokovinin, A., Thomas, S., Sterzik, M., & Udry, S. 2006, *A&A*, **450**, 681
- Tokovinin, A. A. 1997, *A&AS*, **124**, 75
- Trenti, M., Ransom, S., Hut, P., & Heggie, D. C. 2008, *MNRAS*, **387**, 815
- van den Berg, M., Orosz, J., Verbunt, F., & Stassun, K. 2001, *A&A*, **375**, 375
- Weldrake, D. T. F., Sackett, P. D., & Bridges, T. J. 2007, *AJ*, **133**, 1447
- Weldrake, D. T. F., Sackett, P. D., Bridges, T. J., & Freeman, K. C. 2004, *AJ*, **128**, 736

Chapter 12

Kozai cycles, tidal friction and the dynamical evolution of binary minor planets

Perets & Naoz

ApJL, in press (2009)

KOZAI CYCLES, TIDAL FRICTION AND THE DYNAMICAL EVOLUTION OF BINARY MINOR PLANETS

HAGAI B. PERETS¹ AND SMADAR NAOZ²

Draft version May 26, 2009

Abstract

In recent years many binary minor planets (BMPs) have been discovered in the Solar system. Many models have been suggested for their formation, but these encounter difficulties explaining their observed characteristics. Here we show that secular perturbations by the Sun (Kozai mechanism) fundamentally change the evolution and the initial distribution of BMPs predicted by such models and lead to unique observational signatures. The Kozai mechanism can lead to a large periodic oscillations in the eccentricity and inclination of highly inclined BMP orbits, where we predict such effects to be observable with current accuracy within a few years (e.g. for the binary asteroid Huenna). In addition, the combined effects of the Kozai mechanism and tidal friction (KCTF) drives BMPs into short period circular orbits. We predict a specific inclination dependent distribution of the separation and eccentricity of BMPs, due to these effects, including a zone of avoidance at the highest inclinations. Specifically the Kozai evolution could explain the recently observed peculiar orbit of the Kuiper belt binary 2001 QW₃₂₂. Additionally, the KCTF process could lead to BMPs coalescence and serve as an important route for the formation of irregular shaped single minor planets with large axial tilts.

Subject headings:

1. INTRODUCTION

Stable gravitational triple systems require a hierarchical configuration, in which two objects orbit each other in a relatively tight “inner binary”, and the third object orbits the binary in a wider “outer binary”. Although such triples are stable against disruption, their orbits may change shape and orientation on time scales much longer than their orbital period. In particular, the Kozai-Lidov mechanism (Kozai 1962; Lidov 1962) predicts a secular perturbations of the inner binary orbit. So-called “Kozai oscillations” cause the eccentricity and the inclination to fluctuate. The Kozai mechanism is known to be highly important in the evolution of many triple systems (Kozai 1962; Mazeh & Shaham 1979; Harrington 1968; Kiseleva et al. 1998; Carruba et al. 2002; Nesvorný et al. 2003; Fabrycky & Tremaine 2007). It leads to a large (order unity) periodic oscillations (Kozai cycles) in the eccentricity and inclination of inner binaries with high inclinations with respect to the outer binary orbit (hereafter the relative inclination).

In recent years many binary minor planets [BMPs; both binary asteroids and binary trans-Neptunian objects (TNOs)] have been discovered in the Solar system (Richardson & Walsh 2006). BMPs can be regarded as the inner binary members of a triple system in which the sun is the perturbing companion in the outer orbit. Here we study the importance of such perturbations and show that BMPs are susceptible to Kozai oscillations, which play a major role in their evolution. The combined effects of the Kozai mechanism in addition to tidal friction, (Kozai cycles and tidal friction; KCTF (Mazeh & Shaham 1979; Kiseleva et al. 1998)) which becomes important for BMPs with high eccentricities (induced by the Kozai mechanism), change the orbital parameters of

the BMPs. These effects could then erase the observational signatures suggested by the various formation scenarios of BMPs discussed in the literature (Weidenschilling et al. 1989; Weidenschilling 2002; Merline et al. 2002; Goldreich et al. 2002; Funato et al. 2004; Richardson & Walsh 2006; Lee et al. 2007). replacing them with unique and different signatures, that are consistent with current observations.

2. KOZAI OSCILLATIONS

Large Kozai oscillations (see fig. 1; for which we used the Kozai and KCTF evolution code (Fabrycky & Tremaine 2007)) take place when the relative inclination between the inner binary orbit and the outer binary orbit of a triple system is large for initially circular binaries, i.e. $40^\circ \lesssim i \lesssim 140^\circ$ (hereafter Kozai inclinations), with somewhat wider inclination range for initially eccentric BMPs. Systems with Kozai inclinations keep their semi-major axis (SMA) separation, but could be driven into periodic changes of the other orbital parameters of the inner binary. The eccentricity and inclination change in a specific range which depends on these orbital parameters. The maximal eccentricity induced by the Kozai mechanism (assuming small initial eccentricity) is given by

$$e_{max} = \sqrt{1 - (5/3)\cos^2(i_0)}, \quad (1)$$

where e_0 and i_0 are the initial eccentricity and inclination, respectively (the more general expressions for the maximal eccentricity and minimal eccentricity (and inclinations) for arbitrary initial parameters have somewhat more lengthy analytic formulation Perets & Naoz 2009). The typical timescale for Kozai oscillations between the limiting values is given by (Kiseleva et al. 1998)

$$P_K = \frac{2P_{out}^2}{3\pi P_{in}} \frac{m_1 + m_2 + m_3}{m_3} (1 - e_{out}^2)^{3/2}, \quad (2)$$

where P_{out} and P_{in} are the orbital periods of the outer and inner binaries in the triple system, respectively;

Electronic address: hagai.perets@weizmann.ac.il

¹ Weizmann Institute of Science, POB 26, Rehovot 76100, Israel

² Raymond and Beverly Sackler School of Physics and Astronomy, Tel Aviv University, Tel Aviv 69978, Israel

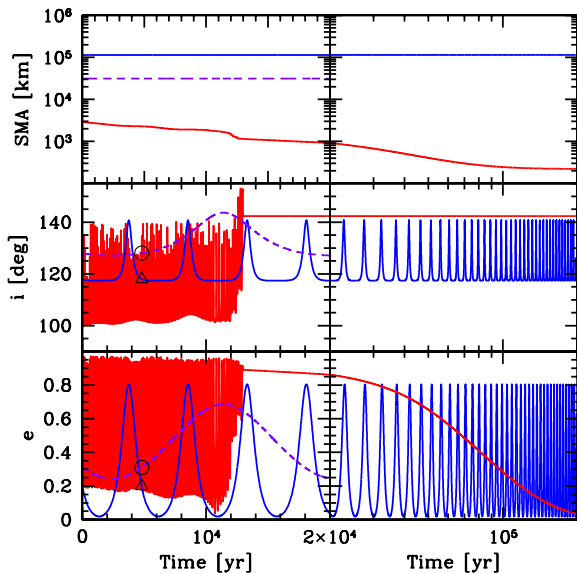


FIG. 1.— Typical Kozai evolution of three BMPs (note logarithmic time scale on the right). Bold blue curves show the Kozai cycles of the binary TNO similar to 2001 QW₃₂₂ [triangle marks its currently observed (Petit et al. 2008) orbital parameters]. The evolution of 2001 QW₃₂₂ is not affected by tidal friction, and probes a wide range of inclinations and eccentricities. The evolution of the TNO binary 2001 QT₂₉₇ is also shown in dashed line [circle marks its currently observed orbital parameters]. Red curves show the evolution of a hypothetical main belt binary asteroid affected both by the Kozai mechanism and by tidal friction. The BMP periodically evolves into high eccentricities and at later times circularize due to tidal forces and migrates to small SMA separation. Note that the final inclination is typically close to 140° at which eccentricities during the Kozai cycle are highest and tidal friction is therefore more efficient. The small inclination oscillations observed at the final stages are due to tidal torques which become important at this stage (Fabrycky & Tremaine 2007). These could have even larger amplitudes if the spin rate of the BMP members is larger.

$m_1 + m_2$ and m_3 are the masses of the inner binary and the third outer member of the triple (the sun in the case of the BMP-sun triple system considered here), respectively; and e_{out} is the eccentricity of the outer binary.

Many of the BMPs observed in the Solar system are known to have large relative inclinations, making them susceptible to Kozai oscillations (see Perets & Naoz 2009 for an extended discussion of the observed inclinations of BMPs). For such systems the timescale for periodic changes in the absence of any additional forces (such as tidal friction or pericenter precession for non-spherical objects), could be as short as a few thousand years (typical for main belt binary asteroids) and up to 10^7 years for some binary TNOs; much shorter than the lifetime of these systems (see 1 for example). The change in eccentricities and inclinations during these timescales could be as large as $\Delta e = e_{max} - e_{min} \simeq 0.99 - 0.05 = 0.94$ and $\Delta i = i_{max} - i_{min} \simeq 86 - 39 = 47^\circ$ for the known systems (e.g. for the binary TNO 2000 OJ67; based upon the orbital parameters determined by Grundy et al. 2009). Note that the short, ~ 46 yrs, Kozai timescale for the BMP Huenna³ may enable a direct observation of the

³ The inclination of Huenna is outside the Kozai region for initially circular binaries, however eccentric binaries are affected by the Kozai mechanism even at lower inclinations.

Kozai effect within the next few years, even with current observations accuracy (we find $e_{max} \simeq 0.23$ and $e_{min} \simeq 0.15$ for Huenna; i.e. eccentricity change rate of $\sim 3.4 \times 10^{-3} \text{ yr}^{-1}$, where current error bars on the eccentricity are of $\pm 6 \times 10^{-3}$; Marchis et al. 2008).

3. KOZAI CYCLES AND TIDAL FRICTION

The SMA separation of BMPs could evolve due to the Kozai mechanism, when tidal friction effects are accounted for. Such effects become important when the pericenter distance between the BMP members becomes small enough during the Kozai cycles. Orbital energy is then dissipated in each pericenter approach by the tidal friction, leading to the evolution of the BMP to smaller SMA separations and more circular orbits (hereafter Kozai migration or KCTF mechanism (Mazeh & Shaham 1979; Kiseleva et al. 1998); see fig. 1). Moreover, such evolution could even lead to the formation of contact binaries (such as currently observed; Sheppard & Jewitt (2004)) or even to mass exchange or coalescence of the BMP members into a single (probably irregularly shaped) minor planet if the separation becomes small enough.

In fig. 2 we show the regions in orbital phase space where the Kozai and KCTF processes become important, where only the dependence on SMAs and inclinations is shown (for simplicity, initial eccentricities of BMPs, just following their formation, are assumed to be negligible; higher initial eccentricities could further strengthen the KCTF effects, making the Kozai and KCTF phase space regions somewhat larger). BMPs in the KCTF region, i.e. BMPs with large inclinations and small SMAs such that during their Kozai evolution their pericenter distance becomes small enough (when their eccentricities become large) for tidal friction to dominate their further evolution (see fig. 2) are expected to have small SMA separations and circularized orbits (i.e. low eccentricities). Therefore the KCTF regime is expected to have a zone of avoidance in its upper region (large SMA separations) from which BMPs are expected to migrate into its lower region (small separations), which is expected to be overpopulated with close BMPs (possibly even contact or coalesced configurations), with low eccentricities. Moreover, the distribution of the inclinations for migrating BMPs in the KCTF could be double peaked, increasing towards 40° and 140° (Fabrycky & Tremaine 2007), where the pericenter distance is smallest during the Kozai cycle, and therefore tidal friction becomes more dominant and may lock the system from further evolution of the inclination at the final stages of the KCTF evolution (see fig. 1 for such behavior). Note, however, that for fast spinning member of BMPs and/or low mass ratio BMPs, inclinations may continue to fluctuate even at late times of the KCTF evolution, and the inclinations distribution could be strongly affected. In addition, the Kozai mechanism may still excite small eccentricities in BMPs in the KCTF regime. Such excitations could be the source of small but non-zero eccentricities of BMPs in the KCTF regime, such as observed for the binary asteroid Emma and the Pluto-Charon system in the Kuiper belt (Stern et al. 2003; Marchis et al. 2008). Such excitations are likely to be higher for BMPs with low mass ratios.

We note that the (usually unknown) asphericity of

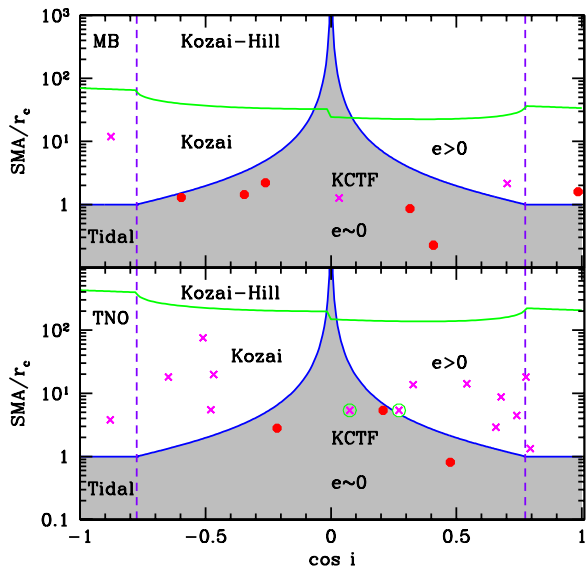


FIG. 2.— The inclination and semi-major axis phase space at which the Kozai, KCTF and Kozai-Hill mechanisms have a dominant role for two observed BMP populations; the binary TNOs (bottom) and the main belt binary asteroids (top). Observed eccentric (\times) and circular (filled circles) BMP orbits are shown. BMPs with two inclination solutions, in which different solutions fall in different regimes are marked by green open circles [otherwise only one solution is shown, corresponding to better χ^2 score; currently observed BMPs will be discussed extensively in a forthcoming paper; Naoz, Perets & Ragozzine, in prep.; full references for the data can also be found on the web (<http://arxiv.org/abs/0809.2095v1>)]. BMPs outside the Kozai region (typically $i \lesssim 40^\circ$ and $i \gtrsim 140^\circ$) are negligibly affected by the Kozai evolution. BMPs in the Kozai region can fundamentally change their inclinations and eccentricities and typically have large eccentricities (> 0.05). BMPs in the shaded region are affected by the Kozai mechanism and/or tidal friction and are expected to have relatively small SMA separations and circularized orbits (< 0.05). Stable BMPs should not exist in the Kozai-Hill region (above the upper arc). The SMA is given in units of the KCTF region baseline, r_c at which BMPs are expected to be circularized.

the binaries components may also affect the BMPs orbital evolution (Chauvineau et al. 1993; Scheeres 1994; Ragozzine & Brown 2009). In addition, minor planets in higher multiplicities (e.g. the triple TNO systems of 2003 EL61) are subjected to mutual forces from additional satellites, not taken into account in our description, which can substantially affect the evolution of the system (Ragozzine & Brown 2009). Such effects are beyond the scope of this paper, where we assume all systems to be binaries with spherical components.

4. KOZAI-HILL INSTABILITY

At the other end, if the apocenter distance of a BMP becomes large enough during the Kozai cycles, the tidal effects of the sun may become dominant. The binary separation then becomes closer to or even larger than the Hill radius of the system; and the BMP is disrupted (hereafter the Kozai-Hill scenario; Perets and Naoz, in preparation). Therefore the Kozai-Hill region (see fig. 2) should be depleted of BMPs. Note that the Hill radius has an inclinations dependence at all inclinations due to the changing strength of the Coriolis force which is proportional to $\cos(i)$ (Innanen 1980; Hamilton & Burns

1991). The effect of the Kozai mechanism is an additional effect which affects only the Kozai region. We use an analytic expression for the critical SMA at which a given BMP becomes unstable, which takes into account both these effects (Perets & Naoz 2009). We note that currently observed BMPs indeed have separations that are a few times smaller than the Hill radius, but this could also be related to other processes, such as disruption of the widest binaries through gravitational encounters with other minor or major planets.

5. DISCUSSION

5.1. KCTF observational signature and BMPs formations scenario

The Kozai, KCTF and Kozai-Hill processes could appreciably affect the survival of BMPs, their orbits and their orbital phase-space distribution. In fig. 2 we show typical examples of the inclination-SMA separation phase-space in which the different Kozai processes take place. The positions of all BMPs with known inclinations in this phase-space are also shown (detailed discussion of the observed inclinations of BMPs is given elsewhere Perets & Naoz 2009). BMPs in the Kozai region (excluding the KCTF region) are not susceptible to tidal friction during the Kozai cycle, since they have lower inclinations and/or semi-major axis, and therefore even at their smallest periastron distance during a Kozai cycle tidal friction is too weak to affect the BMP orbital evolution. The eccentricity and inclinations of such BMPs continuously and periodically change between the minimal and maximal Kozai eccentricity (see e.g. fig. 1) and should therefore have a wide distribution of eccentricities which would be very different from the initial conditions set by the formation mechanism of the BMPs. The initial SMA, however, will be conserved in this case, still reflecting the initial conditions.

We note that the current observations (although currently only a small sample exists) are in good agreement with our predictions. All the BMPs in the Kozai region have relatively high eccentricities (none are circular, defined here as $e < 0.05$). The zone of avoidance at the highest inclinations in the KCTF region is empty, and BMPs in the KCTF region tend to be circular and with smaller SMA separations. The large difference between binary TNOs and binary asteroids is likely to be related to different formation mechanisms (Richardson & Walsh 2006). Note that BMPs formed only at small separations at which tidal friction is important would never be subjected to the pure Kozai mechanism.

The above predictions should be of major concern when trying to constrain BMPs' formation scenarios by observations. Many formation scenarios for BMPs have been described in the literature (see refs. Richardson & Walsh (2006); Noll et al. (2008) for a review) with different predictions for the distribution of BMP SMA separations, eccentricities and inclinations (unfortunately, only few studies explored inclination distribution (Nazzario et al. 2007; Schlichting & Sari 2008); given the importance of the Kozai effect we strongly suggest to explore this in future studies). As we have shown the initial conditions as prescribed by different scenarios will be fundamentally changed by the Kozai and KCTF evolution. In order to find evidence for specific formation scenarios of BMPs, it is therefore essential to take the Kozai evo-

lution of the BMPs into account. For example, typical high eccentricity BMPs produced in some scenarios such as the expected $e > 0.8$ in the exchange scenario of Funato et al. (Funato et al. 2004), or $0.2 \lesssim e \lesssim 0.8$ in the chaos assisted capture scenario (Lee et al. 2007), could be observed with very low eccentricities, either due to the random phase in which they are observed during their Kozai cycle or due to their KCTF evolution which would have circularized their orbit (e.g. fig. 2). Recently (and after the initial presentation of this manuscript), Petit et al. (2008) have reported on the peculiar orbit of the Kuiper Belt Binary 2001 QW₃₂₂, with very large SMA but relatively small eccentricity. Such orbit is difficult to explain through previously suggested BMPs formation scenarios, since a binary with such wide SMA is likely to be produced through the exchange scenario, which would typically produce a highly eccentric binary (Funato et al. 2004). Such orbit, however, is naturally produced through the Kozai mechanism presented here. As shown in fig. 1, the orbit of a binary similar to 2001 QW₃₂₂ could evolve due to the Kozai mechanism from initially high eccentricity and small pericenter distance separation (in fact comparable to the separation of the “regular” Kuiper belt object 2001 QT₂₉₇) to have a low eccentricity and much larger pericenter distance separation, as observed today. Such a binary could therefore have been formed through a binary-single encounter, and then naturally evolve to its current state through Kozai evolution.

Similarly, typical low eccentricity BMPs, such as might be expected to be produced in the dynamical friction capture scenario (Goldreich et al. 2002), could be observed with very high eccentricities. Since these effects occur mainly for BMPs in the main Kozai region, we predict an inclination and SMA separation dependence of the eccentricity distribution of BMPs, with a transition between BMPs at the different regimes described in fig. 2. Similarly the SMA separation distribution would also be changed between the different regimes. In fact, only BMPs outside the Kozai region would preserve the eccentricity and SMA separation signature of their formation scenario (unless changes by other processes not related to the Kozai mechanism), whereas in the other regimes these distributions would be dominated by the Kozai mechanism.

In addition to these predictions, we note the importance of environmental effects when combined with Kozai evolution. In some regions of the solar system BMPs were likely to form and/or to evolve for some time in dense environments where they encountered other minor planets (as suggested or required by most BMP formation and evolutionary scenarios). In such an environment, encounters may change the orbital configuration of the binaries in quite a chaotic way (Heggie 1975) especially for the wider binaries that are more susceptible to encounters (larger cross section). The Kozai timescales (Eq. 2) could be shorter than the typical timescale between consequent encounters. In such cases a BMP entering the KCTF regime for the first time following an encounter, could rapidly migrate to smaller SMA separation, thus decreasing its chance for further encounters which could have otherwise potentially export it outside this phase space region. This KCTF region therefore produces a sink in the phase-space distribution and induces

a flow from small inclinations to high inclinations in the phase-space distribution of BMPs. We predict that the KCTF mechanism, when at work in a collisional environment, would form a KCTF-collisional signature in which the KCTF and the phase-space regions close to it (i.e. mostly the Kozai region) would be overpopulated relative to the other phase space regions (beside the zone of avoidance which should be depleted of BMPs), and a strong inclination-eccentricity correlation should exist. The distribution of observed binary TNOs is suggestive of such a signature (fig. 2). Even with this small sample, we already find that the probability for the eccentricity and inclinations ($|\cos i|$) distributions to be uncorrelated is ~ 0.001 (with correlation coefficient of 0.7; Naoz, Perets & Ragozzine, in prep.). In addition an empty region at the zone of avoidance could be seen in the figure. We predict that more data from future observations will further increase the significance of these signatures.

5.2. Binary spin-orbit correlation and irregularly shaped minor planets

Since KCTF evolution drives BMPs into close configurations, they may become close enough as to evolve into contact configuration or even collisions or mergers (similar suggestion was discussed in the context of merger of inner binary in triple stellar systems due to KCTF; Perets & Fabrycky 2009). These contact/collision/merger products may still show a signature of their KCTF formation scenario producing a relative spin-orbit inclination which is likely to be limited to Kozai inclinations. This Kozai-induced contact/merger scenario could contribute to the formation of contact binaries population (e.g. Sheppard & Jewitt (2004)) and to the existence of large single minor planets with irregular prolonged shapes (e.g. (Hartmann & Cruikshank 1980; Romanishin et al. 2001)). Such scenario would suggest that the prolonged axis of such objects is more likely to be aligned perpendicular to their spin axis (where the latter is expected to have the same biased spin-orbit inclination distribution as the Kozai contact binaries). We note that rotational disruption and direct collisions could also produce irregularly shaped minor planets, but are not expected to produce a bias towards high latitude inclinations. The YORP effect could also form a bias toward specific high inclinations, however this process is efficient only for small asteroids (diameter smaller than 50 km; e.g. Polishook & Brosch 2009, and references therein), and is not expected to affect TNOs at all. If such mergers products are abundant they could effect the relative spin-orbit inclination distribution, and produce tilt axis distribution which is biased towards high latitudes from the orbital plane. Interestingly, such a bias exists in the pole distribution of large binary asteroids (Kryszczyńska et al. 2007, ; not expected to be affected by YORP).

6. SUMMARY

In this letter we have shown that the secular Kozai perturbations by the sun have a major role in the dynamical evolution of binary minor planets. The Kozai mechanism leads to large periodic oscillations in the eccentricity and inclination of highly inclined BMP orbits and the combined effects of the Kozai mechanism and tidal friction drives BMPs into short period circular orbits. We predict an inclination dependent distribution

of the separation and eccentricity of BMPs, due to these effects, including a zone of avoidance at the highest inclinations. Additionally, the KCTF process could lead to BMPs coalescence and serve as an important route for the formation of irregular shaped single minor planets with large axial tilts. Finally we note that similar KCTF processes could strongly affect the evolution of planetary satellites. Although Kozai effects had been discussed in that context (Nesvorný et al. 2003), the combined KCTF evolution, which has not been taken into account, could play an important role in satellite migration.

We would like to thank Dan Fabrycky for supplying us with his KCTF evolution code and for his critical review on an early version of this manuscript. We also acknowledge valuable discussions with Darin Ragozzine, Re'em Sari, Tsevi Mazeh and David Polishook. SN acknowledges support from the ISF grant 629/05. We also acknowledge the generous support by the industrial and commercial club of Israel through the Ilan-Ramon foundation.

REFERENCES

- Carruba, V. et al. 2002, *Icarus*, 158, 434
 Chauvineau, B., Farinella, P., & Mignard, F. 1993, *Icarus*, 105, 370
 Fabrycky, D. & Tremaine, S. 2007, *ApJ*, 669, 1298
 Funato, Y. et al. 2004, *Nature*, 427, 518
 Goldreich, P., Lithwick, Y., & Sari, R. 2002, *Nature*, 420, 643
 Grundy, W. M. et al. 2009, *Icarus*, 200, 627
 Hamilton, D. P. & Burns, J. A. 1991, *Icarus*, 92, 118
 Harrington, R. S. 1968, *AJ*, 73, 190
 Hartmann, W. K. & Cruikshank, D. P. 1980, *Science*, 207, 976
 Heggie, D. C. 1975, *MNRAS*, 173, 729
 Innanen, K. A. 1980, *AJ*, 85, 81
 Kiseleva, L. G., Eggleton, P. P., & Mikkola, S. 1998, *MNRAS*, 300, 292
 Kozai, Y. 1962, *AJ*, 67, 591
 Kryszczyńska, A. et al. 2007, *Icarus*, 192, 223
 Lee, E. A., Astakhov, S. A., & Farrelly, D. 2007, *MNRAS*, 379, 229
 Lidov, M. L. 1962, *Planetary and Space Science*, 9, 719
 Marchis, F. et al. 2008, *Icarus*, 195, 295
 Mazeh, T. & Shaham, J. 1979, *A&A*, 77, 145
 Merline, W. J. et al. 2002, *Asteroids III*, 289
 Nazzario, R. C. et al. 2007, *Advances in Space Research*, 40, 280
 Nesvorný, D. et al. 2003, *AJ*, 126, 398
 Noll, K. S. et al. 2008, *Binaries in the Kuiper Belt*, 345–363
 Perets, H. B. & Fabrycky, D. C. 2009, *ArXiv* 0901.4328
 Perets, H. B. & Naoz, S. 2009, *In prep.*; see *ArXiv:0809.2095v1*
 Petit, J.-M. et al. 2008, *Science*, 322, 432
 Polishook, D. & Brosch, N. 2009, *Icarus*, 199, 319
 Ragozzine, D. & Brown, M. E. 2009, *ArXiv:0903.4213*
 Richardson, D. C. & Walsh, K. J. 2006, *ARAA*, 34, 47
 Romanishin, W. et al. 2001, *PNAS*, 98, 11863
 Scheeres, D. J. 1994, *Icarus*, 110, 225
 Schlichting, H. E. & Sari, R. 2008, *arXiv:0803.0329*
 Sheppard, S. S. & Jewitt, D. 2004, *AJ*, 127, 3023
 Stern, S. A., Bottke, W. F., & Levison, H. F. 2003, *AJ*, 125, 902
 Weidenschilling, S. J. 2002, *Icarus*, 160, 212
 Weidenschilling, S. J., Paolicchi, P., & Zappala, V. 1989, in *Asteroids II*, ed. R. P. Binzel, T. Gehrels, & M. S. Matthews (The University of Arizona Press), 643–658

Chapter 13

A new type of stellar explosions

Perets et al.

Submitted to Nature (2009)

A new type of stellar explosion

H. B. Perets¹, A. Gal-Yam¹, P. Mazzali^{2,3}, D. Arnett⁴, D. Kagan⁵,
A. V. Filippenko⁶, W. Li⁶, S. B. Cenko⁶, D. B. Fox⁷, D. C. Leonard⁸,
D.-S. Moon⁹, D. J. Sand¹⁰, A. M. Soderberg¹⁰, R. J. Foley^{10,11},
M. Ganeshalingam⁶, J. P. Anderson^{12,13}, P. A. James¹³, E. O. Ofek¹⁴,
L. Bildsten^{15,16}, G. Nelemans¹⁷, K. J. Shen¹⁶, N. N. Weinberg⁶,
B. D. Metzger⁶, A. L. Piro⁶, E. Quataert⁶, M. Kiewe¹, and D. Poznanski⁶

¹ Faculty of Physics, Weizmann Institute of Science, POB 26, Rehovot 76100, Israel

² Scuola Normale Superiore, Piazza Cavalieri 7, 56127 Pisa, Italy

³ INAF - Oss. Astron. Padova, vicolo dell'Osservatorio, 5, 35122 Padova, Italy

⁴ Steward Observatory, University of Arizona, 933 North Cherry Avenue, Tucson, AZ 85721, USA

⁵ Department of Astronomy, University of Texas at Austin, Austin, TX 78712, USA

⁶ Department of Astronomy, University of California, Berkeley, CA 94720-3411, USA

⁷ Dept. of Astronomy and Astrophysics, Pennsylvania State University, University Park, PA 16802, USA

⁸ Department of Astronomy, San Diego State University, San Diego, California 92182, USA

⁹ Department of Astronomy and Astrophysics, University of Toronto, 50 St. George Street, Toronto, ON M5S 3H4, Canada

¹⁰ Harvard-Smithsonian Center for Astrophysics, 60 Garden Street, Cambridge, MA 02138, USA

¹¹ Clay Fellow

¹² Departamento de Astronomia, Universidad de Chile, Camino El Observatorio 1515, Las Condes, Santiago, Casilla 36-D,

Chile

¹³ Astrophysics Research Institute, Liverpool John Moores University, Twelve Quays House, Birkenhead CH41 1LD, UK

¹⁴ Department of Astronomy, 105-24, California Institute of Technology, Pasadena, CA 91125, USA

¹⁵ Kavli Institute for Theoretical Physics, Kohn Hall, University of California, Santa Barbara, CA 93106

¹⁶ Department of Physics, University of California, Santa Barbara, CA 93106

¹⁷ Department of Astrophysics, Radboud University Nijmegen, Toernooiveld 1, NL-6525 ED, The Netherlands

The explosive deaths of stars (supernovae; SNe) are generally explained by two physical processes. Young massive stars (with eight or more solar masses, m_{\odot}) undergoing gravitational core-collapse are observed as type Ib/c and II SNe. Type Ia SNe result from thermonuclear explosion of older, Chandrasekhar-mass carbon-oxygen white dwarfs (WDs).¹ Even the most underluminous SNe Ia^{2,3} eject $\sim 1 M_{\odot}$ of C/O burning products.⁴ Here we report our discovery of a faint type Ib SN 2005E, in the halo of the nearby isolated galaxy, NGC 1032. The lack of any trace of recent star formation near the SN location, and the very low ejected mass we find ($\sim 0.3 M_{\odot}$) argues strongly against an explosion of a short-lived, massive star as the origin of this event (Fig. 1). Our spectroscopic observations, as well as the derived nucleosynthetic output, which is dominated by helium burning products rule out SN 2005E as either a sublumino² or

regular¹ SNe Ia (Fig. 2). SN 2005E therefore represents a new type of stellar explosion arising from a low-mass, old stellar system. The ejected mass contains large amounts of calcium, 5-10 times more than observed in any type of SNe.^{5,6} [Calcium-rich SNe, although not as faint as SN2005E, were theoretically predicted,⁷ but never previously observed.] Our nucleosynthetic analysis suggest that large amounts of radioactive ⁴⁴Ti were also produced. Such SNe may thus help resolve fundamental physical puzzles, extending from the composition of the primitive solar system and that of the oldest stars, to the Galactic production of positrons.

We discovered a supernova explosion (SN 2005E; Fig. 1) on Jan. 13, 2005 (UT dates are used throughout this paper) shortly after it occurred (it was not detected on Dec. 24, 2004). Follow-up spectroscopy (Fig. 2) revealed strong lines of helium and calcium, indicating it belongs to the previously identified group of calcium-rich type Ib supernovae.⁸ The SN position is ~ 22.9 kpc (projected) from the center and ~ 11.3 kpc above the disk of its edge-on host galaxy, NGC 1032 (Fig. 1), which is itself at a distance of 34 Mpc. NGC 1032 is an isolated galaxy⁹ showing no signs of interaction, with the closest small satellite galaxy found at a distance of > 120 kpc in projection. Deep follow-up observations of the explosion site, sensitive to both ultraviolet light from hot young stars and emission lines from ionized hydrogen gas, put strict limits on any local star-formation activity at or near the SN location (Fig. 1). In addition, a radio signature, expected from some core-collapse SNe, has not been observed (see Supplementary Information [SI], Section 2). The remote position of SN 2005E in the outskirts (halo) of the galaxy, together with the isolation of NGC 1032 and its classification as an S0/a galaxy (in which the star-formation rate is very low¹⁰), in addition to our limits on local star formation, point to a SN progenitor from an old stellar population (see also SI, Section 2).

Our analysis of the spectra of SN 2005E indicates that it is spectroscopically similar to SNe Ib (Fig. 2; SI, Section 3), showing lines of He but lacking either hydrogen or the hallmark Si and S lines of SNe Ia in its photospheric spectra. The nebular spectrum of this event shows no emission from iron-group elements, which also characterize type Ia SNe. Analysis of this spectrum indicates a total ejected mass of $M_{\text{ej}} \approx 0.2 M_{\odot}$, with a small fraction in radioactive nickel, consistent with the low luminosity of this event (Fig. 3). Such low ejecta mass for a SN of any type has never before been firmly established using nebular spectral analysis. We also used the narrow, fast, and faint light curve together with the measured ejecta velocities ($\sim 11,000 \text{ km s}^{-1}$) to infer the ejected mass (SI, Section 4). We use these data to find consistent results of $M_{\text{ej}} \approx 0.3 \pm 0.1 M_{\odot}$,

assuming that some of the mass is not accounted for by the nebular spectrum analysis, e.g., high-velocity He layers and some slowly moving, denser ejecta that are still hidden below the photosphere at that time. Finally, SN 2005E shows a remarkable amount of calcium in its ejecta, $0.06 M_{\odot}$ ($\sim 0.22 \pm 0.08$ of the total ejecta mass), 5–10 times larger than any other type of SN^{5,6} (25–350 times higher in relative calcium fraction).

The old environment, ejected mass, and nucleosynthetic output of SN 2005E are in stark contrast to those expected from collapsing massive stars, whether formed locally or ejected from a distant location (SI, Sections 5–6). The low ejected mass is also inconsistent with those determined for SNe Ia, restricted to a tight mass range of $\sim 1\text{--}1.3 M_{\odot}$, regardless of their intrinsic luminosity (even the prototype faint SN 1991bg is found in this range).⁴ Furthermore, the light curve of SN 2005E (see SI, section 4) shows a different behavior than that of SNe Ia, declining much faster than even the most subluminal (1991bg like) SNe observed.³ These properties, together with the observed spectra and our nucleosynthetic analysis, rules out SN 2005E as either a regular or peculiar SN Ia. Therefore, we conclude that SN 2005E is the first clearly identified example of a new, different type of SN explosion, arising from a low-mass progenitor.

The spectroscopic signatures of SN 2005E are quite unique, and allow one to identify additional similar events.⁸ Arising from lower-mass progenitors, these events are likely to be found among both old and young stellar populations, i.e., we expect to find such peculiar SNe Ib in both early- and late-type galaxies. Indeed, while the unusual location of SN 2005E triggered the current study, several other calcium-rich subluminal SNe Ib/c similar to SN 2005E have been observed (see SI, Section 7). Of the group of seven subluminal calcium-rich SNe Ib/c we identified, three are observed in old-population environments: SN 2005E presented here, as well as SN 2000ds and SN 2007ke, observed in elliptical galaxies. Moreover, SN 2000ds has pre- and post-explosion *Hubble Space Telescope* images showing no evidence for either star-forming regions or massive stars¹¹ near its location. No radio signature has been observed either.¹²

The rate of calcium-rich, faint, type Ib/c SNe can be estimated, since SN 2005E was discovered as part of the Lick Observatory Supernova Search (LOSS).¹³ This survey is a volume-limited search, with high sensitivity within 60 Mpc for both SNe Ia and faint Ca-rich objects such as SN 2005E. LOSS found 2.3 calcium-rich objects (after correction for incompleteness) and 31.0 SNe Ia in this volume, from which we infer the rate of such calcium-rich SNe to be $7\% \pm 5\%$ of the total SN Ia rate. Further analysis of this group of subluminal calcium-enriched SNe will be discussed in a forthcoming publication.

Given the unique nucleosynthetic products we observed, we ran several nucleosynthesis single-zone simulations¹⁴ in order to investigate possible conditions that may lead to such signatures. We explored the ignition of various initial mixtures of He, C, and O on a grid of temperatures $[(2-4) \times 10^9 \text{ K}]$. We find that our essential results, namely, large calcium yield with little or no sulfur (in particular, the nebular analysis places a limit of calcium/sulfur > 6), and a low mass of radioactive nickel and iron-group elements, can be produced from initial compositions dominated by helium ($X(\text{He}) \geq 0.5$; see SI, Section 9).

Calcium-rich SNe were theoretically predicted to arise from burning helium-rich material on a WD, leading to the full disruption of a sub-Chandrasekhar-mass WD.^{7,15} However, such models predicted the production of SNe far more luminous (and ^{56}Fe rich) than SN 2005E. Several theoretical models were suggested in the literature to possibly produce subluminous SNe, with low-mass, high-velocity ejecta in an old stellar population. These include the accretion-induced collapse (AIC) of a WD (e.g. Refs.^{16,17} and the detonation of an accreted helium shell on a WD in a binary system (the “.Ia” model^{18,19}). These studies did not explore the burning of large helium masses ($> 0.1 M_{\odot}$), nor the production of calcium-rich ejecta; further studies in these directions are in progress.

We conclude that SN 2005E appears to be the first example identified where the theoretically suggested helium detonation process, and its unique nucleosynthetic production,⁷ are observed. Additional characteristics of these explosions, including their old population origin, subluminosity, and low ejected mass, are broadly consistent with the predictions of some theoretical models (.Ia¹⁸ and AIC¹⁷), variants of which may produce the appropriate conditions for such helium detonations. Alternatively, these explosions may require a totally new mechanism.

We note that the recently discovered peculiar subluminous type Ia SN 2008ha^{20,21} also shows prominent calcium-rich emission in its late-time spectrum. This may hint at the involvement of a similar process of explosive helium burning in this peculiar object (see also SI, Section 10).

Our discovery has numerous astrophysical implications. It seems highly likely that we identified explosions arising from very close WD-WD systems, and therefore the rates of such events might be useful in constraining the rates of WD-WD inspirals observable as gravitational wave sources. The unique nucleosynthetic production of large masses of calcium and radioactive ^{44}Ti per explosion could solve puzzles related to the source of calcium (especially ^{44}Ca) in the primitive solar system,²²⁻²⁴ in old, metal-poor halo stars,²⁵

and the enrichment patterns of the interstellar and intracluster medium.²⁶ Production of most of the Galactic ^{44}Ti and its progeny, ^{44}Ca , in a few rare, prolific explosions, can also explain the origins of Galactic ^{44}Ca given the null detection of ^{44}Ti traces in most nearby SN remnants.^{24,27}

Finally, products from inverse β decay of ^{44}Ti may significantly contribute to the Galactic production of positrons.²⁸ Assuming our estimated rates ($\sim 10\%$ of the SN Ia rate) and our ^{44}Ti yield ($0.006\text{--}0.06\text{ M}_{\odot}$; see SI, Section 9), Galactic SNe of the type we describe here will provide a significant contribution to the Galactic bulge component of the positron annihilation line, at least comparable to that of SNe Ia. In fact, within the current uncertainties on the ^{44}Ti yield and SN rates, these events may come within a factor of few of producing all of the observed positrons.²⁹

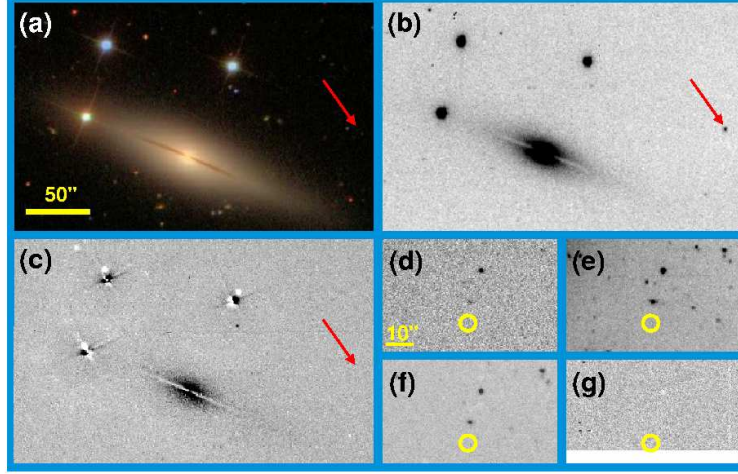


Figure 1. The environment of SN 2005E (technical details about the observations can be found in SI Section 1). (a) NGC 1032, the host galaxy of SN 2005E, as observed by the Sloan Digital Sky Survey (SDSS), prior to the SN explosion. The galaxy is an isolated, edge-on, early-type spiral galaxy, showing no signs of star-formation activity, warping, or interaction. Its luminosity is dominated by the cumulative contribution of a multitude of low-mass old stars (yellow light in this image). Panels (a)-(c) are $275'' \times 175''$; a scale bar is provided, north is up, and east due left. (b) The LOSS¹³ discovery of SN 2005E on Jan. 13, 2005 (shown in negative). Note the remote location of the SN (marked with a red arrow) with respect to its host, 22.9 kpc (projected) from the galaxy nucleus and 11.3 kpc above the disk, whose edge-on orientation is well determined (panel (a)). (c) An image of NGC 1032 in the light of the $H\alpha$ emission line, emitted by interstellar gas ionized by ultraviolet (UV) radiation, and a good tracer of recent star formation. There are no traces of recent star-formation activity (usually appearing as irregular, compact emission sources) near the SN location or anywhere else in the host. Panels (d)-(g) are $64'' \times 36''$; a scale bar is provided. (d) Zoom-in on the location of SN 2005E in pre-explosion SDSS r -band images. No source is detected near the SN location, marked with a yellow circle (radius $3''$; the astrometric uncertainty in the SN location is $< 0.5''$). The SDSS catalog does not list any objects near that position (e.g., putative faint dwarf satellites of NGC 1032), down to a typical limit of $r = 22.5$ mag. (e-f) Deeper photometry of the SN location. A red image is shown in panel (e), while a UV (u -band) image is shown in panel (f). At the distance of NGC 1032, the point source upper limits we find, $M_r < -7.5(-6.9)$ and $M_u < -8.1(-7.1)$ mag at $3(2)\sigma$, respectively, indicate that we would have detected faint star-forming galaxies or star-forming regions at the SN location, or indeed even individual massive red supergiant or luminous blue supergiant stars. (g) Zoom-in on the location of SN 2005E in $H\alpha$ light (see panel (c) for details). No trace of star-formation activity is seen near the SN location.

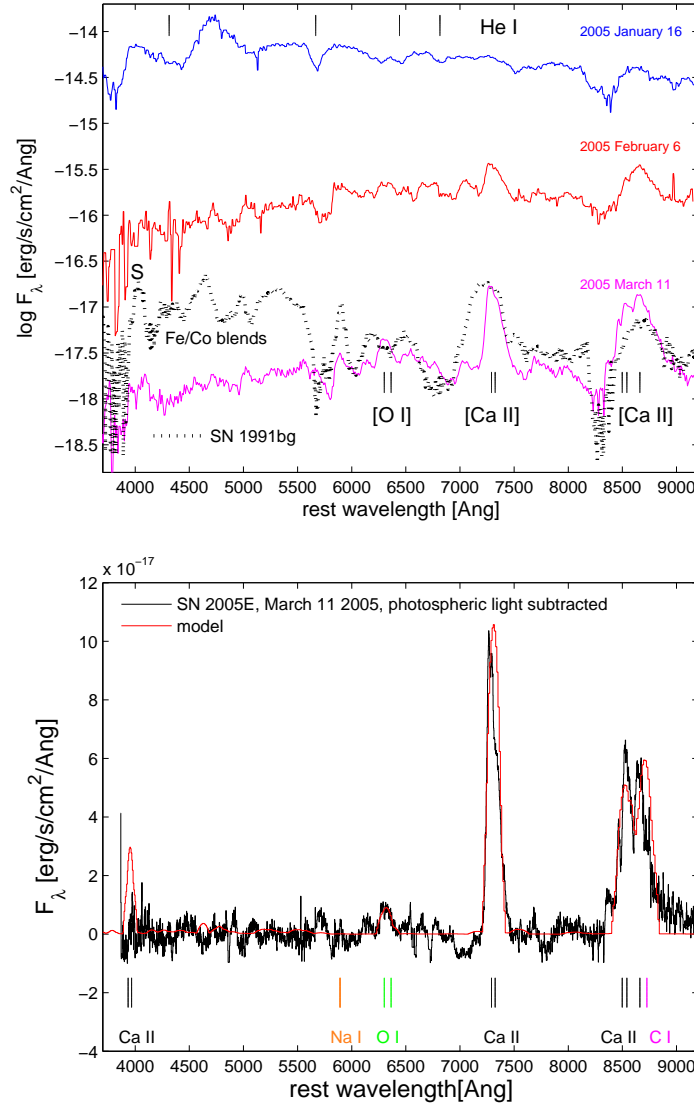


Figure 2. The mass and composition of the SN 2005E ejecta (technical details of observations can be found in SI Section 1). Upper panel: Photospheric spectra of SN 2005E. The top spectrum is obviously photospheric and shows absorption lines of the He I series (marked with black ticks after application of an $11,000 \text{ km s}^{-1}$ blueshift, at the top). Nebular lines of intermediate-mass elements, most notably oxygen and calcium, begin to emerge in the middle spectrum, and dominate the latest nebular spectrum at the bottom. Also note that the typical Si lines of SNe Ia are absent in all spectra, while the nebular spectrum of SN 2005E clearly rules out a type Ia identification (comparison with the underluminous SN 1991bg³⁰ is shown; note the lack of the typical iron group line blends in the blue side). The derived line velocities are consistent with SN 2005E exploding within its putative host galaxy, NGC 1032. Bottom: The nebular spectrum of SN 2005E compared with a model fit. From the fit we can derive elemental abundances and masses in the ejecta of SN 2005E. We find masses of 0.1, 0.02, 0.06, 0.003 M_{\odot} for carbon, oxygen, calcium, and radioactive nickel, respectively. Both the low total ejected mass of $\sim 0.2 M_{\odot}$ and the relative abundances are unique among previously studied events.

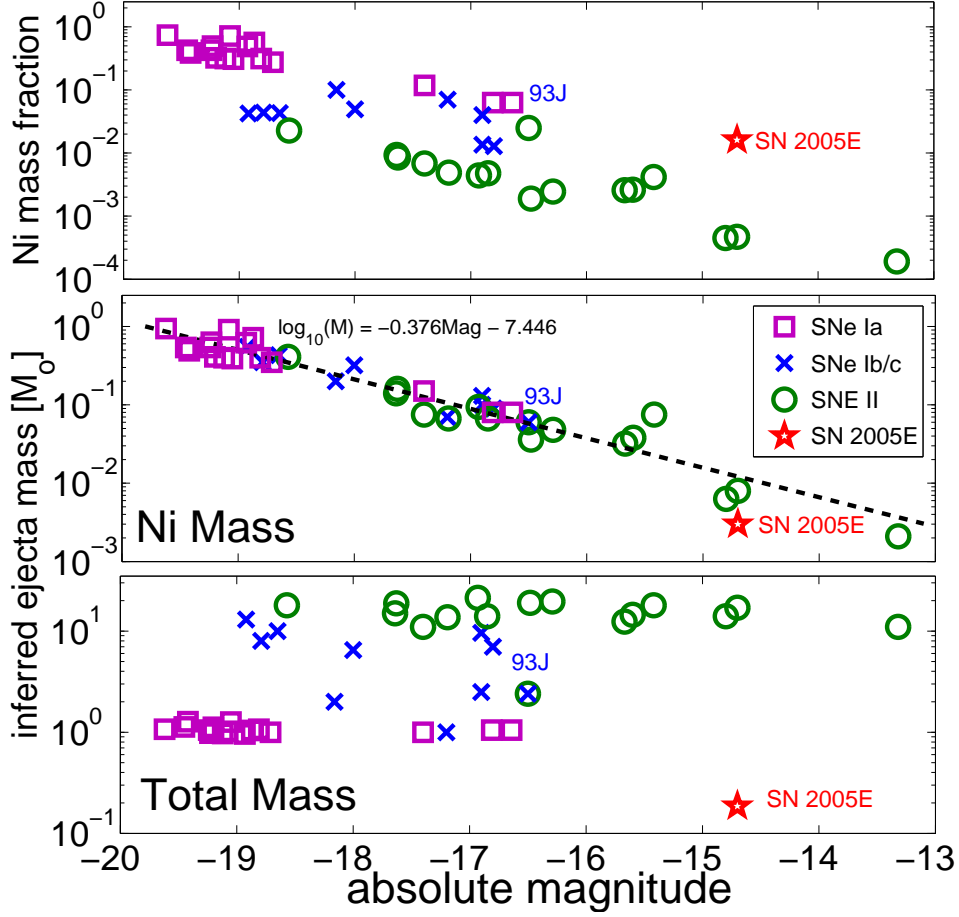


Figure 3. Comparison of the SN 2005E ejecta mass and luminosity with other SNe [SNe Ia, squares; SNe Ib/c, \times marks; SNe II, circles]. The lower panel shows the total ejecta mass inferred for SN 2005E, which is the lowest inferred ejecta mass found for any SN, based on nebular spectra. Its position in the luminosity vs. ejecta-mass phase space is unique, suggesting it is not a member of currently well-known SN families. The middle panel shows the Ni mass inferred for SN 2005E. The small Ni mass inferred for SN 2005E is consistent with its low luminosity, although somewhat lower than might be expected from the extension of the observed Ni mass-luminosity relation observed for other SNe (dashed line and formula). The upper panel shows the Ni ejecta mass fraction $M_{\text{Ni}}/M_{\text{total}}$ inferred for SN 2005E. The sources from which the SN data were collected are listed in the SI, Section 8.

-
1. Filippenko, A. V. Optical spectra of supernovae. *ARAA* **35**, 309–355 (1997).
 2. Filippenko, A. V. *et al.* The subluminal, spectroscopically peculiar type Ia supernova 1991bg in the elliptical galaxy NGC 4374. *AJ* **104**, 1543–1556 October 1992.
 3. Kasliwal, M. M. *et al.* SN 2007ax: An extremely faint type Ia supernova. *ApJL* **683**, L29–L32 (2008).
 4. Mazzali, P. A. *et al.* A common explosion mechanism for type Ia supernovae. *Science* **315**, 825– (2007).
 5. Nomoto, K. *et al.* Nucleosynthesis in type Ia supernovae. *Nuclear Physics A* **621**, 467–476 (1997).
 6. Nomoto, K. *et al.* Nucleosynthesis in type II supernovae. *Nuclear Physics A* **616**, 79–90 (1997).
 7. Woosley, S. E., Taam, R. E. & Weaver, T. A. Models for type I supernova. I - Detonations in white dwarfs. *ApJ* **301**, 601–623 (1986).
 8. Filippenko, A. V. *et al.* Supernovae 2001co, 2003H, 2003dg, and 2003dr. *IAU Circular* **8159**, 2–+ (2003).
 9. Prada, F. *et al.* Observing the dark matter density profile of isolated galaxies. *ApJ* **598**, 260–271 (2003).
 10. Kennicutt, Jr., R. C. Star formation in galaxies along the Hubble sequence. *ARA&A* **36**, 189–232 (1998).
 11. Maund, J. R. & Smartt, S. J. Hubble Space Telescope imaging of the progenitor sites of six nearby core-collapse supernovae. *MNRAS* **360**, 288–304 (2005).
 12. Soderberg, A. M. *et al.* Late-time radio observations of 68 type Ibc supernovae: Strong constraints on off-Axis gamma-ray bursts. *ApJ* **638**, 930–937 (2006).
 13. Filippenko, A. V. *et al.* in *IAU Colloq. 183: Small Telescope Astronomy on Global Scales* (eds Paczynski, B., Chen, W.-P. & Lemme, C.) 121–+ (ASP, 2001).
 14. Arnett, D. *Supernovae and Nucleosynthesis. An Investigation of The History of Matter, from The Big Bang to The Present.* Princeton series in astrophysics, Princeton, NJ: Princeton University Press (1996).
 15. Woosley, S. E. & Weaver, T. A. Sub-Chandrasekhar mass models for type Ia supernovae. *ApJ* **423**, 371–379 (1994).

- 10 *Perets et al.*
16. Nomoto, K. & Kondo, Y. Conditions for accretion-induced collapse of white dwarfs. *ApJL* **367**, L19–L22 (1991).
17. Metzger, B. D., Piro, A. L. & Quataert, E. Nickel-rich outflows from accretion disks formed by the accretion-induced collapse of white dwarfs. *ArXiv* **0812.3656**, (2008).
18. Bildsten, L. *et al.* Faint thermonuclear supernovae from AM Canum Venaticorum binaries. *ApJL* **662**, L95–L98 (2007).
19. Shen, K. J. & Bildsten, L. Unstable helium shell burning on accreting white dwarfs. *ArXiv* **0903.0654**, (2009).
20. Foley, R. J. *et al.* SN 2008ha: An extremely low luminosity and extremely low energy supernova. *ArXiv* **0902.2794**, (2009).
21. Valenti, S. *et al.* An extremely faint stripped-envelope core-collapse supernova and its implications. *Nature, in press* **arXiv:0901.2074**, (2009).
22. Woosley, S. E., Arnett, W. D. & Clayton, D. D. The explosive burning of oxygen and silicon. *ApJS* **26**, 231–+ (1973).
23. Amari, S. *et al.* Interstellar SiC with unusual isotopic compositions - Grains from a supernova? *ApJL* **394**, L43–L46 (1992).
24. Timmes, F. X. *et al.* The production of ^{44}Ti and ^{60}Co in supernovae. *ApJ* **464**, 332–+ (1996).
25. Lai, D. K. *et al.* A unique star in the outer halo of the Milky Way. *ApJL* **697**, L63–L67 (2009).
26. de Plaa, J. *et al.* Constraining supernova models using the hot gas in clusters of galaxies. *A&A* **465**, 345–355 (2007).
27. The, L.-S. *et al.* Are ^{44}Ti -producing supernovae exceptional? *A&A* **450**, 1037–1050 (2006).
28. Chan, K.-W. & Lingenfelter, R. E. Positrons from supernovae. *ApJ* **405**, 614–636 (1993).
29. Knödseder, J. *et al.* The all-sky distribution of 511 keV electron-positron annihilation emission. *A&A* **441**, 513–532 (2005).
30. Mazzali, P. A. *et al.* The properties of the peculiar type IA supernova 1991bg - II. The amount of ^{56}Ni and the total ejecta mass determined from spectrum synthesis and energetics considerations. *MNRAS* **284**, 151–171 January 1997.
31. Oke, J. B. *et al.* The Keck low-resolution imaging spectrometer. *PASP* **107**, 375–+ (1995).

32. Gal-Yam, A. *et al.* in *The Multicolored Landscape of Compact Objects and Their Explosive Origins* (eds di Salvo, T., Israel, G. L., Piersant, L., Burderi, L., Matt, G. *et al.*) 297–303 (IOP Institute of physics publishing LTD, 2007).
33. Oke, J. B. & Gunn, J. E. An efficient low resolution and moderate resolution spectrograph for the Hale telescope. *PASP* **94**, 586–+ (1982).
34. Chu, Y.-H. & Gruendl, R. A. in *Massive Star Formation: Observations Confront Theory* (eds Beuther, H., Linz, H. & Henning, T.) 415–+ (ASP, 2008).
35. Schilbach, E. & Röser, S. On the origin of field O-type stars. *A&A* **489**, 105–114 (2008).
36. Anderson, J. P. & James, P. A. Constraints on core-collapse supernova progenitors from correlations with H α emission. *MNRAS* **390**, 1527–1538 (2008).
37. Dyson, J. E. & Hartquist, T. W. On the structure of intermediate- and high-velocity clouds. *MNRAS* **203**, 1233–1238 (1983).
38. Christodoulou, D. M., Tohline, J. E. & Keenan, F. P. Star-forming processes far from the galactic disk: inoperative or indolent where operative. *ApJ* **486**, 810–+ (1997).
39. Martos, M. *et al.* Spiral density wave shock-induced star formation at high galactic latitudes. *ApJL* **526**, L89–L92 (1999).
40. Heraudeau, P. & Simien, F. Optical and I-band surface photometry of spiral galaxies. I. The data. *AAPS* **118**, 111–155 (1996).
41. Kennicutt, Jr., R. C. & Kent, S. M. A survey of H-alpha emission in normal galaxies. *AJ* **88**, 1094–1107 (1983).
42. Soderberg, A. M. in *Supernova 1987A: 20 Years After: Supernovae and Gamma-Ray Bursters* (eds Immler, S., Weiler, K. & McCray, R.) 492–499 (IOP, 2007).
43. Howell, D. A. *et al.* Gemini spectroscopy of supernovae from the supernova legacy survey: Improving high-redshift supernova selection and classification. *ApJ* **634**, 1190–1201 (2005).
44. Hamuy, M. *et al.* Optical and infrared spectroscopy of SN 1999ee and SN 1999ex. *AJ* **124**, 417–429 (2002).
45. Filippenko, A. V. & Sargent, W. L. W. The unique supernova (1985f) in NGC 4618. *AJ* **91**, 691–696 (1986).
46. Gaskell, C. M. *et al.* Type Ib supernovae 1983n and 1985f - Oxygen-rich late time spectra. *ApJL* **306**, L77–L80 (1986).

- 12 *Perets et al.*
47. Arnett, W. D. Type I supernovae. I - Analytic solutions for the early part of the light curve. *ApJ* **253**, 785–797 (1982).
 48. Stehle, M. *et al.* Abundance stratification in Type Ia supernovae - I. The case of SN 2002bo. *MNRAS* **360**, 1231–1243 July 2005.
 49. Modjaz, M. *et al.* From shock breakout to peak and beyond: Extensive panchromatic observations of the aspherical type Ib supernova 2008D associated with Swift X-ray transient 080109. *ArXiv* **0805.2201**, (2008).
 50. Valenti, S. *et al.* The broad-lined type Ic supernova 2003jd. *MNRAS* **383**, 1485–1500 (2008).
 51. NED *Nasa/ipac extragalactic database* <http://nedwww.ipac.caltech.edu/>.
 52. Blaauw, A. On the origin of the O- and B-type stars with high velocities (the "run-away" stars), and some related problems. *Bulletin of the Astronomical Institutes of the Netherlands* **15**, 265–+ (1961).
 53. Hoogerwerf, R., de Bruijne, J. H. J. & de Zeeuw, P. T. On the origin of the O and B-type stars with high velocities. II. Runaway stars and pulsars ejected from the nearby young stellar groups. *A&A* **365**, 49–77 (2001).
 54. Hills, J. G. Hyper-velocity and tidal stars from binaries disrupted by a massive Galactic black hole. *Nature* **331**, 687–689 (1988).
 55. Brown, W. R. *et al.* Discovery of an unbound hypervelocity star in the Milky Way halo. *ApJL* **622**, L33–L36 (2005).
 56. Edelmann, H. *et al.* HE 0437-5439: An unbound hypervelocity main-sequence B-Type star. *ApJL* **634**, L181–L184 (2005).
 57. Hirsch, H. A. *et al.* US 708 - an unbound hyper-velocity subluminescent O star. *A&A* **444**, L61–L64 (2005).
 58. Eisenhauer, F. *et al.* SINFONI in the Galactic center: Young stars and infrared flares in the central light-month. *ApJ* **628**, 246–259 (2005).
 59. Ghez, A. M. *et al.* Stellar orbits around the Galactic center black hole. *ApJ* **620**, 744–757 (2005).
 60. Miyamoto, M. & Nagai, R. Three-dimensional models for the distribution of mass in galaxies. *Publ. of the Astronomical Society of Japan* **27**, 533–543 (1975).
 61. Shankar, F. *et al.* New relationships between galaxy properties and host halo mass, and the role of feedbacks in galaxy formation. *ApJ* **643**, 14–25 (2006).

62. Gorgas, J., Jablonka, P. & Goudfrooij, P. Stellar population gradients in bulges along the Hubble sequence. I. The data. *A&A* **474**, 1081–1092 (2007).
63. Leonard, P. J. T. The maximum possible velocity of dynamically ejected runaway stars. *AJ* **101**, 562–571 (1991).
64. Leonard, P. J. T. & Duncan, M. J. Runaway stars from young star clusters containing initial binaries. II - A mass spectrum and a binary energy spectrum. *AJ* **99**, 608–616 (1990).
65. Ferrarese, L. & Merritt, D. A fundamental relation between supermassive black holes and their host galaxies. *ApJL* **539**, L9–L12 (2000).
66. Gebhardt, K. *et al.* A relationship between nuclear black hole mass and galaxy velocity dispersion. *ApJL* **539**, L13–L16 (2000).
67. Hills, J. G. Computer simulations of encounters between massive black holes and binaries. *AJ* **102**, 704–715 (1991).
68. Bromley, B. C. *et al.* Hypervelocity stars: Predicting the spectrum of ejection velocities. *ApJ* **653**, 1194–1202 (2006).
69. Abt, H. A. Normal and abnormal binary frequencies. *ARAA* **21**, 343–372 (1983).
70. Morrell, N. & Levato, H. Spectroscopic binaries in the Orion OB1 association. *ApJS* **75**, 965–985 (1991).
71. Kobulnicky, H. A. & Fryer, C. L. A new look at the binary characteristics of massive stars. *ApJ* **670**, 747–765 (2007).
72. Perets, H. B. Runaway and hypervelocity stars in the Galactic halo: Binary rejuvenation and triple disruption. *ApJ, in press* **ArXiv:0802.1004**, (2008).
73. Heber, U. *et al.* The B-type giant HD 271791 in the Galactic halo. Linking run-away stars to hyper-velocity stars. *A&A* **483**, L21–L24 (2008).
74. Yu, Q. & Tremaine, S. Ejection of Hypervelocity Stars by the (Binary) Black Hole in the Galactic Center. *ApJ* **599**, 1129–1138 (2003).
75. Perets, H. B., Hopman, C. & Alexander, T. Massive Perturber-driven Interactions between Stars and a Massive Black Hole. *ApJ* **656**, 709–720 (2007).
76. Perets, H. B. Dynamical and evolutionary constraints on the nature and origin of hypervelocity stars. *ApJ* **690**, 795–801 (2009).

77. Perets, H. B. *et al.* Dynamical evolution of the young stars in the Galactic center: N-body simulations of the S-stars. *ArXiv* **0903.2912**, (2009).
78. Gould, A. & Quillen, A. C. Sagittarius A* Companion S0-2: A Probe of Very High Mass Star Formation. *ApJ* **592**, 935–940 (2003).
79. Gillessen, S. *et al.* Monitoring Stellar Orbits Around the Massive Black Hole in the Galactic Center. *ApJ* **692**, 1075–1109 (2009).
80. Sauer, D. N. *et al.* The properties of the ‘standard’ Type Ic supernova 1994I from spectral models. *MNRAS* **369**, 1939–1948 (2006).
81. Mazzali, P. A., Iwamoto, K. & Nomoto, K. A spectroscopic analysis of the energetic type Ic Hypernova SN 1997EF. *ApJ* **545**, 407–419 (2000).
82. Tominaga, N. *et al.* The unique type Ib supernova 2005bf: A WN star explosion model for peculiar light curves and spectra. *ApJL* **633**, L97–L100 (2005).
83. Li, L.-X. Correlation between the peak spectral energy of gamma-ray bursts and the peak luminosity of the underlying supernovae: implication for the nature of the gamma-ray burst-supernova connection. *MNRAS* **372**, 1357–1365 (2006).
84. Mazzali, P. A. *et al.* The aspherical properties of the energetic type Ic SN 2002ap as inferred from its nebular spectra. *ApJ* **670**, 592–599 (2007).
85. Soderberg, A. M. *et al.* An HST study of the supernovae accompanying GRB 040924 and GRB 041006. *ApJ* **636**, 391–399 (2006).
86. Nadyozhin, D. K. Explosion energies, nickel masses and distances of type II plateau supernovae. *MNRAS* **346**, 97–104 (2003).
87. Zampieri, L. in *1604-2004: Supernovae as Cosmological Lighthouses* (eds Turatto, M., Benetti, S., Zampieri, L. & Shea, W.) 358–+ (ASP, 2005).
88. Li, W. *et al.* SN 2002cx: The most peculiar known type Ia supernova. *PASP* **115**, 453–473 (2003).
89. Jha, S. *et al.* Late-time spectroscopy of SN 2002cx: The prototype of a new subclass of type Ia supernovae. *AJ* **132**, 189–196 (2006).

*

*Correspondence should be addressed to Avishay Gal-Yam (avishay.gal-yam@weizmann.ac.il) and Hagai Perets (hagai.perets@weizmann.ac.il).

Acknowledgements

We would like to thank Udi Nakar and Dani Maoz for helpful comments. We acknowledge observations with the Liverpool Telescope, which is operated on the island of La Palma by Liverpool John Moores University in the Spanish Observatorio del Roque de los Muchachos of the Instituto de Astrofísica de Canarias with financial support from the UK Science and Technology Facilities Council. KAIT and its ongoing operation were made possible by donations from Sun Microsystems, Inc., the Hewlett-Packard Company, AutoScope Corporation, Lick Observatory, the NSF, the University of California, the Sylvia & Jim Katzman Foundation, and the TABASGO Foundation. Some of the data presented herein were obtained at the W. M. Keck Observatory, which is operated as a scientific partnership among the California Institute of Technology, the University of California, and NASA; the Observatory was made possible by the generous financial support of the W. M. Keck Foundation. We are grateful to the staffs of the Lick, Keck, and Palomar Observatories for their assistance. This research has made use of the NASA/IPAC Extragalactic Database (NED) which is operated by the Jet Propulsion Laboratory, California Institute of Technology, under contract with the National Aeronautics and Space Administration. A.G.-Y. acknowledges support by the Israeli Science Foundation, an EU Seventh Framework Programme Marie Curie IRG fellowship, the Benoziyo Center for Astrophysics, Minerva program, a research grant from the Peter and Patricia Gruber Awards, and the William Z. and Eda Bess Novick New Scientists Fund at the Weizmann Institute. A.V.F. is grateful for the support of US NSF grant AST-0607485, US Department of Energy grant DE-FG02-08ER41563, Gary and Cynthia Bengier, the Richard and Rhoda Goldman Fund, and the TABASGO Foundation.

Supplementary Information

(1) Technical observational details for figures 1 and 2

Figure 1 Panel (a) shows the image of NGC 1032 prior to SN 2005E explosion, obtained from the SDSS. Panel (b) shows the LOSS¹³ discovery of SN 2005E on Jan. 13, 2005. LOSS imaging of SN 2005E was obtained using the robotic 76-cm Katzman Automatic Imaging Telescope (KAIT) at Lick Observatory. Panel (c) shows an image of NGC 1032 in the light of the H α emission line, the panel shows the difference between images obtained using a narrow filter (6567 Å and a FWHM of 100Å) with a measured transmission of 40% for H alpha at the redshift of NGC 1032, plus broad R-band observations used for continuum subtraction. Exposure times of 1800 s, were obtained on Oct. 5, 2008 with the RATCam camera mounted on the 2-m Liverpool Telescope at Observatorio del Roque de Los Muchachos (La Palma, Spain). The smooth negative residual ($\sim 7\%$ of the original flux) near the galaxy core probably arises from a combination of slight color gradients of the smooth galactic old population, and H α absorption in the spectra of old stars, and does not indicate real line emission. Panel (d) shows a zoom-in on the location of SN 2005E in pre-explosion SDSS r -band images. Panels (e)-(f) show deep photometry of the SN location using the Low-Resolution Imaging Spectrometer (LRIS)³¹ mounted on the Keck-I 10-m telescope on Feb. 17, 2009 under very good conditions (seeing $\sim 0.7''$). Panel (e) shows a red image with a total exposure time of 840 s, reaching a point-source detection limit of $r < 25.3(25.9)$ mag at $3(2)\sigma$. Panel (f) shows a UV (u -band) image with a total exposure time of 780 s, reaching a point-source detection limit of $u < 24.7(25.7)$ mag at $3(2)\sigma$. Panel (g) shows a zoom-in on the location of SN 2005E in H α light (same observations used to produce panel (c)).

Figure 2 Upper panel: Photospheric spectra of SN 2005E. The top 2 spectra were obtained as part of the Caltech Core-Collapse Project (CCCP)³² using the double spectrograph³³ mounted on the 5-m Hale telescope at Palomar Observatory. Exposure times were 600 s and 900 s on 2006 January 16 and February 6, respectively, with the 158 lines mm^{-1} and 1,200 lines mm^{-1} gratings, yielding an instrumental resolution of ~ 5 Å and ~ 0.5 Å on the red and blue sides, respectively. The CCCP spectra were further rebinned to ~ 5 Å resolution bins to increase the signal-to-noise ratio. The bottom spectrum was obtained using LRIS³¹ mounted on the Keck I 10-m telescope on 2005 March 11. We took an exposure of 600 s using the 560 dichroic and the 400/8500 grating and 600/4000

grism, giving resolutions of 5.6 \AA and 2.4 \AA in the red and blue sides, respectively. For comparison we plot a nebular spectrum of SN 1991bg; see Ref. 30 for a detailed discussion.

(2) Can the progenitor of SN 2005E be a massive star formed in a star-forming region in the halo?

Massive stars are typically formed and observed in giant molecular clouds and young stellar clusters or associations.^{34,35} Core-collapse SNe of massive stars are therefore expected to be typically found close to star forming regions (SFRs). Observations of such SNe are usually consistent with this picture.³⁶ In principle, the discovery of SN 2005E in the halo of NGC 1032 could be attributed to in-situ star formation of a massive star rather than a low-mass older progenitor. However, star formation in the halo environment of a S0/a galaxy would be difficult to understand according to current star-formation theories. For example, star formation during collisions between cloudlets within high-velocity clouds at high galactic latitudes³⁷ has been shown to be much too rare.³⁸ Spiral density waves in the disk may trigger star formation up to a kpc above the Galactic plane,³⁹ but this seems unlikely for the larger height of SN 2005E (which also seems to be positioned beyond the edge of the optical disk). In addition, we note that NGC 1032 shows no evidence for warping or other structures extending beyond the region of the galactic disk to which SN 2005E could be related. We conclude that given the remote location of the supernova in the galactic halo, and the nondetection of any star-formation activity anywhere in the halo or the disk of NGC 1032, it is unlikely that an in-situ formation scenario could explain SN 2005E, unless a yet unknown and unique star-formation mechanism was at work in this case. In contrast, the evidence for a low-mass progenitor of SN 2005E is naturally consistent with the low-mass old stellar population environment in which it was found.

A search for nearby star-forming regions:

We have looked for star-formation tracers both in the halo and the disk of NGC 1032. Star-formation regions (SFRs) produce two classes of emission: continuum emission from young stars and emission lines (dominated by $H\alpha$) produced by ionized gas. We have searched for both classes of emission, and obtained upper limits on the star-formation rates.

$H\alpha$ observations:

$H\alpha$ imaging was obtained with the Liverpool Telescope, and then analyzed using similar methods to those described in detail elsewhere.³⁶ We have determined an upper

limit of 2.02×10^{-17} erg cm $^{-2}$ for the H α flux from the region of SN 2005E. This is a 3σ upper limit obtained from the variation in the sky background, for a $2''$ aperture centered on the SN position and calibrated using an R -band galaxy magnitude taken from the literature.⁴⁰ For the distance of NGC 1032 (34 Mpc) we infer an H α luminosity of 2.79×10^{36} erg s $^{-1}$; correcting this for Galactic extinction (0.098 mag) and for the contribution from [N II] lines⁴¹ we then calculate a corrected limit of $H\alpha_{\text{limit}} = 2.3 \times 10^{36}$ erg s $^{-1}$. Using the conversion rate from Ref. 10 (Eq. 2), we determine an upper limit on the star-formation rate at the SN position of $SFR_{\text{limit}} = 1.8 \times 10^{-5}$ M $_{\odot}$ yr $^{-1}$.

In addition, our H α observations of NGC 1032 show no SFRs closer than the galactic nucleus itself (see Fig. 1), up to our detection limit.

R - and u' -band observations:

Our deep R and u' -band observations using Keck (calibrated onto the SDSS photometric system) rule out point sources near the location of SN 2005E down to $u' < 24.7$ (25.7), $r < 25.3$ (25.9) mag at $3(2)\sigma$ (see Fig. 1). At the distance of NGC 1032, these limits ($M_r < -7.5$ (−6.9) and $M_{u'} < -8.1$ (−7.1) mag at $3(2)\sigma$, respectively) indicate that we would have detected faint star-forming galaxies or star-forming regions at the SN location, or indeed even individual red supergiant or luminous blue supergiant stars. Since massive stars are usually formed and observed in stellar clusters or associations,^{34,35} the lack of nearby supergiants (either red or blue) further argues against local star-formation activity.

Radio signature of a core-collapse SN:

A non-negligible fraction of core-collapse SNe show radio signatures. We have therefore made observations at 8.46 GHz with the VLA radio telescope on Jan. 21.10, 2005. We found a flux of $11 \pm 53 \mu\text{Jy}$ at the optical position of SN 2005E. At the distance of SN 2005E, and assuming an explosion date between Dec. 24, 2004 and Jan. 14, 2005, the radio luminosity limit (2σ) is 1.8×10^{26} erg s $^{-1}$ Hz $^{-1}$ which is a factor of 10 lower than a typical radio-emitting SNe Ib/c on this same timescale.⁴²

(3) Spectroscopic identification of SN 2005E as a type Ib supernova

In Fig. 2 we show optical spectra of SN 2005E. Our first spectrum (Fig. 2 top, blue curve) is clearly photospheric, dominated by absorption lines including the He I series at $\lambda\lambda 4471, 5876, 6678, 7065 \text{ \AA}$, blueshifted by $\sim 11,000$ km s $^{-1}$ (marked with black ticks at the top of Fig. 2), typical of a young SN Ib. Based on pre-discovery nondetections, SN 2005E was 3 – 20 days after explosion at this time. Analysis using the *Superfit* spectral

analysis code⁴³ confirms a type Ib identification, with the best-fit match being with a spectrum of the type Ib/c transition event SN 1999ex⁴⁴ 14 days after maximum light.

Our next spectrum (Fig. 2 middle, red curve) shows the beginning of the transition to the nebular phase, with emerging emission lines of oxygen and calcium. The best-fit spectrum found by *superfit* is that of the type Ic event SN 1990U, but spectra of the type Ib SN 1999di also provide a good fit. Masking of the blueshifted He I 6678 Å line by the emerging strong [O I] $\lambda\lambda$ 6300, 6364 nebular doublet may account for the similarity to type Ic supernovae, with intrinsically much weaker He I lines.

Strong nebular emission lines of [O I] $\lambda\lambda$ 6300, 6364 and [Ca II] $\lambda\lambda$ 7291, 7324 and the near-infrared triplet at $\lambda\lambda$ 8498, 8542, 8662 (tick marks at the bottom of Fig. 2) dominate our latest spectrum of SN 2005E (Fig. 2 bottom, magenta curve). The best fit found by *Superfit* is to the type Ib SN 1985F^{45,46} obtained 89 days after its first observation. Dominated by lines of intermediate-mass elements (O and Ca), the nebular spectrum of SN2005E is similar to that of type Ib events, though calcium is much stronger than usual for these SNe type, while the lack of Fe-group emission lines in the bluer part of the spectrum rules out an identification as a type Ia event of either the normal or subluminous (SN 1991bg like²) varieties.

(4) Ejected mass estimates from the observed light curve and photospheric velocities:

The ejecta mass of a given supernova can be estimated using its light curve and the observed ejecta velocities. The ejecta velocity of a SN is proportional to $(E_{\text{kin}}/M_{\text{ej}})^{1/2}$, where E_{kin} is the kinetic energy and the M_{ej} is the ejecta mass, while the typical duration of a SN light curve is $t_d \propto (M_{\text{ej}}^3/E_{\text{kin}})^{1/4}$.⁴⁷ Combining these equations and assuming that two objects have the same opacity, we have

$$E_{\text{kin},1}/E_{\text{kin},2} = \left(\frac{v_1}{v_2}\right)^3 \left(\frac{t_1}{t_2}\right)^2 \quad (1)$$

and

$$M_{\text{ej},1}/M_{\text{ej},2} = \frac{v_1}{v_2} \left(\frac{t_1}{t_2}\right)^2. \quad (2)$$

Following Ref. 20 who estimated the mass of the subluminous SN 2008ha, we use a normal SN Ia as a reference with $t_d = 19.5$ days and $v = 8,000$ km s⁻¹.⁴⁸ The timescales of SN 2005E are 0.4 – 0.5 times shorter than those of the well-observed type Ib SN 2008D (Fig. S1), which had a rise time of 18 days,⁴⁹ and therefore we estimate the rise time of SN 2005E to be 7 – 9 days. The ejecta velocities we observe from the

photospheric spectra are $11,000 \text{ km s}^{-1}$. We therefore find $E_{\text{kin},05\text{e}}/E_{\text{kin,Ia}} = 0.34\text{--}0.55$ and $M_{\text{ej},05\text{e}}/M_{\text{ej,Ia}} = 0.17\text{--}0.29$. Assuming $E_{\text{kin,Ia}} = 1.3 \times 10^{51} \text{ ergs}$ and $M_{\text{ej,Ia}} = 1.4 M_{\odot}$, we find $E_{\text{kin},05\text{e}} = (4.4\text{--}7.2) \times 10^{50} \text{ ergs}$ and $M_{\text{ej},05\text{e}} = 0.25\text{--}0.41 M_{\odot}$. We note that this widely used method for SN ejecta-mass estimation may have two caveats in our case: helium is less opaque than other elements so we may miss some of the helium mass, and ^{56}Ni may not be the only radioactive energy source as assumed in such estimates.

(5) The possible origin of SN 2005E from a hypervelocity star and its trajectory:

Most of the stars in the Galaxy move at relatively low velocities (a few tens of km s^{-1}) with respect to their Galactic environment. Some massive stars ($\gtrsim 8 M_{\odot}$) are known to have higher velocities, up to $\sim 200 \text{ km s}^{-1}$. These so-called “runaway stars” are ejected from their birth place as a result of binary encounters, or if they have binary companions that explode as SNe,^{52,53} and could therefore be found far from the SFR where they were formed. Hypervelocity stars⁵⁴ (HVSs) move at even higher velocities ($\text{few} \times 10^2\text{--}10^3 \text{ km s}^{-1}$). Such stars are thought to be ejected following dynamical interaction with (or close to) massive black holes.

In 2005, the first HVS was serendipitously discovered in the Galactic halo,⁵⁵ 71 kpc from the Galactic center, with a radial velocity of $853 \pm 12 \text{ km s}^{-1}$. Two additional HVSs, one of them a massive B star with $\sim 9 M_{\odot}$, were discovered shortly thereafter.^{56,57} Follow-up surveys have discovered a total of ~ 20 HVSs with radial velocities in the range $300\text{--}900 \text{ km s}^{-1}$ at distances of $20\text{--}120 \text{ kpc}$ from the Galactic center (GC). A total population of ~ 100 such young B stars is inferred to exist in the Galaxy at these distances (no main-sequence O stars are observed). Given their positions and velocities, all observed HVSs must have been ejected with even higher initial velocities ($> 850 \text{ km s}^{-1}$), if they originated near the massive black hole (MBH) in the center of our Galaxy whose mass is $\sim 3.6 \times 10^6 M_{\odot}$.^{58,59}

If the progenitor of SN 2005E was a massive star, it could have formed in the center or the disk of NGC 1032 and then have been ejected at high velocity to attain its observed location in the halo. In order to find the ejection velocity required for the progenitor of SN 2005E to travel from its birth place to the observed position of SN 2005E, we need to trace its possible trajectory. For this purpose we need to assume some galactic potential for NGC 1032 to be used for the calculations of the HVS trajectory. For the galactic potential we use a two-component model suggested in Ref. 60 composed of a galactic bulge, and a halo (the disk component has a relatively small effect). Ref. 9 finds the virial mass of

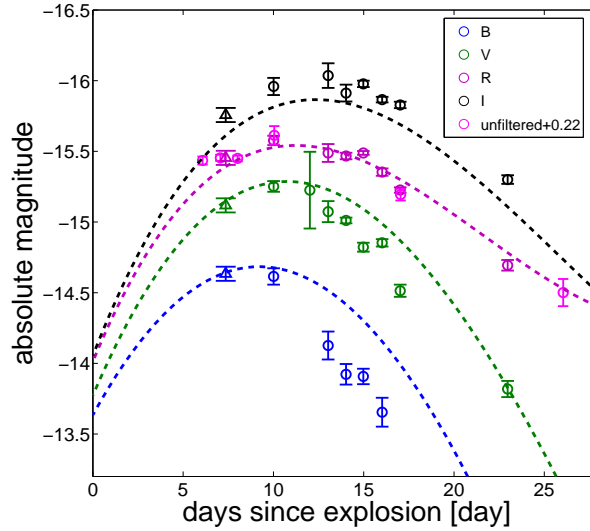


Figure 4. Optical light curves of SN 2005E. Top: We present our observations obtained using the 0.76-m KAIT as part of LOSS¹³ in the *BVRI* bands (blue, green, red, and black empty circles, respectively), as well as unfiltered data (magenta empty circles). Additional point (triangle) was obtained through synthesis of the first spectrum (seen in Fig. 1), scaled to fit the *R*-band photometry. KAIT unfiltered observations are most similar to *R*-band data due to the combined response of its optics and detector, so we have scaled these data to the *R*-band observations. The rapid decline of this object is consistent⁵⁰ with its relatively low absolute magnitude, $M_R \approx -15.5$, calculated assuming a distance of 34 Mpc to NGC 1032 (as given in the NED database⁵¹) and negligible extinction. Estimating the peak date of this SN from the magenta curve (January 7, 2005), our spectra (Fig. 2) were obtained 9, 29, and 62 days after maximum light. The rapid decline observed in the light curve is similar to that of observed subluminous SNe Ia at early times, with a slope of $-0.155 \text{ mag day}^{-1}$, but it does not show a break to a different slope expected at ~ 4.5 days after peak (compare with the analysis of Kasliwal et al.³). Also shown for comparison are third order polynomial fits to the light curves of the well-studied type Ib SN 2008D.⁴⁹ We find that SN 2005E behaves similarly to SN 2008D, but with timescales roughly a factor of 0.45–0.55 shorter (the displayed light curves of SN 2008D are compressed by a factor of 0.52).

galaxies such as NGC 1032 to be $\sim 1.5 \times 10^{12} M_{\odot}$ for magnitudes $-19.5 < M_B < -20.5$ where NGC 1032 has $M_B = -19.8$ mag. This mass is also generally consistent with the formulas in Ref. 61, which gives a total galactic mass of $(2-3) \times 10^{12} M_{\odot}$ from the relation found for the MBH mass and the halo mass. The bulge mass could be estimated from the velocity dispersion in the bulge⁶² to be between $6 \times 10^{10} M_{\odot}$ and $1.3 \times 10^{11} M_{\odot}$, where the bulge size is ~ 1.85 kpc.⁶²

The inferred ejection velocity of the progenitor of SN 2005E from a birth place in the disk (taking the shortest distance from the observed position of SN 2005E to the plane of the galactic disk) is found to be $> 1600 \text{ km s}^{-1}$ for a massive ($\sim 25 M_{\odot}$), short-lived ($\sim 7 \times 10^6$ yr) progenitor, appropriate for a type Ib SN. Such an ejection velocity from the galactic disk would require an ejection mechanism different from that of OB runaways, where the only suggested mechanisms involve an interaction with a MBH. Such a MBH is unlikely to exist in the galactic disk. An ejection velocity of $> 300 \text{ km s}^{-1}$ would be required for a lower mass ($\sim 8 M_{\odot}$) and longer lived ($\sim 4 \times 10^7$ yr) component in a binary progenitor ejected from the disk. Such a velocity is much higher than the typical velocities of OB runaway stars,⁵³ but it could theoretically be accessible for a runaway single star.⁶³ However, runaway binaries are typically ejected at lower velocities (up to 0.3–0.4 of the maximal ejection velocities of single stars⁶⁴), which would again suggest a different ejection mechanism than OB runaways. We conclude that the progenitor of SN 2005E is unlikely to be ejected from the disk by currently suggested high-velocity ejection mechanisms, and (if ejected at all) was more likely to be ejected from the center of NGC 1032.

For the progenitor of SN 2005E to be ejected from the galactic center and reach its current position in the halo during its lifetime, the required ejection velocity would be at least $\sim 3400 \text{ km s}^{-1}$ ($\sim 1600 \text{ km s}^{-1}$) assuming a lifetime of < 7 Myr for a $25 M_{\odot}$ star (< 40 Myr for an $8 M_{\odot}$ binary star). We now calculate whether such ejection velocities are likely, taking into account the conditions in NGC 1032.

Given the velocity dispersion in the bulge of NGC 1032, which is in the range⁶² 200–225 km s^{-1} , we can estimate the mass of the MBH in the nucleus using the $M - \sigma$ relation^{65,66} to be in the range $\sim (1-2) \times 10^8 M_{\odot}$.

We now compare the velocities derived from the trajectories with the average ejection velocity of a star ejected from the galactic nucleus following the disruption of a binary by

a MBH, given by^{67,68}

$$v_{\text{eject}} = 3400 \text{ km s}^{-1} \times \left(\frac{a_{\text{bin}}}{0.8 \text{ AU}} \right)^{-1/2} \left(\frac{M_{\text{bin}}}{50 M_{\odot}} \right)^{1/3} \left(\frac{M_{\text{BH}}}{1.5 \times 10^8 M_{\odot}} \right)^{1/6},$$

where a_{bin} is the semi-major axis of the binary, M_{bin} is the binary mass, and M_{BH} is the MBH mass. Massive binaries usually have components of comparable and frequently equal mass, and are known to have relatively compact orbits, with a large fraction of them ($f_{\text{cbin}} \approx 0.4$) in close binaries ($a_{\text{bin}} < 1 \text{ AU}$; e.g., Refs.^{69–71}). We therefore conclude that the observed position of SN 2005E is consistent with its progenitor being ejected as a massive star following the disruption of a typical very massive binary of $M_{\text{bin}} = 2 \times 25 = 50 M_{\odot}$ and $a_{\text{bin}} \lesssim 0.8 \text{ AU}$, or the disruption of a $M_{\text{triple}} = 3 \times 8 = 24 M_{\odot}$ triple star, with an outer semi-major axis of $a_{\text{bin}} \lesssim 1.5 \text{ AU}$, which would eject a hypervelocity binary.⁷²

The velocity of an observed supernova is difficult to measure. The measured velocities of the supernova ejecta are on the order of a few thousands km s^{-1} and any signature of a pre-explosion velocity of the progenitor is smeared out even for velocities as high as hundreds of km s^{-1} . Even for higher velocities such as expected for a HVS, one would require extreme velocities for the HVS, directed along the line of sight, in order to identify a significant signature of the SN HVS progenitor. The velocities we find for SN 2005E ejecta velocities are consistent with other SN Ib/c ejecta velocities at the various epochs.

(6) The ejection rate of hypervelocity stars:

Although two massive HVS ($> 8 M_{\odot}$; Refs.^{56,73}) are known in our Galaxy, it is difficult to infer the total number of Galactic massive HVSs from the very few examples known, given their serendipitous discovery nature. An estimate can be obtained if most massive HVSs in our Galaxy have been ejected through the Hills binary disruption mechanism^{54,74} (which is the likely case^{75–77}). In this scenario the binary companions of ejected HVSs should have been captured into close orbits around the MBH^{78,74}; the number of such stars should therefore reflect the number of similar HVSs in the Galaxy. Currently, a few tens of main-sequence B stars are observed in such close orbits ($< 0.04 \text{ pc}$ from the MBH; e.g. Ref. 79). Approximately half of these stars (with identified stellar types) are found to be B0–2 V main sequence stars, most likely with masses $> 8 M_{\odot}$. Given the trend of massive binaries to have equal-mass components,⁶⁹ one can then infer a total of ~ 10 – 20 such massive HVSs in our Galaxy. The total number of $> 8 M_{\odot}$ stars in the Galaxy is $\sim 10^6$ stars (e.g., assuming a Miller-Scalo initial mass function); thus, the HVS fraction of the population of massive stars is $\sim 10/10^6 = 10^{-5}$, and we therefore expect a similar fraction of HVS supernova progenitors. If the progenitor of SN 2005E was a

Table 1. The sample of calcium-rich SNe

SN	Absolute B -band peak magnitude	Absolute B -band discovery magnitude	Host galaxy	Host-galaxy type
2000ds	?	-14.35	NGC 2768	E/S0
2001co	-16.12	-15.8	NGC 5559	Sb
2003H	?	-14.46	NGC 2207	Galaxy pair
2003dg	?	-16.06	UGC 6934	Scd
2003dr	-14.04	-13.7	NGC 5714	Sc
2005E	-14.8	-14.7	NGC 1132	S0/Sa
2007ke	-15.45*	-14.7*	NGC 1129	E/S0

Table 2. * B magnitude unavailable; unfiltered used, corrected to B using the measured colors of SN 2005E at peak.

hypervelocity star, the probability of discovering SN 2005E in LOSS, which detected a total of ~ 550 core-collapse SNe from 1998 through 2008, is low. Its discovery would then be either a chance observation of a rare event, or suggests a much higher ejection rate of extragalactic HVSs than observed in our Galaxy. However, given the low-mass ejecta observed for SN 2005E and its additional peculiarities, which cannot be explained by a hypervelocity progenitor, it is more likely that SN 2005E has a different origin.

(7) Additional calcium-rich faint type Ib/c SNe:

In addition to SN 2005E, several other objects were reported as possible members of this class of calcium-rich SNe. We have verified these reports by re-inspection of the spectra, rejecting unconvincing cases, and list all verified Ca-rich events in Table 1.

A full analysis of the photometry and spectroscopy of this extended sample will be presented in a forthcoming publication.

(8) Masses and luminosities of SNe:

In Fig. 3 we compared the nickel mass and the total mass and luminosity of SN 2005E with those of other SNe. The data used in this figure were taken from the literature, as follows. The data for SNe Ia were taken from Ref. 4 and references therein; it includes both typical SNe as well as peculiar and subluminous SNe. The data for SNe Ib/c were collected from Refs. 80, 81, 82, 83, and 84. Additional data concerning the ejected Ni mass were taken from Ref. 85. The data for SNe II were taken from Refs. 86 and 87, and contain both regular and subluminous SNe, most of them SNe IIP.

(9) Nucleosynthetic simulations:

We ran several single-zone simulations using the JINA version of ReacLib (April 2009) for the rates, a 203-nucleus network, and the “explosive nucleosynthesis” procedure.¹⁴ We investigated various initial compositions of He, C, and O, at an density of 10^6 g cm^{-3} , and scanned the temperature range $(2\text{--}4.1) \times 10^9 \text{ K}$. Our main findings are illustrated in Fig. S2 and Table S2. In Fig. S2, we scale the mass fractions to fit the observed calcium abundance, and plot the observed limits on sulfur and ^{56}Ni . We also present the amount of ^{44}Ti produced. A 0.6/0.4 mix of He/O **(a)** works well in reproducing our data only up to $T_9 = 3.5$ where nickel becomes overabundant, and certainly fails at higher T , where S is also a problem. In the allowed phase space ($T_9 < 3.5$), ^{44}Ti is 0.1–0.3 times as abundant as Ca. Increasing the amount of helium **(b)**, only low temperatures ($T_9 = 2.2$) are allowed; in this case radioactive titanium and calcium are almost equally produced. Replacing oxygen by pure carbon **(c)** does not work for nearly equal ratios, as we either get too much S or too much Ni, or both. Decreasing the amount of carbon **(d)** again works only for the lowest temperatures, $T_9 = 2.2$, leading to significant production of ^{44}Ti .

We conclude that helium-rich models with some C/O contamination can recover our essential findings. A prediction is that a substantial amount of ^{44}Ti (at least 1/10 of Ca, and perhaps a comparable amount) will be synthesized. In some cases ^{48}Cr production exceeds that of ^{56}Ni ; its decay may therefore power the light curve (via ^{48}V decay). A realistic model in which the burning shock traverses layers of varying temperature, density, and composition will be investigated in a forthcoming publication.

(10) The origin of SN 2008ha-like SNe:

We note that the low luminosity and calcium-rich late-time spectra of the recently discovered SN 2008ha^{20,21} (see Fig. 7 of Ref. 20), may relate it to our group of calcium-rich faint SNe. Its type Ia identification suggests that its composition contains a larger fraction of C/O burning products than observed for SN 2005E. The first models suggesting the production of calcium-rich SNe through helium detonations^{7,15} showed that helium burning on C/O WDs could produce calcium-rich SNe with various ejecta masses and luminosities, depending on the specific initial conditions used, and could sometimes lead to a C/O deflagration of the accreting WD. One could therefore expect a range of outcomes with varying mixtures of helium (Ca, Ti) and C/O burning (S, Si, Fe, Ni) products. This could be consistent with the wide variety of luminosities (and likely ejecta masses) found in other SNe similar to SN 2008ha,^{88,89,20,21} including the helium-rich SN 2007J. If the

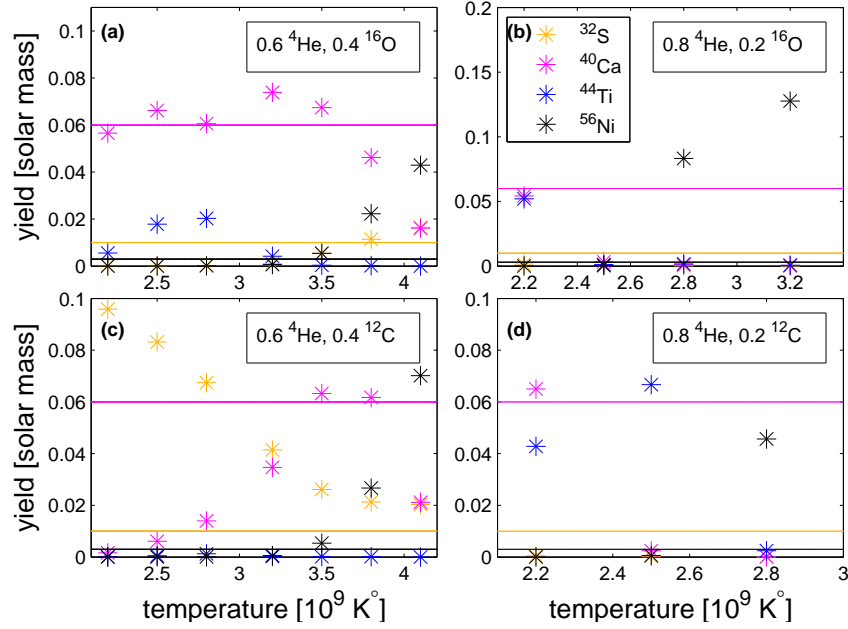


Figure 5. Nucleosynthetic products of the burning of He-rich mixtures with carbon and oxygen (fractions marked in each panel), at various temperatures and an initial density of 10^6 g cm $^{-3}$. The fractions are scaled to best match the observed calcium mass (cyan horizontal line) and compared with the observed limit on sulfur (orange line) and measurement of radioactive ^{56}Ni (black line).

Initial Conditions			Final Values					
T_9	${}^4\text{He}$	${}^{12}\text{C}$	${}^{32}\text{S}$	${}^{40}\text{Ca}$	${}^{44}\text{Ti}$	${}^{48}\text{Cr}$	${}^{52}\text{Fe}$	${}^{56}\text{Ni}$
3.4	8.00×10^{-1}	1.86×10^{-1}	6.18×10^{-5}	1.97×10^{-4}	2.68×10^{-4}	1.34×10^{-4}	2.82×10^{-4}	8.08×10^{-1}
3.4	7.50×10^{-1}	2.36×10^{-1}	2.80×10^{-4}	1.30×10^{-1}	5.03×10^{-3}	9.03×10^{-3}	2.29×10^{-1}	5.82×10^{-1}
3.4	7.00×10^{-1}	2.86×10^{-1}	2.49×10^{-3}	6.10×10^{-1}	1.60×10^{-1}	3.04×10^{-2}	1.65×10^{-1}	1.18×10^{-1}
3.4	6.50×10^{-1}	3.36×10^{-1}	1.12×10^{-1}	5.61×10^{-1}	2.63×10^{-3}	1.84×10^{-2}	2.00×10^{-2}	2.78×10^{-2}
3.4	6.00×10^{-1}	3.86×10^{-1}	2.09×10^{-1}	3.74×10^{-1}	1.13×10^{-3}	9.84×10^{-3}	8.01×10^{-3}	1.97×10^{-2}
3.2	8.00×10^{-1}	1.86×10^{-1}	5.25×10^{-5}	1.74×10^{-4}	2.36×10^{-4}	1.18×10^{-4}	3.15×10^{-4}	8.29×10^{-1}
3.2	7.50×10^{-1}	2.36×10^{-1}	1.69×10^{-6}	1.24×10^{-1}	3.94×10^{-1}	6.66×10^{-2}	4.33×10^{-1}	2.50×10^{-1}
3.2	7.00×10^{-1}	2.86×10^{-1}	4.32×10^{-4}	6.55×10^{-1}	1.14×10^{-1}	8.00×10^{-2}	7.49×10^{-2}	1.95×10^{-2}
3.2	6.80×10^{-1}	2.86×10^{-1}	2.73×10^{-2}	6.76×10^{-1}	2.43×10^{-2}	2.79×10^{-2}	1.37×10^{-2}	9.83×10^{-3}
3.2	6.50×10^{-1}	3.36×10^{-1}	1.63×10^{-1}	4.18×10^{-1}	4.75×10^{-3}	1.07×10^{-2}	4.35×10^{-3}	6.86×10^{-3}
3.2	6.00×10^{-1}	3.86×10^{-1}	2.90×10^{-1}	2.43×10^{-1}	1.56×10^{-3}	5.29×10^{-3}	1.95×10^{-3}	4.02×10^{-3}
3.0	8.00×10^{-1}	1.86×10^{-1}	6.06×10^{-5}	2.15×10^{-4}	3.26×10^{-4}	2.38×10^{-4}	8.69×10^{-2}	7.50×10^{-1}
3.0	7.50×10^{-1}	2.36×10^{-1}	3.85×10^{-9}	2.96×10^{-2}	1.73×10^{-1}	1.78×10^{-1}	4.53×10^{-1}	1.24×10^{-1}
3.0	7.00×10^{-1}	2.86×10^{-1}	1.06×10^{-3}	5.72×10^{-1}	2.71×10^{-1}	4.41×10^{-2}	9.32×10^{-3}	4.16×10^{-3}
3.0	6.50×10^{-1}	3.36×10^{-1}	2.40×10^{-1}	2.88×10^{-1}	2.91×10^{-2}	3.77×10^{-3}	7.91×10^{-4}	2.34×10^{-3}
3.0	6.00×10^{-1}	3.86×10^{-1}	3.85×10^{-1}	1.53×10^{-1}	1.14×10^{-1}	1.51×10^{-3}	2.47×10^{-4}	1.44×10^{-3}

Table 3. The abundances (by mass) of several important nuclei from post-shock burning in a helium-burning layer. A 203-nucleus network was used, with reaction rates taken from an April 2009 download of ReacLib from JINA. The initial composition was ${}^4\text{He}$, ${}^{12}\text{C}$ (see table for initial values; temperature T_9 given in 10^9 K), and 0.014 of ${}^{22}\text{Ne}$ by mass. The values of ${}^4\text{He}$ and ${}^{12}\text{C}$ correspond to different degrees of hydrostatic helium burning prior to explosion. Low values for S/Ca occur only for high ${}^4\text{He}$ abundance. For such low S/Ca, temperature must be $T < 3.2 \times 10^9$ K to avoid overproduction of ${}^{56}\text{Ni}$. Production of ${}^{48}\text{Cr}$ (and ${}^{52}\text{Fe}$) may exceed that of ${}^{56}\text{Ni}$, so that ${}^{48}\text{V}$ decay (half-life 15.98 days) may help power the light curve.¹⁸ ${}^{44}\text{Ti}$ can be copiously produced under these conditions, so that such events may provide a solution to the problem of low emission from ${}^{44}\text{Ti}$ decay. The significant abundance of ${}^{12}\text{C}$ prior to the explosive burning may allow unburned (lower density) regions to explain the relatively large abundance of ${}^{12}\text{C}$ observed. To convert the abundance entries to solar mass units, multiply by the assumed mass of ejecta.

possibility raised here is correct, we expect events of this distinct class of SNe (so-called SN 2002cx-like SNe^{88,89}) to show a calcium-enhanced composition. Such a prediction could be checked in the future through spectral analysis of these SNe.

Chapter 14

Glossary, quantities and useful relations

14.1 GLOSSARY

The following abbreviations appear either in the introductory text or in the published papers in this Thesis.

BH	—	Black hole (general term when black holes of any mass are implied.)
BHB	—	Blue horizontal branch
BMBH	—	Binary massive black hole
BSS	—	Blue straggler star
CO	—	Compact object
CR	—	Compact remnant
DF	—	Distribution function
DM	—	Dark matter
EMRI	—	Extreme mass ratio inspiral source
GC	—	Galactic center
GR	—	General relativity
GW	—	Gravitational wave
HVS	—	Hypervelocity star
IBH	—	Intermediate mass black hole
IMBH	—	Intermediate mass black hole
LISA	—	Laser interferometer space antenna
LSO	—	Last stable orbit
MBH	—	Massive black hole
MC	—	Monte Carlo
MP	—	Massive Perturber
MS	—	Main sequence
NR	—	Non-resonant
NS	—	Neutron star
RLOF	—	Roche lobe overflow
RR	—	Resonant relaxation
SBH	—	Stellar black hole
SN	—	Supernova
TAMS	—	Terminal age main sequence
WD	—	White dwarf
ZAMS	—	Zero age main sequence

14.2 SOME ASTROPHYSICAL QUANTITIES AND USEFUL RELATIONS

Galactic Massive Black Hole

Mass of the Galactic MBH¹: $M_{\bullet} = (3.6 \pm 0.3) \times 10^6 M_{\odot}$

Schwarzschild radius of Galactic MBH: $r_S = \frac{2GM_{\bullet}}{c^2} = 10^{12} \text{ cm}$

Tidal radius of Solar type star near Galactic MBH: $r_t = \left(\frac{M_{\bullet}}{M_{\odot}}\right)^{1/3} R_{\odot} = 10^{13} \text{ cm}$.

Distance to the Galactic center²: $D = 7.62 \pm 0.32 \text{ kpc}$

Dynamical time in GC: $t_d \sim 300 \text{ yr}$ (at 0.03 pc); $t_d \sim 0.2 \text{ Myr}$ (at 3 pc);

Relaxation time in GC: $t_r \sim \frac{0.34\sigma^3}{(GM_{\bullet})^2 n_{\star} \ln \Lambda} \sim \text{few Gyr}$

Keplerian relations

Keplerian relations for energy \mathcal{E} , semi-major axis a , period P , eccentricity e , angular momentum J , circular angular momentum J_c , periapse r_p :

$$a = \frac{GM_{\bullet}}{2\mathcal{E}}; \quad P = \frac{2\pi a^{3/2}}{\sqrt{GM_{\bullet}}} = 2\pi \frac{GM_{\bullet}}{(2\mathcal{E})^{3/2}}; \quad e = 1 - r_p/a = \sqrt{1 - \left(\frac{J}{J_c}\right)^2}$$

$$J_c = \sqrt{GM_{\bullet}a} = \frac{GM_{\bullet}}{\sqrt{2\mathcal{E}}}; \quad J = \sqrt{GM_{\bullet}(1+e)r_p}; \quad r_p = (1-e)a;$$

Distribution functions

Relation between the number of stars $n(\mathcal{E})d\mathcal{E}$ with energies in the range $(\mathcal{E}, \mathcal{E} + d\mathcal{E})$ and the distribution function $f(\mathcal{E})$ (stars per unit $dx^3 dv^3$) for a spherically symmetric system dominated by a Keplerian potential:

$$n(\mathcal{E}) = \pi^3 \sqrt{2} (GM_{\bullet})^3 \mathcal{E}^{-5/2} f(\mathcal{E})$$

Relation between the number density of stars $n(r)$ and the distribution function $f(\mathcal{E})$ (stars per unit $dx^3 dv^3$) for a spherically symmetric system dominated by a Keplerian potential:

$$n(r) = 4\sqrt{2}\pi \int_{-\infty}^{GM_{\bullet}/r} d\mathcal{E} f(\mathcal{E}) \sqrt{\frac{GM_{\bullet}}{r} - \mathcal{E}}$$

General relativity

¹[29]

²[29]

Last stable orbit in GR: $J_{\text{LSO}} = \frac{4GM_\bullet}{c} = \sqrt{8GM_\bullet r_S}$.

Energy and angular momentum losses to GWs for star of mass M_\star orbiting a MBH of mass M_\bullet :

$$\Delta\mathcal{E}_{\text{GW}} = \frac{8\pi}{5\sqrt{2}} f(e) \frac{M_\star c^2}{M_\bullet} \left(\frac{r_p}{r_S} \right)^{-7/2} ; \quad f(e) = \frac{1 + \frac{73}{24}e^2 + \frac{37}{96}e^4}{(1+e)^{7/2}}$$

$$\Delta J_{\text{GW}} = -\frac{16\pi}{5} g(e) \frac{GM_\star}{c} \left(\frac{r_p}{r_S} \right)^{-2} ; \quad g(e) = \frac{1 + \frac{7}{8}e^2}{(1+e)^2}$$

Chapter 15

Bibliography

- [1] Alexander, T. 2005, *Phys. Rep.*, 419, 65
- [2] —. 2007, *ArXiv:0708.0688*
- [3] Alexander, T. & Hopman, C. 2003, *ApJL*, 590, L29
- [4] —. 2009, *ApJ*, 697, 1861
- [5] Alexander, T. & Sternberg, A. 1999, *ApJ*, 520, 137
- [6] Allen, D. A., Hyland, A. R., & Hillier, D. J. 1990, *MNRAS*, 244, 706
- [7] Amir, A., Lahini, Y., & Perets, H. B. 2009, *PRE*, in press (*ArXiv:0902.0890*)
- [8] Baganoff, F. K. et al. 2003, *ApJ*, 591, 891
- [9] Bahcall, J. N. & Wolf, R. A. 1976, *ApJ*, 209, 214
- [10] —. 1977, *ApJ*, 216, 883
- [11] Bailey, M. E. 1983, *MNRAS*, 204, 603
- [12] Bartko, H. et al. 2009, *ApJ*, 697, 1741
- [13] Baumgardt, H., Makino, J., & Ebisuzaki, T. 2004, *ApJ*, 613, 1143
- [14] Berczik, P., Merritt, D., & Spurzem, R. 2005, *ApJ*, 633, 680
- [15] Berczik, P., Merritt, D., Spurzem, R., & Bischof, H.-P. 2006, *ApJL*, 642, L21
- [16] Binney, J. & Tremaine, S. 1987, *Galactic Dynamics* (Princeton, NJ: Princeton University Press)
- [17] Bromley, B. C. et al. 2006, *ApJ*, 653, 1194
- [18] Brown, W. R., Geller, M. J., & Kenyon, S. J. 2009, *ApJ*, 690, 1639

- [19] Brown, W. R., Geller, M. J., Kenyon, S. J., & Kurtz, M. J. 2006, *ApJL*, 640, L35
- [20] Brown, W. R. & others. 2005, *ApJL*, 622, L33
- [21] Brown, W. R. et al. 2006, *ApJ*, 647, 303
- [22] —. 2007, *ApJ*, 660, 311
- [23] —. 2007, *ApJ*, 671, 1708
- [24] Chandrasekhar, S. 1943, *ApJ*, 97, 255
- [25] Cohn, H. & Kulsrud, R. M. 1978, *ApJ*, 226, 1087
- [26] Cox, A. N. 2000, *Allen’s astrophysical quantities* (New York: AIP Press; Springer, 4th ed.)
- [27] Eckart, A., Ott, T., & Genzel, R. 1999, *A&A*, 352, L22
- [28] Edelman, H., Napiwotzki, R., Heber, U., Christlieb, N., & Reimers, D. 2005, *ApJL*, 634, L181
- [29] Eisenhauer, F. et al. 2005, *ApJ*, 628, 246
- [30] Ferrarese, L. & Ford, H. 2005, *Space Science Reviews*, 116, 523
- [31] Ferrarese, L. & Merritt, D. 2000, *ApJL*, 539, L9
- [32] Figer, D. F. et al. 2000, *ApJL*, 533, L49
- [33] Forrest, W. J., Shure, M. A., Pipher, J. L., & Woodward, C. E. 1987, in *AIP Conf. Proc. 155: The Galactic Center*, 153–+
- [34] Frank, J. & Rees, M. J. 1976, *MNRAS*, 176, 633
- [35] Freitag, M., Amaro-Seoane, P., & Kalogera, V. 2006, *ApJ*, 649, 91
- [36] Freitag, M. & Benz, W. 2002, *A&A*, 394, 345
- [37] Fuentes, C. I., Stanek, K. Z., Gaudi, B. S., McLeod, B. A., Bogdanov, S., Hartman, J. D., Hickox, R. C., & Holman, M. J. 2006, *ApJL*, 636, L37
- [38] Gebhardt, K. et al. 2000, *ApJL*, 539, L13
- [39] —. 2003, *ApJ*, 583, 92
- [40] Genzel, R., Eckart, A., Ott, T., & Eisenhauer, F. 1997, *MNRAS*, 291, 219
- [41] Genzel, R., Pichon, C., Eckart, A., Gerhard, O. E., & Ott, T. 2000, *MNRAS*, 317, 348
- [42] Genzel, R., Thatte, N., Krabbe, A., Kroker, H., & Tacconi-Garman, L. E. 1996, *ApJ*, 472, 153

- [43] Genzel, R. et al. 2003, *ApJ*, 594, 812
- [44] Gerhard, O. E. & Binney, J. 1985, *MNRAS*, 216, 467
- [45] Gezari, S., Ghez, A. M., Becklin, E. E., Larkin, J., McLean, I. S., & Morris, M. 2002, *ApJ*, 576, 790
- [46] Gezari, S., Halpern, J. P., Komossa, S., Grupe, D., & Leighly, K. M. 2003, *ApJ*, 592, 42
- [47] Gezari, S. et al. 2006, *ApJL*, 653, L25
- [48] Ghez, A. M. et al. 2003, *ApJL*, 586, L127
- [49] —. 2005, *ApJ*, 620, 744
- [50] Gillessen, S. et al. 2009, *ApJ*, 692, 1075
- [51] Gould, A. & Quillen, A. C. 2003, *ApJ*, 592, 935
- [52] Haller, J. W., Rieke, M. J., Rieke, G. H., Tamblyn, P., Close, L., & Melia, F. 1996, *ApJ*, 456, 194
- [53] Hansen, B. M. S. & Milosavljević, M. 2003, *ApJL*, 593, L77
- [54] Hills, J. G. 1981, *AJ*, 86, 1730
- [55] —. 1988, *Nature*, 331, 687
- [56] —. 1991, *AJ*, 102, 704
- [57] —. 1992, *AJ*, 103, 1955
- [58] Holley-Bockelmann, K. & Sigurdsson, S. 2006, submitted to *MNRAS* (ArXiv:astro-ph/0601520)
- [59] Hopman, C. 2006, PhD thesis, Weizmann Institute of Science
- [60] Hopman, C. & Alexander, T. 2005, *ApJ*, 629, 362
- [61] —. 2006, *ApJ*, 645, 1152
- [62] —. 2006, *ApJL*, 645, L133
- [63] Kenyon, S. J. et al. 2008, *ApJ*, 680, 312
- [64] Kollmeier, J. A. & Gould, A. 2007, *ApJ*, 664, 343
- [65] Kormendy, J. & Richstone, D. 1995, *ARAA*, 33, 581
- [66] Krabbe, A. et al. 1995, *ApJL*, 447, L95
- [67] Levin, Y. 2006, *ApJ*, 653, 1203
- [68] —. 2007, *MNRAS*, 374, 515

- [69] Levin, Y. & Beloborodov, A. M. 2003, *ApJL*, 590, L33
- [70] Levin, Y., Wu, A., & Thommes, E. 2005, *ApJ*, 635, 341
- [71] Lightman, A. P. & Shapiro, S. L. 1977, *ApJ*, 211, 244
- [72] Löckmann, U. & Baumgardt, H. 2007, *ArXiv*:0711.1326
- [73] Lopez-Morales, M. & Bonanos, A. Z. 2008, *ArXiv*: 0802.2945
- [74] Lu, J. R. et al. 2009, *ApJ*, 690, 1463
- [75] Magorrian, J. & Tremaine, S. 1999, *MNRAS*, 309, 447
- [76] Magorrian, J. et al. 1998, *AJ*, 115, 2285
- [77] Maoz, E. 1998, *ApJL*, 494, L181
- [78] Martins, F., Gillessen, S., Eisenhauer, F., Genzel, R., Ott, T., & Trippe, S. 2008, *ApJL*, 672, L119
- [79] McGinn, M. T., Sellgren, K., Becklin, E. E., & Hall, D. N. B. 1989, *ApJ*, 338, 824
- [80] Merritt, D. & Milosavljević, M. 2005, *Living Reviews in Relativity*, 8, 8
- [81] Merritt, D. & Poon, M. Y. 2004, *ApJ*, 606, 788
- [82] Miller, M. C. et al. 2005, *ApJL*, 631, L117
- [83] Milosavljević, M., Merritt, D., Rest, A., & van den Bosch, F. C. 2002, *MNRAS*, 331, L51
- [84] Miralda-Escudé, J. & Gould, A. 2000, *ApJ*, 545, 847
- [85] Murphy, B. W., Cohn, H. N., & Durisen, R. H. 1991, *ApJ*, 370, 60
- [86] Najarro, F., Krabbe, A., Genzel, R., Lutz, D., Kudritzki, R. P., & Hillier, D. J. 1997, *A&A*, 325, 700
- [87] Norman, C. & Silk, J. 1983, *ApJ*, 266, 502
- [88] O’Leary, R. M. & Loeb, A. 2007, *MNRAS*, 1076
- [89] Paumard, T. 2004, in *Proc XXXIXth Moriond meeting: Young Local Universe*, ed. A. Chalabaev, T. Fukui, T. Montmerle, & T. J. (Paris: Editions Frontieres), in press, available at <http://arXiv.org/abs/astro-ph/0407189>
- [90] Paumard, T. et al. 2006, *ApJ*, 643, 1011
- [91] Perets, H. B. 2008, *ArXiv*: 0802.1004
- [92] —. 2009, *ApJ*, 690, 795

- [93] Perets, H. B. & Alexander, T. 2008, *ApJ*, 677, 146
- [94] Perets, H. B. & Fabrycky, D. C. 2009, *ApJ*, 697, 1048
- [95] Perets, H. B., Gualandris, A., Kupi, G., Merritt, D., & Alexander, T. 2009, *ArXiv:0903.2912*
- [96] Perets, H. B., Hopman, C., & Alexander, T. 2007, *ApJ*, 656, 709
- [97] Perets, H. B., Lederhendler, A., Biham, O., Vidali, G., Li, L., Swords, S., Congiu, E., Roser, J., Manicó, G., Brucato, J. R., & Pirronello, V. 2007, *ApJL*, 661, L163
- [98] Perets, H. B. & Naoz, S. 2008, *ApJL*, in press (*ArXiv:0809.2095*)
- [99] Perets, H. B. et al. 2008, *Physical Review Letters*, 100, 170506
- [100] —. 2009, *ApJ*, 697, 2096
- [101] Peters, P. C. 1964, *Physical Review*, 136, 1224
- [102] Polnarev, A. G. & Rees, M. J. 1994, *A&A*, 283, 301
- [103] Preto, M., Merritt, D., & Spurzem, R. 2004, *ApJL*, 613, L109
- [104] Przybilla, N. et al. 2008, *A&A*, 488, L51
- [105] Rauch, K. P. & Ingalls, B. 1998, *MNRAS*, 299, 1231
- [106] Rauch, K. P. & Tremaine, S. 1996, *New Astronomy*, 1, 149
- [107] Schneider, P., Ehlers, J., & Falco, E. E. 1992, *Gravitational Lenses (Gravitational Lenses, XIV, 560 pp. 112 figs.. Springer-Verlag Berlin Heidelberg New York. Also Astronomy and Astrophysics Library)*
- [108] Schödel, R., Ott, T., Genzel, R., Eckart, A., Mouawad, N., & Alexander, T. E. 2003, *ApJ*, 596, 1015
- [109] Schödel, R. et al. 2002, *Nature*, 419, 694
- [110] Shapiro, S. L. & Teukolsky, S. A. 1983, *Black holes, white dwarfs, and neutron stars: The physics of compact objects (Research supported by the National Science Foundation. New York, Wiley-Interscience, 1983, 663 p.)*
- [111] Sherwin, B. D., Loeb, A., & O’Leary, R. M. 2007, *ArXiv: 0709.1156*
- [112] Spitzer, L. J. & Schwarzschild, M. 1951, *ApJ*, 114, 385
- [113] —. 1953, *ApJ*, 118, 106
- [114] Syer, D. & Ulmer, A. 1999, *MNRAS*, 306, 35
- [115] Tamblyn, P., Rieke, G. H., Hanson, M. M., Close, L. M., McCarthy, D. W., & Rieke, M. J. 1996, *ApJ*, 456, 206

- [116] Tanner, A. et al. 2006, *ApJ*, 641, 891
- [117] Tremaine, S. et al. 2002, *ApJ*, 574, 740
- [118] Vidali, G. et al. 2007, *Journal of Physical Chemistry A*, 111, 12611
- [119] Wang, J. & Merritt, D. 2004, *ApJ*, 600, 149
- [120] Wu, X. et al. 2008, *MNRAS*, 386, 2199
- [121] Young, P. J. 1977, *ApJ*, 215, 36
- [122] Yu, Q. & Tremaine, S. 2002, *MNRAS*, 335, 965
- [123] —. 2003, *ApJ*, 599, 1129
- [124] Zhao, H., Haehnelt, M. G., & Rees, M. J. 2002, *New Astronomy*, 7, 385

Chapter 16

List of publications

The following first authored publications appear in this thesis:

1. “Massive perturber-driven interactions between stars and a massive black hole by Perets, Hopman, & Alexander, published in *The Astrophysical Journal*, Volume 656, Issue 2, pp. 709-720 (2007).
2. “Massive perturbers and the efficient coalescence of binary massive black holes by ? , published in *The Astrophysical Journal*, Volume 677, Issue 1, pp. 146-159 (2008).
3. “Dynamical and evolutionary constraints on the nature and origin of hypervelocity stars” by Perets, published in *The Astrophysical Journal*, Volume 690, Issue 1, pp. 795-801 (2009).
4. “Runaway and hypervelocity stars in the Galactic halo: Binary rejuvenation and triple disruption” by Perets, to appear in *The Astrophysical Journal*, in press (2009)
5. “The Galactic potential and the asymmetric distribution of hypervelocity stars” by Perets et al. published in *The Astrophysical Journal*, Volume 697, Issue 2, pp. 2096-2101 (2009).
6. “Dynamical evolution of the young stars in the Galactic center: N-body simulations of the S-stars” by Perets, Gualandris, Kupi, Merritt, & Alexander, to appear in *The Astrophysical Journal*, in press (2009).
7. “Molecular hydrogen formation on amorphous silicates under interstellar conditions” by Perets et al. published in *The Astrophysical Journal*, Volume 661, Issue 2, pp. L163-L166 (2007)
8. “Realization of quantum walks with negligible decoherence in waveguide lattices” by Perets et al., published in *Physical Review Letters*, , vol. 100, Issue 17, id. 170506 (2008)

9. “On the triple origin of blue stragglers” by Perets & Fabrycky, published in *The Astrophysical Journal*, Volume 697, Issue 2, pp. 1048-1056 (2009)
10. “Kozai cycles, tidal friction and the dynamical evolution of binary minor planets” by Perets & Naoz to appear in *ApJL*, in press (2009)
11. “A new type of stellar explosions” by Perets et al., submitted to *Nature* (2009)